UNIVERSIDAD COMPLUTENSE DE MADRID

FACULTAD DE CIENCIAS QUÍMICAS

Departamento de Química Orgánica I

TESIS DOCTORAL

Complejos supramoleculares dador-aceptor basados en éteres corona

MEMORIA PARA OPTAR AL GRADO DE DOCTOR

PRESENTADA POR

Luis Moreira Navarro

Directores

Nazario Martín León
Jean-François Nierengarten

Madrid, 2014

UNIVERSIDAD COMPLUTENSE DE MADRID
FACULTAD DE CIENCIAS QUÍMICAS
Departamento de Química Orgánica I

COMPLEJOS SUPRAMOLECULARES DADOR-ACEPTOR BASADOS EN ÉTERES CORONA

Directores:

Prof. Nazario Martín León
Dr. Jean-François Nierengarten

Memoria que para optar al grado de
DOCTOR EN CIENCIAS QUÍMICAS
presenta

Luis Moreira Navarro

ESTRASBURGO – MADRID
Madrid, 2013

UNIVERSITÉ DE STRASBOURG

ÉCOLE DOCTORALE DES SCIENCES CHIMIQUES

Laboratoire de Chimie des Matériaux Moléculaires – UMR 7509

Laboratorio de Materiales Moleculares Orgánicos

THÈSE

présentée par :

Luis MOREIRA NAVARRO

soutenue le : **5 novembre 2013**

pour obtenir le grade de : **Docteur de l'Université de Strasbourg**

Discipline/ Spécialité : Chimie

Des éthers couronnes pour la construction de systèmes donneur-accepteur supramoléculaires

THÈSE dirigée par :

M Jean-François NIERENGARTEN	Dr., Université de Strasbourg
M Nazario MARTÍN	Pr., Universidad Complutense

RAPPORTEURS :

M Pau BALLESTER	Dr., ICIQ
M Dario BASSANI	Dr., Université Bordeaux 1

AUTRES MEMBRES DU JURY :

M Jean WEISS	Dr., Université de Strasbourg
Mme María del Mar GÓMEZ	Pr., Universidad Complutense
Mme Carmen María ATIENZA	Dr., Universidad Complutense

D. Nazario Martín León, Catedrático de Universidad del Departamento de Química Orgánica de la Universidad Complutense de Madrid, y **D. Jean-François Nierengarten**, Director de Investigación del UMR 7509 del CNRS/Université de Strasbourg.

CERTIFICAN

Que la presente Memoria titulada "Supramolecular crown ether containing donnor-aceptor ensembles" se ha realizado bajo su dirección en el Departamento de Química Orgánica de la Facultad de Ciencias Químicas de la Universidad Complutense de Madrid y el UMR 7509 del CNRS/Université de Strasbourg, por el Licenciado en Ciencias Químicas D. Luis Moreira Navarro y autorizan su presentación para ser calificada como Tesis Doctoral.

Y para que conste, firmo el presente certificado en Madrid a 5 de noviembre de 2013.

Fdo. Dr. Nazario Martín León

Fdo. Dr. Jean-François Nierengarten

M Luis Moreira Navarro was a member of the European Doctoral College of the University of Strasbourg during the preparation of his PhD, from 2009 to 2013, class Charles Darwin.

He has benefited from specific financial supports offered by the College and, along with his mainstream research, has followed a special course on topics of general European interests presented by international experts.

This PhD research project has been led with the collaboration of two universities: the Universidad Complutense de Madrid, Spain and the Université de Strasbourg, France.

A mi padre Luis, a mi madre Pepa y a mi hermana Raquel,
por estar siempre a mi lado,
a las duras y a las maduras,
en España o donde sea.

‘To see what is in front of one's nose requires a constant struggle’
George Orwell

‘Patience is the mother of science’
Spanish proverb

ACKNOWLEDGEMENT

This PhD is the end of a travel which started nearly 6 years ago when I moved to Strasbourg for the first time as part of a joint degree in chemistry. That positive experience encouraged me to later enroll into this international PhD under the supervision of Jean-François Nierengarten in Strasbourg and Nazario Martín in Madrid without whom, this work would not have been possible.

Jean-François, merci beaucoup de ton appui et disponibilité tout ce temps. Merci de m'avoir introduit dans le monde de la chimie supramoléculaire et de m'avoir appris que dans la recherche il vaux la peine d'être patient pour avoir des résultats.

Nazario, muchas gracias por haberte embarcado en esta aventura cotutelada y tu compromiso por sacarla adelante, por todo el apoyo que me has brindado este tiempo y tu preocupación en mi formación académica y profesional. Sin lugar a dudas tus grandes conocimientos de 'lo nano' me han ayudado a ser un mejor químico.

I would also like to mention here Beatriz Illescas, who has been mentoring me since I joined the laboratory in Madrid. **Beti**, muchísimas gracias por tu calidad humana, por tener siempre abiertas las puertas de tu despacho y por todo el apoyo demostrado.

Many thanks to the members of my PhD jury, for their interest in my work and for having accepted its evaluation.

My acknowledgements goes as well to the **Fundación la Caixa**, which trusted in this project and afforded me a scholarship to fund my stay in France, as well as to the **Consolider project**, which funded my stay in Spain.

I am grateful to **Dr. Iwona Nierengarten**, who made the non-linear curve fitting calculations of chapter 4.1, and 4.2, to **Dr. José Santos**, who started the research line of chapter 4.3, collaborating in the synthesis of some of the molecules employed, and to **Joaquin Calbo**, **Juan Aragó**, **Dr. Pedro Viruela** and **Prof. Enrique Ortí** for performing the theoretical calculations on chapter 4.3.

I am also thankful to the people attending the different technical and research centers I've been working with. Notably **Michel Schmitt** from the NMR services in Strasbourg, **Ángel Sánchez**, **Dra. Dolores Molero**, **Dr. Elena Saénz** and **Dr. Margarita Valhondo** from the NMR services in Madrid, **Maite Alonso** and **Mª Jesús Vicente** from the MS services in the Universidad Autónoma de Madrid and **Javier García** and **Laura García** who performed the IR measurements in Madrid. I would also like to thank **Agnès Schmitt**, **Marta Grande**, **Virginia González**, **Nara Alexiou** and **Ana Ferruelo** for helping me with all my administrative issues (and there were plenty of them!).

I am indebted to **Prof. Carmen Carreño**, who started the international joint degree which took me to Strasbourg on a first place.

A huge "MERCI BEAUCOUP" goes to all my colleagues with whom I had the pleasure to work side by side in the Laboratoire de Chimie des Matériaux Moléculaires.

Michel Holler **"Mimiche"** (I am grateful to you for listening to all my chemical problems and always being able to find creative solutions), Julien **"Choupi"** (thanks for guiding me in my first steps in the lab) and especially to my friends inside and outside the lab **Maida** (I still remember –and practice– your arab dancing lessons!), **Meera** (I am glad we met, but would you mind stop being so nice?!), David **"Piou"** (best DJ in a lab ever) and **Rubén** (todo lo que tienes de grande lo tienes de buen tipo). I would also like to thank **Nico**, **Thomas**, **Mathilde** and **Annie** for their friendship.

My 'mercis' go also to the rest of my colleagues in the UMR 7509 for their kindness. Especially to **Camille** (thanks for all those 'papotage' moment) and **Anaïs** (I miss going to the gym together).

Of course, my stay in Strasbourg would have been much worst without the Spanish mafia: **Johanne** (¡eres la mejor collocataire, amiga y confidente que podría haber tenido!), **Carolina** (mira que has tenido paciencia aguantando mis "bromas medievales"), **Marta** (pocas personas me hacen reír tanto como tú), **Alba** (siempre

dispuesta a pasar un buen rato con sus amigos), **Elena** (la de veces que te habremos "escuateado" la casa para cenar o tomar algo), **Mercedes** & **Leti** (gracias por ser mis mamis en Estrasburgo y cuidarme tanto todo el tiempo que compartimos), **Irene** (responsable del mejor tiramisú de toda Alsacia), **Juanjo** (incapaz de dejar indiferente, gracias por los buenos ratos que me has hecho pasar), **David** (un cafecito en el coin caffé sin ti no es lo mismo), **Violeta** (nadie como tú para pasarlo bien, ya sea en el Tribord, en la Académie de la Bière o en el parque de la Citadelle), **Rafa** & **Rafeta** (los anfitriones de las mejores soirées en el club 19), **Marimeri** (la "niña muerta" de la sonrisa perenne en los labios), **Viky** (todavía me río con la historia de los choricitos al infierno) and **Rocio** (¡a ver si nos volvemos a ir de Bienal juntos!).

Finally, but not least, my non-chemist French friends **Diego**, **Philippe**, **Alexandre**, **Alejandro** and **Amehde** welcomed me in their group, discovering me "the French way" and making me feel in Strasbourg a bit more like at home. I also enjoyed the time passed with **Paulux**, thank you so much for everything!

When moving back to Madrid I had the opportunity to work with an amazing –and large– bunch of people in the Laboratorio de Materiales Moleculares Orgánicos who are responsible for having made my time spent here amazing.

Carmen **"Friend"** (no hay bastantes líneas para agradecerte el buen tiempo que me has hecho pasar en el labo y el apoyo que me has prestado, especialmente al final durante la escritura, gracias, friend, por ser como eres), Sonia **"Mali"** (eres el descubrimiento de mi tesis, después de haber trabajado en 5 laboratorios de 3 países distintos tu fuiste la 1ª en seguirme los bailes sin dudarlo), **Javi** (muchas gracias por estar siempre dispuesto a echar una mano en cuanto hace falta y por los buenos momentos fuera del labo), **Sara** (gracias por poner siempre un punto de buen rollo –y de buen olor– con tu presencia), **Juan** (definitivamente el laboratorio sería mucho más aburrido sin ti, ¡gracias por prestarme la radio del coche!), **Antonio** (2 años después, sigo flipando de las cosas bizarras que sabes de química), **Andre(it)a** (el terror de las nenash, no sabes lo que echaré de menos tus palabros), **Silvia** (gracias

organizar tantas excursiones y tener la cámara siempre lista), **Laura** (gracias por ser mi gurú de los nanotubos y el grafeno), Alberto **"Muchachito"** (gracias por traernos un poquito de Colombia a Madrid a través de tu música), **Jaime** (gracias por amenizarnos las sobremesas con tus historias), **Vanesa** (gracias por ese mes de agosto en el que trabajamos codo con codo), **Carmen A.** (muchas gracias por tu amabilidad y estar siempre dispuesta a resolver mis dudas), **Juan Luis "Murcia"** (es increíble la de ideas nuevas que se pueden sacar después de discutir un rato contigo de química), **Mª Ángeles** (muchísimas gracias por todo el trabajo que haces por el grupo y por aguantar la guerra que te he dado con la electroquímica), **Salvatore** (eres un grande de la química, pero ¡¡deja de ir a los toros!!), **Emilio**, **Juan Luis "Toledo"**, **Helena**, **María** & **Alberto** (IMDEICOS, gracias por escuchar y resolver mis penas supramoleculares, ¡siempre vale la pena consultaros!) and **Margarita**, **David**, **Andreas**, **Ángel**, **Enrique**, **Raúl**, **André**, **Damien**, **Marta**, **Fulvio**… gracias por hacerme sentir como en casa.

Thanks, also to the rest of the people working in the Department, especially to **Luis Sánchez** (gracias por poner siempre tantísimo interés en ayudarme) and **Gloria**, **Alberto**, **Paula**, **Fátima A**, **Fátima G**, **Julia**, **Noe** and **Irene** . You made it easier going to work everyday.

Also to my friends in the UAM: **Sonia**, **Ana**, **Marta**, **María**, **Dani**, **Nerea**, **Irene**… and the rest of the "Guisantes locos" **Almudena**, **Anto**, **Constanza**, **Richard** and **Edu** for their friendship.

Finally, as everything in life is not chemistry I would like to mention here all my non-chemist friends in Madrid: **Rubén**, **Gabriel**, **Garcy**, **Beto**, **Cris**, **Amanda**, **Yago**… as well as my closer family: my parents **Luis** and **Josefa**, my sister and brother in law **Raquel** and **Luismi** and my aunt and cousins **Carmen**, **Marta** and **Sofia**. Thank you all for helping me maintaining a balanced, healthy and funny life during this PhD.

Luis Moreira Navarro

Abbreviations and acronyms

In addition to the standard abbreviations and acronyms in organic chemistry (as defined by the *J. Org. Chem.* Author Guidelines) the following terms have been used in this manuscript:

α	Allosteric cooperative factor
α^H	Hydrogen-bond donor constant
A	Acceptor. Absorbance
AFM	Atomic force microscopy
β	Overall constant
bpy	4,4'-Bipyridine
χ	Electronegative. Mole fraction
CC	Gravity-fed column chromatography
CE	Counter electrode
CS	Charge separated
CTV	Cyclotriveratrylene
D	Donor
dba	Dibenzylideneacetone
DCTB	*trans*-2-[3-(4-*tert*-Butylphenyl)-2-methyl-2-propenylidene]malononitrile
DFT	Density functional theory
DMAP	4-(Dimethylamino)pyridine
ε	Dielectric constant. Relative molar absorptivity
EDC	*N*-(3-Dimethylaminopropyl)-*N*'-ethylcarbodiimide
EM	Effective molarity
exTTF	9,10-Di(1,3-dithiol-2-ylidene)-9,10-dihydroanthracene
FC	Flash chromatography
G	Guest
GCE	Glassy carbon electrode
GPC	Gel permeation chromatography

H	Host
$H_2T_{3,5\text{-dimethyl}}PP$	Tetra(3,5-dimethylphenyl)porphyrin
H_2TMP	Tetra(1,3,5-tri-methylphenyl)porphyrin
H_2TPP	Tetraphenylporphyrin
HMTA	Hexamethylenetetramine
K_a	Binding constant
k_{CR}	Charge recombination rate
k_D	Energy decay rate
K_d	Dissociation constant
k_{ET}	Electron transfer rate
k_{ENT}	Energy transfer rate
MW	Microwave
ϕ_{ENT}	Energy transfer efficiency
ϕ_{ET}	Electron transfer efficiency
*o*DCB	1,2-Dichlorobenzene
p	p-value. Probability of binding of the system
PIFA	[Bis(trifluoroacetoxy)iodo]benzene
PM	Parametric method
SCE	Saturated calomel electrode
SE	Supporting electrode
TBAI	Tetrabutylammonium iodide
TBAOH	Tetrabutylammonium hydroxide
TBDPS	*tert*-Butyldiphenylsilyl
TCAQ	Tetracyanoanthraquinodimethane
TMHDA	*N*,*N*,*N*′,*N*′-Tetramethylhexane-1,6-diamine
TTF	Tetrathiafulvalene
VT	Variable temperature
WE	Working electrode
XPhos	2-Dicyclohexylphosphino-2′,4′,6′-triisopropylbiphenyl
ZnTMP	Zinc(II) tetra(1,3,5-tri-methylphenyl)porphyrin

Table of contents

1. Introduction

1. INTRODUCTION

Since the dawn of times, human beings have improved their life quality thanks to the advance of science and technology. Indeed, mastery of these fields has often marked the destination of entire nations. For example, the British Empire would not have been possible without the industrial revolution, spurred by the steam engine developed by James Watt in 1781. In a similar manner, the decadence of the Soviet Union was intimately related to the lack of a modern industry unable to compete with the newest American technologies.

During the last decades, the development of new theories and inventions has increased so much that we are nowadays fully surrounded by 'smart' things. From our clothes, to our buildings, passing through our mobile phones, which seem to be a new extension of our body. Together with the uncountable benefits from this new way of living a number of drawbacks come along, one of the most important being the increasing dependency to electricity, without which our society would move back more than two centuries into the 1800s. This is a major issue if we consider that a huge fraction of our electricity depends on non-renewable fossil fuels, which are currently starting to disappear after years of massive consumption.

As a result, tremendous efforts have been made to find new and better sources of energy. Among them, solar light is one of the most promising given the outstanding potential of sun, which sheds over the Earth more energy in one year than the one that will ever be obtained from all the non-renewable sources available in the planet together (Figure 1.1).[1]

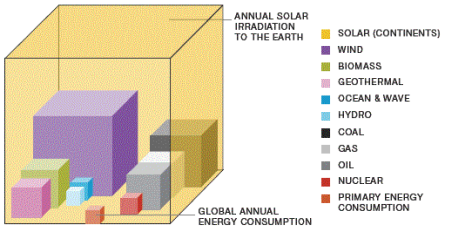

Figure 1.1. Solar irradiation *vs.* established global energy resources. Fossil fuels are expressed with regard to their total reserves while renewable energies to their yearly potential.

[1] Greenpeace and EPIA, "Solar Generation. The global solar photovoltaic outlook.", **2010**.

Solar cells are, without doubt, the most common devices to transform light energy into electricity and even though their efficiencies have dramatically increased in the last years they are still very dependent on their composition.

Currently, multijunction cells offer the best results (44% efficiency), but they suffer from a series of disadvantages including the expensive prize of their components and their low processability.

In sharp contrast, organic cells have emerged as cheap and flexible alternatives which unfortunately are not yet as effective (12% efficiency). However, it must be possible to obtain much better efficiencies from them, as organic devices able to harvest light and convert it into electrochemical potential energy with near quantum efficiency -such as the photosynthetic apparatus- do already exist (in fact, they are the base of life in the planet!)

So, if we consider that both solar cells and the photosynthetic apparatus share a basic functioning (i.e. absorption of light to produce a separation of charges which then recombine) why no human-made device has come even close to the efficiency of nature?

The answer is not yet fully clear but seems to be related to the size of the photosynthetic apparatus, lying in the nano-scale (Figure 1.2), where properties of matter no longer respond to standard physics but to quantum mechanics, which radically changes everything leading to unique phenomena.

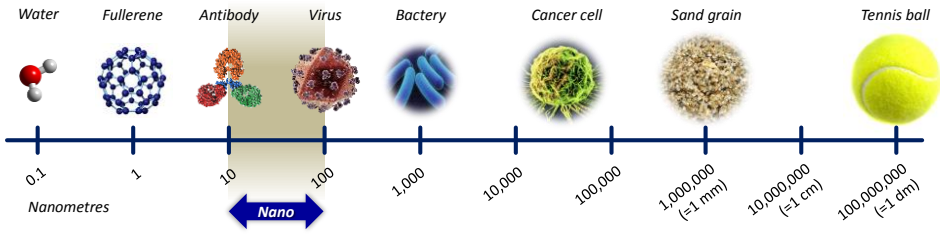

Figure 1.2. Size scale showing how small is “nano”.

In order to reach that scale two different approaches have been followed:

- ***Top-down approach***: consisting in the creation of smaller devices by scaling down the device dimensions. The development of the technologies related to computers is a paradigmatic example: the size of the external memory devices, for example, have evolved from the first 8-inch floppy disks into the cloud computing where no physical device is required by the user at all (Figure 1.3).

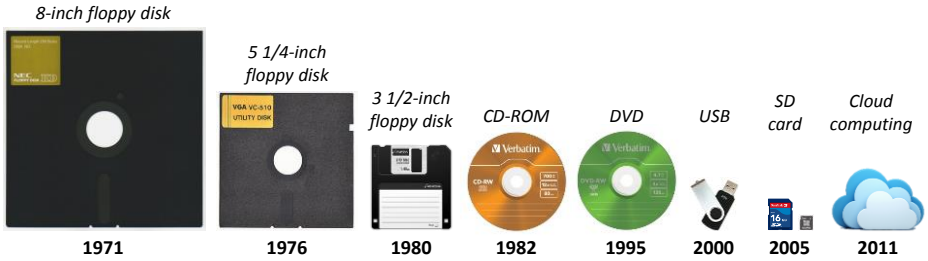

Figure 1.3. Timeline of the evolution of the external memory devices.

- ***Bottom*-up approach**: consisting in arranging smaller components into more complex assemblies. This is the more familiar approach to chemists, who are able to arrange molecules together into larger ensembles (Figure 1.4).

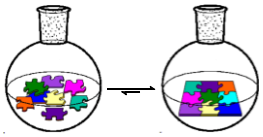

Figure 1.4. Bottom-up approach

For this, the key question is how to control this assembly in order to obtain the desired ensemble and not a random combination of its building blocks. The answer, lies within the field of supramolecular chemistry, which addresses how molecules interact among themselves and which will be the main focus of the present study.

In this context, this study deals with the formation of supramolecular donor-acceptor ensembles which are able to reproduce the key step of the photosynthetic process, i.e. the formation of a charge separated state. The interest will be focused in understanding how electron donor and acceptor molecules can form stable ensembles in a controlled manner.

2. Background

2. BACKGROUND

2.1. SUPRAMOLECULAR CHEMISTRY

In contrast to traditional organic chemistry – based on the synthesis of molecules by covalent bonds – supramolecular chemistry goes a step ahead and is interested in the self-assembly of these covalent building blocks by means of weak intermolecular forces (Scheme 2.1).[2]

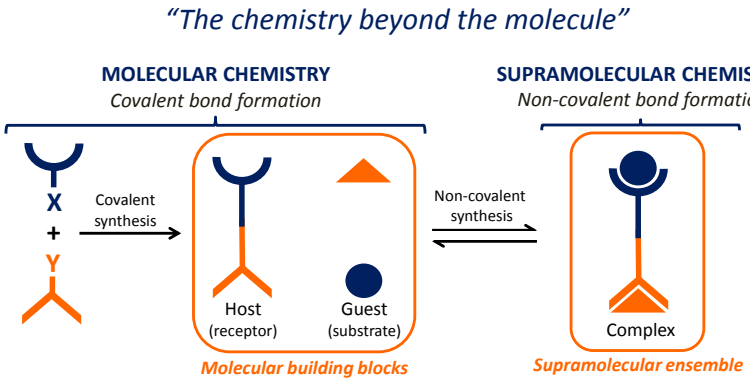

Scheme 2.1. Molecular chemistry *vs.* supramolecular chemistry.

As a result, in 1988 it was described by Nobel Prize Jean-Marie Lehn as the "…chemistry of molecular assemblies and of intermolecular bond".[3] Other definitions present the field as "the chemistry beyond the molecule", "the chemistry of the non-covalent bond" or even "the Lego chemistry", reflecting that one of its main benefits is the synthetic freedom achieved in comparison to covalent methods.

Whereas it is not easy to establish a complete timeline of supramolecular chemistry, as its roots expand to almost the beginning of modern chemistry, it is possible to select some of its milestone moments (Figure 2.1).

[2] a) J.-M. Lehn, *Supramolecular Chemistry. Concepts and Perspectives*, Wiley-VCH, Weinheim, **1995**; b) P. D. Beer, P. A. Gale and D. K. Smith, *Supramolecular Chemistry*, Oxford University Press, Oxford, **1999**; c) J. W. Steed and J. L. Atwood, *Supramolecular Chemistry*, 2nd ed., John Wiley & Sons, Wiltshire, **2009**; d) *Comprehensive Supramolecular Chemistry, Vol. 1-11*, (Ed. J.-M. Lehn, J. L. Atwood, J. E. D. Davies, D. D. Macnicol and F. Vögtle), Pergamon/Elsevier, Oxford, **1996**; e) *Supramolecular Chemistry of Fullerenes and Carbon Nanotubes*, (Ed. N. Martín and J.-F. Nierengarten), Wiley-VCH, Weinheim, **2012**; f) *Supramolecular Chemistry: From Molecules to Nanomaterials*, (Ed. J. W. Steed and P. A. Gale), John Wiley & Sons, **2012**; g) *Analytical Methods in Supramolecular Chemistry*, 2nd ed., (Ed. C. A. Schalley), Wiley-VCH, Weinheim, **2012**.
[3] J.-M. Lehn, *Angew. Chem. Int. Ed.* **1988**, *27*, 89.

Figure 2.1. Milestone moments in supramolecular chemistry history.

Intermolecular forces were first described by van der Waals in 1873. This concept was further expanded by Werner's coordination chemistry[4] but it was not until Fischer's *lock and key* model for enzyme-substrate interactions[5] that the crucial relationship of a molecule with its environment was revealed. Later, Ehrlich stated that a molecule can only have effects in the human body if it is bound, coining the term receptor.[6]

The imagination of synthetic chemists soon spanned and new systems such as crown ethers,[7] cryptands[8] and spherands[9] were obtained (Figure 2.2). Pedersen, Lehn and Cram, their respective designers, were awarded the Nobel Prize in 1987 "for the development and use of molecules with structure-specific interactions of high selectivity".

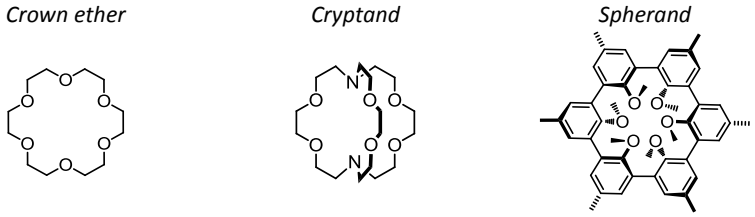

Figure 2.2. Crown ethers, cryptands and spherands where given the Nobel Prize in 1987.

More recently, supramolecular chemistry has enabled to obtain extremely complex and beautiful systems such as the catenanes and molecular knots reported by Sauvage[10] or the Borromean rings synthesized by Stoddart,[11] landmarks in molecular topology. Transition metal directed self-assembled macrocycles and molecular cages developed by Fujita[12]and Stang[13] represent other examples of complex structures easily obtained by using concepts of supramolecular chemistry.

[4] A. Werner, *Z. anorg. Chem.* **1893**, *3*, 267.
[5] E. Fischer, *Ber. Deutsch. Chem. Ges.* **1894**, *27*, 2985.
[6] P. Ehrlich and C. B. Bolduan, *Collected Studies on Immunity*, Wiley, **1906**.
[7] C. J. Pedersen, *J. Am. Chem. Soc.* **1967**, *89*, 7017.
[8] B. Dietrich, J. M. Lehn and J. P. Sauvage, *Tetrahedron Lett.* **1969**, *10*, 2885.
[9] D. J. Cram, T. Kaneda, R. C. Helgeson and G. M. Lein, *J. Am. Chem. Soc.* **1979**, *101*, 6752.
[10] C. O. Dietrich-Buchecker and J.-P. Sauvage, *Angew. Chem. Int. Ed.* **1989**, *28*, 189.
[11] K. S. Chichak, S. J. Cantrill, A. R. Pease, S.-H. Chiu, G. W. V. Cave, J. L. Atwood and J. F. Stoddart, *Science* **2004**, *304*, 1308.
[12] M. Fujita, D. Oguro, M. Miyazawa, H. Oka, K. Yamaguchi and K. Ogura, *Nature* **1995**, *378*, 469.

2.1.1. *Nature of supramolecular interactions*

The term 'supramolecular' involves many and diverse interactions which have in common being weak in comparison to covalent bonds (Figure 2.3). As a result of this diversity, this section is limited to a general overview of these forces.

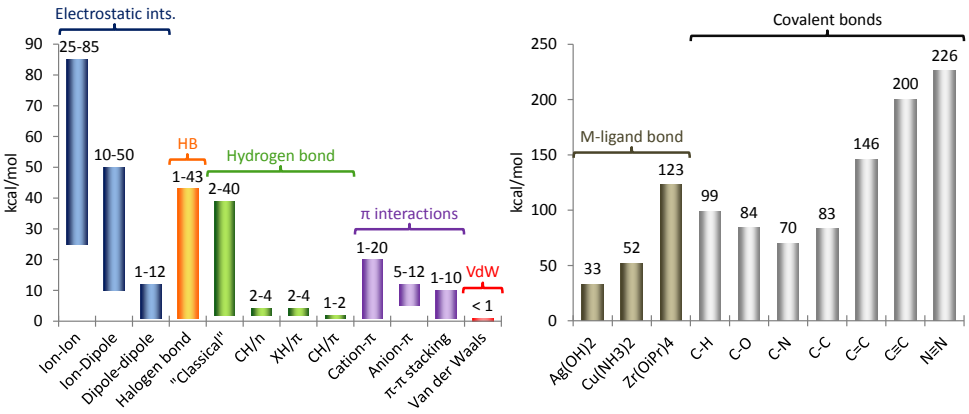

Figure 2.3. Non-covalent *vs.* covalent bonds strength.

a) **Electrostatic interactions** (1-85 kcal/mol)

The strongest supramolecular interactions. They are based in the Coulombic attraction of permanent opposite charges and can be subdivided in *ion-ion* (e.g. tetrabutylammonium chloride), *ion-dipole* (e.g. potassium [18]crown-6) or *dipole-dipole* interactions (e.g. acetone) (Figure 2.4). While ion-ion interactions are non-directional, the relative orientation of charges plays an important role with dipoles.[14]

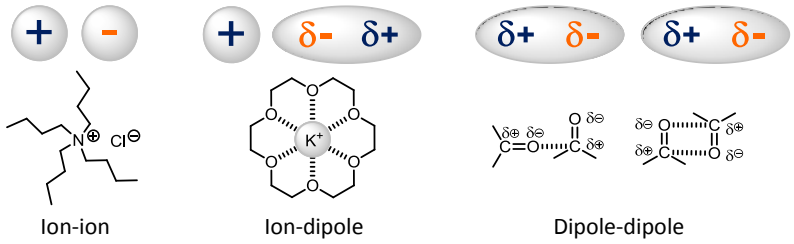

Figure 2.4. Electrostatic interactions.

[13] B. Olenyuk, J. A. Whiteford, A. Fechtenkotter and P. J. Stang, *Nature* **1999**, *398*, 796.
[14] E. V. Anslyn and D. A. Dougherty, *Modern Physical Organic Chemistry*, Univ. Science Books, **2006**.

b) **Halogen bonds** (1-43 kcal/mol)

Arise from a Lewis acid-base interaction between an electron rich site (D, a Lewis base) and a halogen atom (X) acting as a Lewis acid (Figure 2.5). The anisotropic electron density of organic halides makes this a very directional interaction, whose strength increases with the electron-withdrawing nature of the atom/moiety bound to a given halogen (Y) and with the nature of the halogen (I > Br > Cl > F).[15]

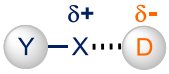

Y = C, N, halogen… **X =** I, Br, Cl, F **D =** N, O, S, Se, Cl, Br, I…

Figure 2.5. Halogen bond.

c) **Hydrogen bonds** (1-40 kcal/mol)

Consist in the directional electron density transfer from rich sites (D, a Lewis base) to a hydrogen atom (Lewis acid) being thus similar in nature to halogen bonds. It is possible to establish a comprehensive classification of all different types by taking into account Pearson's hard and soft acids and base theory (Table 2.1).[16],[17]

Table 2.1. Classification of hydrogen bonds.

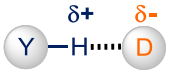

H-BOND TYPE	Y (H-donor)	D (H-acceptor)
"Classical" H-bond	Hard acid RX–H (X = O, N, F)	Hard base Elec. pair of an χ atom (O, N, F, Cl)
CH/n	Soft acid C–H	Hard base Elec. pair of an χ atom (O, N, F, Cl)
XH/π	Hard acid RX–H (X = O, N, F)	Soft base π system
CH/π	Soft acid C–H	Soft base π system

[15] a) P. Metrangolo, H. Neukirch, T. Pilati and G. Resnati, *Acc. Chem. Res.* **2005**, *38*, 386; b) P. Metrangolo, F. Meyer, T. Pilati, G. Resnati and G. Terraneo, *Angew. Chem. Int. Ed.* **2008**, *47*, 6114.
[16] R. G. Pearson, *J. Am. Chem. Soc.* **1963**, *85*, 3533.
[17] a) O. Takahashi, Y. Kohno and M. Nishio, *Chem. Rev.* **2010**, *110*, 6049; b) T. Steiner, *Angew. Chem. Int. Ed.* **2002**, *41*, 48.

d) π interactions (1-20 kcal/mol)

A type of electrostatic interactions dealing with the quadrupoles of π bonds.[18] In standard aromatic rings this quadrupole is positive at the faces of the ring and negative in the plane, thus enabling *cation-π* interactions[19] with alkaline, alkaline earth or ammonium cations (transition metal cations interact in a too strong manner to be considered non-covalent, e.g. ferrocene). *Anion-π* interactions[20] can be rationalized equally, but they appear in the presence of electron deficient aromatic systems (e.g. perfluorobenzene) which present a reversal in the quadrupolar moment (Figure 2.6).

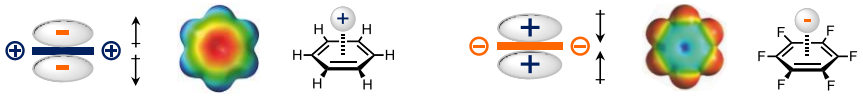

Figure 2.6. Quadrupoles and electrostatic potential surfaces of Ph (left) and PhF_6 (right).

However, the most common π-interactions occur between aromatic rings. Due to their electronic density distribution (Figure 2.6) the so called *π-π* interactions or *π-stacking*[21] usually take place in a parallel displaced or a T-shaped edge-to-face manner. Eclipsed face-to-face dimers are favored by combining electron rich and electron poor rings (Figure 2.7).

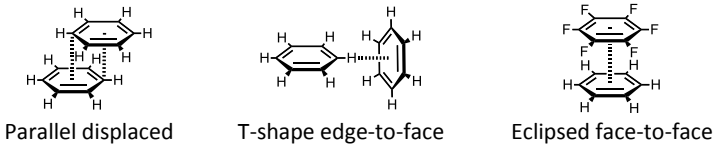

Figure 2.7. π-stacking interactions.

More recently, the close carbonyl-carbonyl interactions of many proteins suggested the existence of *n-π interactions* between the lone pair of electrons of an oxygen atom and the π orbital of the subsequent carbonyl group.[22] This interaction, however, has seldom been used in supramolecular chemistry up to date.

[18] L. M. Salonen, M. Ellermann and F. Diederich, *Angew. Chem. Int. Ed.* **2011**, *50*, 4808.
[19] A. S. Mahadevi and G. N. Sastry, *Chem. Rev.* **2012**, *113*, 2100.
[20] D.-X. Wang and M.-X. Wang, *J. Am. Chem. Soc.* **2012**, *135*, 892.
[21] C. A. Hunter, K. R. Lawson, J. Perkins and C. J. Urch, *J. Chem. Soc., Perkin Trans. 2* **2001**, 651.
[22] G. J. Bartlett, A. Choudhary, R. T. Raines and D. N. Woolfson, *Nat. Chem. Biol.* **2010**, *6*, 615.

e) Van der Waals forces (< 1 kcal/mol)

Also called dispersion forces, are the weakest and less directional of supramolecular interactions. They arise from induced dipoles and therefore exist between almost all atoms and molecules. They can be classified in *ion-induced dipole*, *dipole-induced dipole* and *induced dipole-induced dipole* (London forces) (Figure 2.8).

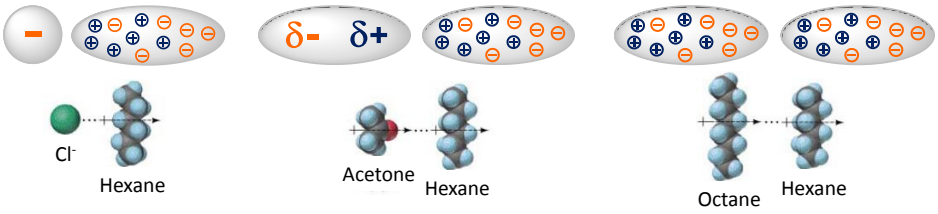

Figure 2.8. Van der Waals forces.

f) Metal-ligand interactions

Are at the core of coordination chemistry and at the interface of covalent and non-covalent bonds as they tend to be stronger than most supramolecular interactions (Figure 2.3) and produce rather short length distances (around 1.8-2.5 Å).[23] Its nature depends on the metal and ranges from an entirely ion-dipole interaction between the cation and an electronic pair of the ligand, to a covalent bond with orbital overlap.

g) Mechanical bond[24]

Combines two or more submolecular components so they cannot be separated without breaking a covalent bond. The most representative systems are *catenanes*, formed by two or more interlocked molecular rings and *rotaxanes*, formed by a ring molecule threaded through an "axle" molecule capped by two molecular stoppers. *Pseudorotaxanes* lacks at least one of the stoppers, thus not being a truly mechanical bond (Figure 2.9).

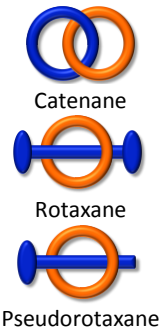

Figure 2.9.

[23] I. Dance, *New J. Chem.* **2003**, *27*, 1.
[24] a) J. F. Stoddart, *Chem. Soc. Rev.* **2009**, *38*, 1802; b) C. Bruns and J. F. Stoddart, in *Beauty in Chemistry, Vol. 323* (Ed.: L. Fabbrizzi), Springer Berlin Heidelberg, **2012**, p. 19.

2.2. DONOR-ACCEPTOR SYSTEMS

From a general point of view, a donor-acceptor (D-A) system is a molecular composite capable of using photon energy to produce a red-ox reaction through a charge-separated (CS) state.[25] Its basic functioning is depicted in Figure 2.10:

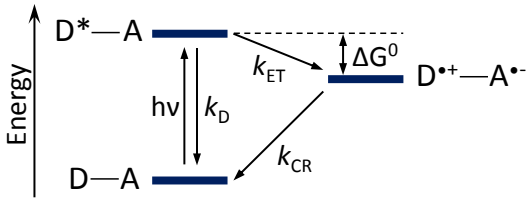

Figure 2.10. Energy diagram for a typical donor-acceptor system.

1. A photon with the necessary hν energy produces an excited state where the gained energy is located either in the excited state donor (D*) or the acceptor (A*) moiety.
2. This extra energy can either decay to the ground state (with a k_D rate) or be employed in transferring an electron from the donor to the acceptor moiety (with a k_{ET} rate), thus leaving a "positive hole". As a result, an "electron-hole pair" is created leading to the desired CS state ($D^{\bullet+}$–$A^{\bullet-}$) if sufficiently long lived.
3. Let to itself, a recombination to the ground state will happen (with a k_{CR} rate) due to Coulombic attraction of the spatially separated electron and positive hole recovering the system at the ground state.

The chemical potential stocked during this process is given by hν + ΔG^0. In order to maximize it, the rate constant for the electronic transfer should be as high as possible ($k_{ET} >> k_D$; $k_{ET} > 10^{10} s^{-1}$ in practice), lifetimes of the CS state should be greater than 1 μs and ΔG^0 should be as small as possible to ensure maximum conversion of photonic energy into chemical potential.

[25] a) K. A. Jolliffe, S. J. Langford, M. G. Ranasinghe, M. J. Shephard and M. N. Paddon-Row, *J. Org. Chem.* **1999**, *64*, 1238; b) J.-P. Sauvage, http://www-chimie.u-strasbg.fr/~lcom/Recherche/transfert1.html.

2.3. FULLERENES

Fullerenes are closed carbon cages discovered in 1985 by Nobel Prizes Kroto, Curl and Smalley during experiments aimed at understanding the mechanisms by which long-chain carbon molecules were formed in the space.[26] They soon became one of the most widely used electron acceptors due to their outstanding properties:

Three-dimensional structure.[27] Fullerenes are formed by 2(n+10) carbon atoms distributed in n hexagons and 12 pentagons. C_{60} (n = 20) is the most stable fullerene, presents a I_h symmetry – as a soccer ball – and two types of bonds: those between two hexagons, the [6-6], measuring 1.38 Å and presenting a double bond character, and those between a pentagon and a hexagon, the [5-6], measuring 1.45 Å and a simple bond character. C_{70}, (n = 25) has an oval shape – as a rugby ball – and four different bond types ranging from 1.37 Å to 1.46 Å (Figure 2.11).

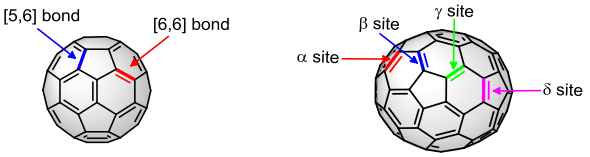

Figure 2.11. C_{60} and C_{70} fullerenes structures.

Low reduction potential.[28] Fullerenes are able to accept up to 6 electrons at a E^0_{red} comparable to those of benzoquinones due to a triply degenerated LUMO orbital. Reduction potentials are virtually the same for both C_{60} and C_{70} (Figure 2.12).

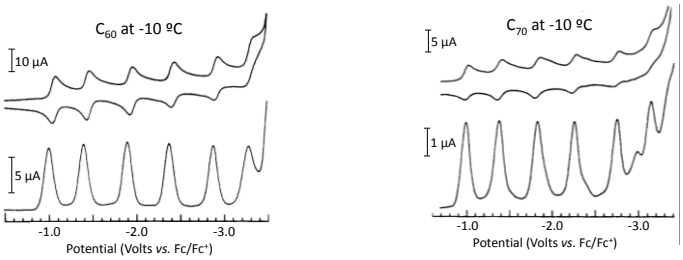

Figure 2.12. Reduction of C_{60} (left) and C_{70} (right) in PhMe/MeCN 5:1 at -10ºC (100 mV/s).

[26] H. W. Kroto, J. R. Heath, S. C. O'Brien, R. F. Curl and R. E. Smalley, *Nature* **1985**, *318*, 162.
[27] a) *Fullerenes. Chemistry and reactions.*, (Ed. A. Hirsch and M. Brettreich), Wiley-VCH, **2005**; b) D. M. Guldi and N. Martin, *Fullerenes: From Synthesis to Optoelectronic Properties*, Springer, **2002**.
[28] a) Q. Xie, E. Pérez-Cordero and L. Echegoyen, *J. Am. Chem. Soc.* **1992**, *114*, 3978; b) N. Martín, L. Sánchez, B. Illescas and I. Pérez, *Chem. Rev.* **1998**, *98*, 2527.

UV-vis absorption at a large range.[29] C_{60} presents various absorption bands between 190 and 410 nm due to allowed 1T1u-1Ag transitions and weak transitions (log ε around 2-3) between 410 and 620 nm from singlet-singlet forbidden transitions due to the high symmetry of C_{60}. The latter are responsible for their purple color.

C_{70} possesses markedly lower molecular symmetry and, accordingly, exhibits much stronger absorption at these wavelengths (log ε > 4) (Figure 2.13).

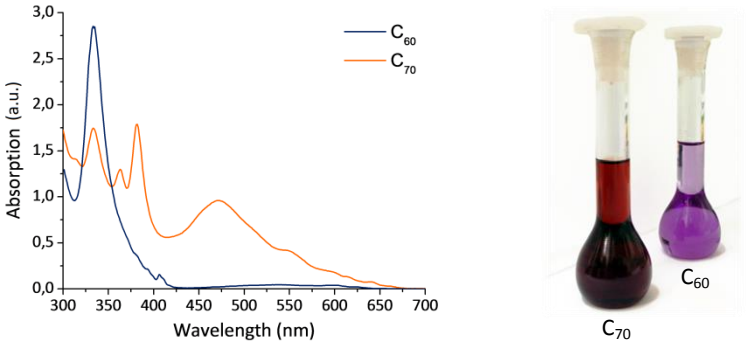

Figure 2.13. UV-Vis spectra of fullerene at rt in ClPh (l=1 cm). $[C_{60}]=4.96x10^{-5}$ M. $[C_{70}]=4.75x10^{-5}$ M.

Low reorganization energies in electron transfer reactions,[30] implying that upon reduction, the charge is spread over the whole 3-dimensional carbon framework. Thus, the charge density in each carbon in $C_{60}^{\bullet -}$ is much smaller than it would be in other electron acceptors, such as benzoquinone, thus reducing the value of the intramolecular reorganization energy (λ_i).

[29] H. Ajie, M. M. Alvarez, S. J. Anz, R. D. Beck, F. Diederich, K. Fostiropoulos, D. R. Huffman, W. Kraetschmer, Y. Rubin, K. E. Schriver, D. Sensharma and R. L. Whetten, *J. Phys. Chem.* **1990**, *94*, 8630.
[30] I. Hiroshi, H. Kiyoshi, A. Tsuyoshi, A. Masanori, T. Seiji, O. Tadashi, S. Masahiro and S. Yoshiteru, *Chem. Phys. Lett.* **1996**, *263*, 545.

2.4. CROWN ETHERS

Crown ethers consist of a cyclic array of ether oxygen atoms linked by organic spacers, typically ethylene groups. They were discovered by Charles J. Pedersen while studying the effects of phenolic ligands on the catalytic properties of the vanadyl group. As part of his research, he designed a synthetic route toward the bis-phenol depicted in Scheme 2.2. However, a secondary by-product was obtained as white crystals insoluble in hydroxylic solvents due to incomplete protection of starting catechol.[31]

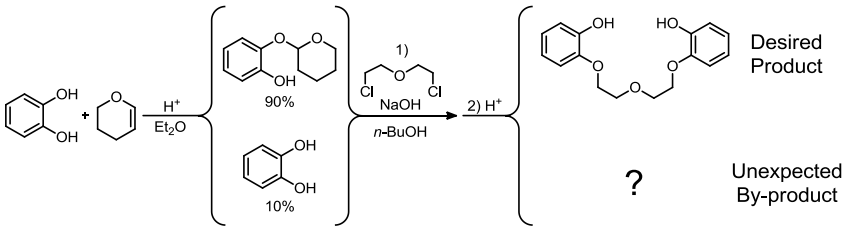

Scheme 2.2. The first crown ether was obtained as a by-product.

Luckily, Pedersen used UV-vis spectroscopy to follow the reactions as phenols exhibit a bathochromic shift of the absorption band upon treatment with an alkali if a hydroxyl position is free, remaining unaltered on the contrary (Figure 2.14.a).

The by-product, slightly soluble in MeOH, gave the typical absorption curve for a phenol. However, after addition of NaOH, the compound became fully soluble and the absorption spectra was distorted in an unexpected manner (Figure 2.14.b). This effect was observed with any soluble sodium salt being thus due to the cation.

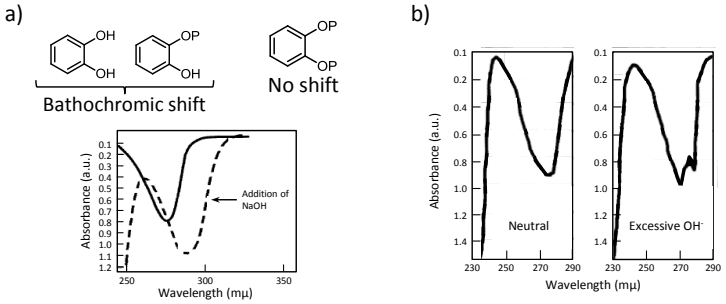

Figure 2.14. a) Effect of NaOH on the UV-vis of bis-phenols and b) on the by-product.

[31] C. Pedersen, *J. Inclusion Phenom.* **1988**, *6*, 337.

Its elementary analysis corresponded to the 2,3-benzo-1,4,7-trioxacyclonane (Figure 2.15), a plausible product in agreement with the reaction scheme and the IR and NMR spectra which proved that there were no free phenolic group.

However, the molecular weight obtained was exactly the double of the expected for such a molecule. Suddenly everything matched, the by-product was a 18-membered ring able to accommodate the cation in the hole in the center of the molecule. Dibenzo[18]crown-6, the first synthetic compound for complexing alkali metal ions, had been obtained (Figure 2.15).

2,3-Benzo-1,4,7-trioxacyclononane Dibenzo[18]crown-6

Figure 2.15. The by-product obtained was the first crown ether.

The molecular model (Figure 2.16) evidenced the beauty of the supramolecular system and the ability of this macrocycle to "crown" cations by complexation, hence their name.

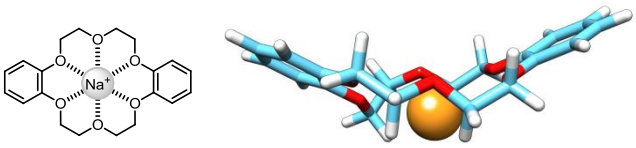

Figure 2.16. Dibenzo[18]crown-6•Na^+ complex.

Their ability to complex a wide variety of substrates was soon evidenced by Pedersen, who reported complexes with alkali, alkaline earth, transition metal and ammonium cations.[7] The stability of these complexes arises from ion-dipole interactions, when complexing metallic cations, or H-bonds, when complexing ammonium cations. It is maximized when the size of the crown ether corresponded to the diameter of the unsolvated ion. However, complexation can be achieved even if the fit is not optimal by complexing several ions (if the crown is too large) or forming a sandwich system consisting of two crown ethers per cation (if the crown is too small).[31]

2.4.1. Nomenclature

It was soon evident that the IUPAC nomenclature was too cumbersome for an effective identification of these compounds. As a result, Pedersen developed a trivial name based in their capacity to "crown" cations[7] consisting of:

- The number and kind of substituents, denoted by their prefix.
- The total number of atoms in the ring (usually given in square brackets).
- The class name, crown.
- The number of oxygen atoms in the polyether ring.

This nomenclature, however, does not define unequivocally the location of the donor atoms or other ring components. As a result, Vögtle and Weber first[32a] and then Cram[31b] designed a more systematic nomenclature where crown ethers are denominated *corands* (originally *coronand*) (Table 2.2). In spite of this, Pedersen's terminology is most frequently found and will be the one used in this manuscript.

Table 2.2. New nomenclature for crown ethers (top) and its comparative with other systems.

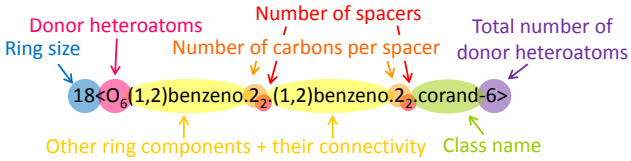

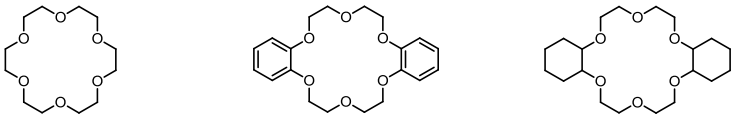

IUPAC	1,4,7,10,13,16-hexaoxacycloocta-decane	2,5,8,15,18,21-hexaoxa-tricyclo[20.4.0.0^{9,14}]hexacosa-1(22),8,11,13,23,24-hexaene	2,5,8,15,18,21-hexaoxa-tricyclo[20.4.0.0^{9,14}]-hexacosane
Pedersen Names	[18]crown-6	Dibenzo[18]crown-6	Dicyclohexano[18] crown-6
Short Notation	[18]C6	DB[18]C6	DCH[18]C6
New system	18<O$_6$2$_6$corand-6>	18<O$_6$(1,2)benzeno.2$_2$.-(1,2)benzeno.2$_2$corand-6>	18<O$_6$(1,2)cyclohexano.2$_2$.(1,2)cyclohexano.2$_2$corand-6>

[32] a) E. Weber and F. Vögtle, *Inorg. Chim. Acta* **1980**, *45*, L65; b) D. J. Cram, *Angew. Chem. Int. Ed.* **1986**, *25*, 1039.

2.4.2. Synthesis

A total of five different variations of Williamson ether synthesis (Scheme 2.3) were originally described by Pedersen to obtain crown ethers.[7] They still constitute the basis of current crown ether synthesis.

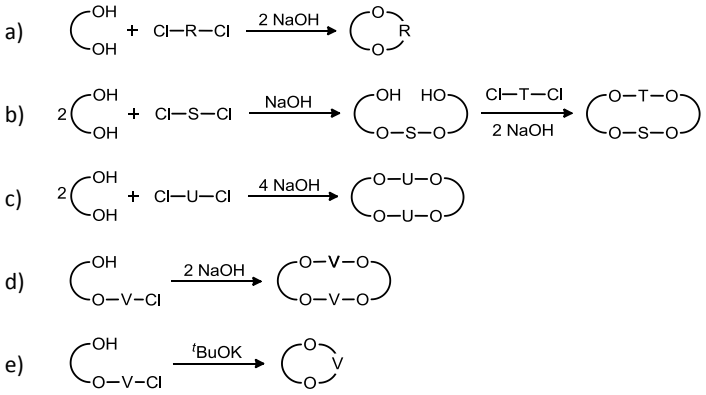

Scheme 2.3. Methods for synthesizing crown ethers (R–V are organic linker groups).

It is interesting to note that the original synthetic route used by Pedersen (Scheme 2.3.c) led to large macrocycles without the use of high dilution techniques rather than polymeric by products.

This extraordinary behavior can be rationalized if we consider that the metal ion is acting as a *template*, being wrapped by the polyheteroatom chain, bringing together the alkoxide anion and the carbon bearing the leaving group. The role of the metal is therefore crucial. Indeed, if we aim to synthesize [18]crown-6 using Et_3N instead of K_2CO_3, the result is a polymeric product rather than the desired product (Scheme 2.4).

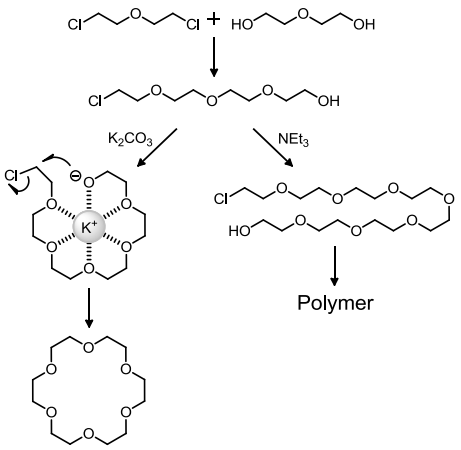

Scheme 2.4. Template effect has a crucial role in the synthesis of crown ethers.

Extensive research has been achieved since the discovery of crown ethers, leading to a vast structural variety of corands[33] (Table 2.3).

Table 2.3. Most common structural variations of crown ethers.

Most common structural variations in crown ethers	Example
a) *Ring-stiffened aryl ether ligands:* leading to a reduced basicity and donor ability of the oxygen atoms.	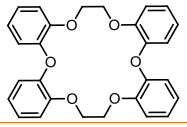
b) *Varied ring size:* every number of ring members and oxygen donors is possible.	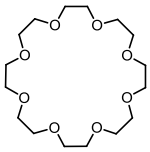
c) *Geometric arrangement of the donor atoms in the ring:* it is possible to separate or bring closer the O atoms.	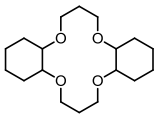
d) *Sulfur as alternative donor site:* all combinations, even pure thiacrowns, are possible.	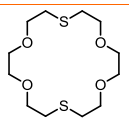
e) *Nitrogen as donor site:* it is possible to introduce N atoms at any position of the macrocycle.	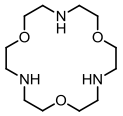
f) *Mixed O, N, S, P-coronands:* N and S can be combined together. P atoms have also been introduced in the ligand.	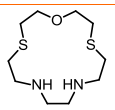
g) *Heteroaromatic coronands:* the donor atom can proceed from a heterocycle such as furane, pyridine or thiophene.	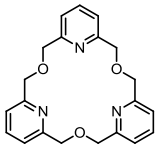
h) *Donor sites incorporated into functional groups:* enabling combination of various properties such as ligand stiffening or different polarization of the binding sites.	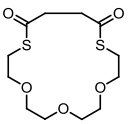
i) *Multisite crown compounds:* leading to assemblies of different geometry which can act cooperatively.	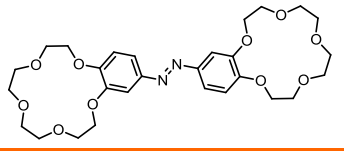

[33] E. Weber and F. Vögtle, in *Host Guest Complex Chemistry I, Vol. 98*, Springer, **1981**, p. 1.

2.4.3. *Supramolecular crown ether*•fullerene complexes

The first systems able to complex C_{60} and C_{70} in solution were two azacrowns with long lipophilic chains (Figure 2.17). Their ability to act as fullerene "baskets" was postulated in view of the additional stability of their Langmuir-Blodgett films upon addition of fullerenes, the morphological changes observed by AFM and the appearance of a new peak at 256 nm in the UV-vis attributed to π-π interactions.[34]

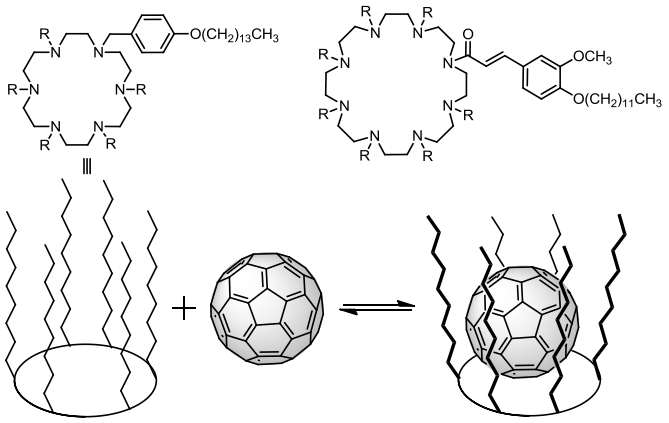

Ringsdorf and co.
Angew. Chem. Int. Ed., **1992**

Figure 2.17. The first system able to complex fullerenes in solution was an azacrown derivative.

Reflux of tetracyclohexano[12]crown-4 and C_{60} in benzene yielded the first complex involving a crown ether (Figure 2.18). The brown solid obtained had a 2:1 stoichiometry as demonstrated by the elemental analysis, ^{13}C-NMR and the appearance of a new UV-vis band at 280 nm attributed to n-π interactions from the oxygen atoms.[35]

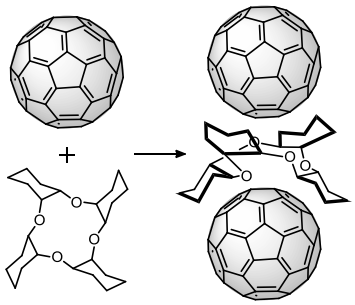

Cruz, Martínez and co.
Supramol. Chem., **1999**

Figure 2.18. Supramolecular complex.

[34] J. Effing, U. Jonas, L. Jullien, T. Plesnivy, H. Ringsdorf, F. Diederich, C. Thilgen and D. Weinstein, *Angew. Chem. Int. Ed.* **1992**, *31*, 1599.
[35] F. Lara, R. Cruz, M. Martínez, R. Martíneza, B. Villaneda, A. Ramírez, E. Moreno, I. Martínez and E. Angeles, *Supramol. Chem.* **1999**, *10*, 185.

The ability of crown ethers to form supramolecular complexes with fullerenes was further evaluated by Mukherjee using ^{1}H-NMR[36a] or UV-vis[36b] (Table 2.4).

Table 2.4. Stability constants for various 1:1 fullerene•crown ether complexes.

a)	b)	c)
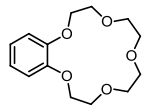	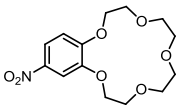	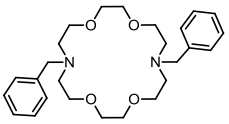
C_{60}: log K_a = 2.8 C_{70}: log K_a = 2.1	C_{60}: log K_a = 2.2 C_{70}: log K_a =3.0	C_{60}: log K_a = 1.9 C_{70}: log K_a = 2.6
d)	**e)**	**f)**
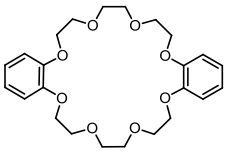	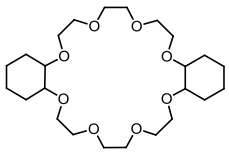	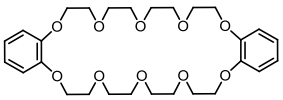
C_{60}: log K_a = 3.8 C_{70}: log K_a = 2.4	C_{60}: log K_a = 2.9 C_{70}: log K_a = 2.6	C_{60}: log K_a = 3.9 C_{70}: log K_a = 2.4
a-d), f) (rt, CCl_4, ^{1}H-NMR) Mukherjee and co. *J. Phys. Chem. B*, **2003**, 4213	e) (rt, CCl_4, UV-vis) Mukherjee and co. *J. Phys. Chem. B*, **2003**, 1189	

As seen from experimental data, only crown ethers **d)** and **f)** exhibit a binding constant large enough (>10^3) to suggest inclusion of fullerenes. Their higher affinity for C_{60} can be due to the crown ether cavity size, too small to include C_{70}.

Crown ether **e)**, the saturated analogue of molecule **d)**, exhibits a lower K_a, most likely due to its higher flexibility leading to a decrease in the cavity size and the absence of additional π-π interactions between the benzene rings and the fullerenes.

Due to their small size, interaction of crown ethers **a)** and **b)** with fullerenes has been proposed to occur through the benzene ring of the crowns.

The preference of electron deficient molecule **b)** for C_{70} may be due to the irregular electronic distribution in this fullerene, which makes their poles more polar than C_{60}.

[36] a) S. Bhattacharya, A. Sharma, S. K. Nayak, S. Chattopadhyay and A. K. Mukherjee, *J. Phys. Chem. B* **2003**, *107*, 4213; b) A. Saha, S. K. Nayak, S. Chottopadhyay and A. K. Mukherjee, *J. Phys. Chem. B* **2003**, *107*, 11889.

Taking into account that transition metals bind stronger to selena and aza-crown ethers than to crown ethers and considering Yoshida's work, which assimilates C_{60} to a 'superatom' analogous to a transition metal,[37] Liu designed a series of seleno and aza-crown ethers and studied their affinity towards C_{60}[38] (Table 2.5)

Table 2.5. Thermodynamic properties of a series of 1:1 C_{60}•aza/selenacrown ether complexes.

	a)	b)	c)	d)
	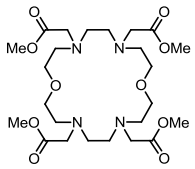	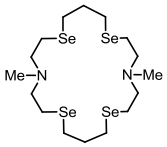	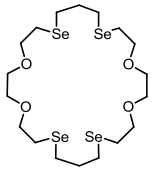	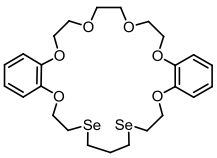
Binding constant	log K_a = 3.1	log K_a = 3.3	log K_a = 3.2	log K_a = 3.2
Cavity size (Å)	—	7.8 x 7.4	7.2 x 7.3	7.8 x 7.6
ΔG^0 *(kJ·mol^{-1})*	-17.9	-18.9	-18.1	-18.0
ΔH^0 *(kJ·mol^{-1})*	-32.5	-70.6	-32.1	-90.7
$T\Delta S^0$ *(kJ·mol^{-1})*	-14.6	-51.7	-14.0	-72.7

(rt, CCl_4, UV-vis)
Liu and co.
J. Inclusion Phenom. Macrocyclic Chem., **2005**, 191

The influence of Se remains unclear if we compare these results with the previous. Whereas K_a with molecule **b)** is larger than with structural related **T.2.4.c)**, affinity for **d)** is lower than for **T.2.4.d)**. Indeed, the key factor seems to be the cavity size. Molecules **b)** and **c)**, both with 4 Se atoms led to different binding constants while the large size of **d)** may compensate having less Se atoms.

Even though systems **b)** and **d)** showed the largest enthalpic gains, probably due to stronger n-π and/or π-π interactions, there is no direct correlation with the K_a due to the entropic factors. The larger $T\Delta S^0$ of molecule **d)** in comparison to **c)** suggests larger conformational changes due to π-π interactions with the aromatic rings.

[37] Y. Yamaguchi and Z.-I. Yoshida, *Chem. Eur. J.* **2003**, *9*, 5430.
[38] Y. Liu, J.-R. Han, Y.-L. Zhao, H.-Y. Zhang and Z.-Y. Duan, *J. Inclusion Phenom. Macrocyclic Chem.* **2005**, *51*, 191.

2.5. PORPHYRINS

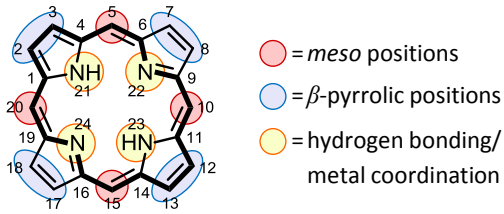

Figure 2.19. Porphyrin structure with its aromatic ring (bold) and numbering.

Porphyrins are 18 π-electron aromatic macrocycles composed of a tetra pyrrolic core with three different positions for functionalization. Two of them on the periphery, the *meso* and *β*-pyrrolic positions, and a third in the inner NH positions, where it is possible to coordinate a metal cation (Figure 2.19).[39] Porphyrins have been extensively used as the donor moiety in D-A systems due to the following properties:

Strong UV absorption bands. The typical UV-vis absorption profile presents a strong band at 380-420 nm (log ε around 5-6), named the Soret band, arising from π-π* transitions from the ground state to the second excited singlet state, and a series of less intense bands in the 480-700 nm, named the Q band, arising from π-π* transitions from the ground state to the first excited singlet state. Free base porphyrin presents 4 Q bands, whereas metalated porphyrins only have 2 due to their higher symmetry[39] (Figure 2.20).

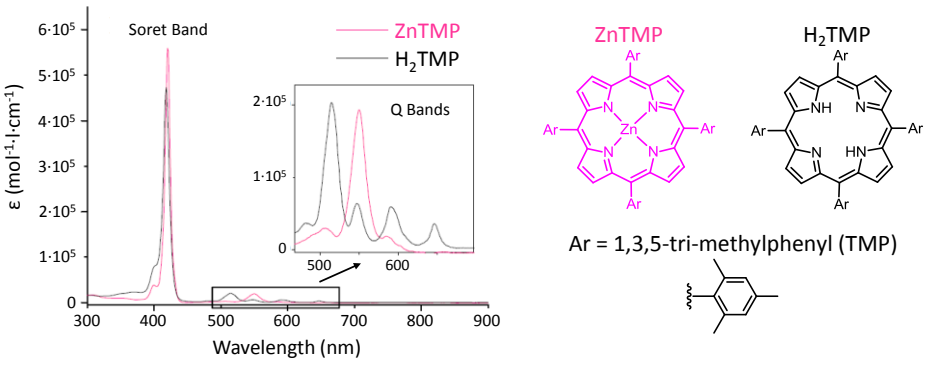

Figure 2.20. UV-vis spectra of H_2TMP and ZnTMP in DCM at rt.

[39] J. L. Sessler, E. Karnas and E. Sedenberg, in *Supramol. Chem.* (Eds.: J. W. Steed and P. A. Gale), John Wiley & Sons, Ltd, **2012**.

Tunable oxidation potential. By changing its substituents[40a] or the central metal[35b] it is possible to modify the oxidation potential of porphyrins in a large range (>0.5 V) to obtain cationic and dicationic species.

Long lived singlet excited state, in the range of nanoseconds.[41]

2.5.1. *Synthesis of porphyrins*

Table 2.6. Types of *meso*-substituted porphyrins.

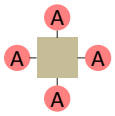	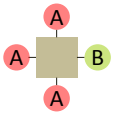	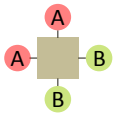	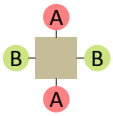	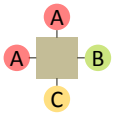	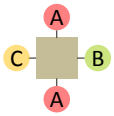	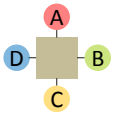
A_4	A_3B	*cis*-A_2B_2	*trans*-A_2B_2	*cis*-A_2BC	*trans*-A_2BC	ABCD

In sharp contrast with naturally occurring porphyrins, which bear substituents in almost all β-positions, synthetic porphyrins are most often modified only in the *meso* positions due to their "easier" synthesis. Regardless this limitation, their structural variety can be very rich (Table 2.6).

In principle, there are three different synthetic approaches to synthesize the seven types of *meso*-substituted porphyrins as depicted in Scheme 2.5:

a) Mixed condensation.
b) Total synthesis.
c) Functionalization of already preformed systems.

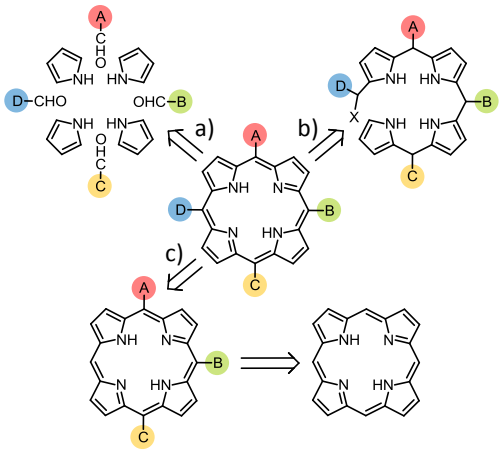

Scheme 2.5. Available routes for *meso*-porphyrins.

[40] a) S. I. Yang, J. Seth, J.-P. Strachan, S. Gentemann, D. Kim, D. Holten, J. S. Lindsey and D. F. Bocian, *J. Porphyrins Phthalocyanines* **1999**, *3*, 117; b) J. H. Fuhrhop and D. Mauzerall, *J. Am. Chem. Soc.* **1969**, *91*, 4174.
[41] a) S. Tobita, Y. Kaizu, H. Kobayashi and I. Tanaka, *J. Chem. Phys.* **1984**, *81*, 2962; b) R. A. Reed, R. Purrello, K. Prendergast and T. G. Spiro, *J. Phys. Chem.* **1991**, *95*, 9720; c) A. Harriman, G. Porter and N. Searle, *J. Chem. Soc., Faraday Trans. 2* **1979**, *75*, 1515.

a) Mixed condensations

Consist in the statistical condensation of aldehydes and pyrrole to yield a mixture of various isomers which are subsequently separated by laborious purification. There are two main methodologies, widely used for obtaining A_4 porphyrins:

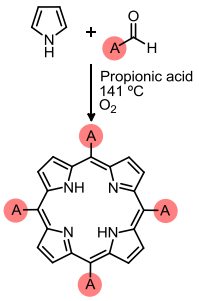

Scheme 2.6.
Adler-Longo method.

The first one was developed by Adler and Longo in 1967.[42] It consists in heating to reflux a mixture of the starting materials in propionic acid under an open atmosphere (atmospheric oxygen is used as oxidant) and subsequent purification by precipitation from the acidic media (Scheme 2.6).

The harsh conditions of this method limit the number of aldehydes that can be used as starting materials.

A milder alternative was developed by Lindsey In the early 1980s. It was a two-step, one-flask route based in 1) the acid catalyzed condensation of starting materials to form a porphyrinogen in a reversible equilibria and 2) its irreversible $6e^-/6H^+$ oxidative dehydrogenation with a soluble oxidant, leading to the desired porphyrin[43] (Scheme 2.7). Experimental conditions involve using $CHCl_3$ or DCM as solvent, TFA or $BF_3{\cdot}OEt_2$ as catalyst, *p*-chloranil or DDQ as oxidant and an inert atmosphere. In order to obtain an appropriate cyclization/polymerization balance concentration of reactants must be around 10^{-2} M.

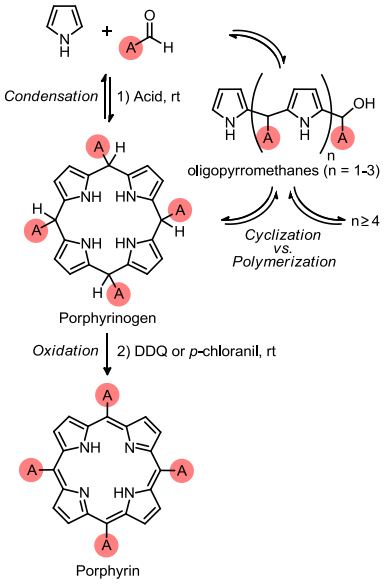

Scheme 2.7.
Lindsey method.

[42] A. D. Adler, F. R. Longo, J. D. Finarelli, J. Goldmacher, J. Assour and L. Korsakoff, *J. Org. Chem.* **1967**, *32*, 476.
[43] a) J. S. Lindsey, H. C. Hsu and I. C. Schreiman, *Tetrahedron Lett.* **1986**, *27*, 4969; b) J. S. Lindsey, I. C. Schreiman, H. C. Hsu, P. C. Kearney and A. M. Marguerettaz, *J. Org. Chem.* **1987**, *52*, 827.

Lindsey's methodology has also been used to obtain A_3B porphyrins, upon statistical condensation of pyrrole with two different aldehydes in a 4:3:1 ratio. The reaction crude yields all the seven possible regioisomers from where the product is obtained in small quantities (typically < 100 mg) after tedious purifications[44] (Scheme 2.8).

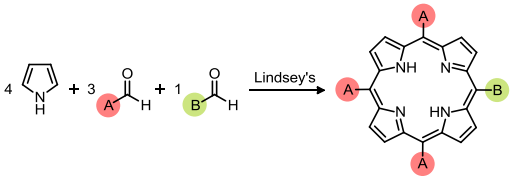

Scheme 2.8. Synthesis of A_3B porphyrin by Lindsey's methodology.

Substitution of pyrrole by a dipyrromethane enables obtaining *trans*-A_2B_2 (Scheme 2.9) and *trans*-A_2BC (Scheme 2.10) porphyrins. However, dipyrromethanes can be rather labile in acidic media, leading to a lot of scrambling (fragmentation followed by an alternate recombination) and, therefore, to a mixture of porphyrins. This can be avoided by using sterically hindered dipyrromethanes.[44]

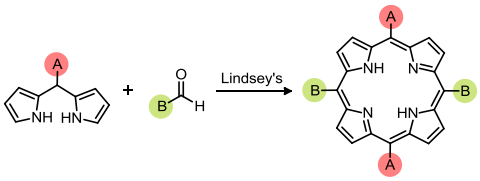

Scheme 2.9. Synthesis of *trans*-A_2B_2 porphyrins by Lindsey's methodology.

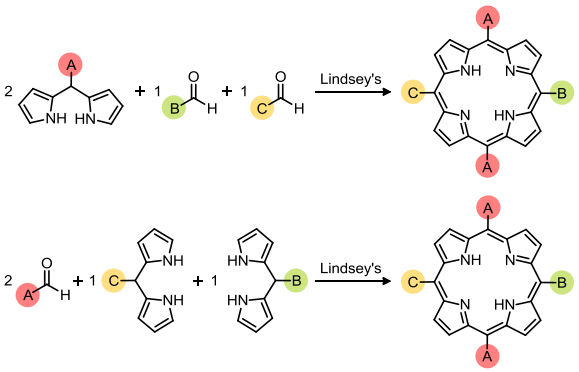

Scheme 2.10. Synthesis of *trans*-A_2BC porphyrins by Lindsey's methodology.

[44] P. D. Rao, S. Dhanalekshmi, B. J. Littler and J. S. Lindsey, *J. Org. Chem.* **2000**, *65*, 7323.

b) Total synthesis

This is the most comprehensive –and synthetic demanding– route, enabling, in principle, obtaining any type of *meso*-porphyrin in a stepwise manner.[44],[45]

Scheme 2.11 is a representative example of this strategy, where the key reactions are 1) the synthesis of an appropriate carbinol, 2) its condensation with a dipyrromethane to obtain a bilane and 3) its intramolecular cyclization to form the porphyrinogen which will be subsequently oxidized into the porphyrin. As with any polypyrromethane, acid scrambling may happen, leading to undesired products.

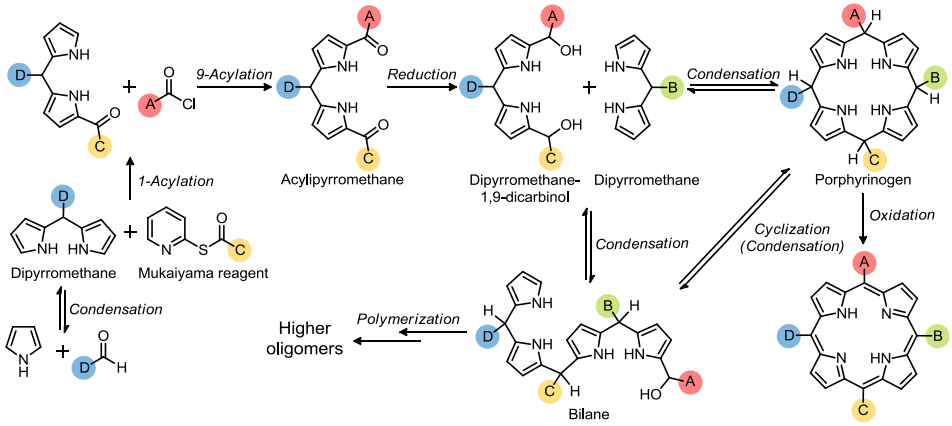

Scheme 2.11. Example of a stepwise synthesis of an ABCD porphyrin.

c) Functionalization of already preformed systems

This route is based on the capacity of porphyrins to participate into electrophilic substitution reactions due to their large degenerated electronic density.[46] A wise selection of the synthetic route can lead to any regioisomer by:

- "Classic" functionalization reactions: formylation, halogenation, nitration…
- Nucleophilic addition of Grignard or organolithium reagents.
- Cross-coupling reactions with organometallics.

[45] J. S. Lindsey, *Acc. Chem. Res.* **2009**, *43*, 300.
[46] a) M. O. Senge, *Chem. Commun.* **2011**, *47*, 1943; b) B. M. J. M. Suijkerbuijk and R. J. M. Klein Gebbink, *Angew. Chem. Int. Ed.* **2008**, *47*, 7396.

d) Directly linked porphyrin arrays

Conjugated porphyrin arrays present special properties such as red-shifted absorption bands, large non-linear optical properties and large π-electron delocalization.[47]

***Meso-meso* singly linked porphyrin arrays** are easily obtained by the Ag^{I} oxidative coupling reaction of metalloporphyrins [M = Zn(II), Mg(II)] with a free *meso* position. The array thus obtained presents high regioselectivity, a rodlike shape, high solubility due to their orthogonal conformations avoiding π-π stacking, easy separation by GPC and two free *meso* positions available for further modification.[48]

The proposed mechanism for this reaction is based in the initial one-electron oxidation of a porphyrin unit by $AgPF_6$ followed by the nucleophilic attack of a neutral porphyrin molecule and its subsequent dehydrogenation.[48] This mechanism is supported by the fact that the coupling reaction is accelerated by addition of I_2, which produces more powerful oxidizing species,[48] and that the same coupling is obtained either by anodic electrochemical oxidation[49] or in the presence of other chemical oxidants such as DDQ, $I_2/AgCO_2CF_3$, $Te(CO_2CF_3)_3$ or PIFA.[50]

The regioselectivity of this reaction can be explained in terms of the HOMO symmetry of the radical cation formed in the process[51] (Scheme 2.12).

- Cu(II), Ni(II), Pd(II) and free base porphyrins favor the a_{1u} HOMO, where the *meso*-carbons become four nodes and the electron density is placed at the β positions. As a result, *meso*-β directly linked bisporphyrins are obtained.
- Zn(II) and Mg(II) porphyrins favor the a_{2u} HOMO, with the electron density centered in the *meso* positions, thus leading to the *meso*-*meso* linked dimer.

[47] a) A. Tsuda and A. Osuka, *Adv. Mater.* **2002**, *14*, 75; b) A. Naoki and O. Atsuhiro, *Chem. Rec.* **2003**, *3*, 225.
[48] A. Osuka and H. Shimidzu, *Angew. Chem. Int. Ed.* **1997**, *36*, 135.
[49] T. Ogawa, Y. Nishimoto, N. Ono, N. Yoshida and A. Osuka, *Chem. Commun.* **1998**, 337.
[50] a) X. Shi and L. S. Liebeskind, *J. Org. Chem.* **2000**, *65*, 1665; b) J. Wojaczyński, L. Latos-Grażyński, P. J. Chmielewski, P. Van Calcar and A. L. Balch, *Inorg. Chem.* **1999**, *38*, 3040; c) L.-M. Jin, L. Chen, J.-J. Yin, C.-C. Guo and Q.-Y. Chen, *Eur. J. Org. Chem.* **2005**, *2005*, 3994.
[51] T. Ogawa, Y. Nishimoto, N. Yoshida, N. Ono and A. Osuka, *Angew. Chem. Int. Ed.* **1999**, *38*, 176.

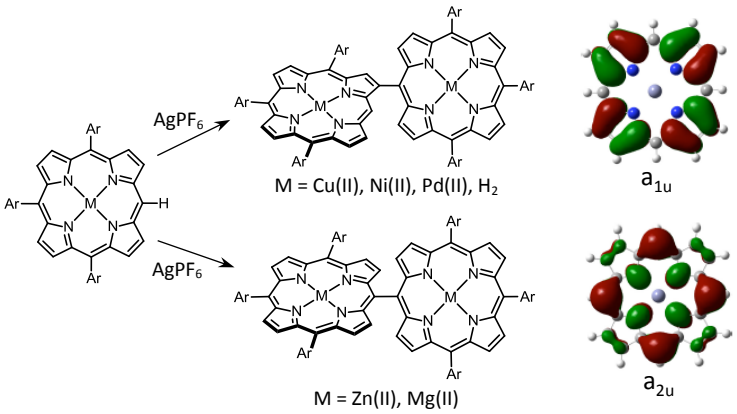

Scheme 2.12. Regioselectivity of the coupling reaction can be explained in terms of the MOs stabilized by the metalloporphyrin.

The absorption spectra of these systems show that the porphyrin subunits in the array retain the individual monomeric porphyrin character, whereas the large splitting of the Soret bands is due to strong exciton coupling.[52]

***Meso-meso*, *β-β*, *β-β* triply linked porphyrin arrays** are obtained by Sc(III)-catalyzed oxidation of a free *meso* position metalloporphyrin or *meso-meso*-linked Zn(II) porphyrin array with DDQ in high yields (Scheme 2.13). The resulting array has planar tape-shaped structure and extensive electronic conjugation, as shown by the significant red shift of the Q bands, reaching into the IR frequency (700-1200 nm).[53]

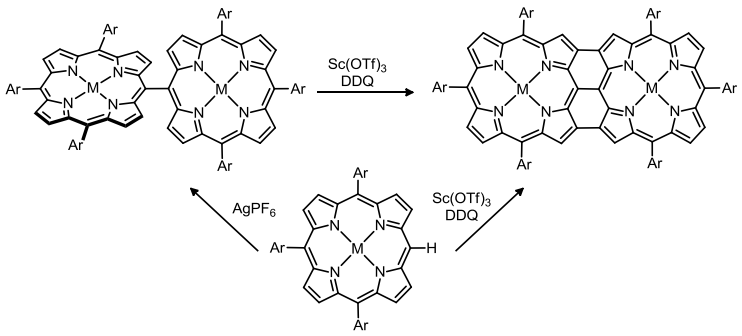

Scheme 2.13. *Meso-meso*, *β-β*, *β-β* triply linked porphyrin arrays.

[52] Y. H. Kim, D. H. Jeong, D. Kim, S. C. Jeoung, H. S. Cho, S. K. Kim, N. Aratani and A. Osuka, *J. Am. Chem. Soc.* **2001**, *123*, 76.
[53] a) A. Tsuda and A. Osuka, *Science* **2001**, *293*, 79; b) S. Hiroto and A. Osuka, *J. Org. Chem.* **2005**, *70*, 4054.

2.5.2. Supramolecular porphyrin•fullerene complexes

Owing to the properties of fullerenes and porphyrins, it is evident the interest of combining these molecules in D-A systems. Whereas this has been done extensively in covalent systems, less research has been done, however, in non-covalent assemblies. A non-comprehensive overview of supramolecular discrete host-guest systems, based in their constituent interactions, follows:

a) π-π interactions

The mutual porphyrin-fullerene attraction was first evidenced in the crystal structure of a fulleropyrrolidine-porphyrin dyad,[54] where the intermolecular distances (2.75 Å) were found to be shorter than typical π-π distances (3.0-3.5 Å) (Figure 2.21).[55]

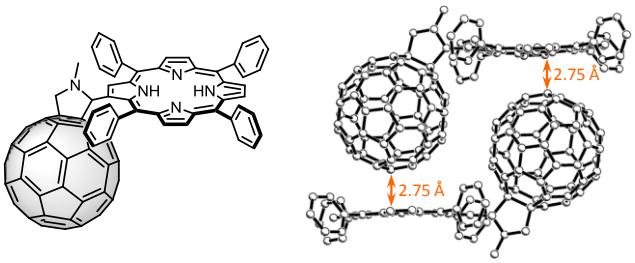

Boyd, Reed and co.
J. Org Chem., **1997**

Figure 2.21. The short porphyrin–C_{60} distance suggested a mutual attraction of both molecules.

Crystal structures of pristine C_{60} with different metallooctaethylporphyrins[56] and tetraphenylporphyrins[57] proved soon the ubiquity of this interaction. NMR studies in PhMe demonstrated that this interaction persisted in solution, as evidenced by the upfield shift of the porphyrin inner N-H pyrrolic protons and fullerene carbon signals.

[54] Y. Sun, T. Drovetskaya, R. D. Bolskar, R. Bau, P. D. W. Boyd and C. A. Reed, *J. Org. Chem.* **1997**, *62*, 3642.
[55] D. R. Evans, N. L. P. Fackler, Z. Xie, C. E. F. Rickard, P. D. W. Boyd and C. A. Reed, *J. Am. Chem. Soc.* **1999**, *121*, 8466.
[56] M. M. Olmstead, D. A. Costa, K. Maitra, B. C. Noll, S. L. Phillips, P. M. Van Calcar and A. L. Balch, *J. Am. Chem. Soc.* **1999**, *121*, 7090.
[57] P. D. W. Boyd, M. C. Hodgson, C. E. F. Rickard, A. G. Oliver, L. Chaker, P. J. Brothers, R. D. Bolskar, F. S. Tham and C. A. Reed, *J. Am. Chem. Soc.* **1999**, *121*, 10487.

This new supramolecular tool came as a surprise as it challenged the traditionally belief that curved guest required curved hosts for effective complexation.[58]

Analysis of the crystallographic data obtained from different C_{60}•porphyrin complexes revealed that in most cases an electron rich 6:6 bond lied centered over the metal of a metalloporphyrin or the protic center of a free base porphyrin. When complexation was accomplished in the presence of C_{70}, the closest atoms were those corresponding to the intersection of three fused six-membered rings (Figure 2.22).

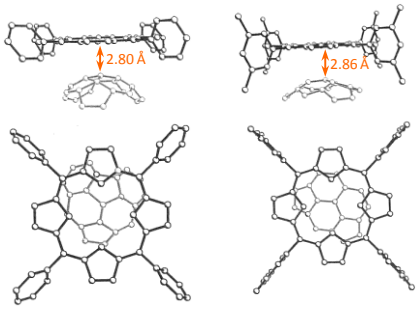

Figure 2.22. Fullerene-porphyrin plane orientation. Left: H_2TPP•C_{60}. Right: $H_2T_{3,5\text{-dimethyl}}PP$•$C_{70}$.

These conformations are those ones offering the greatest contact area and correspond to the most electron rich area of the fullerene, thus pointing to van der Waals forces. The controlled position of the fullerene, over the center of the porphyrin suggests an additional electrostatic component.[57]

However, the nature of this interaction remains controversial. As the center of a porphyrin or metalloporphyrin is electron deficient compared to a fullerene double bond, this would mean that a fullerene (an acceptor) is donating electron density to a porphyrin (a donor).

This counterintuitive conclusion may be rationalized if we consider the fullerene at the specific level of the double bond rather than at the global one.[59]

[58] E. M. Pérez and N. Martín, *Chem. Soc. Rev.* **2008**, *37*, 1512.
[59] P. D. W. Boyd and C. A. Reed, *Acc. Chem. Res.* **2004**, *38*, 235.

In solution, π-π interactions are so weak that it is rare to find examples of discrete host-guest complexes relying only on direct π-π interactions and involving just a single porphyrin unit and a fullerene.

An exception is the phenylene-based dendritic porphyrin of Figure 2.23, whose interior cavity is believed to enable the complexation of fullerene with a moderate binding constant.[60]

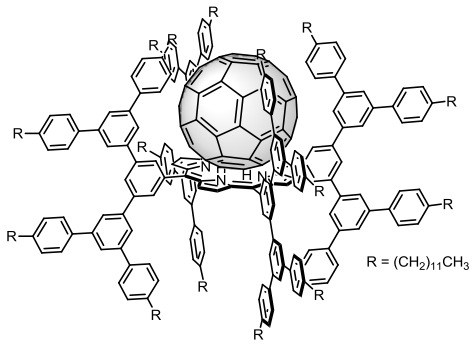

log K_a =4.4 (rt, PhMe, UV-vis)
Kimura, Shirai and co.
J. Am. Chem. Soc., **2002**

Figure 2.23. Example of host-guest system relying on π-π interactions.

In order to overcome this limitation, chemists have resorted to chelation and designed new hosts combining various porphyrin units together. Considering the van der Waals diameter of C_{60} fullerene (10 Å),[27a] a minimum porphyrin-porphyrin distance of around 12 Å is required for such a system (Figure 2.24).

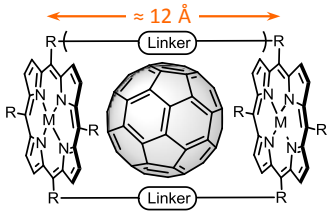

Figure 2.24. Distance between porphyrins should be around 12 Å.

In this regard, multiple porphyrin units have been combined both in an open manner, as in the Reed and Boyd jaws porphyrin where $PdCl_2$[61] and calixarene[62] are used as

[60] M. Kimura, Y. Saito, K. Ohta, K. Hanabusa, H. Shirai and N. Kobayashi, *J. Am. Chem. Soc.* **2002**, *124*, 5274.
[61] a) D. Sun, F. S. Tham, C. A. Reed, L. Chaker, M. Burgess and P. D. W. Boyd, *J. Am. Chem. Soc.* **2000**, *122*, 10704; b) D. Sun, F. S. Tham, C. A. Reed, L. Chaker and P. D. W. Boyd, *J. Am. Chem. Soc.* **2002**, *124*, 6604.

linkers [molecules **b)** and **c)** respectively], and in a cyclic manner such as the porphyrin sandwiches designed by Aida[63] [molecule **a)**], Anderson's trimer[64] [molecule **d)**], Osuka's nanobarrel[65] [molecule **e)**] or Nitschke's cubic cage[66] [molecule **f)**] (Figure 2.25).

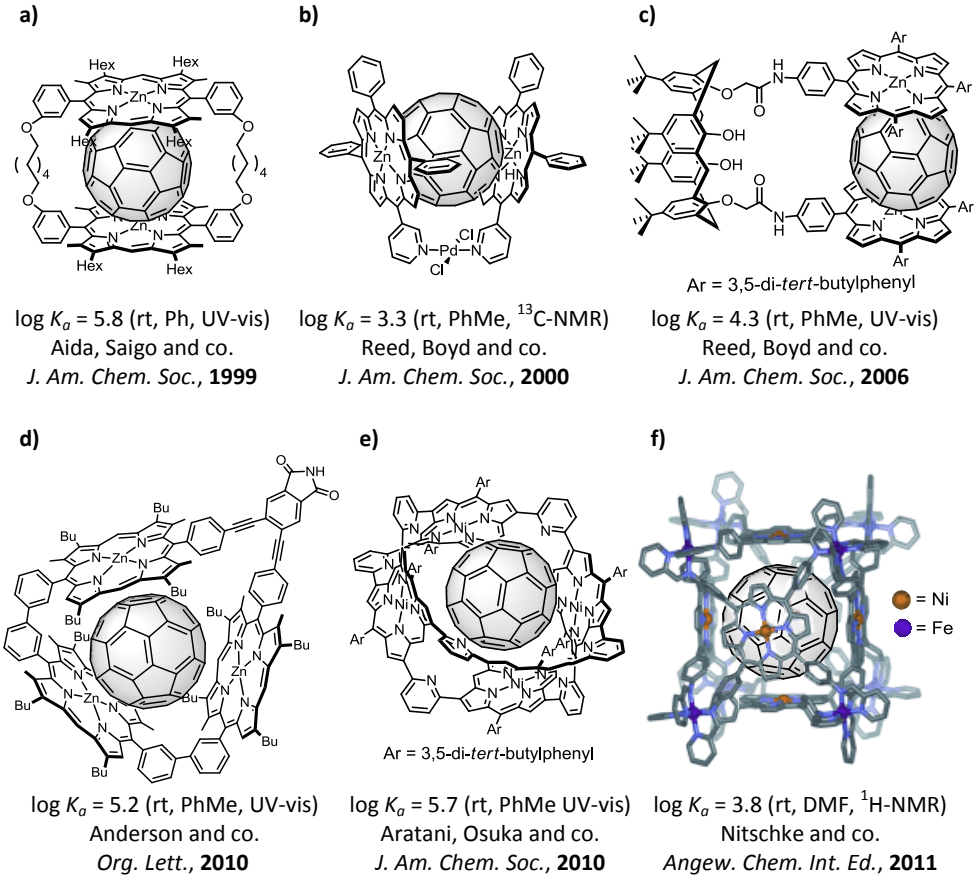

Figure 2.25. Representative examples of porphyrin•C_{60} systems based in π-π interactions.

[62] A. Hosseini, S. Taylor, G. Accorsi, N. Armaroli, C. A. Reed and P. D. W. Boyd, *J. Am. Chem. Soc.* **2006**, *128*, 15903.
[63] a) K. Tashiro, T. Aida, J.-Y. Zheng, K. Kinbara, K. Saigo, S. Sakamoto and K. Yamaguchi, *J. Am. Chem. Soc.* **1999**, *121*, 9477; b) J.-Y. Zheng, K. Tashiro, Y. Hirabayashi, K. Kinbara, K. Saigo, T. Aida, S. Sakamoto and K. Yamaguchi, *Angew. Chem. Int. Ed.* **2001**, *40*, 1857.
[64] G. Gil-Ramírez, S. D. Karlen, A. Shundo, K. Porfyrakis, Y. Ito, G. A. D. Briggs, J. J. L. Morton and H. L. Anderson, *Org. Lett.* **2010**, *12*, 3544.
[65] J. Song, N. Aratani, H. Shinokubo and A. Osuka, *J. Am. Chem. Soc.* **2010**, *132*, 16356.
[66] W. Meng, B. Breiner, K. Rissanen, J. D. Thoburn, J. K. Clegg and J. R. Nitschke, *Angew. Chem. Int. Ed.* **2011**, *50*, 3479.

Systems **a)**, **b)** and **c)** were used to study the role of metals in the complexation. Given the proposed electrostatic nature of this phenomenon, changing the metal atom should have an impact in the stability constant of the final complexes (Figure 2.26).

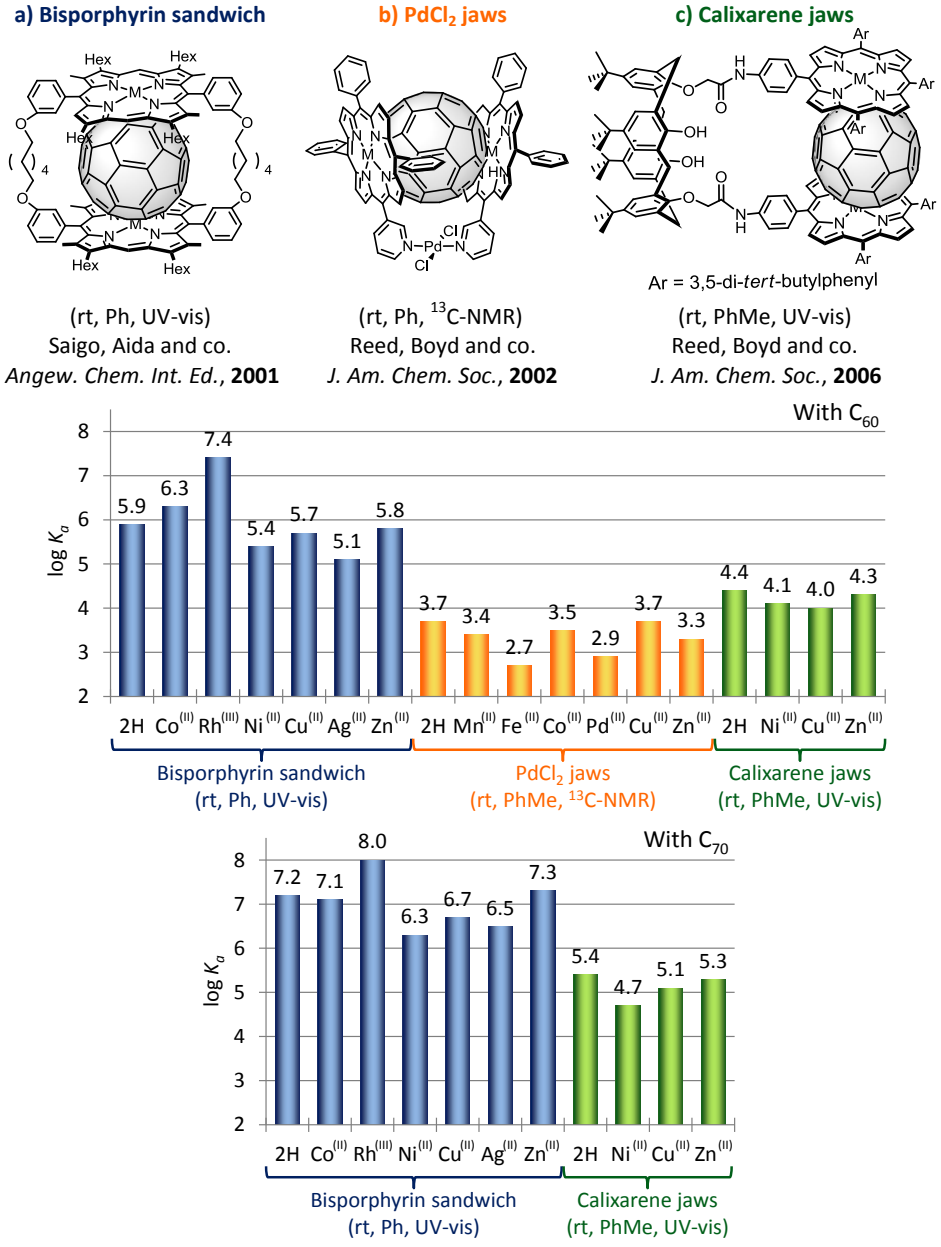

Figure 2.26. Influence of metals in the binding constants K_a values of [60]fullerene (up) and [70]fullerene (down) with different hosts.

The analysis of the experimental data collected did not enable a full interpretation of the impact of metalation. Despite this, some general conclusions can be obtained:

- Bisporphyrins sandwiches exhibit a greater affinity towards fullerenes than $PdCl_2$ and calixarene jaws. This can be due to their greater preorganization.
- Binding constants for C_{70} are around one order of magnitude larger than for C_{60}. This can be a result of the larger π surface available for complexation.[63b]
- The order of binding constants for C_{60} and C_{70} exhibits subtle differences which may be due to differences in solvation energies.[61b]
- Free base porphyrins bind fullerenes with a similar strength than Zn(II) porphyrins and are among the strongest. If porphyrin-fullerene interactions were due only to van der Waals forces, the binding should become larger the richer on electrons the metal of the porphyrin. This result, however, points to the existence of an electrostatic attraction between an electron rich 6:6 double bond of the fullerene and the center of a free base porphyrin.[61b]
- RhMe porphyrin exhibits the largest K_a of the series. This behavior has been rationalized on the capacity of Rh complexes to form fullerene adducts and has also been observed with Ir. Actually, an Ir(III)Me porphyrin (not included in Figure 2.26) holds the world-record in "complex" stability for C_{60} ($\log K_a = 8.1$ in *o*DCB).[67] This phenomenon can also account in a minor extent for the large strength of Co porphyrin complexes.

In all the cases UV-vis titration experiments showed a decrease and a red shift of the porphyrin Soret (Q) band upon addition of fullerene, implying a less energetic π to π* transition from a charge transfer process. This phenomenon has also been observed in covalent dyads and is widely used as a proof of π-π interaction.[62-63]

To sum up, it can be stated that the porphyrin-fullerene mutual attraction arises from a combination of van der Waals interactions with small effects stemming from differences in solvation, electrostatic, coordinate bond formation and charge transfer.

[67] M. Yanagisawa, K. Tashiro, M. Yamasaki and T. Aida, *J. Am. Chem. Soc.* **2007**, *129*, 11912.

b) Metal-ligand interaction

Metal-ligand interactions, based in a Lewis acid-base reaction, are the second most common way to form porphyrin▪fullerene supramolecular dyads. Most of these systems use nitrogen ligands, such as pyridine and imidazole, due to their capacity to form stable dyads with zinc porphyrins. Coordination with imidazole is around one order of magnitude stronger than with pyridine, demonstrating that the electron donor capacity (basicity) of the ligand determines the stability of the complex.[68]

The first examples using pyridine as a ligand were developed in 1999 by Diederich[69a] and D'Souza.[69b] The use of imidazole derivatives allowed the synthesis of the first supramolecular model of the photosynthetic antenna-reaction center (Figure 2.27). The latter system presented an efficient energy transfer (k_{ENT} = 9.2 x 10^9 s^{-1}; ϕ_{ENT} = 0.8) after selective excitation of the boron dipyrrin moiety, creating a singlet excited zinc porphyrin state which is able to produce a subsequent efficient electron transfer to the fullerene (k_{ET} = 4.7 x 10^9 s^{-1}; ϕ_{ET} = 0.9), resulting in a charge-separated state.[70]

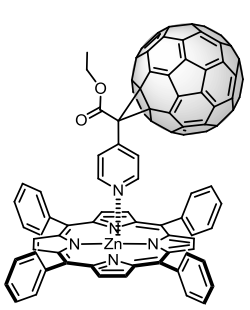

log K_a = 3.5 (rt, PhMe, Fluorescence)
Armaroli, Diederich, Echegoyen and co.
New J. Chem., **1999**

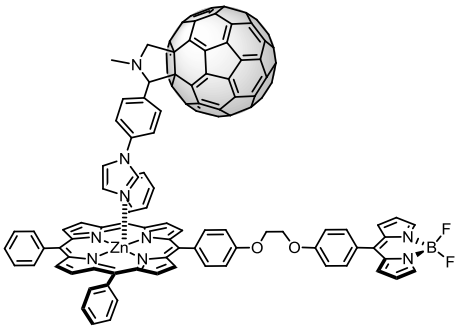

log K_a = 4.2 (rt, *o*DCB, UV-vis)
D'Souza, Ito and co.
J. Am. Chem. Soc., **2004**

Figure 2.27. Examples of fullerene-porphyrin dyads linked through nitrogen ligands.

[68] A. Satake and Y. Kobuke, *Tetrahedron* **2005**, *61*, 13.
[69] a) N. Armaroli, F. Diederich, L. Echegoyen, T. Habicher, L. Flamigni, G. Marconi and J.-F. Nierengarten, *New J. Chem.* **1999**, *23*, 77; b) F. D'Souza, G. R. Deviprasad, M. S. Rahman and J.-P. Choi, *Inorg. Chem.* **1999**, *38*, 2157.
[70] F. D'Souza, P. M. Smith, M. E. Zandler, A. L. McCarty, M. Itou, Y. Araki and O. Ito, *J. Am. Chem. Soc.* **2004**, *126*, 7898.

Supramolecular systems based in this interaction tend to exhibit moderate binding constants (log K_a = 3-4). However, a careful design of the system can increase this value. For example, system $L^2Zn{\bullet}C_{60}BiPy$ exhibits a large increase in the binding constant in comparison with systems $L^1Zn{\bullet}Py$, $L^1Zn{\bullet}C_{60}Py$ or $L^1Zn{\bullet}(Py)_2$ by means of the so called "supramolecular click chemistry" approach, based in the chelate effect (Table 2.7).[71]

Table 2.7. Supramolecular complexes obtained by supramolecular "*click chemistry*".

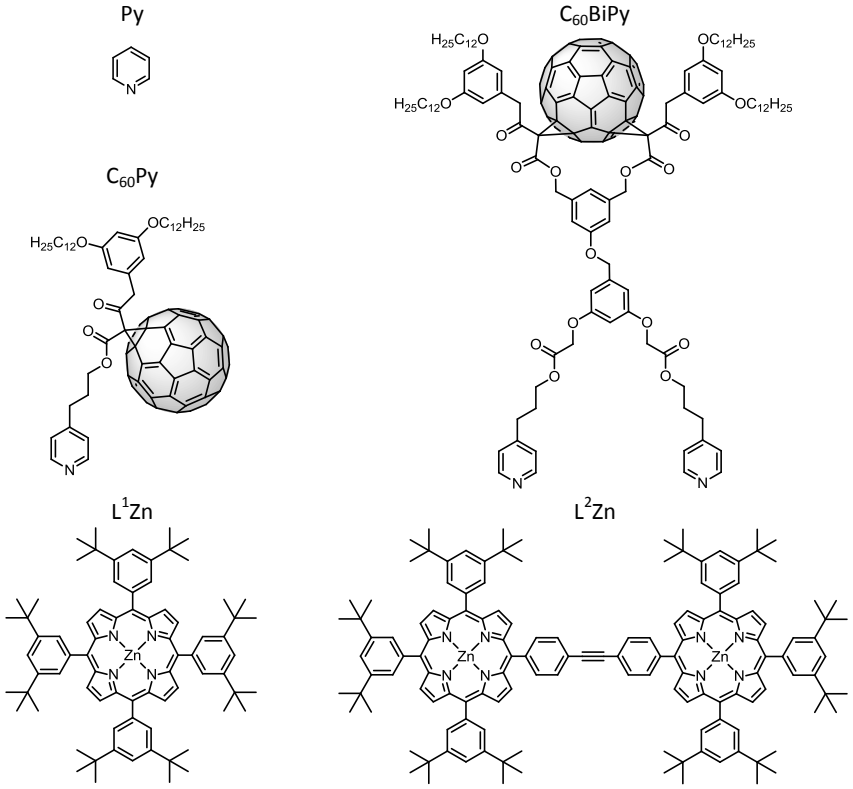

$L^1Zn{\bullet}Py$: log K_a = 3.6	$L^1Zn{\bullet}(Py)_2$: log K_{a1} = 4.0; log K_{a2} = 3.4
$L^1Zn{\bullet}C_{60}Py$: log K_a = 3.5	$L^2Zn{\bullet}C_{60}BiPy$: log K_a = 5.1

(rt, DCM, UV-vis)
Solladié, Nierengarten, Albrecht-Gary and co.
Chem. Commun., **2005**

[71] A. Trabolsi, M. Elhabiri, M. Urbani, J. L. Delgado, F. Ajamaa, N. Solladié, A.-M. Albrecht-Gary and J.-F. Nierengarten, *Chem. Commun.* **2005**, 5736.

c) Hydrogen bond

Hydrogen bonds have also been used as a binding motif due to their high directionality, sensitivity and efficiency in electronic communication, which is even larger than that found in comparable σ or π bonds.[72]

A notable example was the dyad developed by Martín, Rebek and Guldi relying on a two-point amidinium-carboxylate interaction (Figure 2.28). This strong interaction favors the linearity of the system producing faster, more efficient and longer lived (≈1 μs) formation of the radical-ion-pair state than in the covalent analogous.[73]

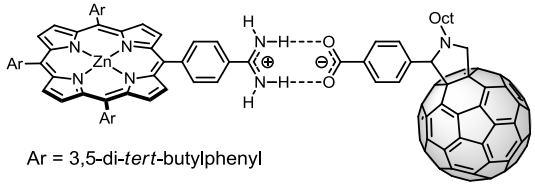

log K_a = 7.3 (rt, PhMe, Fluorescence)
Martín, Rebek, Guldi and co.
Angew. Chem. Int. Ed., **2006**

Figure 2.28. Amidinium-(C_{60})carboxylate dyad.

More recently, the complementarity between Hamilton type receptors[74] and cyanuric acid derivatives (Figure 2.29) has also been employed to self-assemble porphyrins and fullerenes. This six-point binding motif leads to relatively strong binding constants ranging from 10^3 to 10^6 M^{-1} in non-polar solvents such as DCM or PhMe.[75]

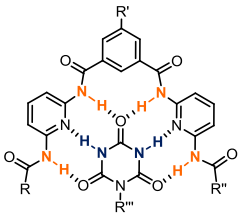

Figure 2.29. Cyanuric acid derivatives and Hamilton-type receptor pattern.

[72] a) J. L. Sessler, B. Wang and A. Harriman, *J. Am. Chem. Soc.* **1993**, *115*, 10418; b) P. de Rege, S. Williams and M. Therien, *Science* **1995**, *269*, 1409.
[73] L. Sánchez, M. Sierra, N. Martín, A. J. Myles, T. J. Dale, J. Rebek, W. Seitz and D. M. Guldi, *Angew. Chem. Int. Ed.* **2006**, *45*, 4637.
[74] S. K. Chang and A. D. Hamilton, *J. Am. Chem. Soc.* **1988**, *110*, 1318.
[75] F. Wessendorf, B. Grimm, D. M. Guldi and A. Hirsch, *J. Am. Chem. Soc.* **2010**, *132*, 10786.

Another recognition pattern involving hydrogen bonds is the ammonium-crown ether complexation. This interaction arises from the attraction between the electronic lone pairs of the heteroatoms in the crown ether and the strongly polarized N^+-H bonds of the ammonium cation. Therefore, its strength decreases in the order primary > secondary > tertiary ammonium ion and is not possible in the absence of hydrogen bonds as in the case of tetramethylammonium.[76]

The selectivity of this interaction can be explained on the basis of the good match between the size of the crown ether cavity (2.60-3.20 Å in [18]C6)[77] and the diameter of the ammonium ion (2.86 Å).[78]

The stability of the fullerene•porphyrin dyads obtained with this strategy is similar to those obtained from pyridine or imidazole fullerene derivatives in metal-ligand interactions. As in the previous case, the nature of the solvents will also have an impact in the binding constant. H-bonding competitive solvents such as DMSO or MeOH will result in weaker complexes and a less favorable conformational change of the crown ether as shown in Figure 2.30.[78]

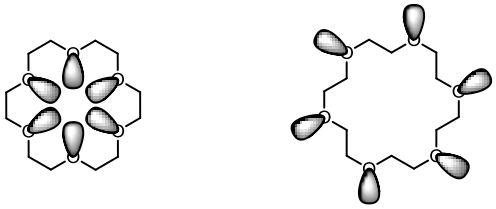

Non-polar solvents Polar solvents

Figure 2.30. Conformational changes of [18]C6 in solvents of different polarity.

A noteworthy example is the photosynthetic reaction center mimic developed by D'Souza where a boron dipyrrin, as energy donor, a Zn porphyrin, as electron donor and a [60]fullerene as electron acceptor are combined together (Figure 2.31).[79]

[76] V. Rüdiger, H.-J. Schneider, V. P. Solov'ev, V. P. Kazachenko and O. A. Raevsky, *Eur. J. Org. Chem.* **1999**, *1999*, 1847.
[77] C. J. Pedersen and H. K. Frensdorff, *Angew. Chem. Int. Ed.* **1972**, *11*, 16.
[78] A. Späth and B. König, *Beilstein J. Org. Chem.* **2010**, *6*, 32.
[79] F. D'Souza, C. A. Wijesinghe, M. E. El-Khouly, J. Hudson, M. Niemi, H. Lemmetyinen, N. V. Tkachenko, M. E. Zandler and S. Fukuzumi, *Phys. Chem. Chem. Phys.* **2011**, *13*, 18168.

The lifetime of the charge-separated state was ≈ 100 μs, the longest ever reported for this type of antenna-reaction center mimics, indicating better charge stabilization as a result of the different disposition of the entities of the supramolecular triad.

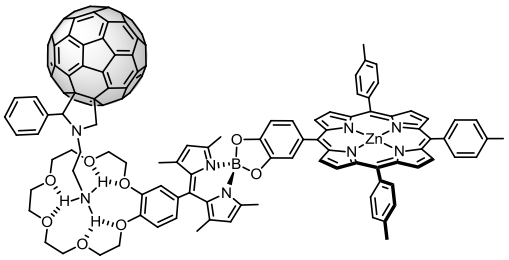

log K_a = 3.3 (rt, PhCN, Fluorescence)
Tkachenko, D'Souza and co.
Phys. Chem. Chem. Phys., **2011**

Figure 2.31. Structure of the boron dipyrrin-zinc porphyrin•fulleropyrrolidine triad.

d) Electrostatic interactions

In spite of its strength, electrostatic interactions have considerably been less exploited. A remarkable example is the 1:1 complex between a dendritic [60]fullerene oligocarboxylate and an octapyridinium zinc porphyrin salt (Figure 2.32). This complex presented a very strong association constant in a phosphate-buffered solution which decreased upon increment of the ionic strength of the media. Transient absorption spectroscopy showed a lifetime of 1.1 μs for the charge-separated state.[80]

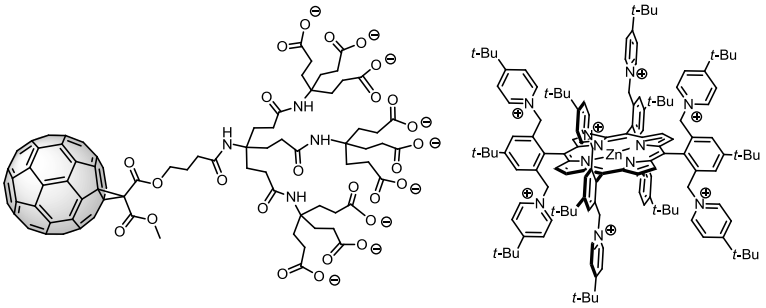

log K_a = 8.5 (rt, H_2O, pH 7.2, Fluorescence)
Guldi, Hirsch, Jux and co.
J. Phys. Chem. B, **2003**

Figure 2.32. Octa-anionic [60]fullerene and octapyridinium zinc porphyrin.

[80] D. Balbinot, S. Atalick, D. M. Guldi, M. Hatzimarinaki, A. Hirsch and N. Jux, *J. Phys. Chem. B* **2003**, *107*, 13273.

e) Mechanical bond

Rotaxane and catenane interlocked systems have also been used to combine porphyrins and fullerenes in a controlled manner.

Takata and Ito mimicked the bacterial photosynthetic center with a donor-acceptor rotaxane rigidified by hydrogen bonding (Figure 2.33). The charge-separated state lifetime obtained for this system was of 0.18 μs.[81]

More rigid systems were reported by Schuster.[82] These systems were synthesized by Sauvage's methodology, consisting in threading a phenantroline strand with a Zn porphyrin stopper through a phenantroline appended C_{60} (Figure 2.33). As a result of the better control of the spatial geometry in these system, the radical ion pair lifetime was 10 times longer (1.17 μs).

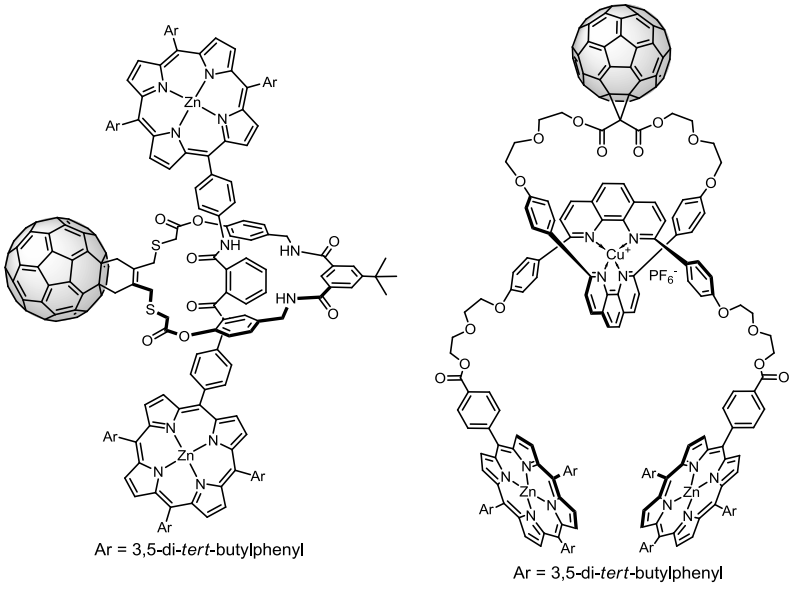

Takata, Ito and co.
Angew. Chem. Int. Ed., **2003**

Schuster and co.
J. Am. Chem. Soc., **2004**

Figure 2.33. Examples of rotaxane type C_{60}•porphyrin dyads.

[81] N. Watanabe, N. Kihara, Y. Furusho, T. Takata, Y. Araki and O. Ito, *Angew. Chem. Int. Ed.* **2003**, *42*, 681.
[82] K. Li, D. I. Schuster, D. M. Guldi, M. Á. Herranz and L. Echegoyen, *J. Am. Chem. Soc.* **2004**, *126*, 3388.

f) Multiple interactions

As a conclusion from the previous examples, the use of single non-covalent interactions may lead to rather weak binding constants and, therefore, relatively unstable complexes where it is difficult to study their properties. A strategy to overcome this drawback is to use multiple interactions, either to preorganize the structure or to include additional recognition motifs.

For example, whereas the supramolecular tweezers developed by Reed and Boyd showed "little evidence of binding" to C_{60},[61b] an analogous structure developed by Li, which presented an additional hydrogen binding motif preorganizing the structure, exhibited a much higher binding constant[83] (Figure 2.34).

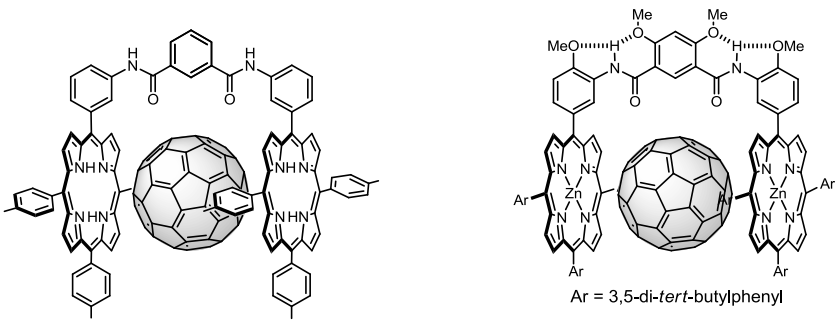

log K_a < 3 (rt, PhMe/$CDCl_3$, ^{1}H-NMR)
Reed, Boyd and co.
J. Am. Chem. Soc., **2002**

log K_a = 4.4 (rt, PhMe, UV-vis)
Li and co.
J. Am. Chem. Soc., **2005**

Figure 2.34. The additional H-bond motif preorganizing the structure leads to higher K_a.

Another system relying on multiple recognition patterns is the ferrocene-porphyrin dyad self-assembled with a supramolecular pyridine developed by D'Souza (Figure 2.35). In this system the ferrocene moiety served both as a primary electron donor and an additional π-π recognition pattern. As a result, the supramolecular pyridine complexes obtained in its presence were 4 times more stable than in its absence.[84]

[83] Z.-Q. Wu, X.-B. Shao, C. Li, J.-L. Hou, K. Wang, X.-K. Jiang and Z.-T. Li, *J. Am. Chem. Soc.* **2005**, *127*, 17460.
[84] F. D'Souza, P. M. Smith, S. Gadde, A. L. McCarty, M. J. Kullman, M. E. Zandler, M. Itou, Y. Araki and O. Ito, *J. Phys. Chem. B* **2004**, *108*, 11333.

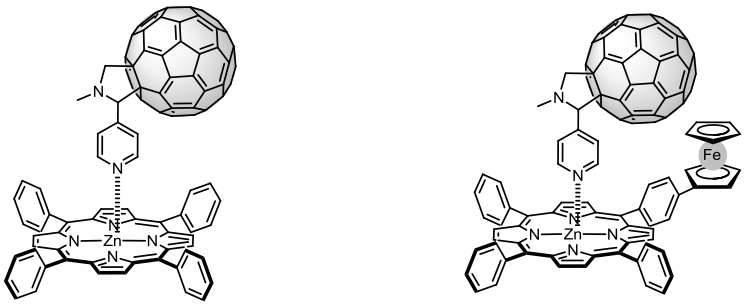

log K_a = 3.8 log K_a = 4.4

(rt, *o*DCB, UV-vis)
D'Souza, Ito and co.
J. Phys. Chem. B., **2004**

Figure 2.35. The ferrocene moiety leads to an increase of K_a due to additional π-π interactions.

This effect has also been observed in polytopic Zn-porphyrin receptors where the presence of the fullerene sub-unit increased 5 times the binding constant in comparison with the complexation with pyridine[85] (Figure 2.36).

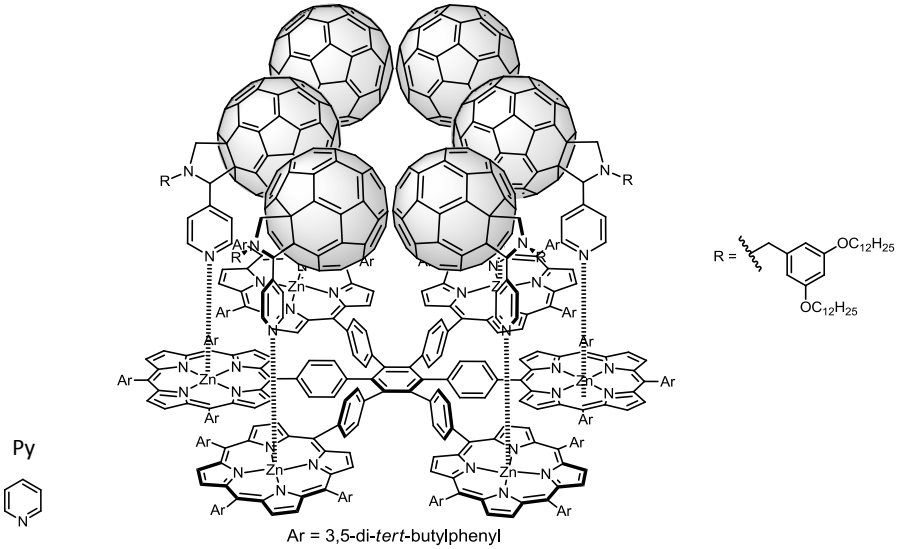

log K_a = 3.7 log K_a = 4.4

(rt, PhMe, UV-vis)
Solladié, Nierengarten, Albrecht-Gary and co.
New J. Chem., **2008**

Figure 2.36. The presence of the fullerene units increases by 5 the stability of the complex.

[85] A. Trabolsi, M. Urbani, J. L. Delgado, F. Ajamaa, M. Elhabiri, N. Solladié, J.-F. Nierengarten and A.-M. Albrecht-Gary, *New J. Chem.* **2008**, *32*, 159.

A remarkable example combining together the ammonium-crown ether interaction and the fullerene-porphyrin π-π stacking was developed in our laboratory in Strasbourg (Figure 2.37).[86]

In contrast to previous examples, based in fullerenes bearing a pyridyl moiety and apically coordinated to the porphyrin, this cup-and-ball C_{60}-porphyrin conjugate enables direct contact between the planar π-surface of the porphyrin and the [60]fullerene sphere. As a result of this additional recognition element, the binding constant was increased by two orders of magnitude in comparison with the complex obtained with [60]fullerene malonate and benzo[18]crown-6.[87]

Studies in the presence of an excess of DBU, which hinders the ammonium-crown ether interaction by deprotonating the ammonium ion, proved this system to function as a molecular switch operated *via* pH.[86]

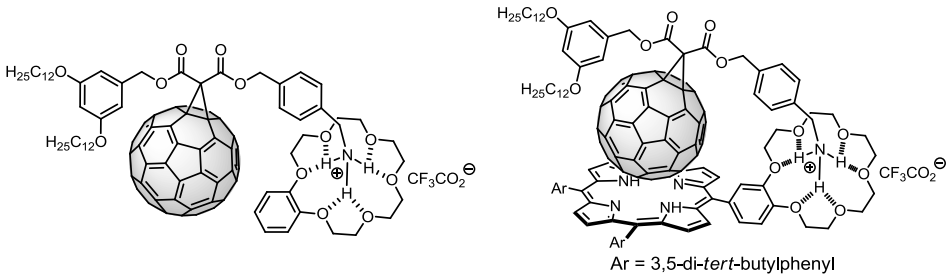

log K_a = 3.3 (rt, $CDCl_3$, ^{1}H-NMR)
Solladié, Van Dorsselaer, Nierengarten and co.
Tetrahedron, **2006**

log K_a = 5.6 (rt, DCM, Fluorescence)
Solladié, Nierengarten and co.
Chem. Commun., **2003**

Figure 2.37. The presence of π-stacking increases K_a by two orders of magnitude.

This strategy has also been successfully used in more complex supramolecular systems where the porphyrin moieties present two *meso* crown ethers in *cis* and *trans* conformations. Effective complexation was evidenced by ^{1}H-NMR and mass spectroscopy.[87]

[86] N. Solladié, M. E. Walther, M. Gross, T. M. F. Duarte, C. Bourgogne and J.-F. Nierengarten, *Chem. Commun.* **2003**, 2412.
[87] N. Solladié, M. E. Walther, H. Herschbach, E. Leize, A. V. Dorsselaer, T. M. F. Duarte and J.-F. Nierengarten, *Tetrahedron* **2006**, *62*, 1979.

Another interesting example involves the fullerene-crown ether and the fullerene-porphyrin complementarity.[88] Even though weak in solution (for example, a control experiment with a free-base porphyrin with no crown ether showed no complexation with C_{60}), these interactions were combined in different cooperative fashions leading to moderately stable complexes (Figure 2.38).

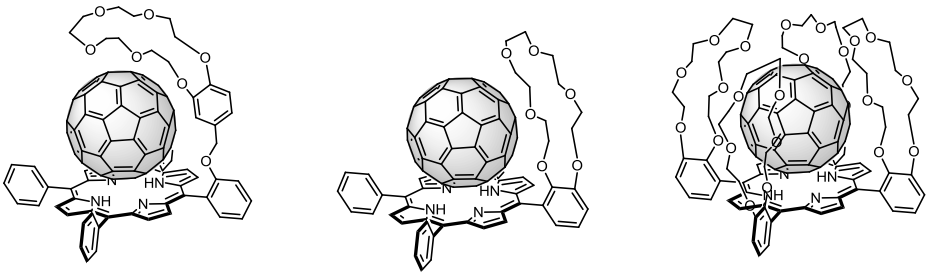

log K_a = 3.75 | log K_a = 3.67 (rt, PhMe, UV-vis) D'Souza, Ito and co. *J. Phys. Chem. A*, **2006** | log K_a = 3.69

Figure 2.38. Structure of benzo[18]crown-6 appended free-base porphyrin complexes.

Remarkably, addition of a potassium tetrakis(4-chlorophenyl)borate excess weakened the complex, as a result of the decreased nucleophility and more rigid structure of the crown ether in the presence of K^+ ions. Addition of [18]crown-6, which captures the cations, reversed the equilibrium, thus recovering the complex (Scheme 2.14).

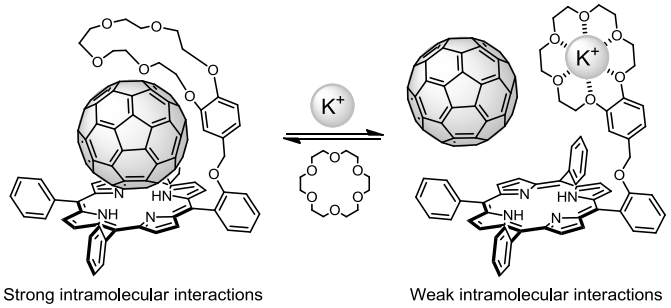

Scheme 2.14. K^+ induced switching of intra to intermolecular association (forward reaction) and [18]crown-6 induced reversible switching (backward reaction).

[88] F. D'Souza, R. Chitta, S. Gadde, M. E. Zandler, A. L. McCarty, A. S. D. Sandanayaka, Y. Araki and O. Ito, *J. Phys. Chem. A* **2006**, *110*, 4338.

g) Extended porphyrins

Supramolecular systems based in fused porphyrin arrays are rare in the bibliography. However, an extraordinary example involving a metalloporphyrin tape and fullerenes was developed by Tashiro and Aida in 2005[89] (Figure 2.39).

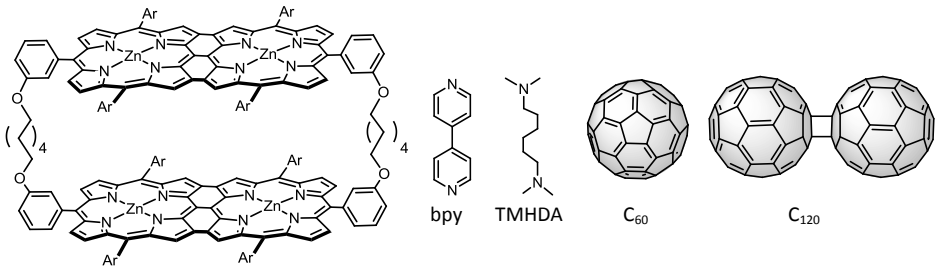

Ar = 3,5-di-*tert*butylpheynyl

Tashiro, Aida and co.
J. Am. Chem. Soc., **2005**

Figure 2.39. Inclusion of diamines and fullerenes by a fused porphyrin array.

Similarly to the monoporphyrin system,[63a] the π-extended porphyrin was able to complex both donor (bpy, TMHDA) and acceptor (C_{60}, C_{120}) molecules in a 1:1 ratio. However, while the host displayed negative homotropic cooperativity for 1:2 systems, a combination of them led to positive heterotropic cooperativity (Scheme 2.15).

Since there is no direct interaction between the C_{60} and diamines in the absence of the porphyrin, and the direction of the CT interactions of the metalloporphyrin with the amines and C_{60} is opposite, this phenomenon is most likely due to an electronic communication between C_{60} and the diamines through the porphyrin.

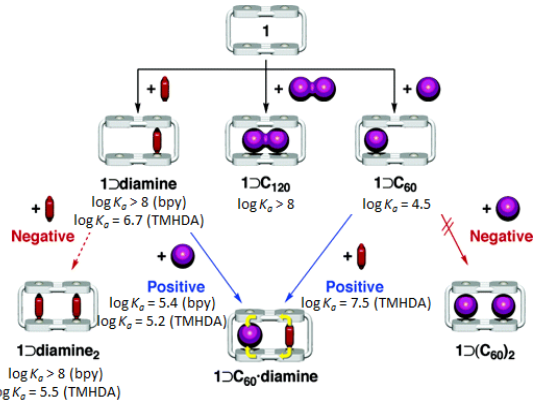

(20°C, PhMe, UV-vis)

Scheme 2.15. The system presents negative homotropic and positive heterotropic cooperativity.

[89] H. Sato, K. Tashiro, H. Shinmori, A. Osuka, Y. Murata, K. Komatsu and T. Aida, *J. Am. Chem. Soc.* **2005**, *127*, 13086.

2.6. exTTF (π-Extended tetrathiafulvalene)

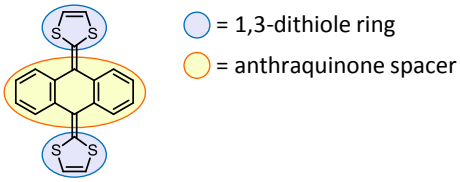

Figure 2.40. exTTF structure.

9,10-Di(1,3-dithiol-2-ylidene)-9,10-dihydroanthracene (exTTF) is a conjugated tetrathiafulvalene (TTF) analogue incorporating two 1,3-dithiole rings connected through a *p*-quinoid spacer (Figure 2.40).[90] This pro-aromatic molecule has widely been used as a donor moiety due to its exceptional properties, including:

Low oxidation potential. exTTFs are strong electron donors exhibiting a two-electron oxidation process to form the dication species (E_{ox}^{1} = 0.44 V *vs*. SCE, in DCM).[91] The gain of aromaticity associated with this process makes this dication very stable.

Non-planar geometry. In the neutral state, the exTTF molecule exhibits a horse saddle structure, clearly differentiating the electron donor and the aromatic face. If oxidized, the geometry changes dramatically into a planar D_{2h}, extending the aromaticity through the whole molecule in which the 1,3-dithiolium aromatic rings are orthogonal to the aromatic central anthracene unit (Figure 2.41).[92]

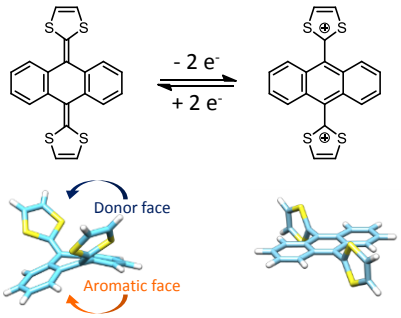

Figure 2.41. The oxidation of exTTF derives in a dramatic change of the geometry.

[90] a) F. G. Brunetti, J. L. López, C. Atienza and N. Martín, *J. Mater. Chem.* **2012**, *22*, 4188; b) Y. Yamashita, Y. Kobayashi and T. Miyashi, *Angew. Chem. Int. Ed.* **1989**, *28*, 1052.
[91] N. Martín, L. Sánchez, C. Seoane, E. Ortí, P. M. Viruela and R. Viruela, *J. Org. Chem.* **1998**, *63*, 1268.
[92] N. Martín and E. Ortí, in *Handbook of Advanced Electronic and Photonic Materials and Devices* (Ed.: N. Hari Singh), Academic Press, Burlington, **2001**, p. 245.

2.6.1. Synthesis

The synthesis of exTTF is quite a straightforward procedure which is fully described in the experimental section. Therefore, here we will only mention that the key step is a Horner–Wadsworth–Emmons reaction between a 9,10-anthraquinone and a phosphonate readily obtained from commercially available vinylene trithiocarbonate.

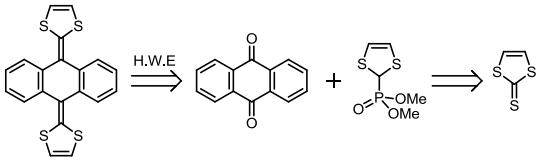

Scheme 2.16. Retrosynthetic analysis of exTTF.

2.6.2. Supramolecular exTTF•fullerene complexes

In spite of the good concave-convex match between exTTF and fullerenes (supported by theoretical calculations predicting binding energies of around 7 kcal·mol^{-1} in the gas phase),[93] attempts to combine both moieties through simply π-π interactions remained elusive at first. A number of different strategies have been developed in order to get over these difficulties:

a) Increasing the electron donor character and the π surface

This has been achieved by synthesizing a novel truxene-TTF derivative, where a third dithiole ring and additional benzene rings were introduced in the same molecule. As predicted by theoretical calculations, and confirmed by experimental findings, this system complexes C_{60} by its aromatic face[94] (Figure 2.42).

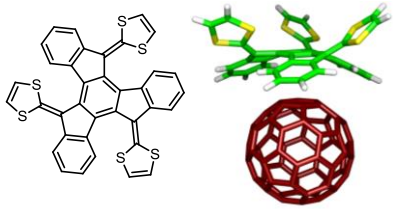

log K_a = 3.1 (rt, $CDCl_3/CS_2$ 1:1, ^{1}H-NMR)
Ortí, Martín and co.
Angew. Chem. Int. Ed., **2007**

Figure 2.42. Truxene-TTF complex.

[93] E. Ortí, *Personal communication*.
[94] E. M. Pérez, M. Sierra, L. Sánchez, M. R. Torres, R. Viruela, P. M. Viruela, E. Ortí and N. Martín, *Angew. Chem. Int. Ed.* **2007**, *46*, 1847.

b) Increasing the number of exTTF units

An alternative approach is combining together various exTTF units. Indeed, the first exTTF-based receptor for pristine C_{60} had a tweezer-like design (Figure 2.43) Interestingly, while in ClPh this system forms a discrete 1:1 host-guest system, in a more polar $CHCl_3$:CS_2 mixture, the system displays homotropic cooperativity leading to higher oligomers, most likely a tetramer.[95] Upon photoexcitation, the lifetime for the CS state of these complex was low, in the range of picoseconds.[96]

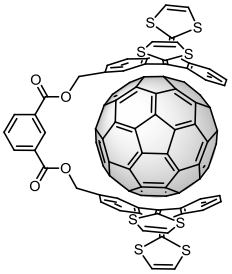

log K_a = 3.5 (rt, ClPh, UV-vis)
Martín and co.
J. Am. Chem. Soc., **2006**

Figure 2.43. exTTF tweezer.

In order to gain further knowledge on the exTTF-fullerene concave-convex complementarity, a series of tweezer analogues was prepared by changing the electron rich exTTF by a TCAQ, a benzoquinone and a TTF unit (Table 2.8).[97]

Table 2.8. Comparison of binding motifs and their binding constants.

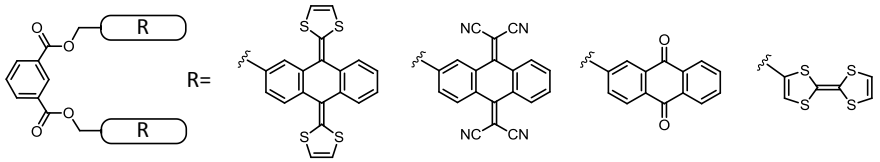

Area	Large	Large	Large	Small
Electronic character	Rich	Very poor	Poor	Rich
Shape	Concave	Concave	Planar	Planar
Binding constant	log K_a = 3.5	log K_a = 3.2	log K_a = 2.9	—

(rt, $CDCl_3$/CS_2 1:1, ^{1}H-NMR)
Ortí, Bietti, Martín and co.
Chem. Commun., **2008**

[95] E. M. Pérez, L. Sánchez, G. Fernández and N. Martín, *J. Am. Chem. Soc.* **2006**, *128*, 7172.
[96] S. S. Gayathri, M. Wielopolski, E. M. Pérez, G. Fernández, L. Sánchez, R. Viruela, E. Ortí, D. M. Guldi and N. Martín, *Angew. Chem. Int. Ed.* **2009**, *48*, 815.
[97] E. M. Pérez, A. L. Capodilupo, G. Fernández, L. Sánchez, P. M. Viruela, R. Viruela, E. Ortí, M. Bietti and N. Martín, *Chem. Commun.* **2008**, 4567.

The following lessons can be obtained from the experimental data:

- Complexation only happens in the presence of large aromatic surfaces, thus demonstrating the major contribution of π-π and van der Waals interactions.
- The higher K_a of electron rich exTTF derivatives compared to electron poor TCAQ suggests a noticeable contribution of coulombic interactions.
- The concave-convex complementarity seems also to play a specific role as TCAQ derivatives bind stronger than benzoquinone derivatives.

The role of the preorganization has also been studied by closing a series of exTTF based tweezers to form a macrocycle with an alkyl linker through a metathesis olefination reaction (Table 2.9).[98]

Table 2.9. log K_a for each of the macrocyclic hosts.

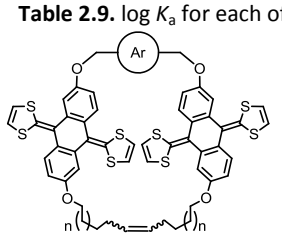

(rt, PhCl, UV-vis)
Pérez, Martín and co.
J. Am. Chem. Soc., **2011**

Ar=	**a)** 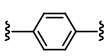		**b)** 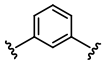		**c)** 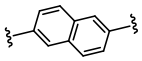	
n	C_{60}	C_{70}	C_{60}	C_{70}	C_{60}	C_{70}
1	4.3	6.0; 12.3	4.0	4.4; 8.3	4.0	4.7
2	6.5	—	4.8	—	5.6	5.6
3	3.5	5.9	4.1	5.4	3.4	6.1

The increase in the preorganization of the macrocycle led to higher K_a for fullerenes. However, strict optimization of the linker's length proved to be a crucial factor as small variations led to changes in the binding constants up to 3 orders of magnitude.

Binding constants for C_{70} were systematically larger than for C_{60}, due to its larger π surface. The bigger surface of this fullerene also enabled to obtain a mixture of 1:1 and 2:1 host/guest complexes with the smaller macrocycles [Ar = **a)**, **b)**; n= 1].

[98] D. Canevet, M. Gallego, H. Isla, A. de Juan, E. M. Pérez and N. Martín, *J. Am. Chem. Soc.* **2011**, *133*, 3184.

Based in these results, more sophisticated systems have also been obtained such as supramolecular self-assembled polymers with a linear[99] (Figure 2.44) or dendritic[100] architecture.

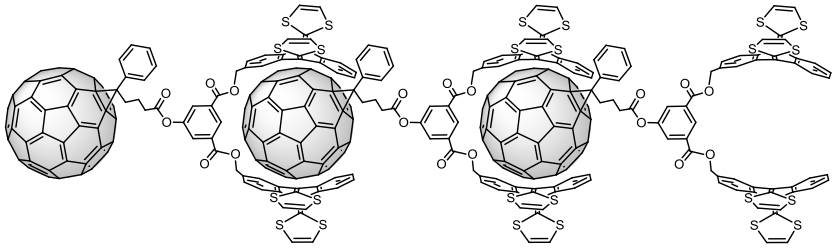

Martín and co.
Angew. Chem. Int. Ed., **2008**

Figure 2.44. Supramolecular polymer obtained from the exTTF-C_{60} complementarity.

Even more exTTF units were introduced in a cyclotriveratrylene (CTV) scaffold through short ether linkages in a system developed by Martín and Mendoza[101] (Figure 2.45).

As expected, the concave surfaces of both the CTV and the exTTF nicely wrapped the fullerene guest, leading to higher stability constants than those found in molecular tweezers without any specific preorganization.

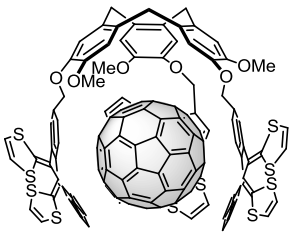

C_{60}: log K_a = 5.3
C_{70}: log K_a = 6.3
(rt, PhCl, UV-vis)
Martín, Mendoza and co.
J. Am. Chem. Soc., **2010**

Figure 2.45. CTV-exTTF host-guest system.

[99] G. Fernández, E. M. Pérez, L. Sánchez and N. Martín, *Angew. Chem. Int. Ed.* **2008**, *47*, 1094.
[100] G. Fernández, E. M. Pérez, L. Sánchez and N. Martín, *J. Am. Chem. Soc.* **2008**, *130*, 2410.
[101] E. Huerta, H. Isla, E. M. Pérez, C. Bo, N. Martín and J. de Mendoza, *J. Am. Chem. Soc.* **2010**, *132*, 5351.

c) Introducing additional recognition motifs

As in the case of porphyrins, the introduction of additional recognition points led to an increase of the overall stability constant of the complex.

For example, an analogous system to the one developed by Nierengarten,[86] with an exTTF unit in the place of the porphyrin, (Figure 2.46) exhibited also a dramatic increase of the K_a of three orders of magnitude compared to the reference system.[102] This value was even larger than the one found with porphyrins, thus evidencing the importance of the concave-convex complementarity.

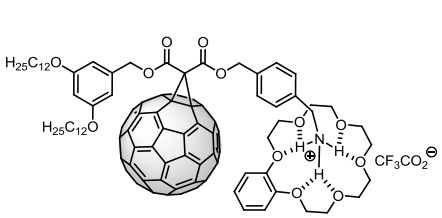

log K_a = 3.3 (rt, $CDCl_3$, ^{1}H-NMR)
Nierengarten and co.
Tetrahedron, **2006**

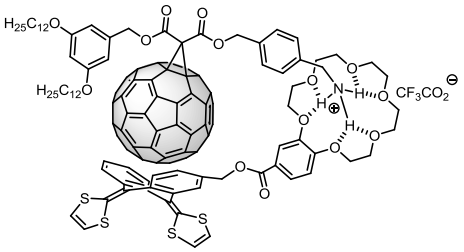

log K_a = 6.3 (rt, $CHCl_3$, UV-vis)
Guldi, Martín and co.
Chem. Commun., **2008**

Figure 2.46. The introduction of an exTTF dramatically increased the binding constant.

Another noteworthy system was developed in our laboratory in Madrid using crown ethers as additional recognition motif (Figure 2.47). In contrast to the porphyrin analogues (Figure 2.38),[88] this system exhibited one of the strongest binding constant for pristine fullerene in a purely organic receptor up to date.[103]

While supposed to arise from n-π or CH-π interactions, the precise nature of the additional stability conferred by crown ethers remains an open question.

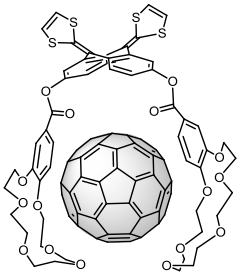

C_{60}: log K_a = 6.7
C_{70}: log K_a = 7.4
(rt, PhCN, UV-vis)
Guldi, Martín and co.
J. Am. Chem. Soc., **2010**

Figure 2.47.

[102] J. Santos, B. Grimm, B. M. Illescas, D. M. Guldi and N. Martín, *Chem. Commun.* **2008**, 5993.
[103] B. Grimm, J. Santos, B. M. Illescas, A. Muñoz, D. M. Guldi and N. Martín, *J. Am. Chem. Soc.* **2010**, *132*, 17387.

Porphyrins and exTTFs have also been recently combined together in a series of strapped porphyrins analogous to the one developed by Aida and Martín (Table 2.10).[104]

Table 2.10. Binding constants towards fullerenes of exTTF-porphyrin derivatives.

a) P = b)

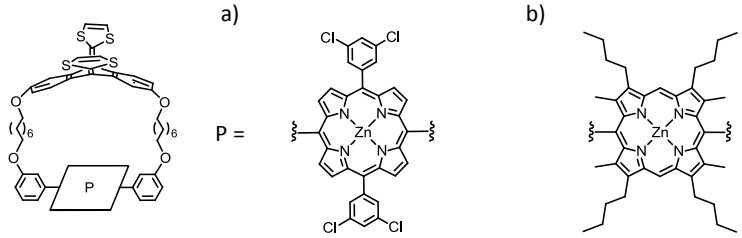

	C_{60}	C_{70}	C_{60}	C_{70}
PhMe	log K_a = 3.6	—	log K_a = 3.9	log K_a = 4.3
PhMe : MeCN (1:1)	log K_a = 4.5	log K_a = 4.6	log K_a = 5.1	log K_a = 5.5

(rt, UV-vis)
Morin and co.
Org. Biomol. Chem., **2012**

Interestingly, system a) does only complex C_{70} in an equimolecular PhMe/MeCN solution and exhibits an unusual lack of preference towards C_{60} *vs*. C_{70}. This behavior was suspected to arise from steric hindrance of the two chlorine atoms pointing into the macrocycle cavity, thus reducing its effective size (Figure 2.48).

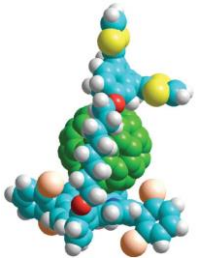

Figure 2.48. Molecular model for system a) with C_{60}.

To verify this, system b), without bulky substituents, was obtained. The higher selectivity and binding constants found may be due to a small increase in the pocket size, as well as to the alkyl chains in the pyrrol subunits which can force the porphyrin to adopt a concave conformation due to steric effect (Figure 2.49).

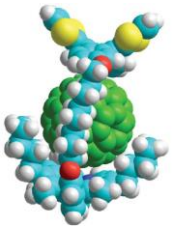

Figure 2.49. Molecular model for system b) with C_{60}.

[104] J.-B. Giguere and J.-F. Morin, *Org. Biomol. Chem.* **2012**, *10*, 1047.

d) Using other interactions

Even though most of the supramolecular complexes derived from exTTF rely on π-π interactions, a few examples using other interactions have also been developed. For example, a hydrogen bond pseudo-rotaxane with a fullerene-based secondary ammonium salt was obtained via hydrogen bond (Figure 2.50). However, the stability of this complex was very low, probably due to the big and hindered cavity.[105]

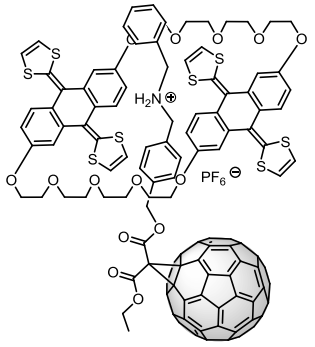

log K_a = 1.7 (rt, $CDCl_3/CDC_3N$ 1:1, ^{1}H-NMR)
Martín and co.
Tetrahedron, **2006**
Figure 2.50. ExTTF pseudo-rotaxane.

To overcome this limitation, a series of exTTF-based secondary ammonium salts were complexed with a smaller DB[24]C8fullerene.[106] Even though higher K_a values were obtained (Figure 2.51), CV experiments revealed that complexation did not influence the redox properties of the components, suggesting that they are not close enough.

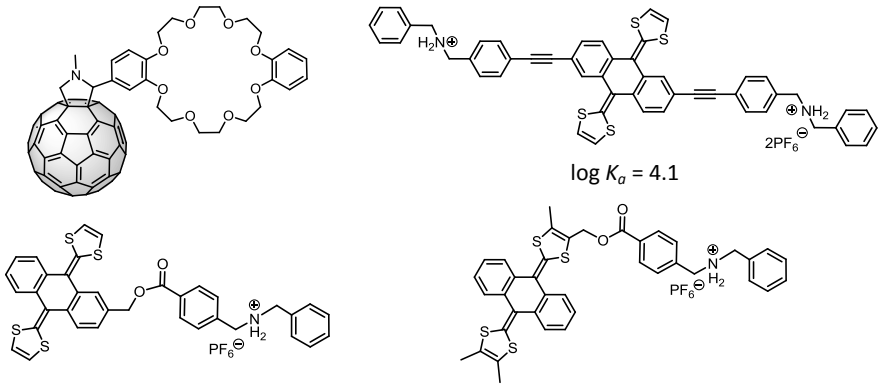

log K_a = 4.1

log K_a = 3.1

log K_a = 2.9

(rt, DCM/CH_3CN 1:1, Fluorescence)
Martín, Guldi and co.
Eur. J. Org. Chem., **2007**

Figure 2.51. Stability constants of different DB[24]C8 fullerocrown ethers with ammonium salts.

[105] M. C. Díaz, B. M. Illescas, N. Martín, J. F. Stoddart, M. A. Canales, J. Jiménez-Barbero, G. Sarova and D. M. Guldi, *Tetrahedron* **2006**, *62*, 1998.
[106] B. M. Illescas, J. Santos, M. C. Díaz, N. Martín, C. M. Atienza and D. M. Guldi, *Eur. J. Org. Chem.* **2007**, *2007*, 5027.

3. Objectives

3. OBJECTIVES

Based on the examples seen in Chapter 2, and especially in the systems previously developed in our laboratories in Strasbourg[86] and Madrid,[103] we have synthesized a series of new supramolecular ensembles in order to further study and exploit the affinity of porphyrins and crown ethers towards [60]fullerene.

Chapter 4.1. *Effect of the metal atom on the binding constant between metalated porphyrins and C_{60}.*

In this chapter we have combined π-π stacking and ammonium-crown ether interactions to obtain new and thermodynamically stable supramolecular metalloporphyrin·C_{60} dyads. The central metal atom in the porphyrin moiety has systematically been changed and its impact on the binding constant evaluated.

Chapter 4.2. *Supramolecular properties of directly linked porphyrin arrays.*

Inspired by the results of the previous systems, we have further functionalized the porphyrin moiety to obtain both a *meso-meso* appended porphyrin dimer and a triply linked *meso-meso*, *β-β*, *β'-β'*, porphyrin tape. The supramolecular properties of these arrays –largely unexplored up to date– have been studied.

Chapter 4.3. *Unveiling the nature of crown ether-C_{60} interactions.*

This chapter studies why the introduction of crown ethers in an exTTF based molecular tweezer led to extraordinary affinity towards C_{60}.[103] For this, a new series of exTTF-(crown ether)$_2$ host molecules with crown ethers of different size and nature has been obtained. The binding constants of theses systems have been obtained and compared with the DFT calculations of the systems.

Chapter 4.4. Crown ether + 2 exTTF.

Two new (exTTF)$_2$-crown ether derivatives have been synthesized in order to further exploit the potentiality of crown ethers in the design of C_{60} receptors as well as the impact of geometrical constraints on the host properties.

4. Results and discussion

4. RESULTS AND DISCUSSION

4.1. EFFECT OF THE METAL ATOM ON THE BINDING CONSTANT BETWEEN METALATED PORPHYRINS AND C_{60}

4.1.1. Synthesis of the building blocks

Host porphyrins **12-M** were obtained as depicted in their retrosynthetic analysis (Scheme 4.1). The key reactions were a Suzuki-Miyaura cross-coupling reaction over derivative **9**, which was in turn obtained by a regioselective iodination of substrate **8**, resulting from the mixed condensation of dipyrromethane **3** and aldehyde **6**.

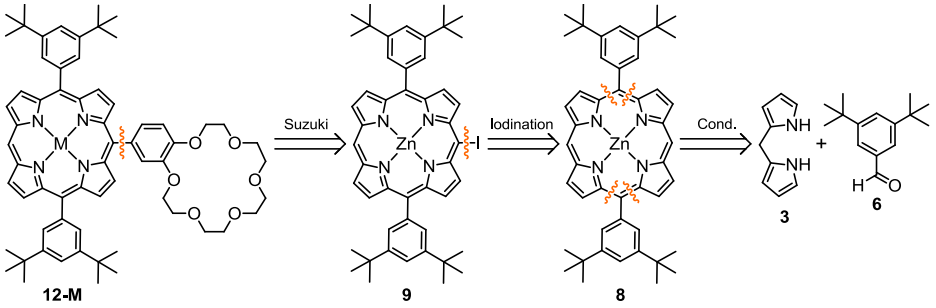

Scheme 4.1. Retrosynthetic analysis of host porphyrins **12-M**.

For the guest molecule **21**, the key reaction was a Bingel cycloaddition over C_{60} from derivative **19**. This asymmetric malonate was in turn obtained by esterification reaction of molecule **18**, derived from alcohol **17** (Scheme 4.2).

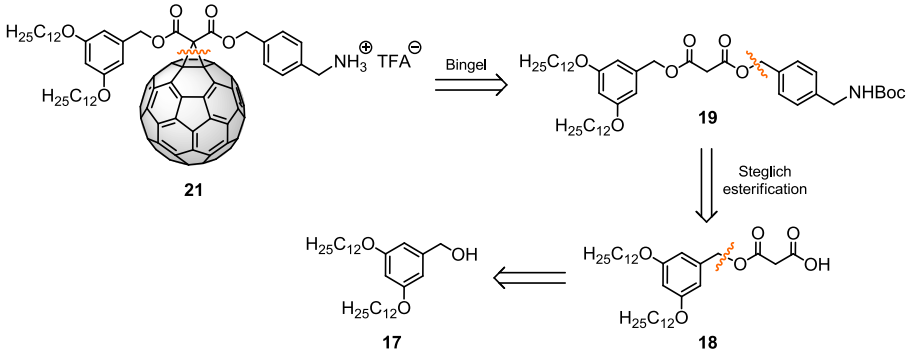

Scheme 4.2. Retrosynthetic analysis of guest methanofullerene **22**.

a) Synthesis of the host

Synthesis of asymmetric porphyrins is often a complex task involving multistep synthetic procedure and affording the final product in low yields. The complete synthesis of host porphyrins **12-M** (M = 2H, Zn, Co, Ni, Cu) is depicted in Scheme 4.3.

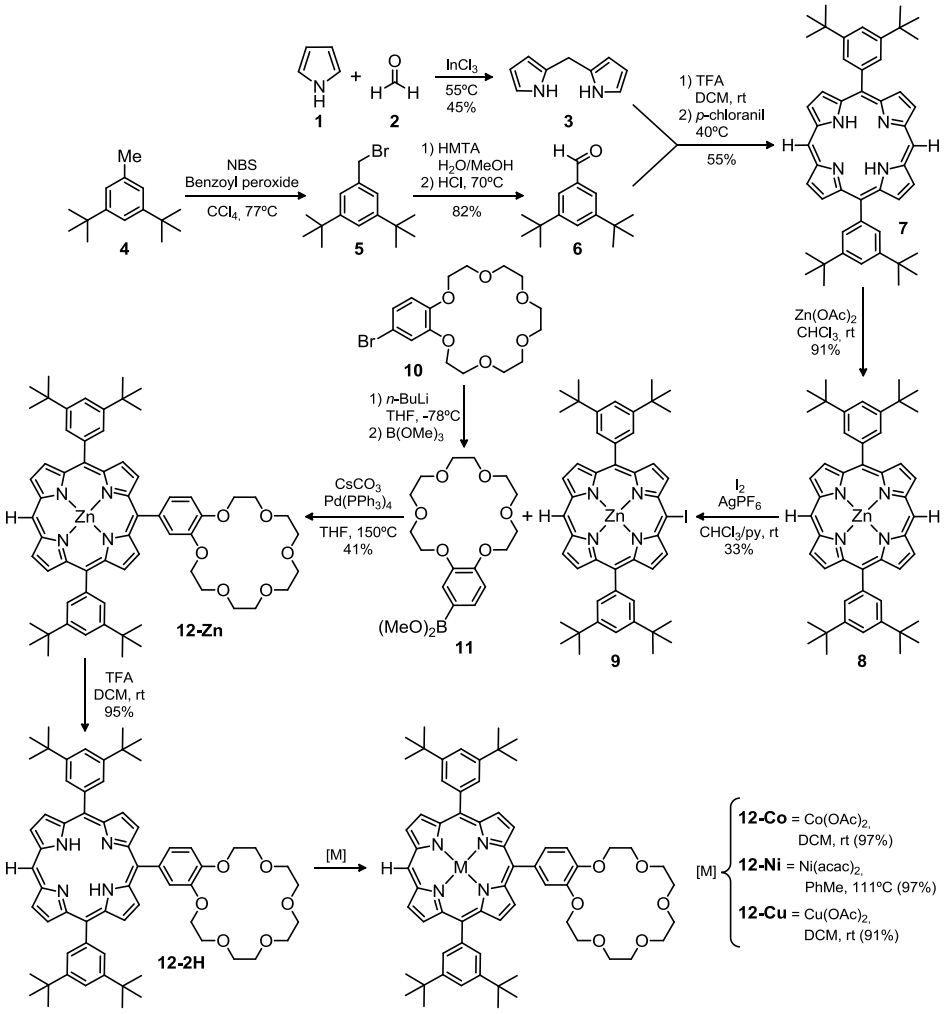

Scheme 4.3. Synthetic route for the preparation of different host porphyrins **12-M**.

Dipyrromethane **3** was obtained by $InCl_3$ catalyzed solventless condensation of pyrrole **1** and formaldehyde **2**, generated *in situ* from paraformaldehyde. By using an excess of pyrrole, the formation of linear and cyclic oligomers is largely prevented, thus allowing to produce the desired dipyrromethane **3** in a reasonable yield.

3,5-di-*tert*-butylbenzaldehyde **6** was prepared by Sommelet oxidation[107] (Scheme 4.4) of molecule **5**, which was obtained by radical bromination of commercially available 3,5-di-*tert*-butyltoluene (**4**).

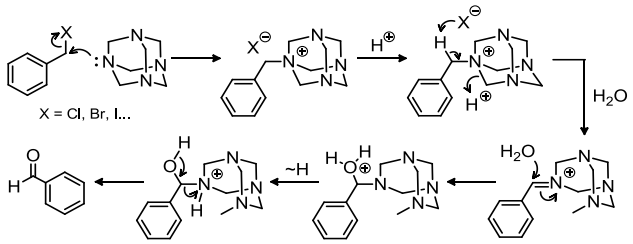

Scheme 4.4. Sommelet oxidation is believed to occur by nucleophilic attack of HMTA over a benzyl halide producing an imine which is then hydrolyzed to furnish the aldehyde.

Condensation of dipyrromethane **3** and aldehyde **6** under Lindsey conditions afforded free base porphyrin **7** in a moderate yield. Purification of this derivative was achieved by gravity-fed column chromatography (SiO_2 gel) as the use of pressure could promote π-stacking phenomena between by-products, thus difficulting the purification process.

Treatment of derivative **7** with $Zn(OAc)_2$ gave the corresponding metalloporphyrin **8**, which was then halogenated regioselectively in the *meso* position to yield porphyrin **9**. Interestingly, the presence of pyridine in the reaction medium is essential to change the course of this reaction from *meso*-*meso* coupling to *meso*-iodination.[108]

Halogen-metal exchange of **10** with *n*-BuLi and subsequent quenching with $B(OMe)_3$ led to boronate **11**, which was then coupled by a microwave activated Suzuki reaction to halogenated porphyrin **9** (conveniently Zn metalated to avoid the insertion of Pd in the porphyrin cavity) to yield porphyrin **12-Zn** after tedious purifications. The reaction was maintained till TLC control showed dehalogenation of **9**.

Subsequent demetalation under acidic conditions afforded **12-2H** which was then treated with different metal salts to obtain **12-Co**, **12-Ni**, and **12-Cu** in excellent yields.

[107] a) M. Sommelet, *C. R. Chim.* **1913**, *157*, 852; b) Z. Wang, in *Comprehensive Organic Name Reactions and Reagents*, John Wiley & Sons, Inc., **2010**.
[108] A. Nakano, H. Shimidzu and A. Osuka, *Tetrahedron Lett.* **1998**, *39*, 9489.

This stepwise approach contrasts with the traditional synthesis of *meso*-appended crown porphyrins, based in the mixed condensation of pyrrole and the appropriate aldehydes,[86],[109] and allowed us to afford the targeted molecules in better yields and in a more controlled manner, as we largely avoid the generation of by-products from polypyrrolic rearrangement.

All new products were satisfactorily characterized by standard analytical and spectroscopic techniques. Demetalation of the porphyrin **12-Zn** was evidenced by the appearance of a ^{1}H-NMR signal at -2.91 ppm, corresponding to the internal NH protons (as a result of the ring current effect of the aromatic porphyrin ring), and the appearance of four Q bands in the UV-vis, as a result of the lower symmetry of the porphyrin. Alternatively, disappearance of the upfield ^{1}H NMR signal and the presence of only two Q bands was considered a reliable proof for successful metalation. As an example, the ^{1}H-NMR of molecule **12-Zn** is shown in Figure 4.1. Complete assignment of the protons was possible with additional NOESY experiments.

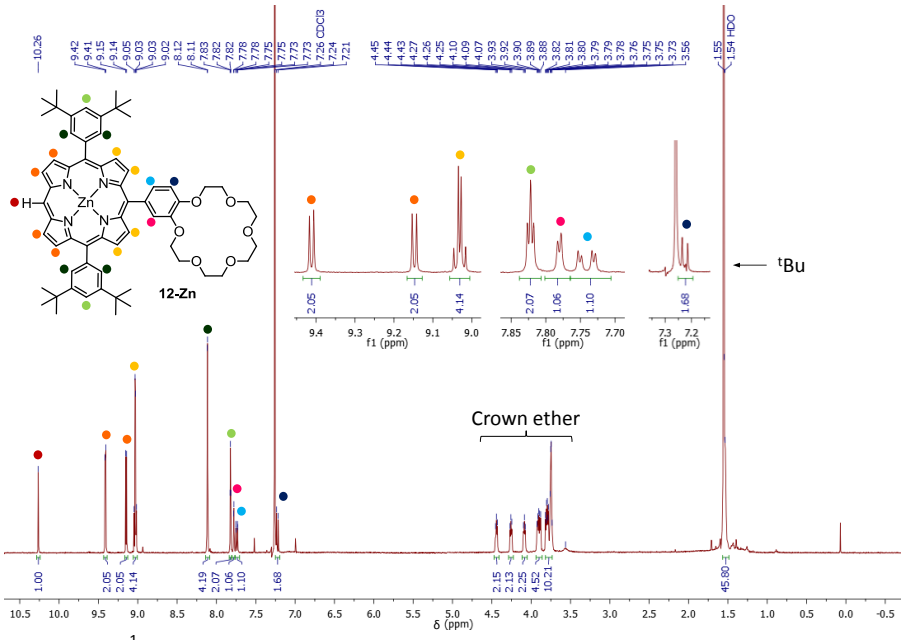

Figure 4.1. ^{1}H-NMR ($CDCl_3$, 400 MHz, 298 K) of host molecule **12-Zn**. Aromatic signals are depicted by colored bullets.

[109] P. Even and B. Boitrel, *Coord. Chem. Rev.* **2006**, *250*, 519.

b) Synthesis of the guest

The synthesis of non-symmetric methanofullerene derivatives such as **21** requires the synthesis of its corresponding asymmetric malonic ester derivative (Scheme 4.5):

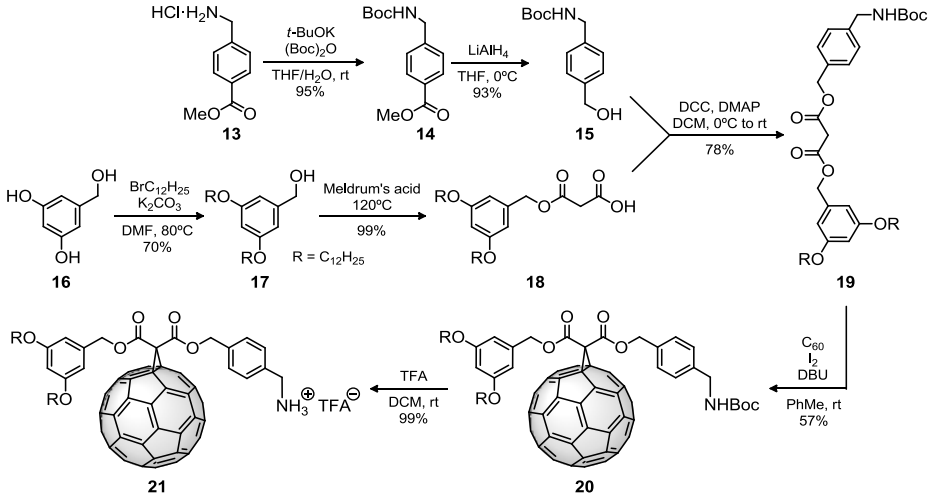

Scheme 4.5. Synthetic route for guest methanofullerene **21**.

For this, the amine group of the commercially available methyl 4-(aminomethyl)benzoate hydrochloride **13** was protected by reaction with di-*tert*-butyl dicarbonate to yield derivative **14**, which was then converted into benzylic alcohol **15**.

In parallel, solubilizing dodecyl chains were attached to molecule **16** by Williamson etherification of the phenolic groups producing **17**. Solventless reaction with Meldrum's acid yielded acid **18**, which was then esterified with benzylic alcohol **15** under a modified Steglich esterification[110] to afford malonic ester **19**.

[60]fullerene was then functionalized with derivative **19** by a Bingel reaction[111] (nucleophilic addition of *in situ* generated stabilized α-halocarbanion to the C_{60} core, followed by an intramolecular nucleophilic substitution leading to the cyclopropanation) to yield molecule **20**. Final deprotection of the Boc group with TFA afforded quantitatively methanofullerene **21** as its trifluoroacetate salt.

[110] B. Neises and W. Steglich, *Angew. Chem. Int. Ed.* **1978**, *17*, 522.
[111] C. Bingel, *Chem. Ber.* **1993**, *126*, 1957.

4.1.2. Formation and characterization of supramolecular ensembles

Complexation studies of supramolecular ensembles **[12-M·21]** were realized by monitoring the changes in the absorption spectra of the porphyrin moiety **12-M** after addition of increasing quantities of fullerene derivative **21** at rt (Scheme 4.6). DCM was chosen as solvent due to its low polarity and H-bonding character (ε = 9.1; α^H = 1.9),[112] ensuring minimal interferences with the ammonium-crown ether interactions while being a good solvent for the building blocks. Further details on the titration experiments can be found in Annex I.

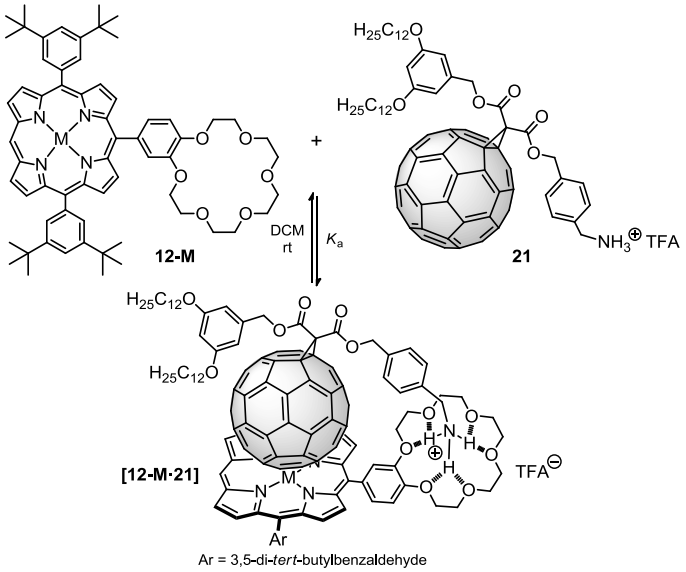

Scheme 4.6. Formation of the supramolecular complexes **[12-M·21]** from their building blocks.

A representative example of the series is the formation of complex **[12-Zn·21]**. Addition of increasing quantities of **21** to **12-Zn** resulted in a red shift of the Soret band (λ_{max} = 416 nm → 423 nm) (Figure 4.2) which was also observed in the rest of complexes (see Annex III.1.1). This shift has been accounted for by the charge transfer from the axial ligand to the porphyrin ring,[113] and is widely used as an evidence of the presence of intermolecular π-stacking of both chromophores.[114]

[112] C. A. Hunter, *Angew. Chem. Int. Ed.* **2004**, *43*, 5310.
[113] M. Nappa and J. S. Valentine, *J. Am. Chem. Soc.* **1978**, *100*, 5075.
[114] F. D'Souza and O. Ito, *Chem. Commun.* **2009**, 4913.

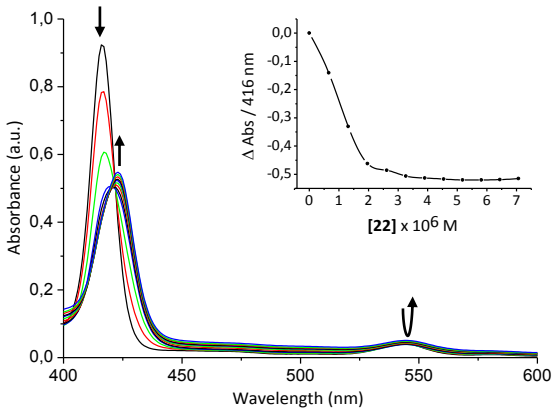

Figure 4.2. UV-vis spectral changes observed upon complexation of **12-Zn** ($1.88 \cdot 10^{-6}$ M) by **21** (0-4 equiv by 0.35 equiv step) in DCM. Inset shows the binding isotherm at 416 nm.

The appearance of a single isosbestic point suggests a single equilibrium between the free and the complexed species.[115] Given the unlikely formation of a 1:2 complex by simultaneous collision of three molecules this is most probably a 1:1 complex.

This stoichiometry is in line with that found in the analogous system developed by Nierengarten[86] and was also evidenced by positive ESI-MS (a technique which allows transferring pre-existing ions in solution to the gas phase in a very soft manner)[116] of an equimolar mixture of **12-Zn** and **21** in DCM (see Annex III.1.2).

Also, mathematical analysis of the titration data by Specfit (see Annex I) only fitted for a 1:1 model, estimating the different K_a values of **[12-M·21]** as reported in Table 4.1.

Table 4.1. Binding constants of systems **[12-M·21]**.

Complex	log K_a ± 3σ
[12-2H·21]	5.5 ± 0.2
[12-Co·21]	6.3 ± 0.2
[12-Ni·21]	5.9 ± 0.1
[12-Cu·21]	6.3 ± 0.3
[12-Zn·21]	6.9 ± 0.2

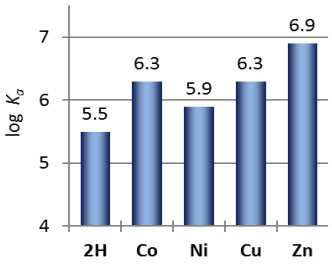

[115] K. A. Connors, *Binding Constants: The Measurement of Molecular Complex Stability*, Wiley, **1987**.
[116] J. Fenn, M. Mann, C. Meng, S. Wong and C. Whitehouse, *Science* **1989**, *246*, 64.

The binding constant obtained for **[12-Zn·21]** was very high, nicely evidencing the complementarity of the ammonium-crown ether interaction and π stacking in the system as well as the influence of the chelate cooperativity (see Annex II).

The K_a obtained for **[12-2H·21]** was roughly the same than the value obtained in the analogous system previously developed in our lab, where the free *meso* position was occupied by a third 3,5-di-*tert*-butylphenyl moiety (Figure 2.37).[86]

Interestingly, the pattern of the binding constants obtained for the **[12-M·21]** complexes was very different to that previously reported by Reed, Boyd[61a],[62] and Aida[63b], where free base porphyrin host systems systematically bound pristine fullerene with a similar strength than their Zn(II) porphyrin analogous and no clear correlation could be obtained (Figure 2.26).

In our case, the binding constants series obtained with the **[12-M·21]** complexes correlate with the one expected for a porphyrin·C_{60} system governed by van der Waals forces, where K_a becomes larger when the number of electrons in the porphyrin increases. The exception to this "rule of thumb" would be the great stability of **[12-Co·21]**, which can be accounted on the base of the strong interactions between fullerenes and group 9 metals (Co, Rh, Ir) as seen in Chapter 2. The special behavior of **12-Co** is also evidenced by the great red shift experienced by its Soret band ($\Delta\lambda_{max}$ = 24 nm) suggesting a large charge transfer (See Annex III.1.1).

It is also important to note that all the previous examples described in the literature consisted on the complexation of pristine C_{60}, whose low solubility limited the crucial choice of solvents for the titration experiment. Indeed, it has been evidenced an inverse correlation between the binding of C_{60} and its solubility in various solvents in a series of supramolecular complexes, suggesting that desolvation of C_{60} is a major contributor to the energetics of its binding in solution.[62] The use of methanofullerene **21** has elegantly circumvented this limitation while basically retaining the original properties of the fullerene moiety.

a) Assessment on the chelate effect

Interested by the high binding constant obtained in the complex **[12-Zn·21]** we studied its chelate effect by calculating its effective molarity (EM), a parameter accounting for the ring-closing *vs.* oligomerization tendency of the system (see Annex II). For this, we have evaluated each of the interactions leading to the complex independently and compared them to the K_a obtained as depicted in Scheme 4.7.

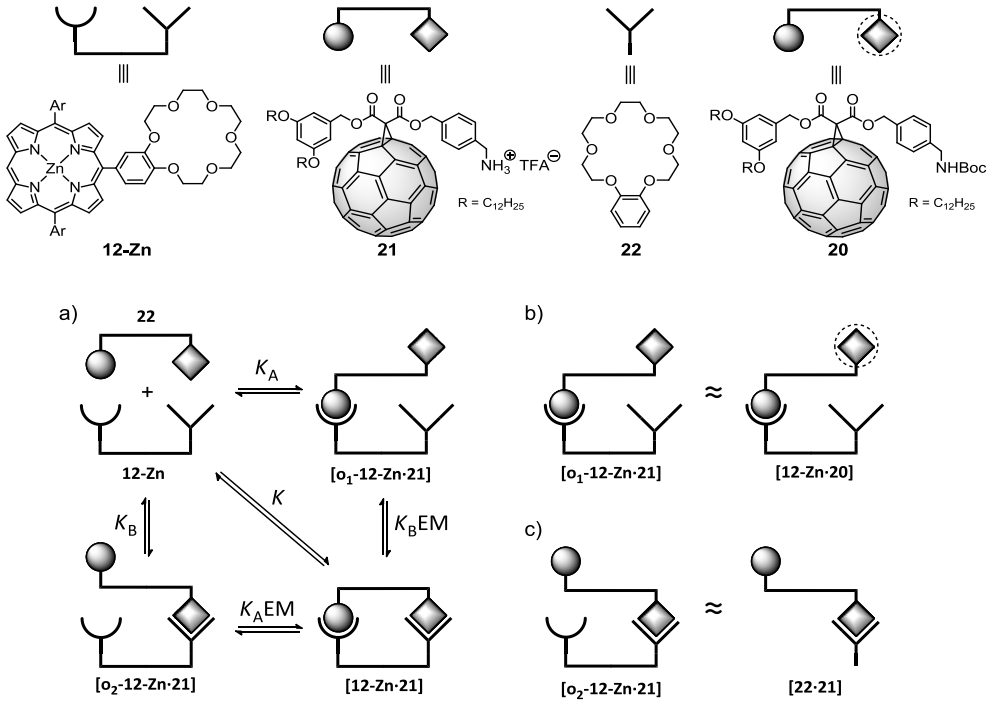

Scheme 4.7. a) The EM of the chelated complex can be obtained by evaluating its individual contributions independently. b) π-stacking was evaluated by combining **12-Zn** and methanofullerene **20**. Ammonium-crown ether complementarity was evaluated by combining together **21** and reference crown ether **22**.

To start with, the π-stacking between the [60]fullerene and the porphyrin was evaluated by combining porphyrin conjugate **12-Zn** with methanofullerene **20**, where the ammonium moiety is under its protected Boc form, thus preventing the interaction with the crown ether. Our first approximation was made by monitoring the complexation induced absorption changes of the Soret band in **12-Zn** upon

increasing quantities of **20** in $CHCl_3$. Experimental data evidenced the additivity of building blocks' absorbance, even in the presence of a large excess of methanofullerene **20**, thus ruling out any interaction measurable by UV-vis spectroscopy. Therefore, we resorted to ^{1}H-NMR spectroscopy and monitored the complexation induced shift of the signal corresponding to the free *meso* proton in **12-Zn** upon increasing quantities of **20** in $CDCl_3$ at rt. The shift was extremely tiny but non-linear curve fitting with the software Equilibria[117] found a binding constant of log K_a = 1.3 (see Annex III.1.3).

The ammonium-crown ether interaction had been previously evaluated in our lab by ^{1}H-NMR spectroscopy where increasing amounts of commercially available benzo crown ether **22** were added over fullerene derivative **21** in $CDCl_3$ at rt, yielding a binding constant of K_a=2100 ± 100 M^{-1}.[87]

Finally, in order to have a homogeneous set of data, the UV-vis titration of **12-Zn** with **21** was repeated in $CHCl_3$ obtaining a value of log Ka = 5.1 ± 0.1 (See Annex III.1.3). This value was lower than that obtained in DCM and can be explained by the larger H-bond acceptor nature of $CHCl_3$ (α^H = 2.2),[112] which hinders the complexation.

Taking into account the aforementioned results, we can calculate EM through equation **(1)**

$$EM = \frac{K}{K_A K_B} = \frac{10^{5.1}}{10^{1.3} \cdot 10^{3.3}} = 3.16\ M \qquad \textbf{(1)}$$

This value serves as a rough estimation of the chelate cooperativity and reflects how the introduction of π-stacking as additional recognition pattern increases the association constant more than 3 orders of magnitude compared to the binding of **21** with **22**. This dramatic increase in the stability results even more surprising if we consider the weakness of the supramolecular complexes obtained just by π-stacking of both chromophores.

[117] P. G. Young and K. A. Jolliffe, *Org. Biomol. Chem.* **2012**, *10*, 2664.

b) ^{1}H-NMR titration of 12-Zn with 21

In view of all these data we performed a final experiment studying the complexation induced changes in the ^{1}H-NMR of the host molecule **12-Zn** upon increasing quantities of **21** (Figure 4.3).

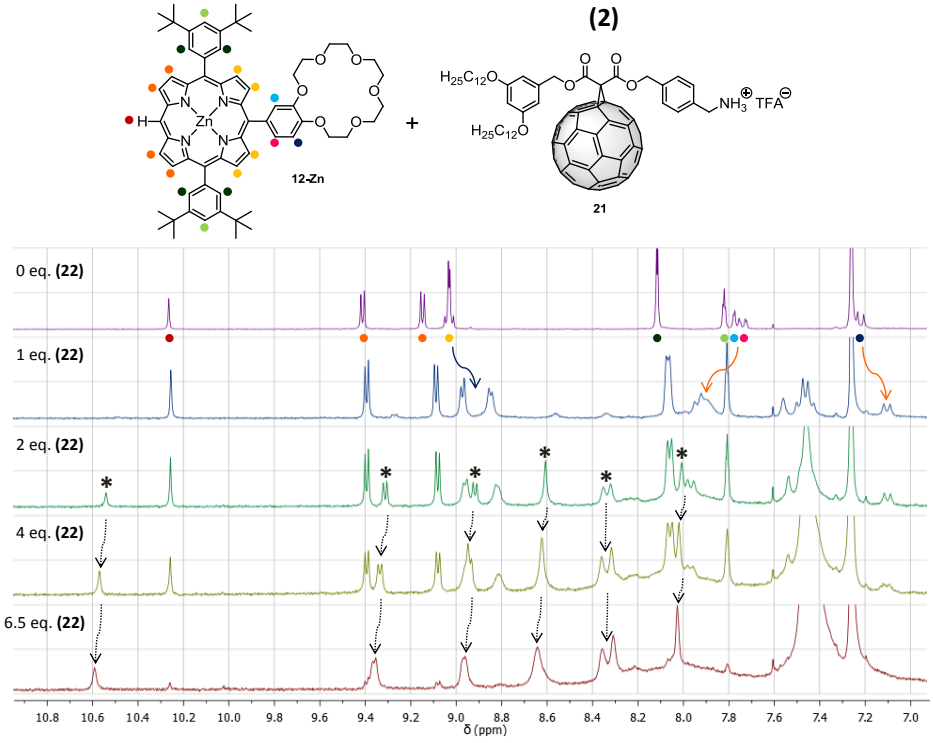

Figure 4.3. ^{1}H-NMR titration of **12-Zn** ($1.81 \cdot 10^{-3}$M, $CDCl_3$, rt) with increasing quantities of **21**.

To start with, the addition of 1 equivalent of guest molecule **21** produced a split of the chemical shift of the β-pyrrolic protons of **12-Zn** (blue arrow) and a shift of the aromatic protons of the crown ether moiety to both higher and lower fields (orange arrows) suggesting that this moiety is involved in a fast equilibrium (on the NMR time scale).

The addition of a second equivalent of **21** resulted in the appearance of a new set of signals (signaled by *) suggesting the existence of a slow equilibrium (on the NMR

time scale). It is noteworthy the appearance of a new signal with a dramatic down-field shift (approx. 0.35 ppm) ascribable to the *meso* proton. Further addition of guest molecule resulted in a small shift of these new signals and their increase till the disappearance of the original set of peaks.

At this stage it is important to make the following considerations:

- Taking into account the high binding constant obtained for this system (log K_a 6.9 ± 0.2) we can state that at the concentration used in ^{1}H-NMR (≈10^{-3} M) the equilibrium is fully shifted to the right, and thus we can consider that the complex is fully formed (p-value ≈ 1).
- Taking in consideration the EM obtained (≈ 3 M), we can consider that no oligomeric species are present ([**21**]^o << EM).
- At this concentration range, we can't consider any more that the salt **21** is nearly completely ionized and thus we would need to work with molecular activities –difficult to calculate– rather than concentrations (see Annex I.2).

As a result, we can only state that the new set of signals are most likely due to the formation of further aggregates with higher stoichiometries. In addition, the dramatic down-field shift observed for the *meso* and pyrrole protons in **12-Zn** suggests that these aggregates are located over the porphyrin macrocycle. Temperature variable ^{1}H-NMR experiments (rt → - 40^{o}C) on a 1:2 mixture of **12-Zn** and **21** in $CDCl_3$ were performed hopping to freeze any conformation but they did not provide any meaningful information (see Annex III.1.4).

Finally, ESI-MS analysis of a millimolar 1:4 mixture of **12-Zn** and **21** in $CHCl_3$ did only showed the peak corresponding to the 1:1 stoichiometry suggesting the weakness of the intermolecular forces in the higher aggregates (see Annex III.1.2).

4.2. SUPRAMOLECULAR PROPERTIES OF DIRECTLY LINKED PORPHYRIN ARRAYS

This chapter is mainly focused on the supramolecular properties of porphyrin arrays **23** and **24**. Despite the great molecular complexity of these dimers, their symmetry has allowed us to carry out the respective synthesis in a relatively easy experimental procedure from porphyrin **12-Zn** by a divergent route as depicted in Scheme 4.8. Previously used methanofullerene **21** was maintained as guest molecule.

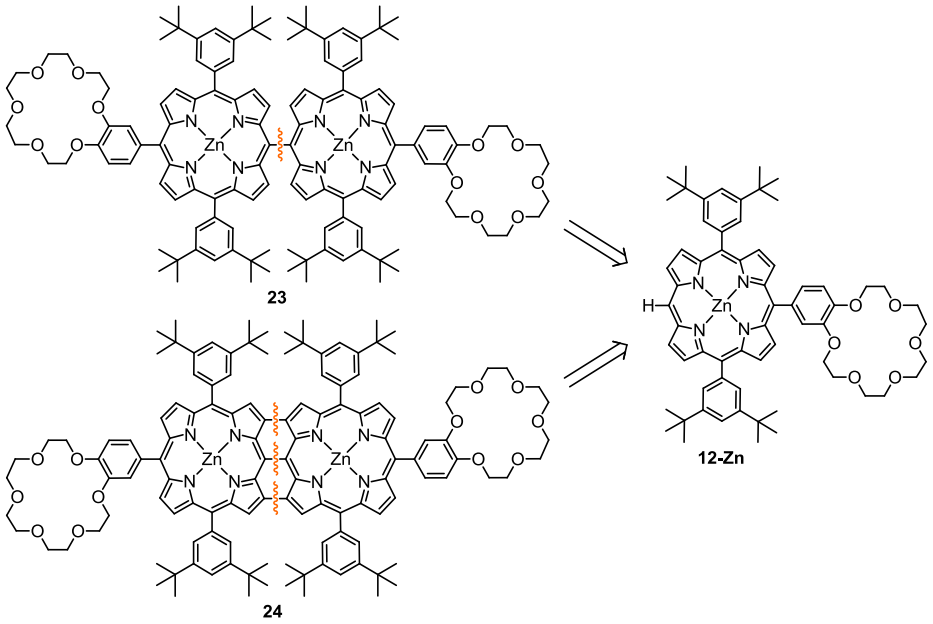

Scheme 4.8. Retrosynthetic analysis of porphyrin arrays **23** and **24**.

4.2.1. meso-meso dimers

a) Synthesis of the *meso-meso* linked porphyrin dimer 23

Porphyrin dimer **23** was obtained by Ag^{I}–promoted oxidative *meso-meso* coupling of porphyrin **12-Zn** in $CHCl_3$. ^{1}H-NMR of the crude proved partial demetalation of the substrate and as a result the reaction was followed by treatment with a Zn(II) salt to ensure full metalation (Scheme 4.9). Purification was easily achieved by gravity-fed chromatography and GPC due to the great solubility of these type of derivatives.

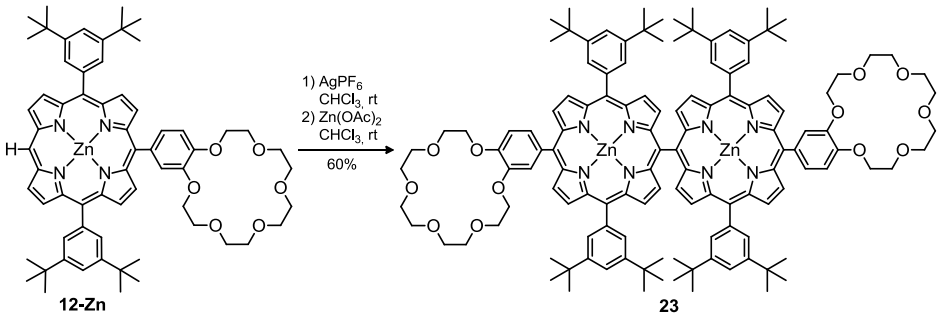

Scheme 4.9. Synthesis of porphyrin dimer **23**.

Analysis of the ^{1}H-NMR of the aromatic region provided valuable information on the structure (Figure 4.4). To start with, as expected, the characteristic *meso* proton (brown bullet), strongly deshielded by the aromatic ring current, was no longer present. Also, pyrrolic protons where shifted up to -0.85 ppm, in good agreement with an approximate perpendicular arrangement of both subunits where the ring current of one porphyrin moiety affects the protons of the other. At this point, however, we were not able to assign all the signals.

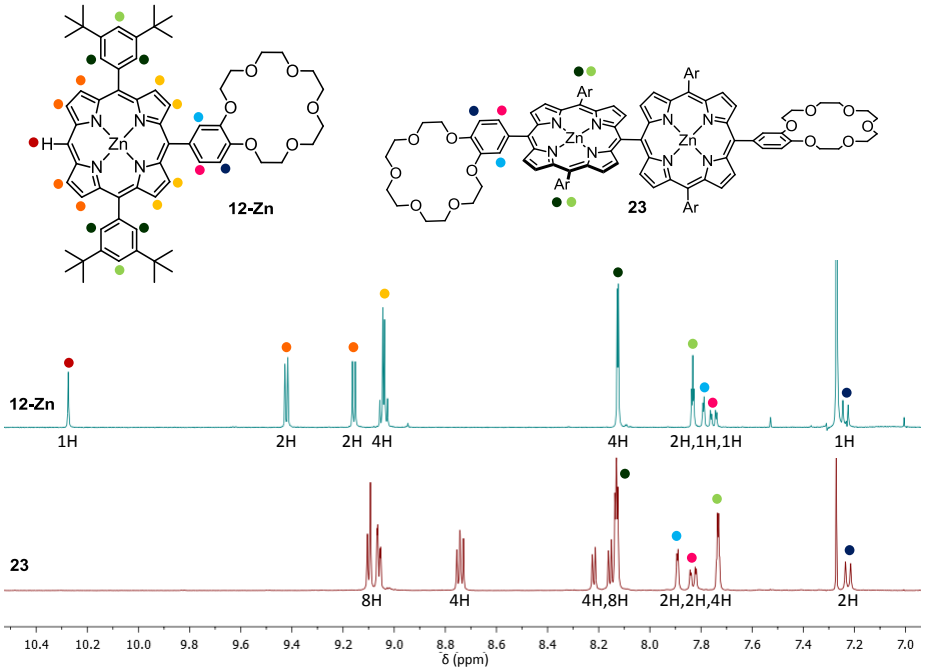

Figure 4.4. ^{1}H-NMR comparison of the monomer porphyrin **12-Zn** with *meso-meso* dimer **23**.

Through-space correlation NOESY experiments allowed us to fully assign all the protons in the molecule as seen in Figure 4.5.

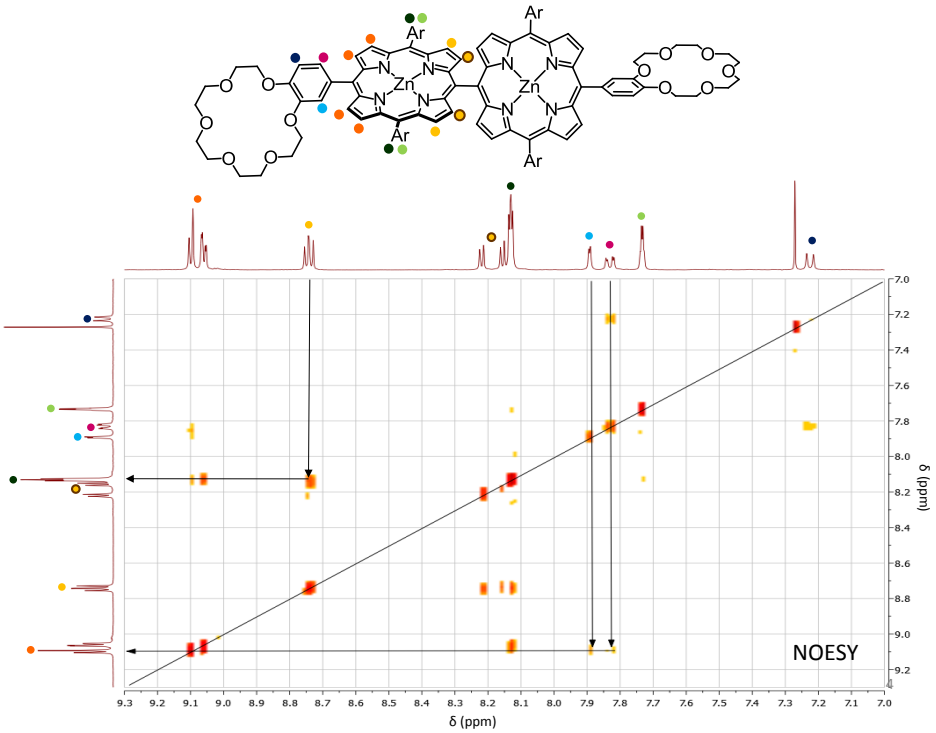

Figure 4.5. NOESY experiment of **23**.

Compound **23** was also characterized by UV-vis spectroscopy. As can be seen in Figure 4.6 its absorption spectrum corresponded to that of a typical *meso-meso* dimer, with a large splitting of the Soret band due to strong exciton coupling and a Q band modestly shifted towards the red. This result suggests that each of the porphyrin subunits retain its individual monomeric porphyrin character.[52]

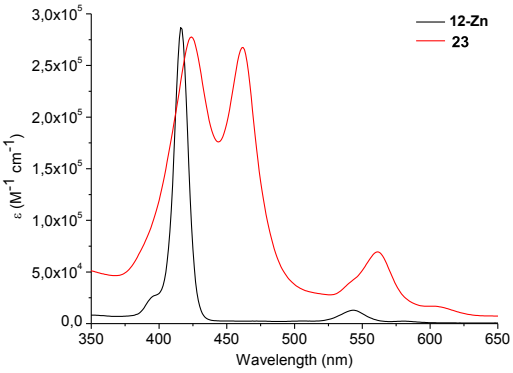

Figure 4.6. Comparison of the UV-vis spectra of **12-Zn** (black) and **23** (red).

Interestingly, the shape of the pyrrolic signals in the ^{1}H-NMR was not the expected for an AB system, thus suggesting the presence of axial chirality across the porphyrin-crown ether bond.

In order to further study this chirality, variable temperature ^{1}H-NMR studies were performed (0-100^{o}C). The increase in the temperature led to an increase in the kinetic energy of the system and, thus, the crown ether moiety started to rotate along its axis overcoming the steric hindrance.

As a result, all pyrrolic protons were equally affected by the crown ether, changing the apparent symmetry of the system and reducing the complexity of the spectra as evidenced by the appearance of two clear AB systems in the pyrrolic region (Figure 4.7). A similar effect was observed in the signals corresponding to the crown ether moiety (see Annex III.2.1).

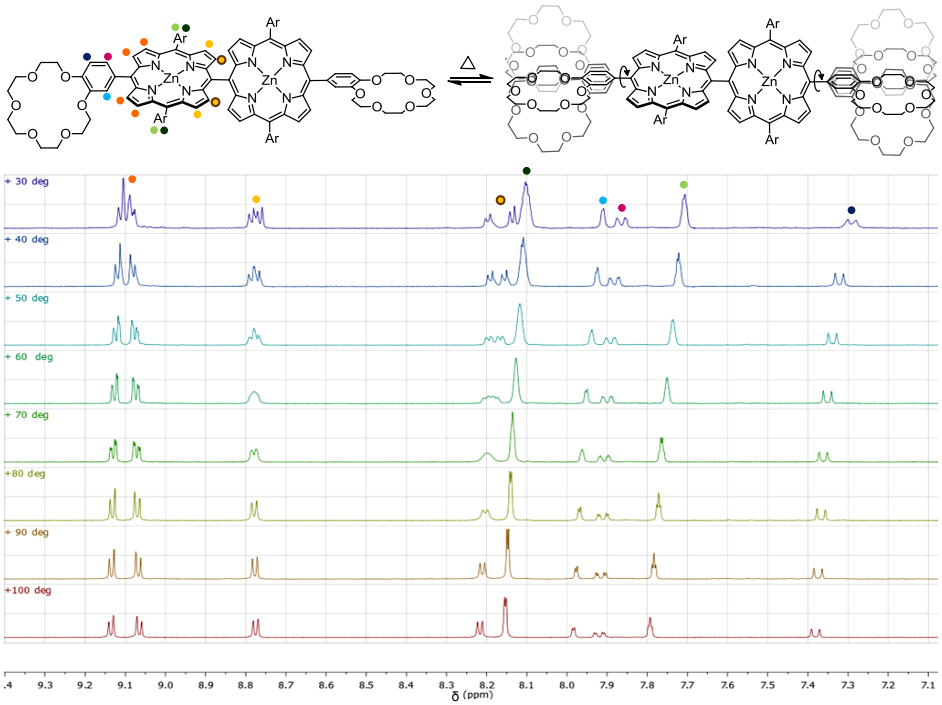

Figure 4.7. ^{1}H-NMR VT experiments (0-100^{o}C) of **23** in $ClCD_2CD_2Cl$.

The absence of rotation around the porphyrin-porphyrin axis at those temperatures was evidenced by UV-vis spectroscopy. If the porphyrins' disposition would be tilted from the orthogonality each of the Soret bands would be split leading to 4 peaks and their absorbance would decrease while increasing that of the Q bands as a result of the change in the symmetry.[118] In our case, nothing of this was observed when heating a solution of **23** in ClPh to 90ºC (see Annex III.2.1).

The activation free energy for the rotation, $\Delta G^{\neq}$, around the porphyrin-crown ether moiety can be obtained from the coalescence temperature (T_C) of the pyrrolic protons (orange bullets) by the following procedure. First we calculated the rate constant (k_c) of the AB system according to equation **(2)** where Δν is the separation in Hz between the two signals in the absence of rotation and J_{AB} is their mutual coupling constant.

$$k_C = 2.22\sqrt{\Delta\nu^2 + 6J_{AB}^2}\ \text{Hz} \qquad \textbf{(2)}$$

With this value we can then calculate $\Delta G^{\neq}$ from equation **(3)**, which is derived from the Eyring equation.[119]

$$\Delta G^{\neq} = 4.58\ T_C\left(10.32 + \log\frac{T_C}{k_C}\right)\ \text{cal·mol}^{-1} \qquad \textbf{(3)}$$

In our case, the $\Delta G^{\neq}$ found was around 17 kcal·mol^{-1} (Figure 4.8). This high value arises from the steric hindrance between the pyrrolic protons of the porphyrins and the ortho protons of the aromatic rings from the crown ether moiety.

J_{AB} = 4.72 Hz
$\Delta\nu_1$ = 8.33 Hz
T_{C1} = 333 K
K_{C1} = 31.6 Hz
$\underline{\Delta G^{\neq} = 17.3\ \text{kcal·mol}^{-1}}$

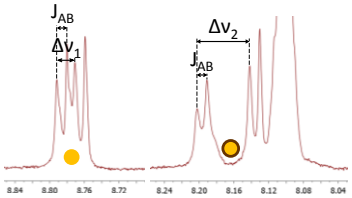

J_{AB} = 4.72 Hz
$\Delta\nu_2$ = 24.32 Hz
T_{C2} = 343 K
K_{C2} = 59.78 Hz
$\underline{\Delta G^{\neq} = 17.4\ \text{kcal·mol}^{-1}}$

Figure 4.8. Experimental values used for calculating $\Delta G^{\neq}$.

[118] D. Kim and A. Osuka, *J. Phys. Chem. A* **2003**, *107*, 8791.
[119] H. Günther, *NMR spectroscopy: basic principles, concepts, and applications in chemistry*, Wiley, **1995**.

b) Formation and characterization of supramolecular ensembles

Complexation studies of supramolecular ensembles **[23·21]** and **[23·21$_2$]** were performed by monitoring the changes in the absorption spectra of the porphyrin dimer **23** in DCM after addition of increasing quantities of fullerene derivative **21** at rt (Scheme 4.10).

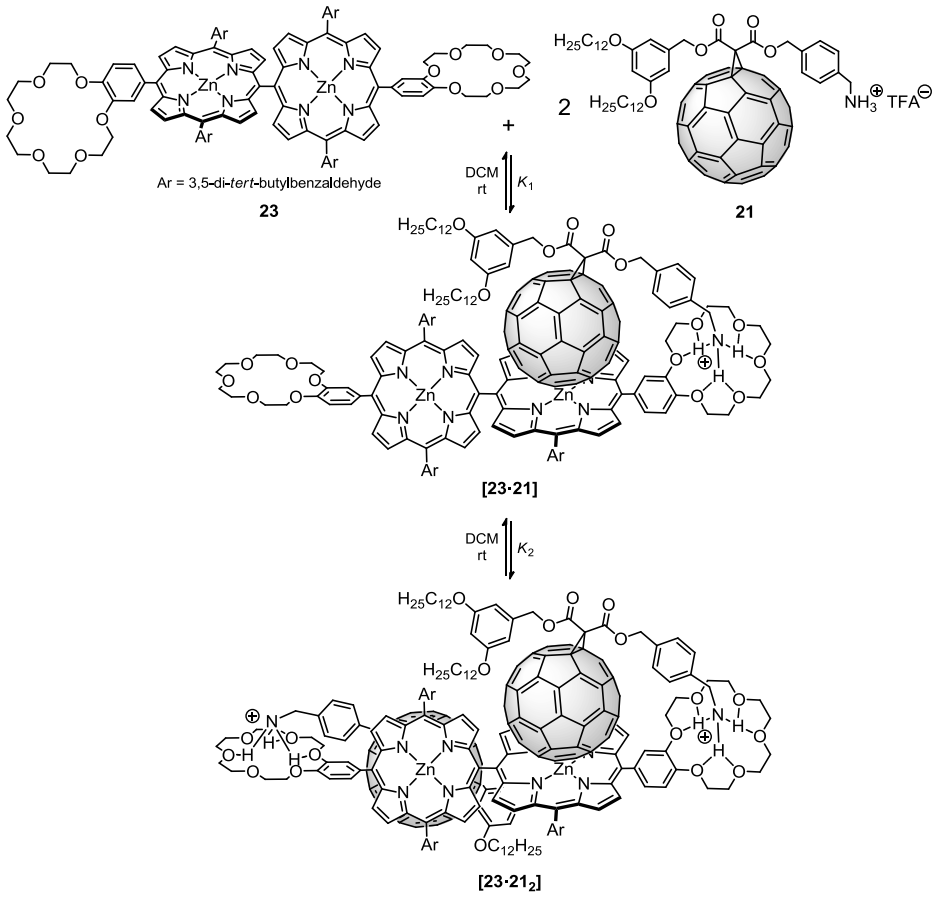

Scheme 4.10. Supramolecular complexes obtained from building blocks **23** and **21**.

Addition of increasing quantities of **21** to **23** resulted in a red shift of its Soret bands (λ_{1max} = 422 nm $\rightarrow$ 427 nm; λ_{2max} = 458 nm $\rightarrow$ 463 nm) evidencing the presence of intermolecular π-π interactions between the host and guest (Figure 4.9).

Based on the structure and the results previously obtained, a 1:2 stoichiometry was foreseen for this system, where one molecule of ammonium-fullerene **21** would be complexed by each of the porphyrin-crown ether subunits in **23** (Scheme 4.11). ESI-MS over a 1:2 mixture of **23** and **21** in DCM corroborated this by exhibiting a double charged ion peak at *m/z* 2461.0, which can be assigned to the 1:2 complex after loss of the TFA counteranions (calculated *m/z* 2461.0). The peak corresponding to the 1:1 mixture was not detected under these conditions, suggesting that **[23·21$_2$]** is the most abundant species in the analyzed solution (see Annex III.2.2).

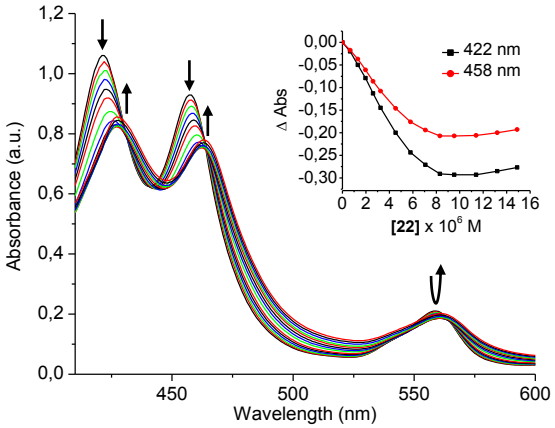

Figure 4.9. UV-vis spectral changes observed during the complexation of porphyrin dimer **23** ($4.72 \cdot 10^{-6}$ M) by addition of **21** (0-3.4 equiv by 0.3 equiv step) in DCM at rt. Inset shows the binding isotherm of the Soret bands.

Even though formed by a myriad of internal micro equilibria leading to semicomplexed species, the complexation of **23** by **21** can be simplified into a 2 steps process taking into account the tendency towards ring-closing of this system as evidenced in the model complex **[12-Zn·21]** (Scheme 4.11). Non-linear curve fitting to a 1:2 model yielded the binding constants of this system as reported by Table 4.2.

Table 4.2. Stepwise binding constants obtained for **[23·21$_2$]**.

log K_a ± 3σ	
log K_1	8.7 ± 1.4
log K_2	5.4 ± 0.9

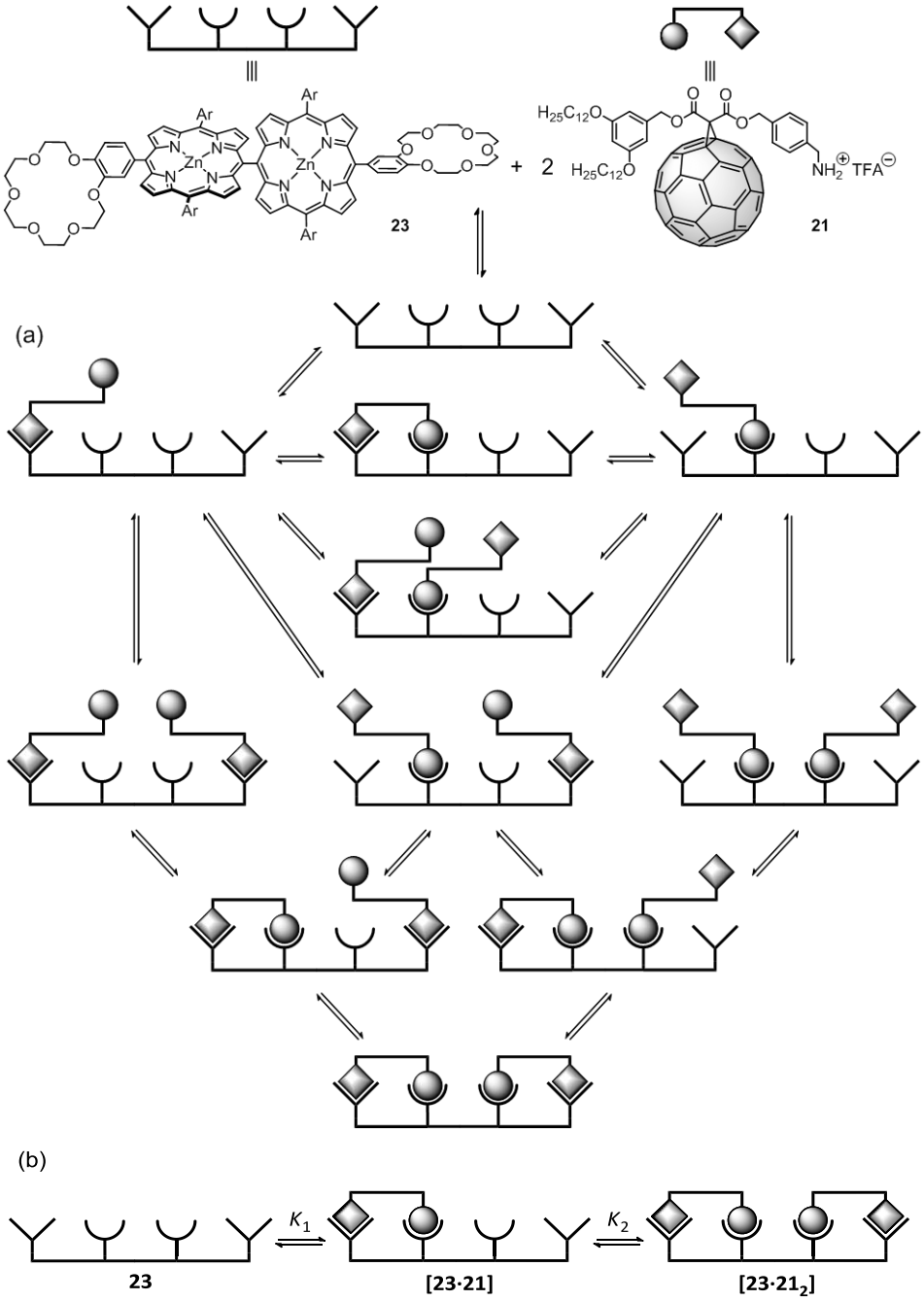

Scheme 4.11. The microscopic internal equilibria producing semicomplexed species (a) could be simplified into a 2 steps process (b) given the tendency towards ring closing of this system.

Surprisingly, the binding constant obtained for K_1 is much larger than that obtained in the case of the monoporphyrin (log K_1=8.7 *vs.* log K_a=6.9 respectively). Molecular modeling studies of the system evidences a close distance between the fullerene moiety and both porphyrin subunits (Figure 4.10), suggesting the existence of an additional interaction with the neighboring porphyrin moiety. This complementary recognition motif can be thus a plausible explanation for the experimental findings.

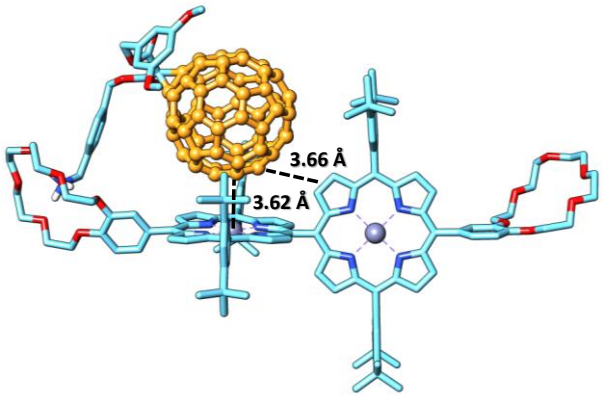

Figure 4.10. Spartan modelization of **[23·21]** (semi-empirical PM3 method, dodecyl chains have been substituted by methyl groups for ease of calculations) suggesting the existence of fullerene-porphyrin interactions with both porphyrin subunits.

A look at the shape of the binding isotherm also evidenced that it was not a standard hyperbola, thus pointing to possible cooperative effects (see Annex II). Even though each of the porphyrin subunits exhibits chelate cooperativity, we could consider the interaction between subunits as allosteric and, therefore, calculate the cooperative factor α as shown in **(4)** where $K \approx K_1$. The result clearly shows a negative cooperativity.

$$\alpha = \frac{K_1 K_2}{K^2} = \frac{K_2}{K_1} = \frac{10^{5.4}}{10^{8.7}} = 0.0005 \qquad \textbf{(4)}$$

This result can be explained on the base of the electronic communication between porphyrin moieties as in the porphyrin tape-sandwich developed by Aida.[89] Thus a complexation of a first fullerene molecule by a porphyrin subunit can deplete the electronic density of that porphyrin and its neighbor's, thus decreasing the affinity of the latter towards fullerenes.

4.2.2. Porphyrin tapes

a) Synthesis of porphyrin tape 24

Triply fused porphyrin tape **24** has been synthesized by using Sc^{III}-catalyzed oxidation of porphyrin **12-Zn** together with DDQ. These harsh conditions led to the product in an efficient manner. As in the previous case, the reaction was followed by treatment with a Zn(II) salt to ensure full metalation of the product (Scheme 4.12).

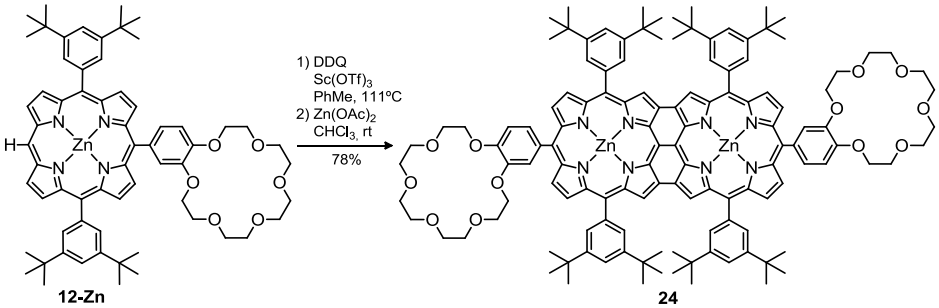

Scheme 4.12. Synthesis of porphyrin tape **24**.

Unfortunately, it was not possible to characterize this compound by NMR due to the formation of aggregates leading to very broad signals. However, its characteristic absorption spectrum, with a strong deformation and red shift of the bands reaching the IR (Figure 4.11) and MS allowed us to unambiguously characterize the product.

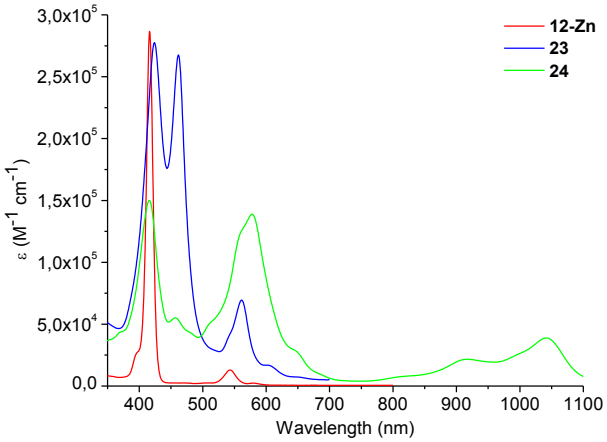

Figure 4.11. Comparison of the UV-vis spectra of **12-Zn** (red), **23** (blue) and **24** (green).

b) Formation and characterization of supramolecular ensembles

Complexation of **24** by **21** at rt was followed by monitoring the changes in the absorption spectra of the porphyrin array **24** (Scheme 4.13).

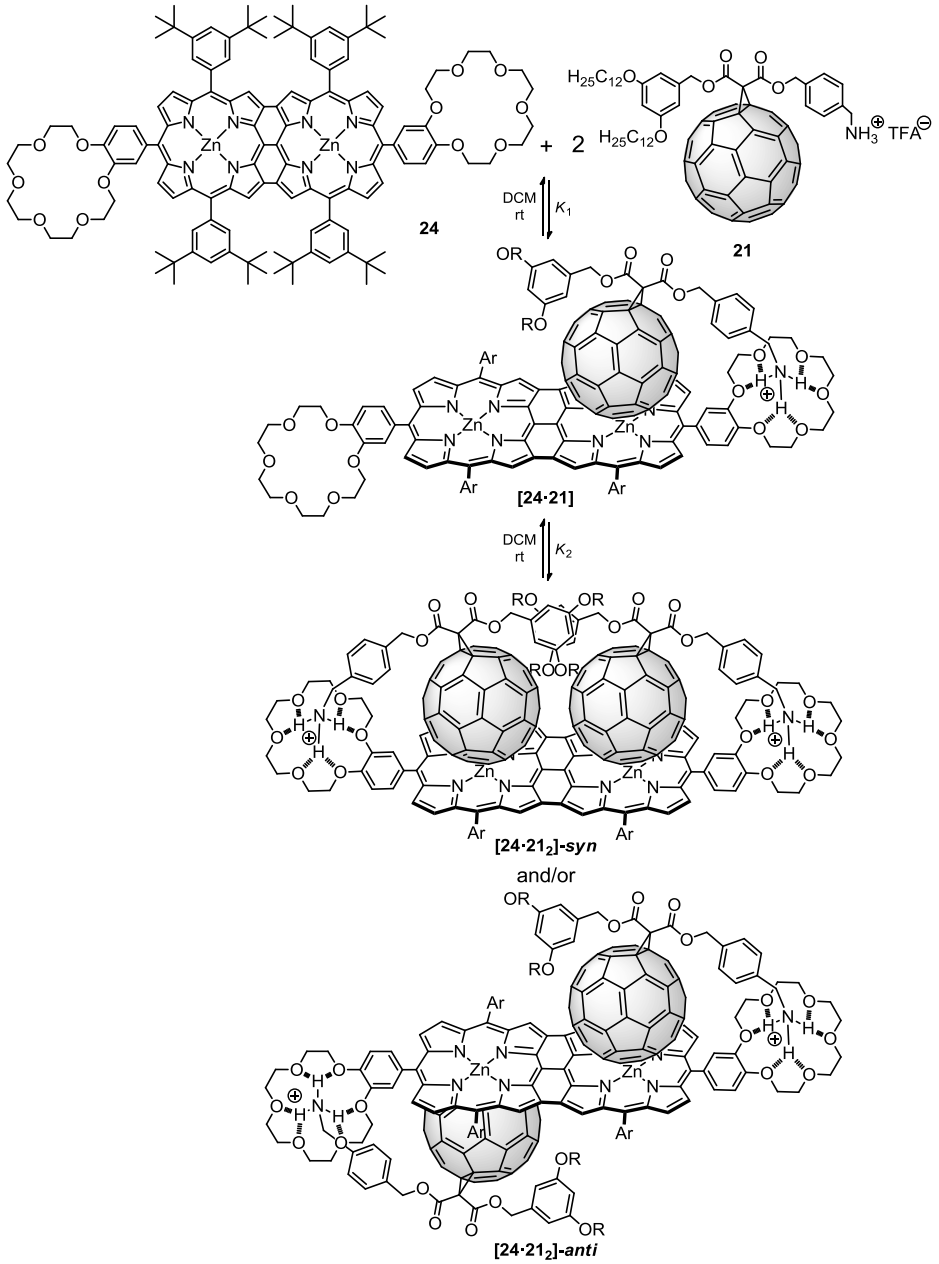

Scheme 4.13. Supramolecular complexes obtained from building blocks **24** and **21**.

Addition of increasing quantities of **21** to **24** in DCM resulted in the expected red shift of the Soret bands (λ_{1max} = 416 nm → 426 nm; λ_{2max} = 578 nm → 581 nm) arising from intermolecular porphyrin·fullerene π stacking. The Q-bands were also shifted to the red (λ_{3max} = 917 nm → 941 nm; λ_{4max} = 1042 nm → 1063 nm) (Figure 4.12).

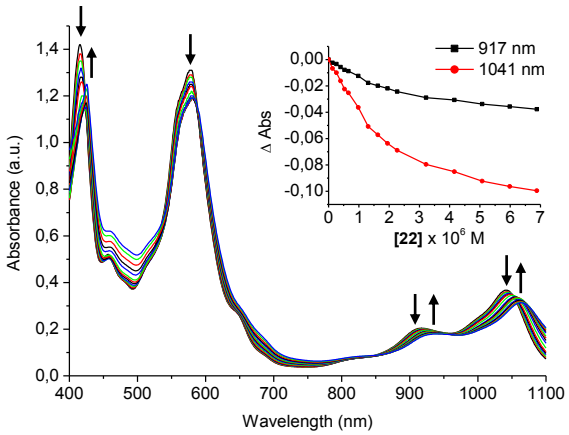

Figure 4.12. UV-vis spectral changes observed during the complexation of porphyrin array **24** ($1.18 \cdot 10^{-8}$ M) by addition of **21** (0-10.5 equiv by 0.7 equiv step) in DCM at rt. Inset shows the binding isotherm of the Q-bands.

ESI-MS analysis of a 1:2 mixture of **24** and **21** in DCM exhibited a double charged ion peak at *m/z* 2459.1 which can be assigned to the 1:2 complex after loss of the TFA counteranions (calculated 2459.0 *m/z*). The peak corresponding to the 1:1 mixture was not detected under these conditions (see Annex III.2.2).

As in the case of dimer **23**, the equilibria present in the systems could be simplified into a two-step binding process (Scheme 4.11). Non-linear curve fitting was therefore adjusted to a 1:2 system. Fitting was better when performed over the Q bands region (750-1100 nm) than over the Soret bands region, yielding the binding constants of the process as reported in Table 4.3.

Table 4.3. Stepwise binding constants obtained for **[24·21$_2$]**.

log K_a ± 3σ	
log K_1	6.8 ± 0.5
log K_2	5.4 ± 0.3

The shape of the binding isotherm obtained in this system was neither the expected rectangular hyperbola for a non-cooperative system (see Annex II). Calculations of the allosteric cooperativity factor by equation **(5)** justified the shape of the binding isotherm in sight of the negative cooperativity of the system.

$$\alpha = \frac{K_2}{K_1} = \frac{10^{5.4}}{10^{6.8}} = 0.04 \qquad \textbf{(5)}$$

The negative cooperativity obtained can be explained by a similar rationale than the one used for the *meso-meso* dimer, i.e. complexation of a fullerene moiety lowers the electronic density of the complexing porphyrin and its neighbor's, decreasing the affinity of the latter towards fullerenes. Interestingly, the cooperativity factor obtained this time is much larger than the one obtained for **[23·21$_2$]** (α=0.005).

As depicted in Scheme 4.13, the combination of 1 equivalent of host molecule **24** and two of guest molecule **21** can yield two different regioisomers, **[24·21$_2$]-*syn*** and **[24·21$_2$]-*anti***. Although it is not possible to ascertain which conformer is preferred in solution by spectroscopic measurements, modelization of **[24·21$_2$]-*syn*** (Figure 4.13) evidenced the possibility of having additional π-π interactions between both fullerene moieties, which are not possible in **[24·21$_2$]-*anti*** for geometrical reasons. The presence of this complementary interaction could be an explanation for the larger α value obtained in **[24·21$_2$]**, thus pointing to the *syn* conformer as that preferred in solution.

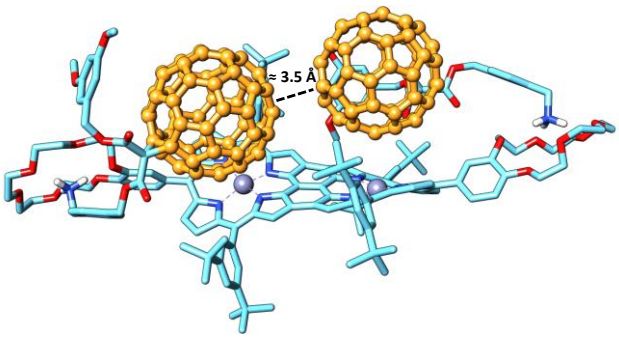

Figure 4.13. Spartan modelization of **[24·21$_2$]-*syn*** (semi-empirical PM3 method, dodecyl chains have been substituted by methyl groups for ease of calculations).

4.3. UNVEILING THE NATURE OF CROWN ETHER-C_{60} INTERACTIONS

4.3.1. Synthesis of the building blocks

Our exTTF based receptors were synthesized by a common synthetic route consisting in the esterification reaction of a crown ether carboxylic acid and 2,6-dihydroxy-exTTF **33** which, in turn, is obtained by a Horner-Wadsworth-Emmons reaction from anthraflavic acid **30** (Scheme 4.14).

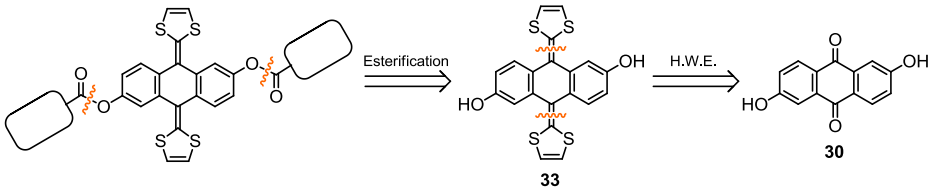

Scheme 4.14. Retrosynthetic analysis of the exTTF receptors.

Whereas (Benzo[18]crown-6)-4'-carboxylic acid **52** and (Benzo[15]crown-5)-4'-carboxylic acid **53** are commercially available, other crown ether derivatives had to be synthesized.

Thus, carboxylic acid **41** was obtained from catechol **36** by two successive *O*-alkylations and via intermediate **38** (Scheme 4.15).

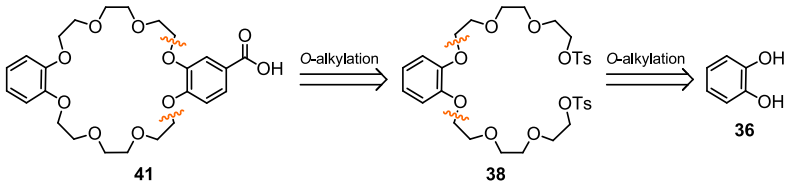

Scheme 4.15. Retrosynthetic analysis of carboxylic acid **41**.

Azacrown ether **47** synthesis involved a *N*-alkylation over benzocaine **42** followed by *O*-alkylation on intermediate **44** (Scheme 4.16).

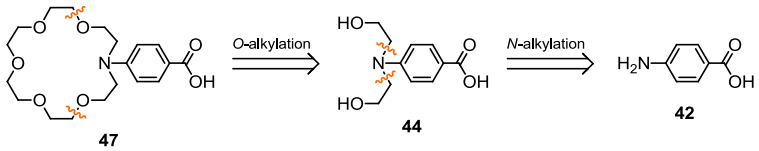

Scheme 4.16. Retrosynthetic analysis of carboxylic acid **47**.

Finally, azacrown ether **51** was obtained from **49** by a Hartwig-Buchwald cross coupling followed by basic hydrolysis (Scheme 4.17).

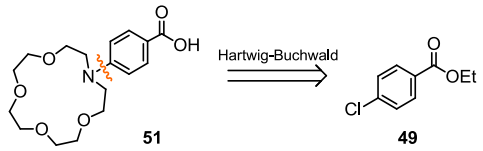

Scheme 4.17. Retrosynthetic analysis of carboxylic acid **51**.

a) Synthesis of 2,6-dihydroxy-exTTF

The required phosphonate for the Horner-Wadsworth-Emmons reaction was synthesized by a four steps procedure well established in our group. Commercially available vinylene trithiocarbonate **25** was methylated with Me_2SO_4, reduced with $NaBH_4$ and treated with HBF_4 to produce the respective intermediates **26**, **27** and **28**. Final treatment of cation **28** with $P(OMe)_3$ yielded phosphonate **29** in an excellent yield (Scheme 4.18).

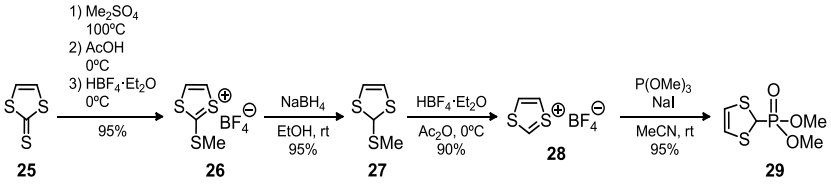

Scheme 4.18. Synthesis of phosphonate **29**.

Addition of *n*-BuLi over phosphonate **29** led to a very reactive, antiaromatic, 8π, anion which reacted readily with quinone **31** to form derivative **32**. Molecule **31** was obtained from anthraflavic acid **30** after protection of its hydroxy groups with TBDPS. Final treatment with TBAF led to the targeted exTTF **33** quantitatively (Scheme 4.19).

Purification of all the exTTF derivatives was made by flash chromatography using 1% Et_3N as cosolvent to prevent their degradation to the corresponding semiquinone derivative.

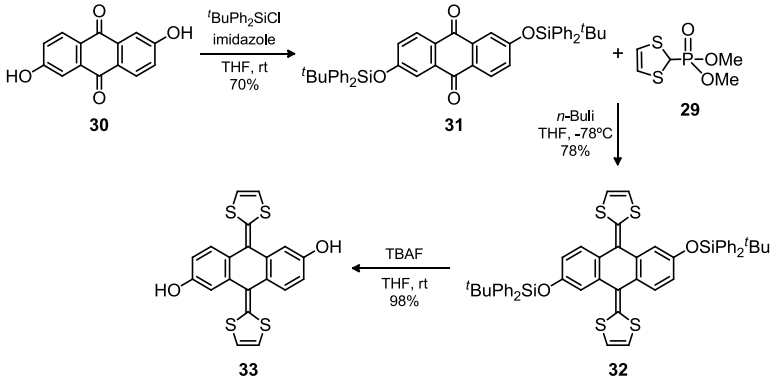

Scheme 4.19. Synthesis of 2,6-dihydroxy-exTTF **33**.

b) Synthesis of crown ether carboxylic acids

(Dibenzo[24]crown-8)-4'-carboxylic acid **41** was obtained from triethylene glycol **34** which was mono tosylated with TsCl to afford compound **35**. Subsequent reaction with catechol **36** in the presence of K_2CO_3 yielded diol **37**, whose hydroxy groups where again tosylated to produce molecule **38**. Macrocyclization with ethoxycarbonylcatechol **39** under basic conditions produced ester **40** in moderate yield, which was finally hydrolyzed to obtain the desired carboxylic acid **41** (Scheme 4.20).

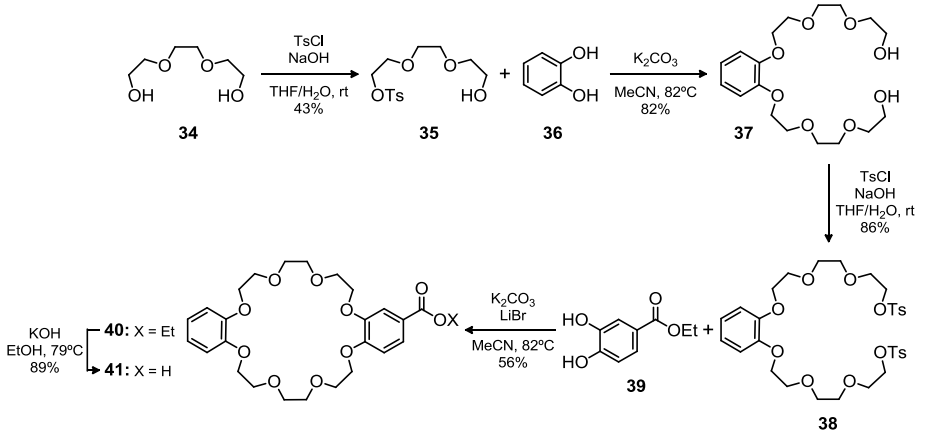

Scheme 4.20. Synthesis of (dibenzo[24]crown-8)-4'-carboxylic acid **41**.

N-(phenylaza[18]crown-6)-4'-carboxylic acid **47** was synthesized from benzocaine **42** and 2-chloroethanol **43** to yield intermediate **44**. Reaction with tetraethylene glycol di(*p*-toluenesulfonate) **45** afforded macrocycle **46**, which was finally hydrolyzed with KOH to obtain the desired product **47** (Scheme 4.21).

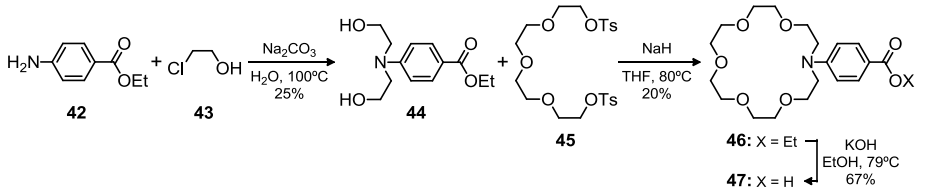

Scheme 4.21. Synthesis of *N*-(phenylaza[18]crown-6)-4'-carboxylic acid **47**.

Finally, *N*-(phenylaza[15]crown-5)-4'-carboxylic acid **51** was obtained by a Buchwald-Hartwig cross coupling amination[120] (Scheme 4.23) of aza[15]crown-5 **48** and ethyl-4-chlorobenzoate **49** to yield crown ether ester **50**. Basic hydrolysis of the ester afforded the targeted carboxylic acid **51** in moderate yield (Scheme 4.22).

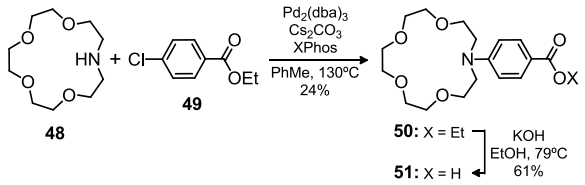

Scheme 4.22. Synthesis of *N*-(phenylaza[15]crown-5)-4'-carboxylic acid **51**.

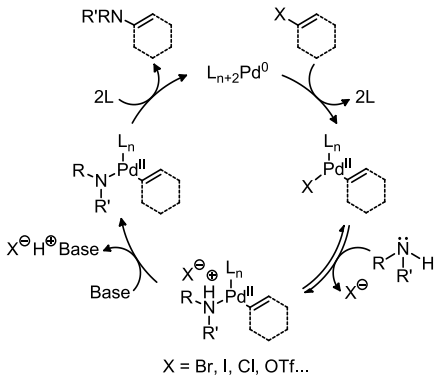

Scheme 4.23. Mechanism of the Buchwald-Hartwig amination.

[120] J. F. Hartwig, *Angew. Chem. Int. Ed.* **1998**, *37*, 2046.

c) Synthesis of exTTF-based receptors

The condensation of 2,6-dihydroxy-exTTF **33** with the carboxylic acids was achieved by two different methods:

The first one was based in the conversion of the corresponding acid into its acyl chloride by treatment with $(COCl)_2$ and a catalytic amount of DMF. This method was used with carboxylic acids **41** and **53**, obtaining the corresponding tweezers **55** and **57**. However, it was not effective with azacrown acid **47**. As a result, from that moment we changed conditions and employed EDC·HCl as a coupling reagent and DMAP as a catalyst. This method was effective with carboxylic acids **52**, **47**, **51** and **54** yielding their respective receptors **56**, **58** and **59** and **60** (Scheme 4.24).

All intermediates and products were unambiguously characterized by standard spectroscopic and analytical techniques. As an example, the ^{1}H-NMR of molecule **59** is shown in Figure 4.14.

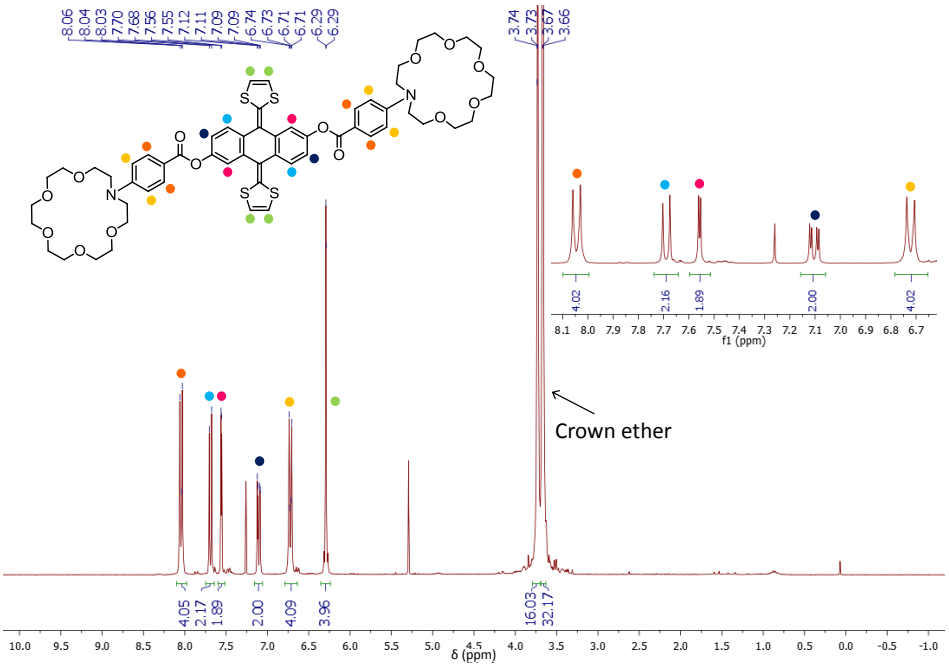

Figure 4.14. ^{1}H-NMR of host molecule **58**. Aromatic signals are depicted by colored bullets.

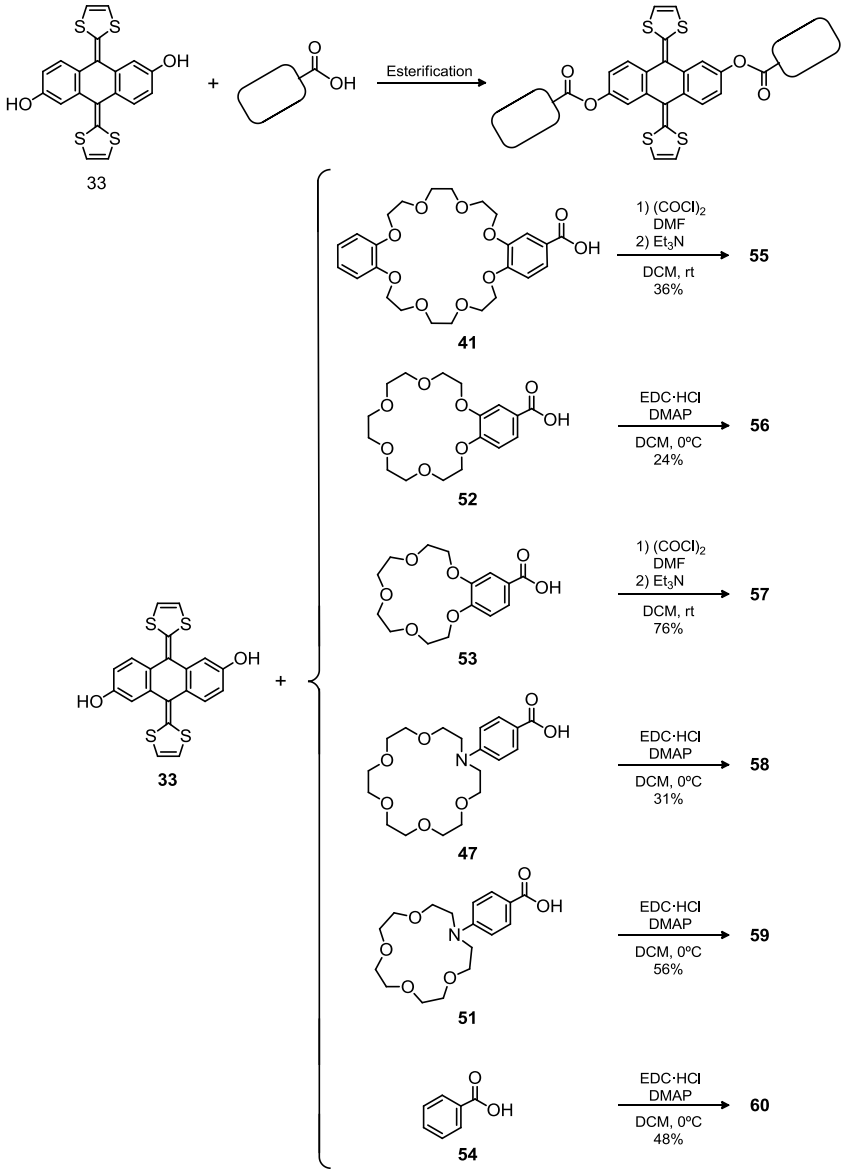

Scheme 4.24. Synthesis of exTTF based receptors **55**, **56**, **57**, **58**, **59** and **60**.

4.3.2. Formation and characterization of supramolecular ensembles

Prior to the study of the properties of our supramolecular ensembles we decided to evaluate their stability in solution. As previously reported by Beeby, Low and Bryce, exTTF derivatives form a radical cation upon photoionization in chlorinated hydrocarbon solutions, which subsequently disproportionates into its dication in degassed solutions or photodegrades into its semiquinone in aerated solutions[121] (Scheme 4.25).

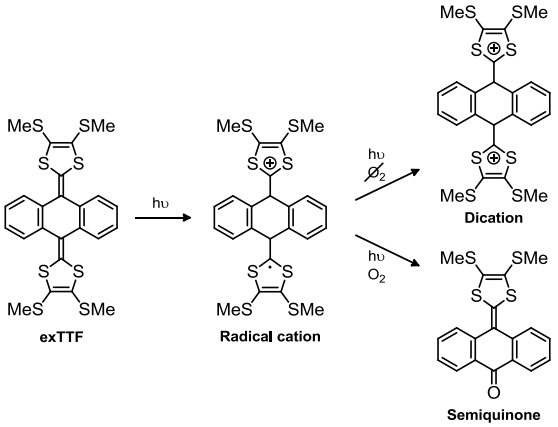

Scheme 4.25. Photoevolution of an exTTF derivative upon irradiation.

Thus, we first prepared a 10^{-5} M solution of **59** in ClPh without preventing air or light exposure and measured its UV-vis spectrum at different times. A "fresh" aliquot was taken at each measurement to avoid re-irradiation over the sample.

As with any neutral exTTF, the spectrum consisted of two strong bands at 367 and 435 nm. These bands did not change during the experiment proving the system to be stable in solution under these conditions. However, radiation with an UV lamp (365 nm) for 30 min led to a decrease of these bands and the appearance of a new one at 478 nm (Figure 4.15) arising from an intramolecular charge transfer in the semiquinone derivative. This result is in agreement with the findings of Beeby, Low and Bryce[121] and was confirmed by the appearance of a new red spot in the TLC.

[121] A. E. Jones, C. A. Christensen, D. F. Perepichka, A. S. Batsanov, A. Beeby, P. J. Low, M. R. Bryce and A. W. Parker, *Chem. Eur. J.* **2001**, *7*, 973.

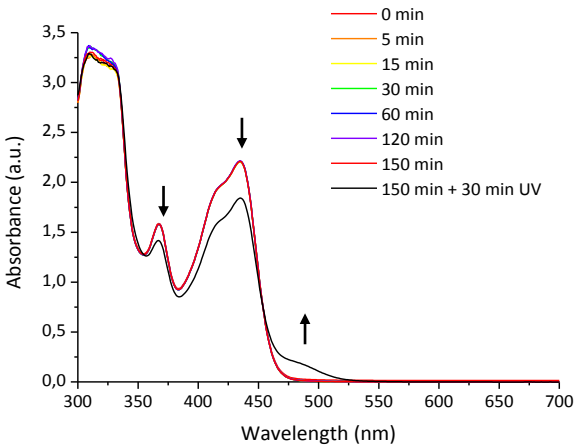

Figure 4.15. Stability of **59** in ClPh.

Then, we repeated the experiment in the presence of an equimolar amount of C_{60}. UV-vis spectroscopy showed **59** to exhibit an analogous response to C_{60} to the one seen for radiation, i.e. a decrease in the 435 nm and 367 nm exTTF bands and the appearance of a new broad band at 475 nm corresponding to the semiquinone derivative, as can be checked by the appearance of the characteristic red spot in TLC (Figure 4.16). These results thus evidence the impact of fullerenes as photosensitizers towards the exTTF platform.

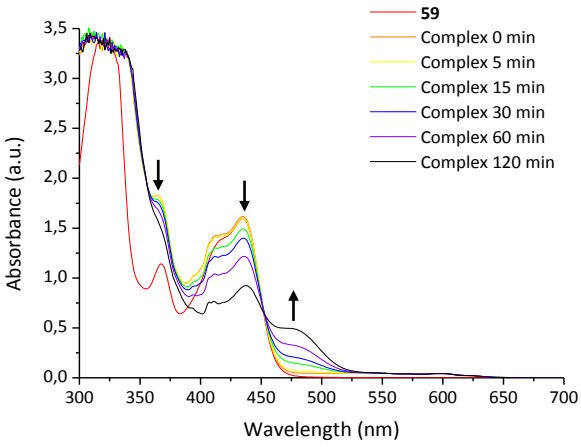

Figure 4.16. Stability of a **[59·C_{60}]** 1:1 mixture.

This sensitivity towards C_{60}, however, seems to be intimately related to the structure of the exTTF host molecule. When the stability experiments were repeated with an equimolecular **[57·C_{60}]** mixture, the decrease in the 435 nm band and the appearance of the 475 nm band was almost negligible (Figure 4.17).

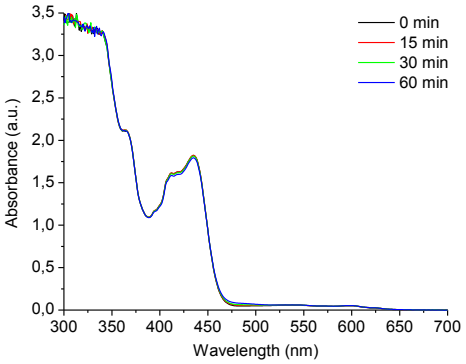

Figure 4.17. Stability of a **[57·C_{60}]** 1:1 mixture.

In order to account for these results and avoid any possible decomposition during the characterization of the ensembles, we took the following precautions: 1) Stock solutions of exTTF derivatives and C_{60} were degassed by bubbling Ar through them several minutes; 2) Host·guest mixtures were prepared in amber glass vials; 3) A new solution was prepared for each of the titration points and 4) C_{60} was only added immediately before the measurement.

Complexation studies were realized by monitoring the changes in the exTTF moiety spectra after adding increasing quantities of C_{60} at rt (Scheme 4.26). ClPh was chosen as solvent due to its high boiling point (131°C) ensuring minimal concentration variations related to evaporation and due to the high solubility of C_{60} (7 mg/mL) in it.

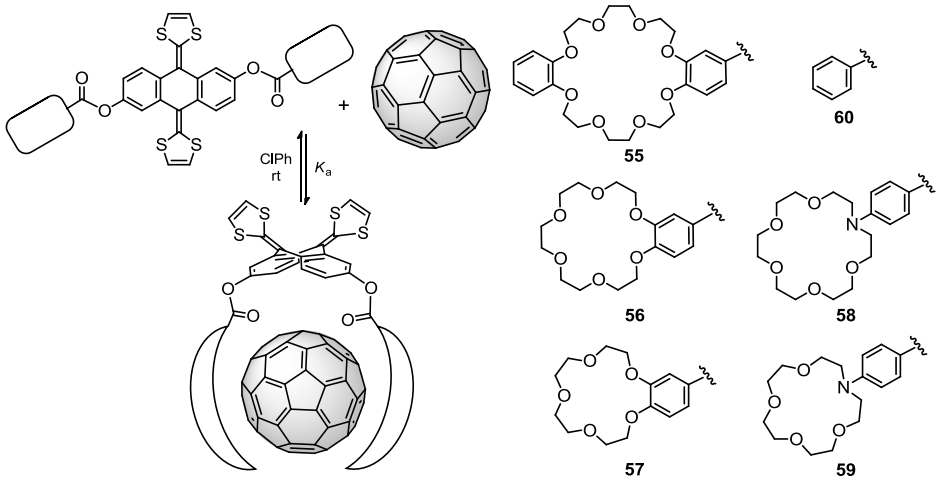

Scheme 4.26. Complexes obtained from exTTF based tweezers **55**, **56**, **57**, **58**, **59** and **60**.

As an example, the spectroscopic changes observed for **59** upon titration with C_{60} are depicted in Figure 4.18. At first sight there is an increase in the absorbance of all the bands due to spectral overlap. However, treatment of the data with Specfit software afforded the simulated profile of all the species in solution and revealed that upon complexation there is a decrease in the absorbance of the band at 435 nm and the appearance of a large charge transfer band at 475-650 nm.

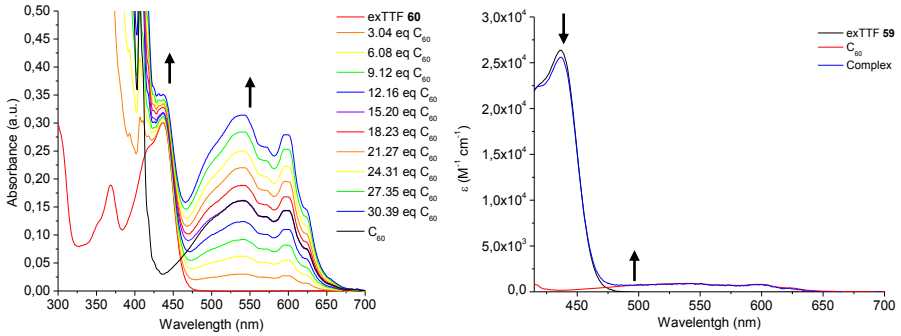

Figure 4.18. UV-vis spectral changes observed during the complexation of **59** by addition of C_{60} in ClPh at rt (left) and simulated profile of all species in solution (right).

Analogous results were observed in all cases and are in agreement with previous reports.[95],[98],[102] TLC analysis of the mixture revealed the absence of decomposition, as evidenced by the non-appearance of the red spot of semiquinone derivatives.

The large affinity of **55** towards C_{60} required to work in such high dilution conditions that the complexation induced spectroscopic changes were out of the range detection of the UV-vis spectrometer and thus only an approximate value is provided.

Based on our previous results,[103] a 1:1 stoichiometry was foreseen for these systems, which was evidenced in all the cases by MS over an equimolecular mixture of exTTF receptor and C_{60} in ClPh (see Annex III.3.1). As ESI-MS requires the presence of pre-existing ions in the solution, which was not the case of our molecules, and we preferred to avoid forming them *in situ* by the use of acids or base as cosolvents to maintain the integrity of the ensembles, we decided to use MALDI instead as the ionization source, which is not as soft as ESI but has been successfully used in the ionization of supramolecular ensembles. Solutions of the complexes were prepared

immediately before their analysis, mixed with the matrix (DCTB) and introduced into the spectrometer. Best results were obtained by using a linear negative mode in combination with a deflection to remove the signal of C_{60}.

This stoichiometry was also supported by the best fit of the experimental data to a 1:1 model. Binding constants of the system were obtained as reported in Table 4.4.

Table 4.4. Binding constants of the exTTF-(crown ether)$_2$ molecular tweezers.

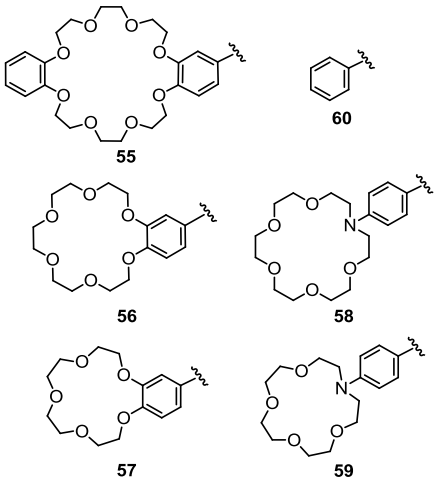

* Results previously published.[103]

Host	log K_a ± 3σ
55	> 7
56*	6.7 ± 0.2
57	4.1 ± 0.1
60	3.3 ± 0.4
58	5.1 ± 0.3
59	3.4 ± 0.3

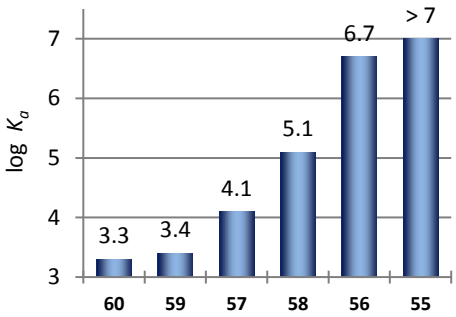

As can be seen from the experimental findings, the nature and size of the crown ether has a clear impact on the affinity towards [60]fullerene leading to a range of K_a oscillating more than three orders of magnitude. Azacrown ethers led to slightly lower binding constants whereas the larger the crown ether, the stronger the binding was.

Finally, it is interesting to note that host molecule **60** is the first example of an exTTF-based receptor for fullerenes relying only in one unit of exTTF and π-stacking interactions. This evidences the usefulness of expanding the conjugated surface available and may lead to new exTTF based receptors.

a) Electrochemical studies

Complexation of C_{60} by the exTTF derivatives was also studied by electrochemical means. Cyclic voltammetry was employed to monitor the complexation induced shift of the oxidation peak of the exTTF moiety and the reduction peaks of C_{60} in a 1:1 host/guest mixture. Measurements were carried out in ClPh in order to be able to estimate the binding constants of the system and 20% of MeCN was added in order to ensure the solubility of the supporting electrolyte.

Due to the higher instability of nitrogen containing exTTF conjugates, CV measurements were only made in systems **60**, **57**, **56** and **55**. As an example, the complexation induced changes of host molecule **55** upon addition of 1 equiv of C_{60} are depicted in Figure 4.19.

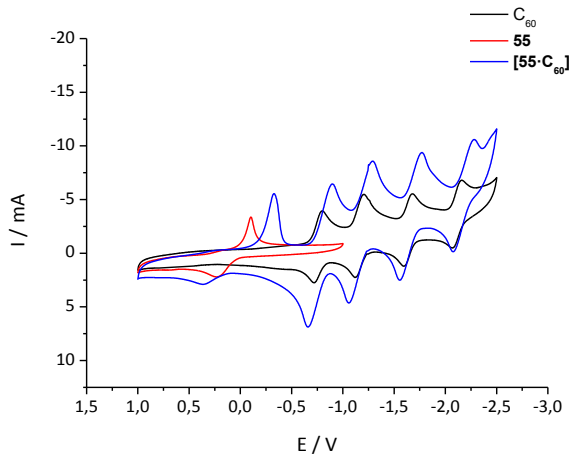

Figure 4.19. Cyclic voltammetry of C_{60}, **55**, and a 1:1 **55**/C_{60} mixture (SR: 100 mV/s. ClPh/MeCN 4:1. SE: *n*-Bu_4NPF_6 (0.1 M). WE: GCE. CE: Pt wire. 298 K).

The CVs of the exTTF derivatives show the characteristic two-electron quasi-reversible oxidation wave, corresponding to the oxidation to the respective dications. The cathodic shift of the wave corresponding to the reversion of dication to the neutral form is ascribed to the high activation barrier when re-reducing the dication, and is related to the planarization of the aromatic part of the molecule. Also, the CV of C_{60} shows the four first quasi-reversible one-electron reductions of fullerene, which is

able to accept up to six electrons in solution. The irregular shape of the exTTF waves can be explained on the basis of adsorption over the working electrode surface.

As can be seen in Figure 4.19, both the anodic peak of the exTTF moiety and the cathodic peaks of [60]fullerene were shifted, evidencing a donor-acceptor interaction in the ground state between the exTTF and the C_{60}. The same behavior was observed in the rest of the series (see Annex III.3.2) as summarized in Table 4.5.

Table 4.5. Redox potentials for C_{60} and compounds **60**, **57**, **56** and **55**.

	E^1_{ox} (a. p.)	E^1_{red} (c. p.)	E^2_{red} (c. p.)	E^3_{red} (c. p.)	E^4_{red} (c. p.)
C_{60}	—	-0.80	-1.19	-1.68	-2.16
60	0.20	—	—	—	—
[60·C_{60}]	0.30	-0.83	-1.23	-1.70	-2.19
57	0.22	—	—	—	—
[57·C_{60}]	0.37	-0.85	-1.24	-1.72	-2.23
56	0.26	—	—	—	—
[56·C_{60}]	0.33	-0.85	-1.24	-1.72	-2.22
55	0.23	—	—	—	—
[55·C_{60}]	0.36	-0.90	-1.30	-1.76	-2.28

Experimental conditions: V *vs*. Ag/Ag^+. Scan rate: 100 mV/s. Solvent: ClPh/MeCN 4:1. SE: *n*-Bu_4NPF_6 (0.1 M). WE: GCE. CE: Pt wire. 298 K.

These values do not lead to any correlation between the red-ox potentials of the donor and acceptor moieties and the binding constants of the supramolecular complexes obtained. This may evidence that other interactions such as n-π, CH-π and π-π -and not only donor-acceptor complementarity- are relevant in the formation of the supramolecular structures.

b) Computational studies

Computational studies were realized in collaboration with Prof. Enrique Ortí and his group in the Universitat de València.

A first analysis of the different conformations of the host molecules was made by using semiempirical PM7 calculations, proving that the energy differences between them are negligible (less than 1 kcal/mol) and that the largest differences arose from the rotation along the C-O (ester) single bond (see Annex III.3.3).

The geometrical parameters and the association energies of the complexes were obtained by DFT calculations in the vacuum (optimization level B97D/cc-pVDZ) and assuming a C_2 symmetry for the complexes as reported in Table 4.6 (see Annex III.3.3).

Table 4.6. Geometrical parameters of the complexes obtained from the exTTF based tweezers.

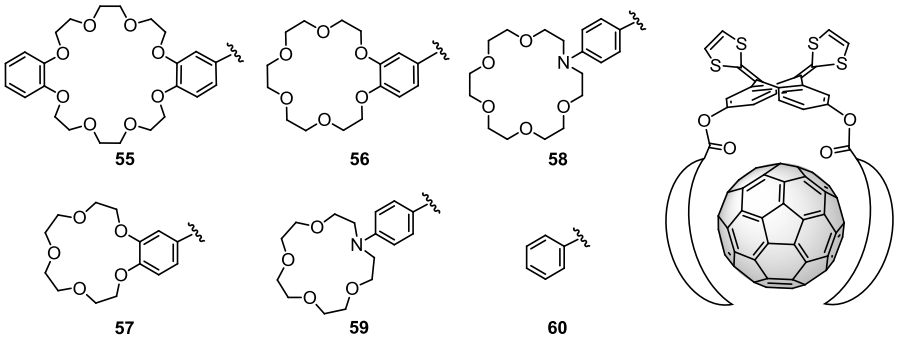

Host	nº H-C (< 3.20 Å)	nº O-C (< 3.80 Å)	bz-C (Å)	bz-bz (Å)	O-C (Å)	N-C (Å)	E_a (kcal/mol)	log K_a ± 3σ (rt, ClPh, UV)
55	12	10	2.96*	3.36*	3.37*	—	-54.36	> 7
56	10	12	2.95	3.45	3.42	—	-44.76	6.7 ± 0.2
58	10	10	3.06	3.37	3.14	3.50	-43.33	5.1 ± 0.3
57	8	8	2.99	3.46	3.30	—	-39.69	4.1 ± 0.1
59	10	4	3.41	3.37	3.25	4.14	-36.77	3.4 ± 0.3
60	—	—	3.25	3.45	3.16	—	-22.85	3.3 ± 0.4
exTTF	—	—	—	3.42	—	—	-10.24	—

* Asymmetric structure. The second bz-C, bz-bz and O-C distances are 2.99, 3.60 and 3.52 Å, respectively.

On the one hand, the interactions with the crown ether moiety are evidenced by the number of short H-C and O-C distances from C_{60}, corresponding respectively to CH-π and n-π interactions. The nitrogen atom in the azacrown ethers was also able to establish n-π interactions.

On the other hand, the interactions with the exTTF moiety and the peripheral rings are evidenced by the shortest distance between the centroid of each aromatic ring or the sp^3 oxygen and C_{60}, corresponding respectively to π-π and n-π interactions.

Therefore, the affinity of our molecular tweezers towards [60]fullerene arises from an interplay of π-π, n-π and CH-π interactions. As an example, the interactions present in **[58·C_{60}]** are depicted in Figure 4.20.

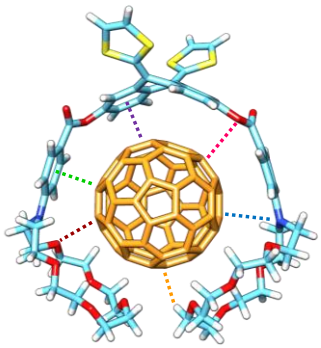

Figure 4.20. Stabilization of the exTTF-crown ether tweezers arises from a combination of n-π (•, • and •), π-π (• and •) and CH-π (•) interactions.

In view of the data obtained, the key parameters seem to be the CH-π and n-π interactions from the crown ether moiety as the larger they become, the larger the binding energy is, and as π-π and n-π interactions from the exTTF moiety/peripheral aromatic rings remain in the same range for all complexes. However, the later still play an important role in the binding of C_{60} as evidenced in **[60·C_{60}]**.

The additional benzene rings present in the crown ether moiety of **55** are also able to participate in the π stacking of both chromophores (bz-C distances are 3.13 and 3.68 Å) providing an additional recognition pattern. The lower affinity of azacrown ethers seems to be due to the geometrical changes, leading to more distorted structures.

Finally, the influence of embracing the fullerene by the crown ether was also studied using host molecules **56** and **57** as references and a PM7 level of calculation. Calculations evidence that this movement provides a huge stabilization of around 25-30% of the total binding energy (Table 4.7). This stabilization being higher, the larger the crown ether is.

Table 4.7. Effect of the embracing stabilization on the relative binding energy.

Conformer	E_{PM7} (kcal/mol)	ΔE_{PM7} (kcal/mol)
56 "open"	-50.71	-20.54
56 "closed"	-71.25	
57 "open"	-50.49	-17.63
57 "closed"	-68.12	

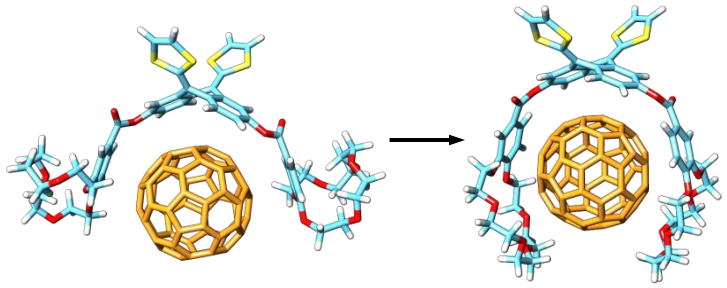

[56·C_{60}] "open" **[56·C_{60}]** "closed"

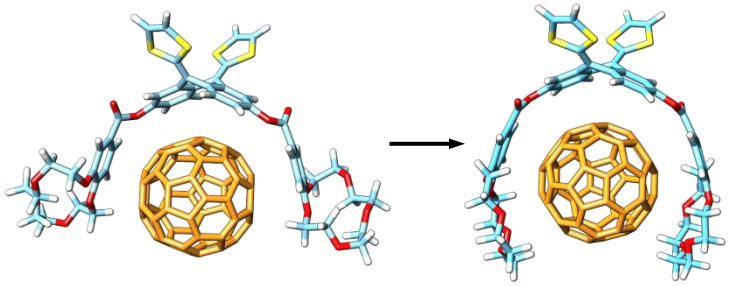

[57·C_{60}] "open" **[57·C_{60}]** "closed"

4.4. DESIGN AND SYNTHESIS OF NEW $(EXTTF)_2$-CROWN ETHER MOLECULAR TWEEZERS

4.4.1. Synthesis of the building blocks

The synthetic route to receptors **74** and **75** was based on the esterification of the corresponding exTTF derivative over carboxylic acid **73**, which in turn was obtained from catechol **69** after two *O*-alkylation reactions (Scheme 4.27).

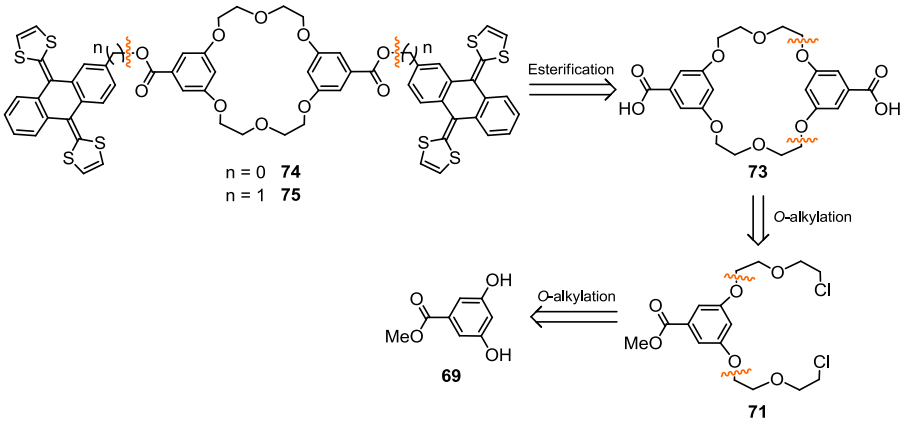

Scheme 4.27. Retrosynthetic analysis of receptors **74** and **75**.

The key reaction to obtain exTTF derivatives **64** and **68** was a Horner-Wadsworth-Emmons reaction over their corresponding alcohols, **61** and **65** (Scheme 4.28).

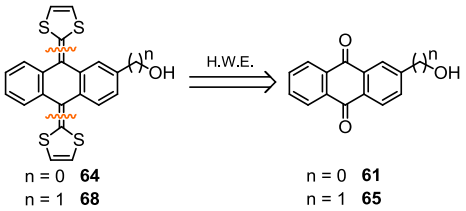

Scheme 4.28. Retrosynthetic analysis of the exTTF derivative moieties **64** and **68**.

a) Synthesis of exTTF derivatives

2-hydroxy-exTTF **64** and 2-hydroxymethyl-exTTF **68** were synthesized following a common synthetic route which starts from their corresponding alcohols **61** and **65**. Protection of their hydroxy groups with TBDPS produced their respective quinones **62**

and **66**, which were then reacted with the *in situ* generated carbanion of phosphonate **29** [see "4.3.1.a) Synthesis of 2,6-dihydroxy-exTTF", p. 91, for more details on the synthesis of the phosphonate] to yield exTTF derivatives **63** and **67**. Final deprotection of the protected alcohols afforded the targeted products **64** and **68**. (Scheme 4.29 and Scheme 4.30). The synthesis of molecule **64** proved to be more challenging due to its lower solubility.

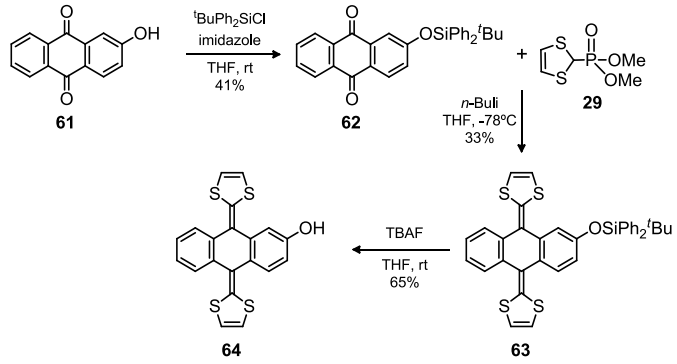

Scheme 4.29. Synthetic route to 2-hydroxy-exTTF **64**.

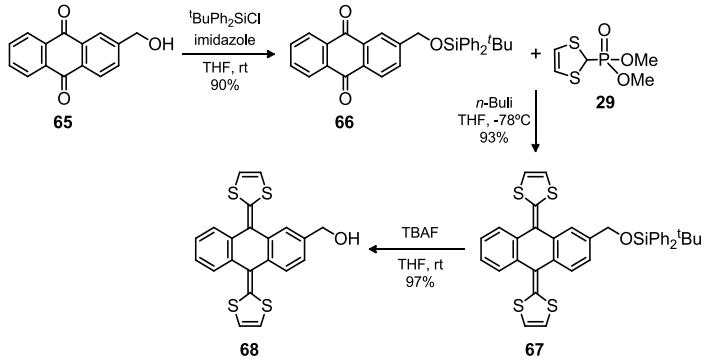

Scheme 4.30. Synthetic route to 2-hydroxymethyl-exTTF **68**.

b) Synthesis of the host

Commercially available methyl 3,5-dihydroxybenzoate **69** was first converted into its disodium salt by treatment with NaH and then reacted with a large excess of 2-chloroethyl ether **70** to produce intermediate **71**. Subsequent syringe pump

addition of **69** in the presence of K_2CO_3 as base, TBAI and high dilution conditions yielded macrocycle **72** in moderate yield. Hydrolysis of the methyl esters by TBAOH afforded the dicarboxylic acid **73** where both 2-hydroxy-exTTF **64** and 2-hydroxymethyl-exTTF **68** were introduced in moderate yield by a esterification reaction using EDC·HCl and DMAP as coupling agents, thus obtaining receptors **74** and **75** (Scheme 4.31).

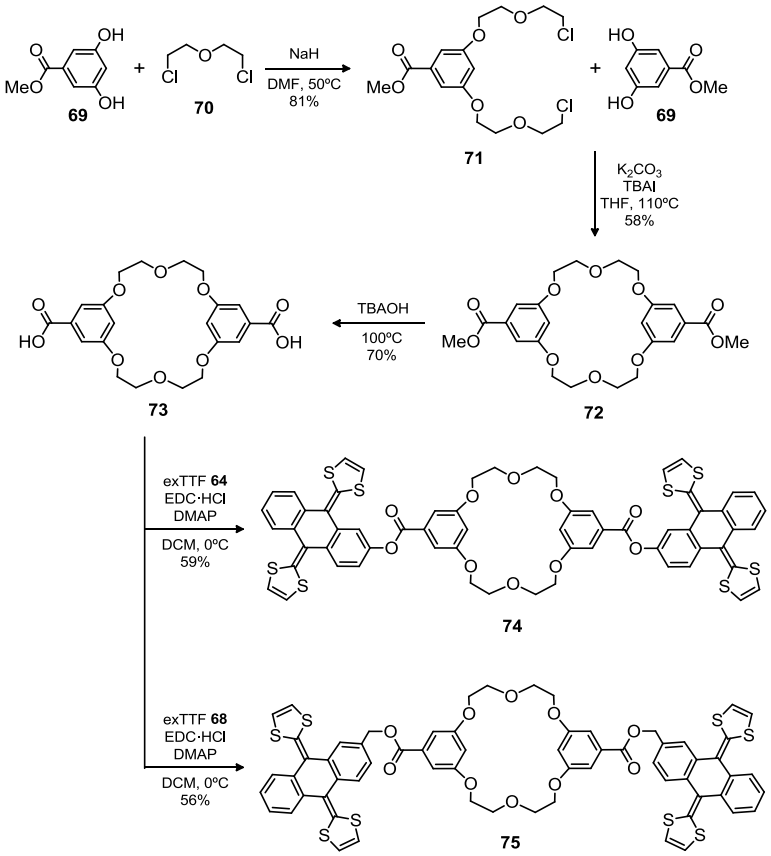

Scheme 4.31. Synthetic route to exTTF based receptors **74** and **75**.

Both receptors were unambiguously characterized by spectroscopic methods. As an example, the ^{1}H-NMR of molecule **75** is shown in Figure 4.21.

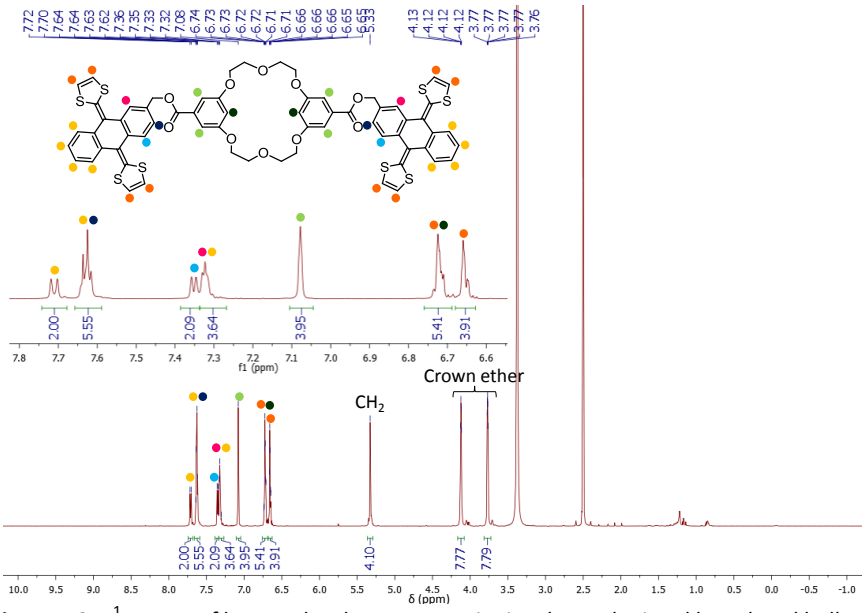

Figure 4.21. ^{1}H-NMR of host molecule **75**. Aromatic signals are depicted by colored bullets.

4.4.2. Formation and characterization of supramolecular ensembles

Complexation of C_{60} by **74** and **75** was followed by monitoring the changes in the absorption spectra of the exTTF moiety at rt upon addition of increasing quantities of C_{60} (Scheme 4.32). The same experimental conditions and precautions as in Chapter 4.3. (see p. 98) were used.

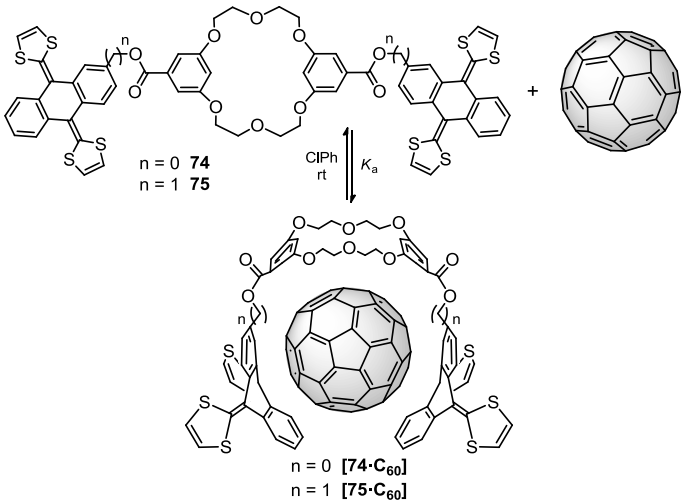

Scheme 4.32. Complexes obtained from exTTF based tweezers **74** and **75**.

As in the previous exTTF-based tweezers, the spectroscopic changes observed for **74** and **75** upon titration with C_{60} correspond to an increase in the absorbance of all the bands identical to the observed in Figure 4.18. Treatment of the data with Specfit revealed that, upon complexation, these systems also experience a decrease in the absorbance of the band at 435 nm and the appearance of a large charge transfer band at 475-650 nm.

The 1:1 stoichiometry foreseen for these systems was evidenced by MS-MALDI over an equimolecular mixture of the molecular tweezer and C_{60} in ClPh (see Annex III.4.1). As in the previous cases, best results were obtained by using a linear negative mode in combination with a deflection to remove the signal of C_{60}. The stoichiometry was also supported by the best fit of the experimental data to a 1:1 model. Binding constants of the systems were obtained as reported in Table 4.8.

Table 4.8. Binding constants of the $(exTTF)_2$-crown ether molecular tweezers.

Complex	log K_a ± 3σ
[74·C_{60}]	5.0 ± 0.4
[75·C_{60}]	6.5 ± 0.6

In spite of the widespread principle of preorganization, which states that the affinity towards a guest molecule increases when the host has a well defined structure,[122] the use of rigid host molecule **74** led to a lower binding constant than in more flexible host **75**. In view of the experimental results, this larger flexibility is a key factor in the affinity towards fullerene.

As a corollary, we can state that it is important to find an equilibrium between the synthetic costs of obtaining highly preorganized hosts and the benefits of having flexible systems which may have a better chance to adapt to the guest surface.[123],[124]

[122] J. B. Wittenberg and L. Isaacs, in *Supramol. Chem.*, John Wiley & Sons, Ltd, **2012**.
[123] a) M. C. Misuraca, T. Grecu, Z. Freixa, V. Garavini, C. A. Hunter, P. W. N. M. van Leeuwen, M. D. Segarra-Maset and S. M. Turega, *J. Org. Chem.* **2011**, *76*, 2723; b) Z. Zhong, X. Li and Y. Zhao, *J. Am. Chem. Soc.* **2011**, *133*, 8862.

Noteworthy, the binding constant obtained with **[74·C_{60}]** is lower than its exTTF-(crown ether)$_2$ analogue **[56·C_{60}]**. This demonstrates the great potential of crown ethers as recognition motifs for fullerenes, comparable –or even better– than that of the well established complementary exTTF.

a) Electrochemical studies

Complexation of C_{60} by **74** and **75** was also studied by electrochemical means. Cyclic voltammetry measurements were carried out under the same conditions used in Chapter 4.3 (see p. 101). As in the previous cases, the CVs of the exTTF derivatives showed the characteristic wave corresponding to their oxidation to their respective dications, while C_{60} exhibited its four first reduction waves.

Upon complexation, both the anodic peak of the exTTF moiety and the cathodic peaks of C_{60} were shifted in the two complexes (Table 4.9), evidencing a donor-acceptor interaction in the ground state between both moieties (see Annex III.4.2).

However, as for exTTF-(crown ether)$_2$ derivatives, the magnitude of the shifts does not correlate with the binding constants of the supramolecular complexes obtained, suggesting that other interactions, apart from the donor-acceptor complementarity, are relevant in the formation of the supramolecular structures.

Table 4.9. Redox potentials for compounds **74** and **75** and their complexes with C_{60}.

	E^1_{ox} (a. p.)	E^1_{red} (c. p.)	E^2_{red} (c. p.)	E^3_{red} (c. p.)	E^4_{red} (c. p.)
C_{60}	—	-0.80	-1.19	-1.68	-2.16
74	0.27	—	—	—	—
[74·C_{60}]	0.21	-0.82	-1.21	-1.69	-2.19
75	0.14	—	—	—	—
[75·C_{60}]	0.21	-0.81	-1.22	-1.70	-2.23

Experimental conditions: V vs Ag/Ag^+. Scan rate: 100 mV/s. Solvent: ClPh/MeCN 4:1. SE: *n*-Bu_4NPF_6 (0.1 M). WE: GCE. CE: Pt wire. 298 K.

[124] H. J. Hogben, J. K. Sprafke, M. Hoffmann, M. Pawlicki and H. L. Anderson, *J. Am. Chem. Soc.* **2011**, *133*, 20962.

5. Conclusions

5. CONCLUSIONS

The work developed in this study has provided valuable information on the key role of crown ethers in the supramolecular chemistry of fullerenes.

Notably, we have gained further knowledge in the nature of two supramolecular interactions which were not very well understood previously: π-π stacking between C_{60} and porphyrins and the affinity of crown ethers towards fullerenes.

We have also further studied the supramolecular properties of porphyrin arrays, largely unexplored up to now.

The respective results obtained in each of the systems developed in the present study can be summarized as follows:

Chapter 4.1. *Effect of the metal atom on the binding constant between metalated porphyrins and C_{60}.*

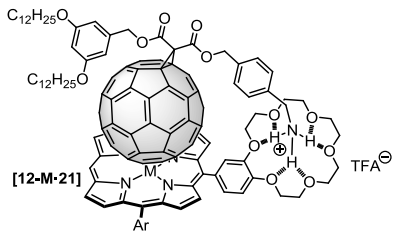

- A new series of cup-and-ball C_{60}–porphyrin conjugates with different metal atoms has been obtained. The study of their supramolecular properties has allowed us to gain further knowledge on the nature of the π-stacking between both chromophores, suggesting that it is mainly governed by van der Waals forces.
- The chelate cooperativity of these complexes has been assessed by calculating the effective molarity of the system. For this, each of the interactions leading to the complex has been evaluated separately. A value of 3.16 M has been obtained.
- Their ability to form further aggregates with higher stoichiometries has been suggested by ^{1}H-NMR studies and, therefore, it cannot be ruled out.

Chapter 4.2. *Supramolecular properties of directly linked porphyrin arrays.*

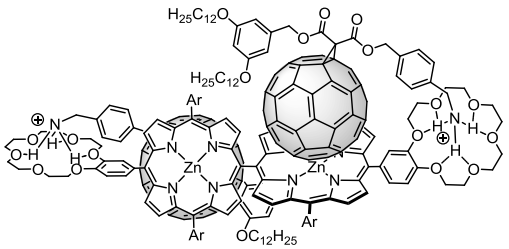

[23·21$_2$]

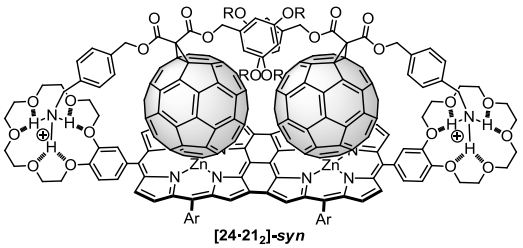

[24·21$_2$]-*syn*

- The supramolecular properties of both *meso-meso* and *meso-meso*, *β-β*, *β'-β'* porphyrin arrays have been studied. The electronic communication between both porphyrin moieties has been demonstrated to have a strong impact on their affinity for C_{60}, resulting in negative cooperative effects.
- The orthogonal disposition of both porphyrins in **[23·21$_2$]** offers an additional recognition motif for C_{60}. This led to an increase of the binding constant in the 1:1 complexes in comparison to the value obtained by using a monoporphyrin as host.
- The possibility of having additional π-interactions between the fullerene subunits in **[24·21$_2$]-*syn*** has been suggested.

Chapter 4.3. *Unveiling the nature of crown ether-C_{60} interactions.*

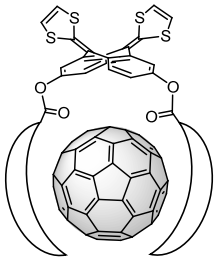

- A new series of exTTF-(crown ether)$_2$ molecular tweezers with different ring size and composition has been synthesized in order to unveil the nature of crown ether-C_{60} supramolecular interactions.

- DFT calculations on the modelized complexes suggest that the affinity of our receptors towards C_{60} arises from an interplay of π-π, n-π and CH-π interactions.
- The great stability arising from "embracing" the fullerenes (25-30% of the total) has been evidenced.

Chapter 4.4. *Design and synthesis of new (exTTF)$_2$-crown ether molecular tweezers.*

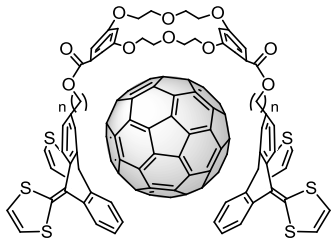

n = 0 **[74·C_{60}]**
n = 1 **[75·C_{60}]**

- Two new (exTTF)$_2$-crown ether molecular tweezers with different degrees of flexibility have ben synthesized.
- The use of rigid host molecule **[74·C_{60}]** led to a lower binding constant than in more flexible **[75·C_{60}]**. This proves that an increase in the preorganization of the host molecule does not always lead to higher affinities towards the guest, being also important to search a proper complementarity between host and guest.
- The binding constant of **[75·C_{60}]** is comparable to the one obtained for their exTTF-(crown ether)$_2$ analogue, further demonstrating the great potential of crown ethers as recognition motifs for fullerenes.

6. Experimental section

6. EXPERIMENTAL SECTION

6.1. GENERALITIES

Reagents were used as purchased from commercial sources without further purification with the exception of pyrrole, which was filtered through an Al_2O_3 gel column prior to use to remove polymers. Solvents were dried and distilled using standard techniques.[125] All reactions were performed in standard glassware under an inert Ar atmosphere.

Microwave reactions: were performed in sealed vessels in an Anton Paar Monowave 300. Reaction mixture temperature was controlled with an external surface sensor.

Analytical thin-layer chromatography: was performed using aluminum coated Merck Kieselgel 60 F_{254}. Visualization was made by I_2 vapor or UV light (λ = 254 or 365nm).

Purification of crude reaction mixture: was achieved either by a) flash chromatography (FC) using SiO_2 gel (Merck, Kieselgel 60, 40-63 µm, 230-400 mesh) or neutral Al_2O_3 gel (Panreac), b) gravity-fed column chromatography (CC) using SiO_2 gel (Scharlau, Kieselgel 60, 0.06-0.2 mm, 70-230 mesh) or c) gel permeation chromatography (GPC) (Biorads Biobeds SX-1). Demetalated SiO_2 gel was prepared as previously reported:[126] 1 kg of SiO_2 gel was mechanically stirred with 2 L of 10% HCl until complete wetting was assured. The acidic aq phase was decanted off, and the silica subsequently washed 15–20 times with distilled H_2O by decantation until pH≈4. Subsequently, 1 L of distilled H_2O was added along with 1 mL of aq ammonia (25%). The aq phase was decanted and the silica oven-dried at 150 °C for a minimum of 24 h prior to use for chromatography.

Melting points: were determined on a Gallenkamp apparatus and are uncorrected.

[125] W. L. F. Armarego and C. L. L. Chai, *Purification of Laboratory Chemicals*, Elsevier, **2003**.
[126] T. E. Nielsen, S. L. Quement, M. Juhl and D. Tanner, *Tetrahedron* **2005**, *61*, 8013.

NMR spectra: were recorded on a Bruker DPX-300, Bruker AC-400 or Bruker AVIII-700 spectrometer at 298K using partially deuterated solvents as internal standards. Multiplicities are denoted as follows: s = singlet, d = doublet, t = triplet, m = multiplet, br = broad, dd = double doublet.

IR spectra: were determined on a Bruker Tensor 27 (ATR device) spectrometer. Only neat picks are reported.

UV-vis spectra: were recorded with a Shimadzu Spectrophotometer UV-3600 at 298K. Temperature variable experiments were performed in a JASCO Corp., V-630.

Mass spectra: were realized by the mass spectra services at the Universidad Autónoma de Madrid. MALDI-TOF experiments were taken on a Brucker Ultraflex III using DCTB + NaI as matrix. ESI-MS spectra were performed on a Q-Star Applied Biosystem mass spectrometer.

Cyclic voltammetry: was performed using an Autolab PGStat 30. Measurements were made in a double-walled cell (Metrohm EA 876-20). A glassy carbon working electrode (Metrohm 6.0804.010) was used after being polished with alumina (30 μ) for 1 min, and platinum wire was used as the counter electrode. A $Ag/AgNO_3$ electrode was used as reference. *n*-Bu_4NPF_6 (0.1 M) was used as supporting electrolyte and ClPh/MeCN 4:1 as solvent. The samples were purged with Ar prior to measurement. Scan rate was 100 mV/s.

6.2. SYNTHESIS OF COMPOUNDS

2,2'-Dipyrrylmethane, 3.[127]

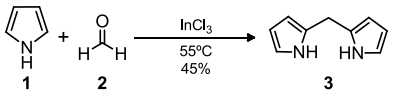

A mixture of pyrrole **1** (347 mL, 5.00 mol) and formaldehyde **2**, generated *in situ* from paraformaldehyde (1.50 g, 0.05 mol) in a 500-mL flask was degassed with a stream of Ar for 10 min. The mixture was heated at 55°C for about 10 min to obtain a clear solution. $InCl_3$ (1.11 g, 0.05 mol) was then added, and the mixture was stirred at 55 °C for 2.5 h. The heat source was removed, and K_2CO_3 (20.7 g, 0.15 mol) was added. The mixture was stirred for 1 h and then filtered. The filtrate was concentrated, and the pyrrole was recovered. The crude solid obtained after removing pyrrole was extracted with 20% AcOEt/cyclohexane. The solvent was evaporated *in vacuo*. Crystallization ($MeOH/H_2O$, 4:1) afforded **3** as pale white crystals (3.29 g, 45%).

^{1}H NMR (250 MHz, $CDCl_3$) δ: 7.62 (m, 2H), 6.60 (m, 2H), 6.19 (m, 2H), 6.07 (bs, 2H), 3.92 (s, 2H).

3,5-Di-*tert*-butyl(bromomethyl)benzene, 5.[127b]

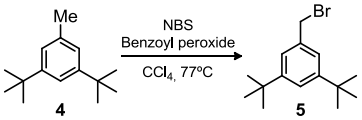

A mixture of commercially available 3,5-di-*tert*-butyltoluene **4** (90 g, 0.44 mol), NBS (135 g, 0.66 mol) and benzoyl peroxide (1g, 0.04 mol) in CCl_4 (800 mL) was refluxed for 3h. The solution was cooled, filtered and concentrated under reduced pressure. The crude residue **5** (125 g) was used without further purification in the next step.

[127] a) J. K. Laha, S. Dhanalekshmi, M. Taniguchi, A. Ambroise and J. S. Lindsey, *Org. Process Res. Dev.* **2003**, *7*, 799; b) M. J. Plater, S. Aiken and G. Bourhill, *Tetrahedron* **2002**, *58*, 2405.

3,5-Di-*tert*-butylbenzaldehyde, 6.[127b]

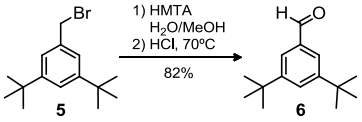

A mixture of compound **5** (125 g, 0.44 mol) and HMTA (256 g, 1.83 mol) in MeOH/H_2O (500 mL, 1:1) was refluxed for 4h. Concentrated aq HCl (150 mL) was added dropwise and the mixture refluxed for 30 min. The solution was cooled and extracted with DCM, the solvent removed *in vacuo* and the residue recrystallized from EtOH/H_2O to give the product **6** (79 g, 82%) as a white crystalline solid.

^{1}H NMR (250 MHz, $CDCl_3$) δ: 10.00 (s, 1H), 7.71 (m, 3H), 1.35 (s, 18H).

5,15-*Bis*-(3,5-di-*tert*-butylphenyl)porphyrin, 7.[128]

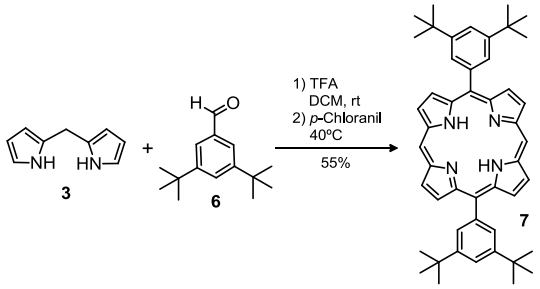

In a round bottom flask, a solution of **3** (2.4 g, 16.42 mmol) and **6** (3.8 g, 17.40 mmol) in DCM (4 L) was deoxygenated by bubbling Ar through for 1 h. TFA (432 mg, 3.66 mmol) was added dropwise, and the mixture was vigorously stirred in the dark for 16 h at rt. *p*-Chloranil (12.32 g, 50.10 mmol) was added and the mixture heated to 70°C for 2 h, then it was concentrated *in vacuo*. CC (SiO_2, cyclohexane/DCM, 1:1 + 1% Et_3N v/v) and precipitation from DCM upon addition of MeOH yielded **7** as a violet solid (3.12 g, 55%).

^{1}H NMR (300 MHz, $CDCl_3$) δ: 10.31 (s, 2 H), 9.41 (d, *J* = 4.5 Hz, 4 H), 9.15 (d, *J* = 4.5 Hz, 4 H), 8.16 (d, *J* = 2.0 Hz, 4 H), 7.85 (t, *J* = 2.0 Hz, 2 H), 1.59 (s, 36 H), -3.00 (s, 2H).

[128] D. Bonifazi, G. Accorsi, N. Armaroli, F. Song, A. Palkar, L. Echegoyen, M. Scholl, P. Seiler, B. Jaun and F. Diederich, *Helv. Chim. Acta* **2005**, *88*, 1839.

Zinc(II) 5,15-*Bis*-(3,5-di-*tert*-butylphenyl)porphyrin, 8.[128]

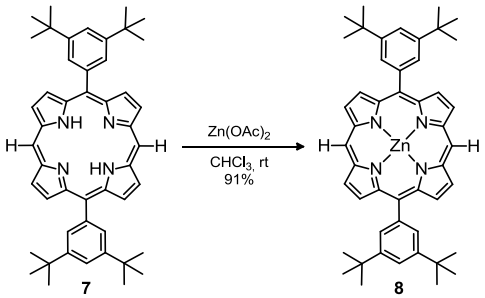

To a vigorously stirred solution of the free base porphyrin **7** (2.6 g, 3.79 mmol) in $CHCl_3$ (150 mL), a solution of $Zn(OAc)_2{\cdot}(H_2O)_2$ (8.32 g, 37.90 mmol) in MeOH (150 mL) was added in the dark at 25°C. After 2 h, the organic phase was washed with H_2O, dried (Na_2SO_4) filtered and evaporated *in vacuo*. CC (SiO_2, cyclohexane/DCM, 2:1 + 1% Et_3N v/v) and precipitation from DCM upon addition of MeOH provided the titled compound **8** as a red powder (2.48 g, 91%).

^{1}H NMR (300 MHz, $CDCl_3$) δ: 10.34 (s, 2 H), 9.46 (d, *J* = 4.5 Hz, 4 H), 9.21 (d, *J* = 4.5 Hz, 4 H), 8.15 (d, *J* = 2.0 Hz, 4 H), 7.85 (t, *J* = 2.0 Hz, 2 H), 1.58 (s, 36 H).

Zinc(II) 5,15-*Bis*-(3,5-di-*tert*-butylphenyl)-10-iodoporphyrin, 9.[128]

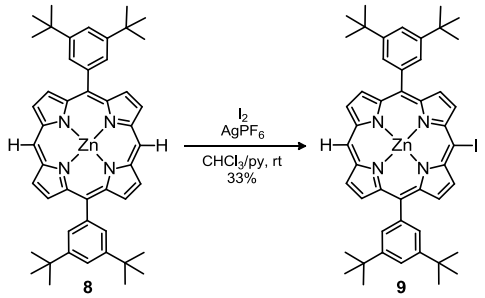

To a 100-mL round-bottomed flask charged with a solution of the Zn(II) porphyrin **8** (630 mg, 0.87 mmol) and I_2 (220 mg, 0.87 mmol) in $CHCl_3$/py 30:1 (65 mL), a solution of $AgPF_6$ (223 mg, 0.87 mmol) in MeCN (5 mL) was added at 25°C. The reaction, which was monitored by TLC (cyclohexane/DCM 1:1), was completed within 13 min, then H_2O (20 mL) was added. The organic layer was washed with H_2O, dried (Na_2SO_4), filtered and evaporated *in vacuo*. CC (SiO_2, cyclohexane/DCM, 1:1 + 1% Et_3N v/v) yielded the product **9** as a red solid (250 mg, 33%).

^{1}H NMR (300 MHz, CS_2/$CDCl_3$ 1:1) δ: 10.22 (s, 1 H), 9.83 (d, *J* = 4.5 Hz, 2 H), 9.36 (d, *J* =4.8 Hz, 2 H), 9.07 (d, *J* = 4.5 Hz, 2 H), 9.04 (d, *J* = 4.8 Hz, 2 H), 8.07 (d, *J* = 1.8 Hz, 4 H), 7.82 (t, *J* = 1.8 Hz, 2 H), 1.58 (s, 36 H).

4-Dimethylbenzo[18]crown-6-boronate, 11.[129]

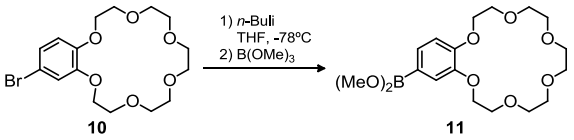

To a stirred solution of commercially available 4-bromobenzo[18]crown-6 **10** (420 mg, 1.07 mmol) in 6 mL of THF at -78 °C 1.3 mL of *n*-butyllithium (2.14 mmol, 1.6 M in hexane) was added. After 1 h of stirring at -78 °C, 1.0 mL of $B(OMe)_3$ was added quickly in one portion. The resulting solution was stirred at -78 °C for 45 min. MeOH (0.5 mL) was added, and the mixture was allowed to warm to rt. The solvent was removed by evaporation below rt, and several portions of MeOH were repeatedly (three times) added and removed to eliminate the excess $B(OMe)_3$. The crude product **11** was used without further purification in the next step.

Zinc(II) 5,15-*Bis*-(3,5-di-*tert*-butylphenyl)-10-(benzo-18C6)-porphyrin, 12-Zn.

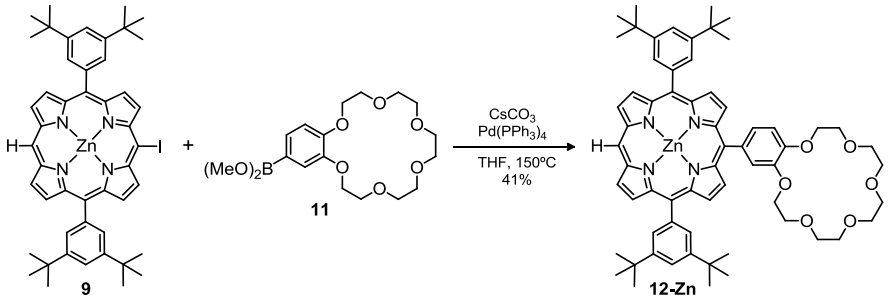

A solution of **9** (185 mg, 0.21 mmol), **11** (243 mg, 0.63 mmol), Cs_2CO_3 (75 mg, 0.23 mmol) and $Pd(PPh_3)_4$ (36 mg, 0.03 mmol) in dry THF was degassed by three freeze-and-thaw cycles, then heated at 150°C in a MW reactor for 1h. The crude was filtered (Celite, DCM) and concentrated *in vacuo*. Subsequent CC (demetalated SiO_2,

[129] C.-L. Chuang, O. dos Santos, X. Xu and J. W. Canary, *Inorg. Chem.* **1997**, *36*, 1967.

cyclohexane/DCM, 3:1 + 1% Et_3N v/v) and GPC (DCM) afforded compound **12-Zn** (75 mg, 41%) as a dark red solid.

mp: 189-190°C.

^{1}H NMR (400 MHz, $CDCl_3$) δ: 10.26 (s, 1H), 9.41 (d, *J* = 4.5 Hz, 2H), 9.15 (d, *J* = 4.5 Hz, 2H), 9.05-9.02 (m, 4H), 8.12 (d, *J* = 1.8 Hz, 4H), 7.82 (t, *J* = 1.8 Hz, 2H), 7.78 (d, *J* = 2.0 Hz, 1H), 7.74 (dd, *J* = 8.0, 2.0 Hz, 1H), 7.22 (d, *J* = 8.0 Hz, 1H), 4.44 (t, *J* = 4.6 Hz, 2H), 4.26 (t, *J* = 4.6 Hz, 2H), 4.09 (t, *J* = 4.6 Hz, 2H), 3.95-3.87 (m, 4H), 3.83-3.71 (m, 10H), 1.55 (s, 36H).

^{13}C NMR (101 MHz, $CDCl_3$) δ: 150.6, 150.1, 149.9, 148.7, 148.2, 146.5, 142.1, 136.3, 132.9, 132.2, 132.0, 131.6, 130.1, 127.9, 122.0, 121.0, 120.9, 120.5, 111.4, 105.7, 70.5, 70.4, 70.3, 70.2, 69.3, 69.1, 68.7, 35.2, 32.0.

FTIR (DCM) ν: 2957, 1590, 1361, 1246, 1132, 1060, 992, 928, 794, 719 cm^{-1}.

UV-vis (DCM) λ_{max} (log ε): 394 (4.72), 416 (5.76), 543(4.42), 581(3.72) nm.

MS (MALDI) *m/z*: 1081.5 $[M + Na]^+$.

HRMS (MALDI) *m/z* calcd for $C_{64}H_{74}N_4NaO_6Zn$ 1081.4792. Found 1081.4747.

5,15-*Bis*-(3,5-di-*tert*-butylphenyl)-10-(benzo-18C6)-porphyrin, 12-2H.

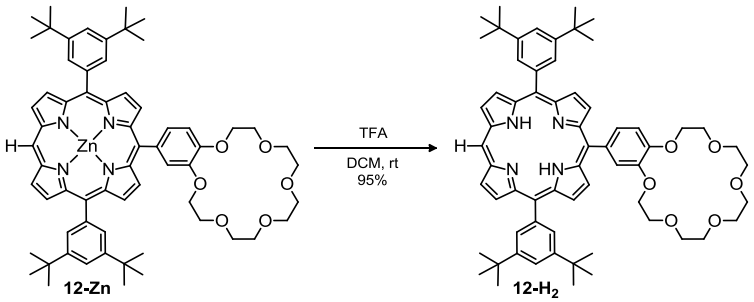

To a stirred solution of **12-Zn** (135 mg, 0.13 mmol) in DCM (15 mL), TFA (0.15 mL, 1.90 mmol) was added. The mixture was stirred at rt overnight and quenched with Et_3N (2 mL). The organic phase was washed with H_2O, dried (Na_2SO_4) and evaporated. FC (Al_2O_3, DCM) gave **12-2H** (120 mg, 95%) as a dark violet solid.

mp: 178-180°C.

^{1}H NMR (300 MHz, $CDCl_3$) δ: 10.21 (s, 1H), 9.34 (d, *J* = 4.7 Hz, 2H), 9.07 (d, *J* = 4.8 Hz, 2H), 8.99-8.90 (m, 4H), 8.13 (d, *J* = 1.9 Hz, 4H), 7.86-7.81 (m, 2H), 7.80 (d, *J* = 1.9 Hz, 1H), 7.75 (dd, *J* = 8.1, 1.8 Hz, 1H), 7.24 (d, *J* = 8.0 Hz, 1H), 4.47 (t, *J* = 4.6 Hz, 2H), 4.29 (t, *J* = 4.6 Hz, 2H), 4.13 (t, *J* = 4.6 Hz, 2H), 3.98-3.91 (m, 4H), 3.86-3.79 (m, 10H), 1.57 (s, 36H), -2.91 (s, 2H).

^{13}C NMR (101 MHz, $CDCl_3$) δ: 149.1, 148.9, 147.1, 140.9, 136.1, 131.7, 131.5, 131.2, 131.0, 130.2, 127.9, 121.2, 121.1, 120.9, 120.2, 112.1, 104.7, 77.5, 77.1, 76.8, 71.2, 71.2, 71.1, 71.0, 70.9, 70.0, 69.9, 69.5, 69.4, 35.2, 31.9.

FTIR (DCM) v: 3316, 2956, 1590, 1361, 1247, 1130, 963, 915, 796, 714 cm^{-1}.

UV-vis (DCM) λ_{max} (log ε): 415 (5.81), 511 (4.48), 546 (4.00), 584 (4.00), 641 (3.70) nm.

MS (MALDI) *m/z*: 1019.6 $[M + Na]^+$.

HRMS (MALDI) *m/z* calcd for $C_{64}H_{76}N_4NaO_6$ 1019.5657, found 1019.5633.

Cobalt(II) 5,15-*Bis*-(3,5-di-*tert*-butylphenyl)-10-(benzo-18C6)-porphyrin, 12-Co.

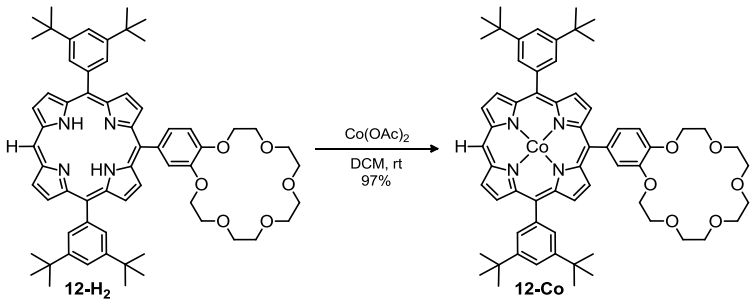

A solution of **12-2H** (40 mg, 0.04 mmol) and $Co(AcO)_2$ (35 mg, 0.30 mmol) in $CHCl_3$ (40 mL) was stirred at rt overnight, then concentrated under reduced pressure. FC (Al_2O_3, DCM) gave compound **12-Co** (41 mg, 97%) as an orange solid.

mp: 182-184^{o}C

FTIR (DCM) v: 2961, 2904, 2869, 1593, 1507, 1465, 1384, 1363, 1339, 1297, 1247, 1135, 1068, 997, 928, 827, 797, 717 cm^{-1}.

UV-vis (DCM) λ_{max} (log ε): 409 (5.36), 432 (4.74), 526 (4.20) nm.

MS (MALDI) *m/z*: 1076.5 $[M + Na]^+$.

HRMS (MALDI) *m/z* calcd for $C_{64}H_{74}CoN_4NaO_6$ 1076.4833. Found 1076.4816.

Niquel(II) 5,15-*Bis*-(3,5-di-*tert*-butylphenyl)-10-(benzo-18C6)-porphyrin, 12-Ni.

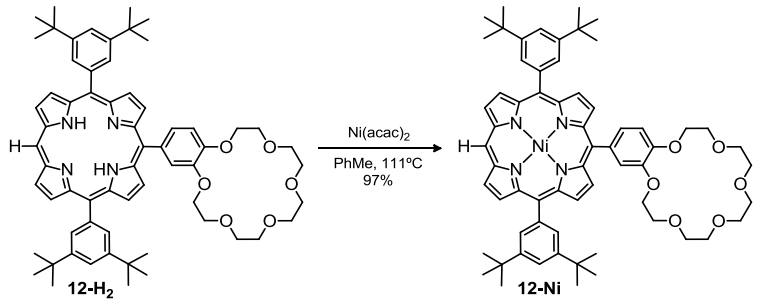

A solution of free base porphyrin **12-2H** (60 mg, 0.06 mmol) and $Ni(acac)_2$ (77 mg, 0.30 mmol) in toluene (60 mL) was heated to reflux for 3h, then concentrated under reduced pressure and purified by FC (Al_2O_3, DCM). Compound **12-Ni** (61 mg, 97%) was obtained as a red solid.

mp: 178-180°C.

^{1}H NMR (400 MHz, $CDCl_3$) δ: 9.84 (s, 1H), 9.14 (d, *J* = 4.7 Hz, 2H), 8.95 (d, *J* = 4.7 Hz, 2H), 8.84 (s, 4H), 7.92 (d, *J* = 1.8 Hz, 4H), 7.76 (t, *J* = 1.8 Hz, 2H), 7.61-7.51 (m, 2H), 7.16 (d, *J* = 8.0 Hz, 1H), 4.44-4.37 (m, 2H), 4.26-4.19 (m, 2H), 4.11-4.04 (m, 2H), 3.96-3.84 (m, 4H), 3.84-3.72 (m, 10H), 1.51 (s, 36H).

^{13}C NMR (101 MHz, $CDCl_3$) δ: 149.1, 148.8, 147.3, 143.2, 143.1, 142.9, 142.7, 140.2, 134.5, 132.9, 132.4, 132.1, 132.0, 129.0, 127.0, 121.3, 120.1, 119.9, 119.0, 112.2, 104.5, 71.1, 71.1, 71.0, 70.9, 69.9, 69.8, 69.4, 69.2, 35.2, 31.9.

FTIR (DCM) ν: 2956, 2926, 2869, 1702, 1667, 1593, 1460, 1264, 1205, 1183, 1136, 1074, 799, 728, 701 cm^{-1}.

UV-vis (DCM) λ_{max} (log ε): 411 (5.84), 522 (4.72), 551 (4.20) nm.

MS (MALDI) *m/z*: 1053.4 $[M]^+$.

HRMS (MALDI) *m/z* calcd for $C_{64}H_{74}N_4NaNiO_6$ 1075.4854, found 1075.4837.

Copper(II) 5,15-*Bis*-(3,5-di-*tert*-butylphenyl)-10-(benzo-18C6)-porphyrin, 12-Cu.

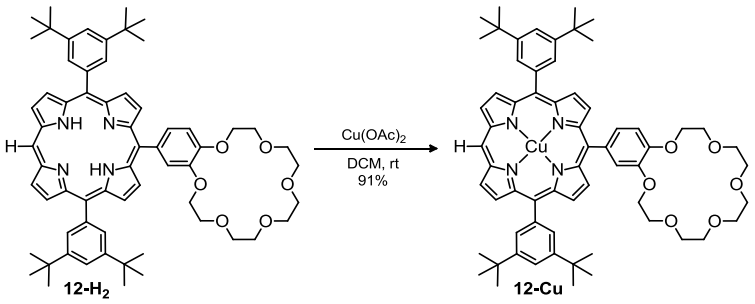

To a solution of **12-2H** (80 mg, 0.08 mmol) in DCM, a solution of $Cu(AcO)_2$ (72 mg, 0.40 mmol) in MeOH (50 mL) was added. The mixture was stirred at rt overnight, then concentrated under reduced pressure and purified by FC (Al_2O_3, DCM). Compound **12-Cu** (77 mg, 91%) was obtained as a red solid.

mp: 228-230^{o}C.

FTIR (DCM) ν: 2955, 2925, 2868, 1592, 1506, 1455, 1362, 1333, 1294, 1263, 1245, 1210, 1128, 1066, 997, 965, 949, 926, 825, 799, 783, 733, 698, 644 cm^{-1}.

UV-vis (DCM) λ_{max} (log ε): 392 (4.50), 412 (5.61), 534 (4.20) nm.

MS (MALDI) *m/z*: 1080.5 $[M + Na]^+$.

HRMS (MALDI) *m/z* calcd for $C_{64}H_{74}CuN_4NaO_6$ 1080.4797. Found 1080.4764.

Methyl 4-[(*tert*-butoxycarbonylamino)methyl]benzoate, 14.[130]

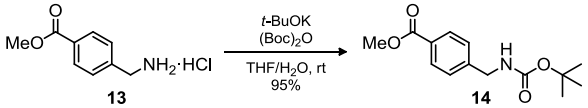

To a solution of methyl 4-aminomethylbenzoate hydrochloride **13** (619 mg, 3.07 mmol) in THF:H_2O 6:1 (84 mL), *t*-BuOK (379 mg, 3.38 mmol) and Boc_2O (303 mg, 3.68 mmol) were added. The mixture was stirred at rt overnight. The layers were separated and the organic layer was washed with brine, dried ($MgSO_4$), filtered and evaporated *in vacuo*. FC (SiO_2, cyclohexane/DCM, 10:90, then DCM/MeOH, 99:1) gave compound **14** (777 mg, 95%) as a white solid.

[130] A. Zistler, S. Koch and A. Dieter Schluter, *J. Chem. Soc., Perkin Trans. 1* **1999**, 501.

^{1}H NMR (300 MHz, $CDCl_3$) δ: 7.58 (d, *J* = 8.2 Hz, 2H), 7.34 (d, *J* = 8.2 Hz, 2H), 4.90 (br s, 1H), 4.37 (d, *J* = 6 Hz, 2H), 3.91 (s, 3 H), 1.46 (s, 9H).

tert-Butyl 4-(hydroxymethyl)benzylcarbamate, 15.[87]

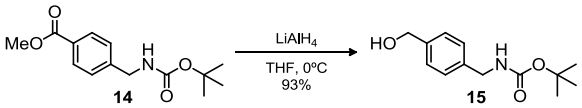

A 1 M $LiAlH_4$ solution in dry THF (4 mL, 4.00 mmol) was added dropwise to a stirred solution of **14** (0.9 g, 3.39 mmol) in dry THF (100 mL) at 0°C. The reaction was stirred for 5 h at 0°C, then MeOH was carefully added. The resulting mixture was filtered (Celite, AcOEt) and evaporated. FC (SiO_2, DCM/MeOH, 98:2) yielded **15** (0.75 g, 93%) as a colorless glassy product.

^{1}H NMR (300 MHz, $CDCl_3$) δ: 7.31 (dd, 4H), 4.83 (broad s, 1H), 4.69 (d, *J* = 6 Hz, 2H), 4.31 (d, *J* = 6 Hz, 2H), 1.67 (br s, 1H), 1.46 (s, 9H).

3,5-*Bis*(dodecyloxy)benzyl alcohol, 17.[131]

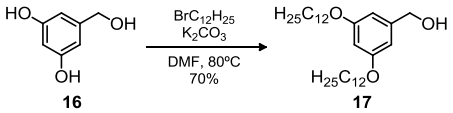

A mixture of 3,5-dihydroxybenzyl alcohol **16** (15.0 g, 0.11 mol), K_2CO_3 (62.7 g, 0.45 mol), and 1-bromododecane (56.84 g, 0.23 mol) in DMF (220 mL) was heated at 70°C for 48 h. After cooling, the resulting mixture was filtered and evaporated to dryness. The brown residue was taken up in DCM. The organic layer was washed with a sat. aq NaCl solution and then with H_2O, dried ($MgSO_4$), filtered, and evaporated to dryness. Recrystallization from hexane yielded **17** (36.2 g, 70%) as colorless crystals.

^{1}H NMR (200 MHz, $CDCl_3$) δ: 6.51 (d, *J* = 2 Hz, 2 H), 6.39 (t, *J* = 2 Hz, 1 H), 4.60 (s, 2 H), 3.93 (t, *J* = 6.5 Hz, 4 H), 1.80-1.70 (m, 4 H), 1.50-1.20 (m, 36 H), 0.90 (t, *J* = 6.5 Hz, 6 H).

[131] J.-F. Eckert, J.-F. Nicoud, J.-F. Nierengarten, S.-G. Liu, L. Echegoyen, F. Barigelletti, N. Armaroli, L. Ouali, V. Krasnikov and G. Hadziioannou, *J. Am. Chem. Soc.* **2000**, *122*, 7467.

[3,5-*Bis*(dodecyloxy)benzyl]hydrogenpropanedioate, 18.[132]

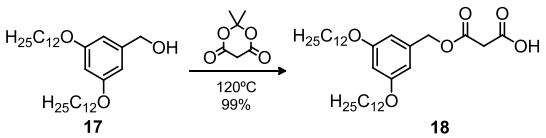

A mixture of alcohol **17** (26.64 g, 55.87 mmol) and Meldrum's acid (8.05 g, 55.87 mmol) was heated at 120ºC for 3 h. The reaction mixture was cooled to rt, dissolved in DCM and evaporated to dryness, providing the desired product **18** (31.10 g, 99%) as pale yellow crystals.

^{1}H NMR (200 MHz, $CDCl_3$) δ: 6.47 (d, *J* = 2 Hz, 2 H), 6.42 (t, *J* = 2 Hz, 1 H), 5.14 (s, 2 H), 3.93 (t, *J* = 6 Hz, 4 H), 3.50 (s, 2 H), 1.77 (m, 4 H), 1.26 (m, 36 H), 0.88 (t, *J* = 6 Hz, 6 H).

3,5-*Bis*(dodecyloxy)benzyl 4-[(*tert*-butoxycarbonylamino)methyl]benzyl malonate, 19.[87]

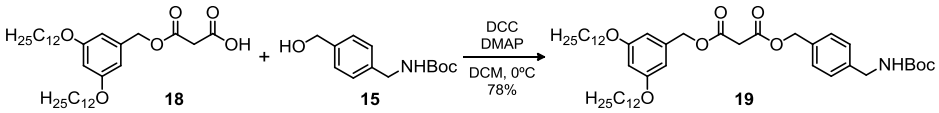

To a stirred solution of alcohol **15** (0.74 g, 3.14 mmol), carboxylic acid **18** (1.94 g, 3.45 mmol) and DMAP (0.15 g, 1.26 mmol) in DCM (100 mL) at 0ºC, DCC (2.57 g, 12.46 mmol) was added in small portions. After 1 h, the mixture was allowed to slowly warm to rt, then stirred for 12 h, filtered (Celite) and evaporated to dryness. FC (SiO_2, DCM/hexane, 4:1) yielded the desired malonate **19** (1.93 g, 78%) as a colorless oil.

^{1}H NMR (300 MHz, $CDCl_3$) δ: 7.28 (dd, 4H), 6.46 (d, *J* = 2 Hz, 2H), 6.41 (t, *J* = 2 Hz, 1H), 5.16 (s, 2H), 5.09 (s, 2H), 4.84 (br s, 1H), 4.31 (d, *J* = 6 Hz, 2H), 3.91 (t, *J* = 7 Hz, 4H), 3.47 (s, 2H), 1.75 (m, 4H), 1.44 (s, 9H), 1.30 (m, 36H), 0.88 (t, *J* = 7 Hz, 6H).

[132] D. Felder, M. Gutiérrez Nava, M. P. Carreón, J.-F. Eckert, M. Luccisano, C. Schall, P. Masson, J.-L. Gallani, B. Heinrich, D. Guillon and J.-F. Nierengarten, *Helv. Chim. Acta* **2002**, *85*, 288.

3,5-*Bis*(dodecyloxy)benzyl 4-[(*tert*-butoxycarbonylamino)methyl]benzyl 2,2-[1,2-[6,6]-methano-[60]-fullerene] malonate, 20.[87]

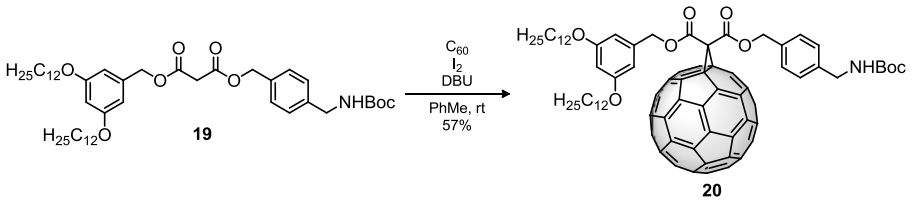

To a stirred solution of fullerene C_{60} (300 mg, 0.41 mmol), I_2 (116 mg, 0.45 mmol) and malonate **19** (326 mg, 0.41 mmol) in freshly distilled toluene (500 mL) at rt, DBU (0.16 mL, 1.04 mmol) was added. Stirring was maintained for 12 h at rt. The resulting mixture was then filtered through a short plug of SiO_2 (toluene) and evaporated to dryness. FC (SiO_2, DCM/hexane 7:3) yielded methane fullerene **20** (0.71 g, 57%) as a dark brown solid.

^{1}H NMR (300 MHz, $CDCl_3$) δ: 7.35 (dd, 4H), 6.56 (d, *J* = 2 Hz, 2H), 6.42 (t, *J* = 2 Hz, 1H), 5.47 (s, 2H), 5.39 (s, 2H), 4.87 (br s, 1H), 4.32 (d, *J* = 6 Hz, 2H), 3.89 (t, *J* = 7 Hz, 4H), 1.75 (m, 4H), 1.43 (s, 9H), 1.30 (m, 36H), 0.88 (t, *J* = 7 Hz, 6H).

Compound 21.[87]

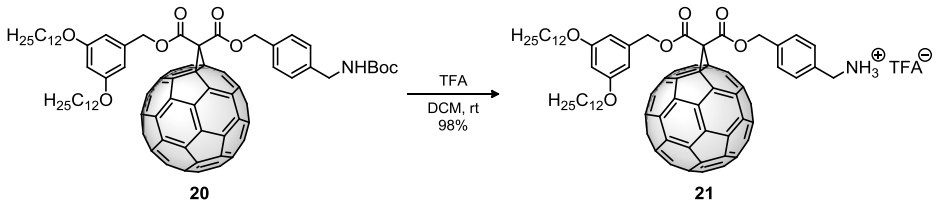

A solution of **20** (393 mg, 0.26 mmol) and TFA (20 mL) in DCM (40 mL) was stirred at rt for 4 h. The mixture was then washed with H_2O, dried ($MgSO_4$), filtered and evaporated to dryness. Recrystallization from DCM/hexane yielded **21** (397 mg, 98%) as a dark brown solid.

^{1}H NMR (300 MHz, $CDCl_3$) δ: 7.46 (dd, *J* = 8 Hz, 4H), 6.51 (d, *J* = 2 Hz, 2H), 6.37 (t, *J* = 2 Hz, 1H), 5.46 (s, 2H), 5.37 (s, 2H), 4.16 (s, 2H), 3.86 (t, *J* = 7 Hz, 4H), 1.67 (m, 4H), 1.25 (m, 36H), 0.87 (t, *J* = 7 Hz, 6H).

5,15-*Bis*-(3,5-di-*tert*-butylphenyl)-10-(benzo-18C6) *meso-meso* linked zinc(II) diporphyrin, 23.

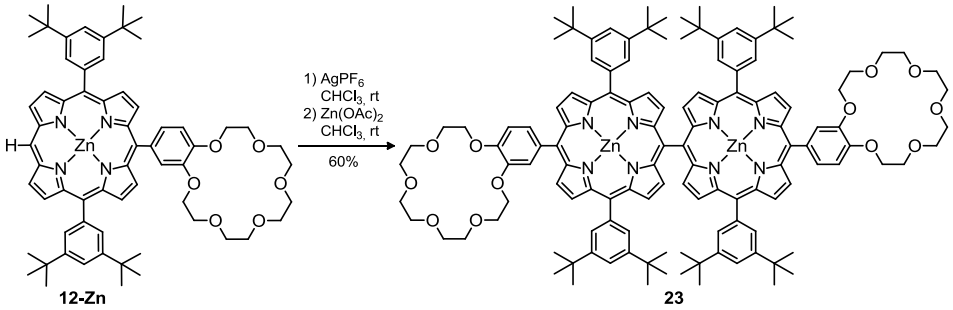

To a 1M solution of **12-Zn** (0.230 g, 0.22 mmol) in $CHCl_3$ shielded from light, a 0.12 M solution of $AgPF_6$ (83 mg, 0.33 mmol) in MeCN was added. The mixture was stirred at rt for 12 h, then quenched with H_2O. The organic phase was washed with H_2O, dried (Na_2SO_4) and concentrated. A solution of the residue in $CHCl_3$ was treated with a sat. solution of $Zn(OAc)_2 \cdot 2H_2O$ in MeOH (2 mL) at reflux for 2 h. The organic phase was washed, dried, filtered and concentrated. Subsequent CC (demetalated SiO_2, DCM/MeOH, 98:2 + 1% Et_3N v/v) and GPC (DCM) gave compound **23** (137 mg, 60%) as a brown solid.

^{1}H NMR (400 MHz, $CDCl_3$) δ: 9.09-9.04 (m, 8H), 8.76-8.70 (m, 4H), 8.21 (d, *J* = 4.6 Hz, 2H), 8.18-8.09 (m, 10H), 7.88 (d, *J* = 1.9 Hz, 2H), 7.82 (dd, *J* = 8.0, 1.9 Hz, 2H), 7.72 (m, 4H), 7.21 (d, *J* = 8.2 Hz, 2H), 4.37-4.22 (m, 8H), 3.96-3.81 (m, 8H), 3.74-3.56 (m, 24H), 1.47 (d, *J* = 1.5 Hz, 72H).

^{13}C NMR (101 MHz, $CDCl_3$) δ: 155.0, 151.1, 150.4, 150.2, 148.7, 148.6, 147.1, 141.9, 136.3, 134.0, 132.3, 132.2, 132.1, 129.8, 128.0, 123.4, 121.5, 120.9, 120.8, 119.7, 112.2, 71.0, 70.9, 70.8, 69.8, 69.7, 69.4, 35.1, 31.8, 31.6.

FTIR (DCM) ν: 3676, 2988, 2901,1451, 1394, 1242, 1066, 880 cm^{-1}.

UV-vis (DCM) λ_{max} (log ε): 422 (5.35), 457 (5.29), 559 (4.65), 605 (3.80) nm.

MS (MALDI) *m/z*: 2141.9 $[M + Na]^+$.

HRMS (MALDI) *m/z* calcd for $C_{128}H_{146}N_8NaO_{12}Zn_2$ 2141.9541. Found 2141.9531.

5,15-*Bis*-(3,5-di-*tert*-butylphenyl)-10-(benzo-18C6) *meso-meso, β-β, β-β*, triply linked zinc(II)-diporphyrin, 24.

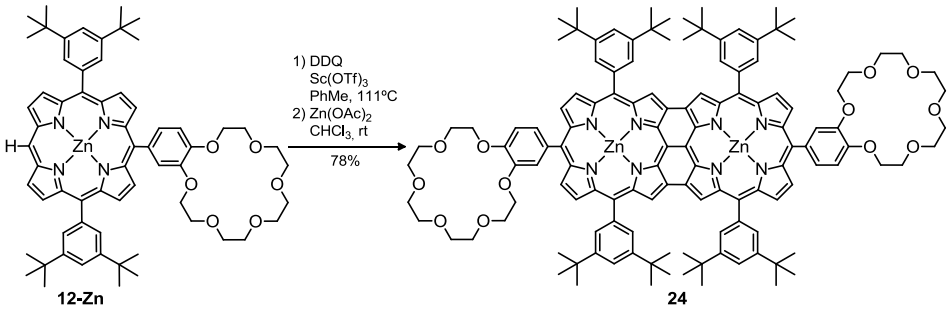

To a solution of **12-Zn** (235 mg, 0.22 mmol) in freshly distilled toluene (110 mL), DDQ (150 mg, 0.66 mmol) and $Sc(OTf)_3$ (326 mg, 0.66 mmol) were added. The resulting reaction mixture was refluxed for 1 hour in the dark, then quenched by the addition of THF (10 mL). The resulting mixture was passed through a short Al_2O_3 column and the solvent evaporated. The residue obtained was dissolved in $CHCl_3$ and treated with a saturated solution of $Zn(OAc)_2 \cdot 2H_2O$ in MeOH (2 mL) at reflux for 2 h. The organic phase was washed with H_2O, dried (Na_2SO_4), filtered out and concentrated to dryness. CC (demetalated SiO_2, acetone + 1% Et_3N v/v) and precipitation from THF upon addition of cyclohexane afforded compound **24** (203 mg, 78%) as a black solid.

FTIR (KBr) v: 3675, 2944, 1451, 1394, 1240, 1066, 881, 801 cm^{-1}.

UV-vis (DCM) λ_{max} (log ε): 307 (4.48), 346 (4.27), 372 (4.36), 416 (4.89), 457 (4.47), 578 (4.86), 646 (4.18), 824 (3.62), 921 (4.02), 1042 (4.32) nm.

MS (MALDI) *m/z*: 2137.9 $[M + Na]^+$.

HRMS (MALDI) *m/z* calcd for $C_{128}H_{142}N_8NaO_{12}Zn_2$ 2137.9228. Found 2137.9244.

2-Methylthio-1,3-dithiol tetrafluoroborate, 26.[133]

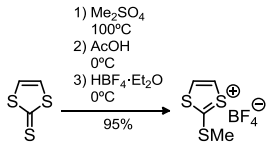

25 **26**

A stirred solution of vinylene trithiocarbonate **25** (0.658 g, 4.90 mmol) in Me_2SO_4 (5 mL, 52.72 mmol) is heated at 90-100ºC for 30 min or until dissolution is complete. The mixture is cooled to 0ºC and AcOH (glacial, 1 mL) is added. After stirring for 10 min, $HBF_4{\cdot}Et_2O$ (0,80 g, 4.90 mmol) is added and stirred for a further 10 min. Cold Et_2O (100 mL) is added, precipitating as a red solid which is collected by filtration and washed thoroughly with cold Et_2O. Recrystallization from DCM affords salt **26** as a red solid (1.10 g, 95%).

^{1}H NMR (300 MHz, DMSO) δ: 8.73 (s, 2H), 3.17 (s, 3H).

2-Methylthio-1,3-dithiol, 27.[133]

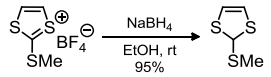

26 **27**

Finely-ground $NaBH_4$ (0.178 g, 4.70 mmol) is added portionwise over 30 min to a stirred solution of salt **26** (1.10 g, 4.65 mmol) in dry EtOH (30 mL) at 0ºC. The mixture is stirred for a further 2h at rt; the solvent is evaporated, H_2O (30 mL) added and the residue extracted with DCM. The organic layer is dried ($MgSO_4$) and concentrated *in vacuo* to afford the crude product **27** as a red oil of sufficient purity for next reaction (664 mg, 95%).

^{1}H NMR (300 MHz, $CDCl_3$) δ: 6.12 (s, 1H), 6.07 (s, 2H), 2.20 (s, 3H).

[133] a) A. J. Moore and M. R. Bryce, *Synthesis* **1991**, *1991*, 26; b) L. Sánchez, Thesis, Universidad Complutense de Madrid, **1997**.

1,3-Dithiolium tetrafluoroborate, 28.[133]

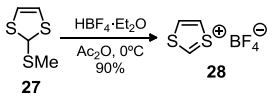

27 **28**

$HBF_4{\cdot}Et_2O$ (10.25 mL, 75.38 mmol) is added dropwise over 10 min to a stirred solution of compound **27** (10.30 g, 68.53 mmol) in Ac_2O (100 mL) at 0ºC. After stirring for a further 15 min, dry Et_2O (100 mL) is added and stirring continued for 30 min. The solid is collected by filtration and washed thoroughly with Et_2O obtaining **28** as a white solid (11.72 g, 90%) of sufficient purity for further reaction.

^{1}H NMR (300 MHz, DMSO) δ: 6.79 (s, 1H), 9.37 (s, 2H).

Dimethyl 1,3-Dithiol-2-ylphosphonate, 29.[134]

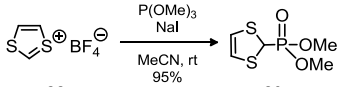

28 **29**

Freshly distilled trimethyl phosphite (0.62 mL, 5.3 mmol) and NaI (0.8 g, 5.34 mmol) were added successively to a stirred solution of the cation salt **28** (1.0 g, 5.34 mmol) in dry MeCN (50 mL) at 20°C. A slightly exothermic reaction immediately took place. Stirring was continued for 2 h, whereupon the solvent was evaporated under reduced pressure. H_2O (25 mL) was added to the residue and the mixture extracted into DCM. The combined extracts were dried ($MgSO_4$), filtered and the solvent evaporated under reduced pressure. The residue was chromatographed (Al_2O_3, AcOEt) to afford phosphonate ester **29** (1.05 g, 95%) as a deep-red hygroscopic oil.

^{1}H NMR (300 MHz, $CDCl_3$) δ: 5.98 (2 H, s), 4.73 (d, *J* = 4.5 Hz, 1 H), 3.75 (d, *J* = 10.5 Hz, 6 H).

[134] A. J. Moore and M. R. Bryce, *J. Chem. Soc., Perkin Trans. 1* **1991**, 157.

2,6-*Bis*([*tert*-butyl-diphenylsilyl)oxy]anthraquinone, 31.[135]

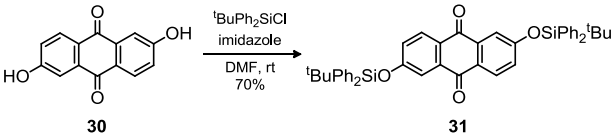

30 **31**

To a solution of 2,6-dihydroxyanthraquinone **30** (5.00 g, 20.81 mmol) in DMF (250 mL), *tert*-butyl(chloro)diphenylsilane (13.75 g, 50.0 mmol) followed by imidazole (14.17 g, 208 mmol) were added. The reaction was stirred at rt for 16 h. DMF was removed *in vacuo*, the residue dissolved in DCM, washed with H_2O, dried ($MgSO_4$), filtered and concentrated *in vacuo*. FC (SiO_2, hexane/DCM, 2:1) afforded compound **31** (10.56 g, 70%) as a yellow solid.

mp: 226-228ºC.

^{1}H NMR ($CDCl_3$) δ: 7.95 (d, *J* = 8.5 Hz, 2H), 7.73-7.68 (m, 8H), 7.63 (d, *J* = 2.7 Hz, 2H), 7.45-7.33 (m, 12H), 6.94 (dd, *J* = 8.5, 2.7 Hz, 2H), 1.13 (s, 18H).

2,6-*Bis*[(*tert*-butyldiphenylsilyl)oxy]-exTTF, 32.[136]

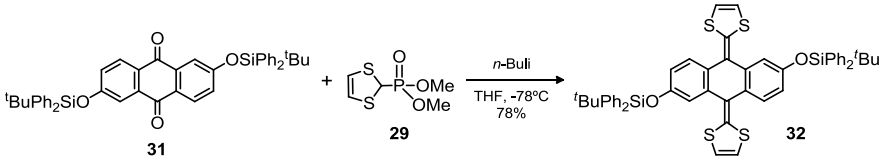

31 **29** **32**

To a solution of 1,3-dithiol phosphonate **29** (4.65 g, 21.91 mmol) in dry THF (50 mL) at -78ºC, *n*-butyllithium (1.6 M in hexane, 15 mL, 24.10 mmol) was added dropwise with stirring over 10 min. Stirring was continued for 1 h, after which a solution of compound **31** (2.61 g, 3.65 mmol) in dry THF was added. The resulting mixture was kept at -78ºC for 1h and then let to reach rt overnight, whereupon the solvent was evaporated under reduced pressure. H_2O (100 mL) was added to the residue and the mixture extracted into DCM. The organic layer was dried (Na_2SO_4), filtered and evaporated under reduced pressure. The residue was purified by FC (SiO_2, hexane/DCM, 3:1 + 1% Et_3N v/v). Precipitation from $CHCl_3$ by hexane afforded compound **32** (2.55 g, 78%) as a yellow solid.

[135] G. J. Marshallsay and M. R. Bryce, *J. Org. Chem.* **1994**, *59*, 6847.
[136] J. Santos, Thesis, Universidad Complutense de Madrid, **2010**.

^{1}H NMR (300 MHz, $CDCl_3$) δ: 7.73 (m, 8H), 7.41 (m, 12H), 7.33 (d, *J* = 8.4Hz, 2H), 7.03 (d, *J* = 2.2 Hz, 2H), 6.89 (dd, *J* = 8.4, 2.2 Hz, 2H), 6.73 (s, 4H), 1.10 (s, 18H).

2,6-Dihydroxy-exTTF, 33.[136]

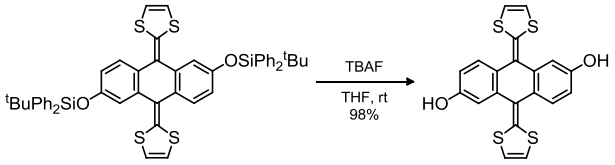

32 **33**

To a solution of compound **32** (710 mg, 0.80 mmol) in 100 mL of dry THF, *n*-Bu_4NF (1 M in THF, 2.3 mL, 2.30 mmol) was added. The mixture was stirred at rt for 16h, whereupon the solvent was evaporated under reduced pressure. H_2O was added to the residue and the mixture extracted into DCM. The organic layer was dried over Na_2SO_4, filtered, concentrated under reduced pressure and purified by FC (SiO_2, hexane/AcOEt, 1:9) to yield **33** as a yellow solid (323 mg, 98%).

mp: 232-234°C.

^{1}H NMR (200 MHz, $CDCl_3$) δ: 7.35 (d, *J* = 8.5 Hz, 2H), 7.05 (d, *J* = 2.3 Hz, 2H), 6.31 (dd, *J* = 8.5, 2.3 Hz, 2H), 6.75 (s, 4H).

8-Tosyloxy-3,6-dioxaoctanol, 35.[137]

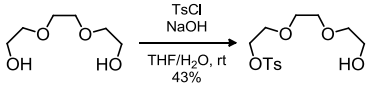

34 **35**

To a mixture of triethylene glycol **34** (35 mL, 0.26 mol) and NaOH (8 g, 0.20 mol) in THF (40 mL)/H_2O (40 mL) in an ice bath, a solution of tosyl chloride (24 g, 0.13 mmol) in THF (80 mL) was added dropwise for 3h. The reaction mixture was stirred overnight. THF was then evaporated under reduced pressure. The residue was extracted with AcOEt, dried ($MgSO_4$), filtered and concentrated. FC (SiO_2, DCM/petroleum ether, 2:1, then Et_2O) afforded **35** (17.0 g, 43%).

^{1}H NMR (500 MHz, $CDCl_3$) δ: 7.80 (d, *J* = 8.0 Hz, 2H), 7.34 (d, *J* = 8.0 Hz, 2H), 4.17 (m, 4H), 3.70 (m, 4H), 3.61 (s, 4H), 3.56 (m, 2H), 2.45 (s, 3H), 2.30 (bs, 1H, OH).

[137] X.-Z. Zhu and C.-F. Chen, *J. Am. Chem. Soc.* **2005**, *127*, 13158.

1,2-*Bis*[2-[2-(2-hydroxyethoxy)ethoxy]ethoxy]benzene, 37.[137]

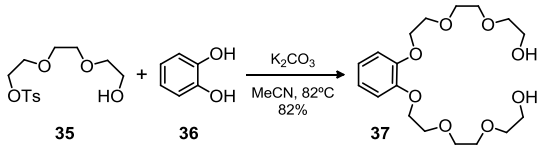

35 36 37

A mixture of catechol **36** (3.1 g, 0.03 mol), **35** (17.3 g, 0.06 mol) and K_2CO_3 (16 g, 0.12 mol) in dry MeCN (200 mL) was refluxed for 60 h. The reaction mixture was filtered and then concentrated under reduced pressure. The crude product was purified by FC (SiO_2, AcOEt, then acetone) to afford the desired product **37** (8.62 g, 82%).

^{1}H NMR (200 MHz, $CDCl_3$) δ: 6.9 (s, 4H), 3.5-4.3 (m, 24H), 3.1 (s, 2H).

1,2-Phenylene-*bis*(oxyethylenoxyethylenoxyethylene) ditosylate, 38.[137]

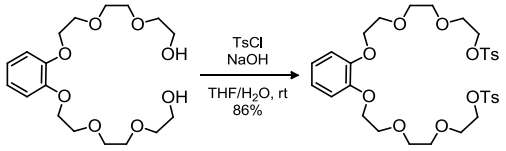

37 38

To a mixture of **37** (7.32 g, 19.6 mmol) and NaOH (3 g, 75 mmol) in THF (20 mL)/ H_2O (20 mL) in an ice bath, a solution of tosyl chloride (7.5 g, 39.5 mmol) in THF (60 mL) was added dropwise for 3h. The reaction mixture was stirred overnight. THF was then evaporated under reduced pressure. The residue was extracted with AcOEt, dried ($MgSO_4$), filtered and concentrated. FC (SiO_2, DCM/hexane 1:1 then AcOEt) afforded **38** (11.5 g, 86 %).

^{1}H NMR (200 MHz, $CDCl_3$) δ: 7.79 (d, *J* = 8.1 Hz, 4H), 7.33 (d, *J* = 8.1 Hz, 4H), 6.91 (s, 4 H), 4.11–4.18 (m, 8 H), 3.81–3.84 (m, 4 H), 3.65–3.79 (m, 8 H), 3.59–3.61 (m, 4 H), 2.42 (s, 6 H).

Ethyl (dibenzo[24]crown-8)-4'-carboxylate, 40.[138]

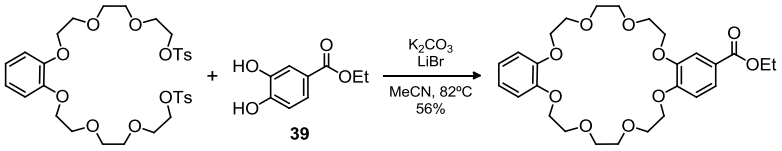

38 39 40

A solution of **39** (1.62 g, 8.89 mmol), K_2CO_3 (5.04 g, 36.46 mmol) and a catalytic amount of LiBr in MeCN (1 L) was heated to reflux for 1 h. A solution of **38** (6.14 g, 8.99 mmol) in MeCN (500 mL) was then added dropwise over 12 h and the mixture was heated to reflux for 48 h. Filtration and concentration of the filtrate *in vacuo* left an oil which was taken up in DCM (200 mL) and washed with 0.1 M HCl and sat. aq NaCl solution. Drying ($MgSO_4$), evaporation and FC (SiO_2, DCM-MeOH 99:1) afforded **40** (2.62 g, 56%) as a white solid.

^{1}H NMR (200 MHz, $CDCl_3$) δ: 7.65 (dd, *J* = 2.0, 8.3 Hz, 1 H); 7.54 (d, *J* = 2.0 Hz, 1 H), 6.86–6.90 (m, 4 H), 6.85 (d, *J* = 8.3 Hz, 1 H), 4.34 (q, *J* = 7.0 Hz, 2 H), 4.13–4.24 (m, 8 H), 3.90–3.98 (m, 8 H), 3.79–3.86 (m, 8 H), 1.37 (t, *J* = 7.0 Hz, 3 H).

(Dibenzo[24]crown-8)-4'-carboxylic acid, 41.[139]

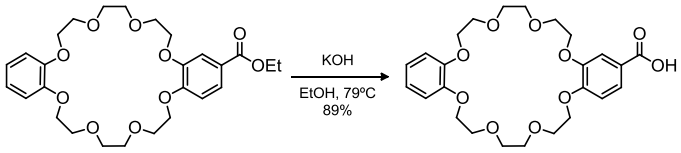

40 41

A 250-mL one-necked, round-bottomed flask was charged with **40** (3.16 g, 6.24 mmol) and EtOH (100 mL). A solution of aq KOH (4M, 10 mL) was added dropwise and the reaction mixture was heated at reflux for 12 h. Upon completion of the reaction the solvent was removed to give an off-white solid, which was redissolved in H_2O and neutralized with H_2SO_4. The solution was extracted with DCM, and the organic layers were combined, dried over $MgSO_4$, and concentrated to give a solid, which was recrystallized from EtOH providing **41** as a white solid (2.73 g, 89%).

[138] F. Diederich, L. Echegoyen, M. Gómez-López, R. Kessinger and J. Fraser Stoddart, *J. Chem. Soc., Perkin Trans. 2* **1999**, 1577.
[139] N. Yamaguchi, L. M. Hamilton and H. W. Gibson, *Angew. Chem. Int. Ed.* **1998**, *37*, 3275.

^{1}H NMR ($CDCl_3$) δ: 7.71 (dd, *J* = 1.6, 8.4 Hz, 1H); 7.56 (d, *J* = 1.6 Hz, 1H), 6.88 (m, 5H), 4.20 (t, *J* = 4.0 Hz, 4H), 4.15 (t, *J* = 4.0 Hz, 4H), 3.93 (m, 8H), 3.84 (m, 8H).

Ethyl [*bis*(2-hydroxyethyl)amino]-4'-benzoate, 44.[140]

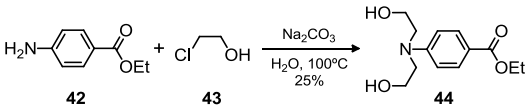

42 **43** **44**

A stirring mixture of benzocaine **42** (5 g, 30.27 mmol), Na_2CO_3 (12.5 g, 117.94 mmol) and 2-chloroethanol **43** (4.3 mL, 63.56 mmol) in H_2O (500 mL) is refluxed for seven days. After allowing the suspension to cool down, DCM was added (100 mL), and the resulting mixture was filtered. After removing the organic layer, the aq layer was concentrated and then extracted with DCM. All the mixed organic layers were dried over Na_2SO_4, filtered and evaporated. The resulting oil was purified by FC (SiO_2, DCM, then DCM/MeOH, 100:2 and up to 95:5), obtaining **44** as a white solid (1.9 g, 25%).

^{1}H NMR (300 MHz, $CDCl_3$) δ: 7.43 (dd, *J* = 8.4, 1.9 Hz, 2H), 7.72 (d, *J* = 8.5 Hz, 2H), 7.69 (d, *J* = 1.9 Hz, 2H), 7.57 (d, *J* = 2.3 Hz, 2H), 7.12 (dd, *J* = 8.4, 2.3 Hz, 2H), 6.93 (d, *J* = 8.5 Hz, 2H), 6.31 (s, 4H), 4.25-4.22 (m, 8H), 3.97-3.92 (m, 8H), 3.79-3.78 (m, 16H).

Ethyl *N*-(phenylaza[18]crown-6)-4'-carboxylate, 46.

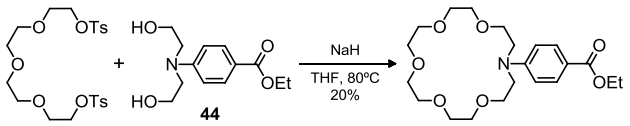

45 **44** **46**

To a suspension of NaH (152 mg, 6.33 mmol) in anhydrous THF (20 mL) at 0ºC, a solution of **44** (400 mg, 1.58 mmol) in THF (10 mL) was added dropwise. The resulting mixture was heated at 30-40ºC for 1.5 h. Then a solution of tetraethyleneglycol ditosylate **45** (800 mg, 1.74 mmol) in THF was added and the reaction was heated at 80ºC for 5 days. After evaporating the solvent, the resulting residue was purified by FC (SiO_2, DCM/MeOH, 200:1) yielding **46** as a transparent oil (131.3 mg, 20 %).

[140] W. C. J. Ross, *J. Chem. Soc.* **1949**, 183.

^{1}H NMR (300 MHz, $CDCl_3$) δ: 7.80 (d, *J* = 9.0 Hz, 2H), 6.57 (d, *J* = 9.0 Hz, 2H), 4.23 (q, *J* = 7.1 Hz, 2H), 3.67 – 3.52 (m, 24H), 1.28 (t, *J* = 7.0 Hz, 3H).

^{13}C NMR (75 MHz, $CDCl_3$) δ: 166.9, 151.3, 131.4, 117.3, 110.5, 70.9, 70.8, 70.8, 70.7, 70.6, 69.8, 68.5, 66.6, 60.1, 51.3, 14.5.

MS (ESI) *m/z*: 434.2 $[M + Na]^+$.

_N_-(Phenylaza[18]crown-6)-4'-carboxylic acid, 47.

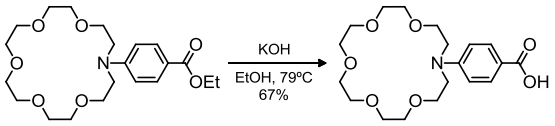

46 **47**

A 100 mL one-necked, round-bottomed flask was charged with ethyl *N*-(phenylaza[18]crown-6)-4'-carboxylate **46** (130 mg, 0.32 mmol) and EtOH (30 mL). A solution of aq KOH (107 mg, 1.91 mmol in 10 mL) was added dropwise and the reaction mixture was heated at reflux for 12 h. Upon completion of the reaction the solvent was removed to give an off-white solid, which was redissolved in H_2O (50 mL) and neutralized with H_2SO_4. The solution was extracted with DCM, and the organic layers were combined, dried over Na_2SO_4, and concentrated to give **47** as a white solid, which was of enough purity to continue with the next step (82 mg, 67 %).

^{1}H NMR (300 MHz, $CDCl_3$) δ: 7.94 (d, *J* = 8.94 Hz, 2H), 6.67 (d, *J* = 8.94 Hz, 2H), 3.72-3.67 (m, 24H).

^{13}C NMR (75 MHz, $CDCl_3$) δ: 171.9, 152.0, 132.3, 116.1, 110.7, 71.0, 70.9, 70.9, 70.9, 70.8, 70.7, 69.9, 68.5, 66.7, 51.4.

MS (ESI) *m/z*: 381.9 $[M - H]^-$

Ethyl *N*-(phenylaza[15]crown-5)-4'-carboxylate, 50.

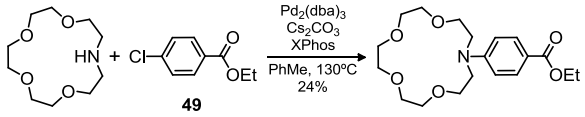

48 49 50

A solution of ethyl 4-chlorobenzoate **49** (0.214 mL, 1.37 mmol), aza[15]crown-5 **48** (300 mg, 1.37 mmol), $Pd_2(dba)_3$ (37 mg, 0.04 mmol), Cs_2CO_3 (500 mg, 1.53 mmol) and XPhos (78 mg, 0.164 mmol) in dry toluene (10 mL) was deoxygenated via three freeze-pump-thaw cycles, then heated in a MW at 130ºC for 1 h. The resulting mixture was filtered (Celite, DCM) and concentrated *in vacuo*. The resulting residue was taken in DCM and washed with H_2O. The organic phase was dried (Na_2SO_4), filtered and concentrated under reduced pressure. FC (Al_2O_3, DCM/hexane, 2:1 then DCM/EtOH, 50:1) gave the desired crown ether **50** (159 mg, 24%) as a white solid.

^{1}H NMR (300 MHz, $CDCl_3$) δ: 7.89 (d, *J* = 9.1 Hz, 2H), 6.67 (d, *J* = 9.1 Hz, 2H), 4.31 (q, *J* = 7.1 Hz, 2H), 3.85-3.55 (m, 20H), 1.35 (t, *J* = 7.1 Hz, 3H).

^{13}C NMR (75 MHz, $CDCl_3$) δ: 167.1, 151.2, 131.5, 117.5, 110.7, 77.6, 77.2, 76.7, 71.5, 70.5, 70.3, 68.5, 60.2, 52.8, 14.6.

MS (MALDI) *m/z*: 390.1 $[M + Na]^+$

***N*-(phenylaza[15]crown-5)-4'-carboxylic acid, 51.**

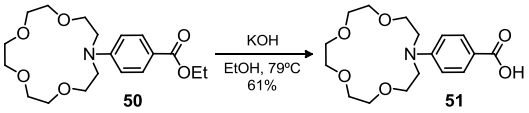

50 51

To a solution of crown ether **50** (272 mg, 0.74 mmol) in 10 mL of EtOH/H_2O (9:1), KOH (250 mg, 4.44 mmol) was added. The reaction mixture was heated under reflux for 1 h. Upon completion of the reaction, the solvent was removed to give an off-white solid, which was redissolved in H_2O (20 mL) and neutralized with aq HCl 1M. The solution was extracted with AcOEt, and the organic layers were combined, dried (Na_2SO_4), filtered and concentrated *in vacuo* to give **51** as a white solid of enough purity to continue with the next step (154 mg, 61 %).

^{1}H NMR (300 MHz, $CDCl_3$) δ: 7.93 (d, *J* = 9.0 Hz, 2H), 6.64 (d, *J* = 9.1 Hz, 2H), 3.78 (t, *J* = 6.0 Hz, 5H), 3.65 (m, 16H).

^{13}C NMR (75 MHz, $CDCl_3$) δ: 172.00, 151.83, 132.30, 116.15, 110.72, 77.58, 77.16, 76.74, 71.46, 70.42, 70.22, 68.38, 52.89, 29.83, 14.23.

MS (MALDI) *m/z*: 362.2 $[M + Na]^+$.

HRMS (MALDI) *m/z* calcd for $C_{17}H_{25}NNaO_6$ 362.1574. Found 362.1558.

2,6-*Bis*[(dibenzo[24]crown-8)-4'-carbonyloxy]exTTF, 55.

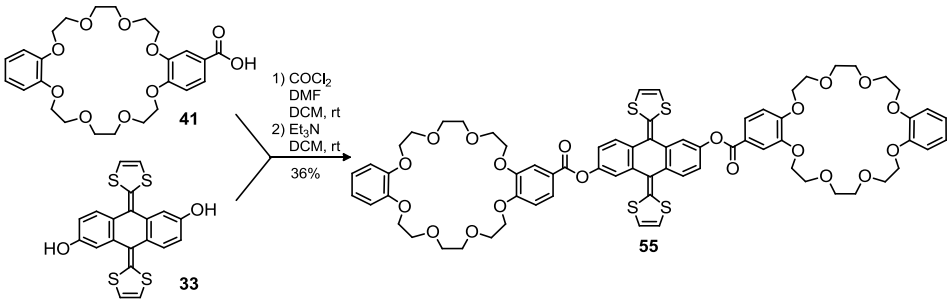

To a stirring solution of carboxylic acid **41** (125 mg, 0,25 mmol) and a catalytic amount of DMF in anhydrous DCM (20 mL), oxalyl chloride (0.1 mL, 0.93 mmol) was added. After 30 min at rt, the solvent was removed under reduced pressure, the resulting residue was diluted with anhydrous DCM (30 mL) and Et_3N (0.1 mL, 0.66 mmol) and 2,6-dihydroxy-exTTF **33** (50 mg, 0.12 mmol) were added. The reaction mixture was stirred at rt until no precipitate was observed. Purification of the reaction crude was performed by subsequent FC (SiO_2, DCM/MeOH/NH_3, 90:10:0.3) and FC (Al_2O_3, DCM/MeOH, 200:1), obtaining the titled product **55** (60 mg, 36%) as a yellow powder.

^{1}H NMR (300 MHz, $CDCl_3$) δ: 7.86 (dd, *J* = 8.4, 2.0 Hz, 2H), 7.72 (d, *J* = 8.4 Hz, 2H), 7.69 (d, *J* = 2.0 Hz, 2H), 7.58 (d, *J* = 2.3 Hz, 2H), 7.12 (dd, *J* = 8.4, 2.3 Hz, 2H), 6.93 (d, *J* = 8.4 Hz, 2H), 6.31 (s, 4H), 4.30 – 4.16 (m, 8H), 4.00 – 3.89 (m, 8H), 3.81 – 3.75 (m, 8H).

^{13}C NMR (75 MHz, $CDCl_3$) δ: 164.9, 153.9, 148.9, 148.7, 137.1, 136.9, 133.1, 126.0, 125.0, 122.2, 120.8, 119.0, 118.5, 117.6, 117.3, 115.1, 112.3, 71.3, 70.6, 70.5, 69.5, 69.4, 69.2, 68.8.

FTIR (DCM) ν: 2924, 2856, 1726, 1596, 1505, 1454, 1428, 1264, 1187, 1128, 1054, 960, 733, 701 cm^{-1}.

UV-vis (DCM) λ_{max} (log ε): 353 (3.98), 369 (4.14), 421 (4.25), 437 (4.31) nm.

MS (MALDI) *m/z*: 1383.3 $[M + Na]^+$.

HRMS (MALDI): *m/z* calcd for $C_{70}H_{72}NaO_{20}S_4$: 1383.3392. Found: 1383.3371.

2,6-*Bis*[(benzo[18]crown-6)-4'-carbonyloxy]exTTF, 56.[103]

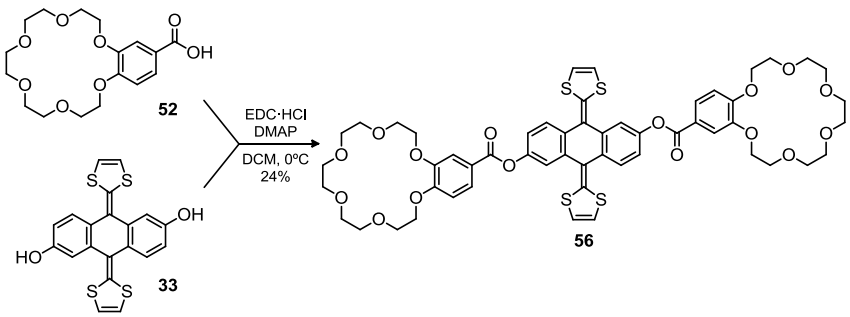

To a solution of 2,6-dihydroxy-exTTF **33** (50 mg, 0.12 mmol), commercially available (benzo[18]crown-6)-4'-carboxylic acid **52** (96 mg, 0.27 mmol) and DMAP (45 mg, 0.37 mmol) in dried DCM (10 mL), EDC hydrochloride (70 mg, 0.37 mmol) was added portionwise at 0ºC. The resulting mixture was stirred for 2h at rt. After evaporation of the solvent under reduced pressure, the mixture was purified by FC (SiO_2, DCM/MeOH, 100:4). Compound **56** was obtained as a yellow solid (32 mg, 24%).

^{1}H NMR (300 MHz, $CDCl_3$) δ: 7.87 (dd, *J* = 8.5, 1.9 Hz, 2H), 7.73 (d, *J* = 8.5 Hz, 2H), 7.71 (d, *J* = 1.9 Hz, 2H), 7.58 (d, *J* = 2.3 Hz, 2H), 7.13 (dd, *J* = 8.5, 2.3 Hz, 2H).

^{13}C NMR (75 MHz, $CDCl_3$) δ: 165.1, 153.6, 149.1, 148.6, 137.3, 137.1, 133.3, 126.2, 125.1, 122.4, 121.0, 119.3, 118.7, 117.8, 117.6, 114.8, 112.3, 71.2, 71.9, 71.0, 70.9, 69.6, 69.5, 69.2.

2,6-*Bis*[(benzo[15]crown-5)-4'-carbonyloxy]exTTF, 57.

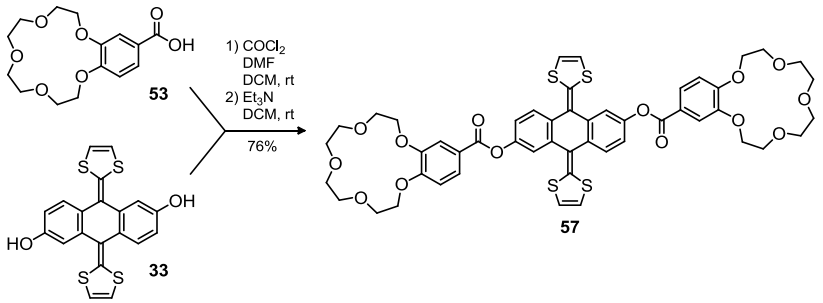

To a stirring solution of (benzo[15]crown-5)-4'-carboxylic acid **53** (100 mg, 0.32 mmol) and a catalytic amount of DMF in anhydrous DCM (20 mL), oxalyl chloride (0.1 mL, 0.93 mmol) was added at rt. After 30 min, the solvent was removed under reduced pressure, the resulting residue was diluted with anhydrous DCM (30 mL) and Et_3N (0.1 mL, 0.66 mmol) and 2,6-dihydroxy-exTTF **33** (62 mg, 0.15 mmol) were added. The reaction mixture was stirred at rt until no precipitate was observed. Purification of the reaction crude was performed by FC (Al_2O_3, DCM/MeOH, 100:0.2). The resulting product **57** was obtained as a yellow powder (38 mg, 76%).

^{1}H NMR (300 MHz, $CDCl_3$) δ: 7.43 (dd, *J* = 8.4, 1.90 Hz, 2H), 7.72 (d, *J* = 8.5 Hz, 2H), 7.69 (d, *J* = 1.9 Hz, 2H), 7.57 (d, *J* = 2.3 Hz, 2H), 7.12 (dd, *J* = 8.4, 2.34 Hz, 2H), 6.93 (d, *J* = 8.5 Hz, 2H), 6.31 (s, 4H), 4.25-4.22 (m, 8H), 3.97-3.92 (m, 8H), 3.79-3.78 (m, 16H).

^{13}C NMR (75 MHz, $CDCl_3$) δ: 165.1, 154.1, 159.1, 148.9, 137.2, 137.1, 133.3, 126.1, 125.1, 122.4, 121.0, 119.2, 118.7, 117.7, 117.5, 115.3, 112.4, 71.5, 70.7, 70.6, 69.7, 69.4, 69.0.

FTIR (DCM) ν: 2870, 1728, 1599, 1547, 1512, 1463, 1428, 1347, 1270, 1188, 1135, 1059, 960, 931, 755, 656 cm^{-1}

UV-vis (DCM) λ_{max} (log ε): 353 (4.04), 368 (4.22), 420 (4.36), 436 (4.42) nm.

MS (MALDI) *m/z*: 1023.2 $[M + Na]^+$, 1000.2 $[M]^+$.

HRMS (MALDI): *m/z* calcd for $C_{50}H_{48}NaO_{14}S_4$ 1023.1819. Found 1023.1810.

2,6-*Bis*[(*N*-phenylaza[18]crown-6)-4'-carbonyloxy]exTTF, 58.

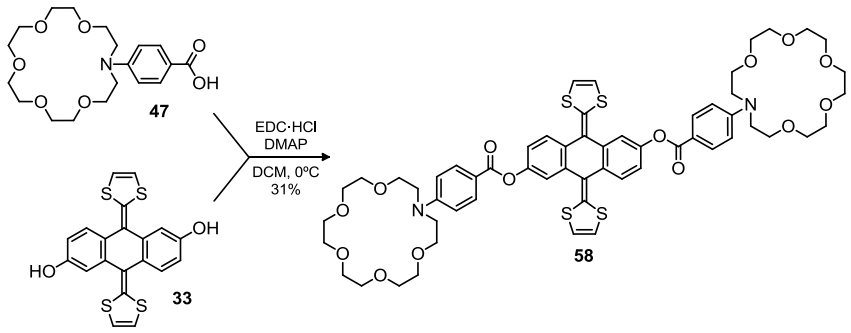

To a stirring solution of 1,6-dihydroxy-exTTF **33** (41 mg, 0.10 mmol) and carboxylic acid **47** (81 mg, 0,21 mmol) in dry DCM (20 mL) at 0ºC, EDC hydrochloride (42 mg, 0.22 mmol) and DMAP (27 mg, 0.22 mmol) were added portionwise. The resulting solution was allowed to slowly warm up to rt and then stirred overnight. The reaction mixture was diluted with 20 mL of DCM and sequentially washed with Na_2CO_3 sat. aq solution, HCl 1 M, and $NaHCO_3$ sat. solution, dried over Na_2SO_4, filtered and evaporated under reduced pressure. The resulting residue was purified by FC (Al_2O_3, DCM/MeOH, 100:0.2). Receptor **58** was obtained as a yellow solid (33 mg, 31 %).

^{1}H NMR (300 MHz, $CDCl_3$) δ: δ 8.04 (d, *J* = 9.0 Hz, 4H), 7.69 (d, *J* = 8.4 Hz, 2H), 7.56 (d, *J* = 2.3 Hz, 2H), 7.10 (dd, *J* = 8.4, 2.3 Hz, 2H), 6.72 (d, *J* = 9.0 Hz, 4H), 6.29 (d, *J* = 1.0 Hz, 4H), 3.74 – 3.73 (m, 16H), 3.67 - 3.66 (m, 32H).

^{13}C NMR (75 MHz, $CDCl_3$) δ: 165.3, 152.0, 149.2, 136.8, 136.5, 132.8, 132.4, 125.8, 121.1, 119.2, 118.6, 117.6, 117.2, 116.1, 110.8, 77.6, 77.2, 76.7, 71.0, 70.9, 70.9, 70.9, 68.5, 51.5.

FTIR (DCM) ν: 2919, 2860, 1716, 1602, 1522, 1464, 1403, 1351, 1263, 1176, 1110, 1062, 995, 760, 732, 699 cm^{-1}.

UV-vis (DCM) λ_{max} (log ε): 325 (4.96), 368 (4.32), 418 (4.40), 435 (4.46) nm.

MS (MALDI) *m/z*: 1165.3 $[M + Na]^+$, 1142.3 $[M]^+$.

HRMS (MALDI) *m/z* calcd for $C_{58}H_{66}N_2NaO_{14}S_4$ 1165.3289. Found 1165.3290.

2,6-*Bis*[(*N*-phenylaza[15]crown-5)-4'-carbonyloxy]exTTF, 59.

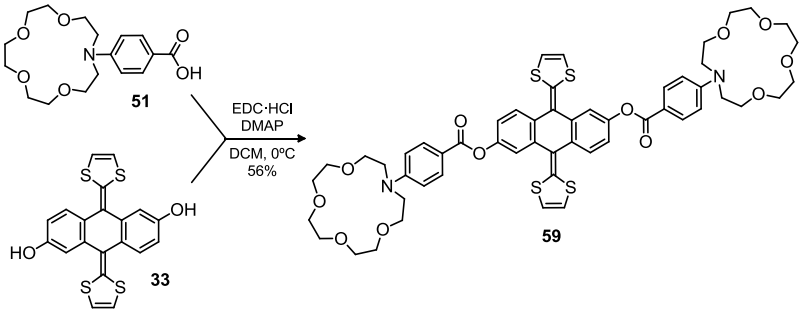

To a stirring solution of 1,6-dihydroxy-exTTF **33** (40 mg, 0.10 mmol) and carboxylic acid **51** (70 mg, 0.21 mmol) in dry DCM (20 mL) at 0ºC, EDC hydrochloride (57 mg, 0.30 mmol) and DMAP (37 mg, 0.30 mmol) were added portionwise. The resulting solution was allowed to slowly warm up to rt and then stirred overnight. The reaction mixture was diluted with 20 mL of DCM and sequentially washed with $NaHCO_3$ sat. aq solution, aq HCl 1 M, and H_2O, dried over Na_2SO_4, filtered and evaporated under reduced pressure. The resulting residue was purified by FC (Al_2O_3, DCM/MeOH, 100:0.2). Receptor **59** was obtained as a yellow solid (58 mg, 56 %).

^{1}H NMR (300 MHz, $CDCl_3$) δ: 8.05 (d, *J* = 8.6 Hz, 4H), 7.69 (d, *J* = 8.4 Hz, 2H), 7.56 (d, *J* = 2.4 Hz, 2H), 7.11 (dd, *J* = 8.4, 2.4 Hz, 2H), 6.70 (d, *J* = 8.6 Hz, 4H), 6.30 (s, 4H), 3.80 – 3.78 (m, 8H), 3.70 – 3.64 (m, 32H).

^{13}C NMR (126 MHz, $CDCl_3$) δ: 165.35, 149.23, 136.87, 136.53, 132.82, 132.38, 125.88, 121.16, 119.20, 118.64, 117.62, 117.24, 116.19, 110.85, 71.49, 70.47, 70.26, 68.35, 52.95.

FTIR (DCM) ν: 2865, 1716, 1601, 1547, 1521, 1465, 1394, 1353, 1263, 1176, 1124, 1062, 995, 829, 761, 732, 699, 659 cm^{-1}.

UV-vis (DCM) λ_{max} (log ε): 324 (4.90), 368 (4.25), 417 (4.33), 435 (4.40) nm.

MS (MALDI) *m/z*: 1077.3 $[M + Na]^+$, 1054.3 $[M]^+$.

HRMS (MALDI) *m/z* calcd for $C_{54}H_{58}N_2O_{12}S_4$ 1054.2867. Found 1054.2873.

2,6-*Bis*[benzoate-4'-carbonyloxy]exTTF, 60.

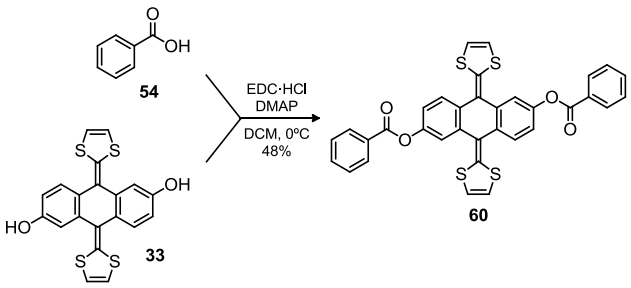

To a solution of 2,6-dihydroxy-exTTF **33** (100 mg, 0.24 mmol), benzoic acid **54** (62 mg, 0.51 mmol) and DMAP (74 mg, 0.61 mmol) in dried DCM (50 mL), EDC hydrochloride (116 mg, 0.61 mmol) was added portionwise at 0ºC. The resulting mixture was stirred for 2 h at rt. After evaporation of the solvent under reduced pressure, the mixture was purified by FC (SiO_2, DCM/MeOH, 100:4). Compound **60** was obtained as a yellow solid (71 mg, 48%).

^{1}H NMR (300 MHz, $CDCl_3$) δ: 8.29 – 8.20 (m, 4H), 7.74 (d, *J* = 8.4 Hz, 2H), 7.70 – 7.61 (m, 2H), 7.60 (d, *J* = 2.4 Hz, 2H), 7.58 – 7.48 (m, 4H), 7.15 (dd, *J* = 8.4, 2.4 Hz, 2H), 6.32 (s, 4H).

^{13}C NMR (75 MHz, $CDCl_3$) δ: 165.2, 148.8, 137.2, 137.0, 133.8, 133.2, 130.4, 129.7, 128.7, 126.0, 120.7, 119.0, 118.4, 117.6, 117.3, 77.6, 77.4, 77.2, 76.7.

FTIR (DCM) ν: 2922, 1735, 1547, 1509, 1465, 1258, 1189, 1025, 799, 708 cm^{-1}.

UV-vis (DCM) λ_{max} (log ε): 353 (4.22), 369 (4.40), 420 (4.53), 437 (4.60) nm.

MS (MALDI) *m/z*: 620.1 $[M]^+$.

HRMS (MALDI): *m/z* calcd for $C_{34}H_{20}O_4S_4$ 620.0239. Found 620.0220.

2-(*Tert*-butyl-diphenylsilyloxy)anthraquinone, 62.

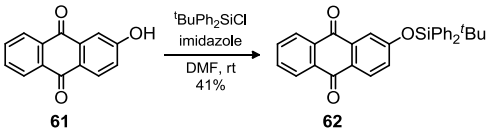

61 **62**

To a solution of 2-hydroxy-9,10-anthraquinone **61** (1.00 g, 4.46 mmol) in dry DMF (50 mL) at rt, *tert*-butyl(chloro)diphenylsilane (1.5 mL, 5.77 mmol), and imidazol (1.52 g, 22.30 mmol) were added. The mixture was stirred for 16 h at rt. The mixture was concentrated *in vacuo* and the residue taken in DCM. The organic phase was washed with H_2O, dried (Na_2SO_4), filtered and the solvent was removed under reduced pressure. Purification of the product was achieved by FC (SiO_2, hexane/DCM, 2:1 + 1% Et_3N v/v) followed by washing with MeOH. Compound **62** (845 mg, 41%) was obtained as a yellow solid.

^{1}H NMR (300 MHz, $CDCl_3$) δ: 8.30 – 8.17 (m, 2H), 8.04 (d, *J* = 8.5 Hz, 1H), 7.78 – 7.70 (m, 6H), 7.69 (d, *J* = 2.6 Hz, 1H), 7.53 – 7.32 (m, 6H), 7.02 (dd, *J* = 8.6, 2.6 Hz, 1H), 1.15 (s, 9H).

^{13}C NMR (75 MHz, $CDCl_3$) δ: 183.18, 182.32, 161.16, 135.55, 134.17, 133.79, 133.76, 131.76, 130.52, 129.75, 128.20, 128.16, 127.45, 127.21, 125.52, 117.82, 77.58, 77.16, 76.74, 26.56, 19.66.

FTIR (DCM) ν: 1673, 1590, 1428, 1325, 1301, 1264, 1237, 1114, 896, 803, 731, 701, 636, 613 cm^{-1}.

MS (MALDI) *m/z*: 485.2 $[M + Na]^+$.

HRMS (MALDI) *m/z* calcd for $C_{30}H_{26}NaO_3Si$ 485.1543. Found 485.1531.

2-(*Tert*-butyl-diphenylsilyloxy)-exTTF, 29.

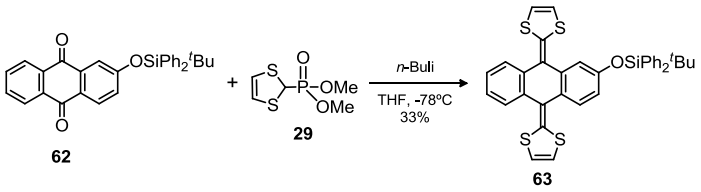

62 29 63

To a solution of phosphonate ester **29** (10 g, 47.12 mmol) in dry THF (100 mL) at -78°C, *n*-BuLi (1.6 M in hexanes) (35 mL, 51.83 mmol) was added dropwise with a syringe. After 30 min at -78°C, a solution of **62** in dry THF (3.63 g, 7.85 mmol) was added with a syringe into the solution of the phosphonate carbanion. The mixture was stirred for 1 h at -78°C and then allowed to warm to rt, and let to stand overnight. The THF was evaporated under reduced pressure, brine (100 mL) added and the residue extracted with DCM. The combined extracts were dried (Na_2SO_4), filtered out, and the solvent was removed under reduced pressure. Purification of products was achieved by FC (SiO_2, hexane/DCM, 4:1 + 1% Et_3N v/v). The titled product **63** (1.58 g, 33%) was obtained as a yellow solid.

^{1}H NMR (300 MHz, $CDCl_3$) δ: 7.79-7.75 (m, 4H), 7.67 – 7.60 (m, 2H), 7.46 – 7.36 (m, 7H), 7.29 – 7.22 (m, 2H), 7.05 (d, *J* = 2.5 Hz, 1H), 6.76 (dd, *J* = 8.4, 2.5 Hz, 1H), 6.26 (s, 2H), 6.15 (dd, *J* = 27.6, 6.7 Hz, 2H), 1.12 (s, 9H).

^{13}C NMR (75 MHz, $CDCl_3$) δ: 153.5, 136.6, 136.2, 135.8, 135.6, 135.5, 135.4, 133.3, 129.9, 129.8, 128.8, 127.9, 126.0, 125.8, 125.0, 124.9, 117.5, 117.1, 117.0, 116.7, 116.0, 77.5, 77.2, 77.0, 76.6, 31.0, 26.5, 19.5.

FTIR (DCM) ν: 3070, 2957, 2930, 2857, 1560, 1546, 1515, 1465, 1427, 1311, 1285, 1264, 1238, 1112, 1011, 951, 872, 822, 800, 755, 733, 701, 661, 643, 612 cm^{-1}.

MS (MALDI) *m/z*: 634.2 $[M]^+$.

HRMS (MALDI) *m/z* calcd for $C_{36}H_{30}OS_4Si$ 634.0943. Found 634.0923.

2-Hydroxy-exTTF, 64.

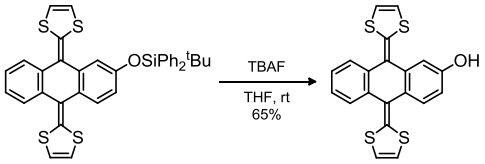

63 **64**

To a solution of **63** (1.50 g, 2.36 mmol) in dry THF (150 mL) at rt, *n*-Bu_4NF (1M in THF) (7 mL, 7.00 mmol) was added. The mixture was stirred at rt for 16 h obtaining a yellow precipitate which was filtered and purified by FC (SiO_2, hexane/DCM, 1:1 + 1% Et_3N v/v then DCM/MeOH 9:1 + 1% Et_3N v/v). The product **64** (608 mg, 65%) was obtained as a yellow solid.

^{1}H NMR (300 MHz, DMSO) δ: δ 9.78 (s, 1H), 7.61 (m, 2H), 7.45 (d, *J* = 8.4 Hz, 1H), 7.32 (m, 2H), 7.07 (d, *J* = 2.4 Hz, 1H), 6.88 – 6.43 (m, 5H).

^{13}C NMR (75 MHz, DMSO) δ: 155.7, 136.2, 136.2, 134.9, 134.7, 133.2, 126.3, 126.1, 126.0, 126.0, 124.7, 124.6, 121.0, 120.9, 118.2, 118.0, 117.8, 112.8, 111.5.

FTIR (DCM) ν: 3066, 1602, 1577, 1547, 1514, 1466, 1450, 1283, 1264, 1225, 1158, 798, 754, 734, 702, 677, 635 cm^{-1}.

MS (MALDI) *m/z*: 396.0 $[M]^+$.

HRMS (MALDI) *m/z* calcd for $C_{20}H_{12}OS_4$ 395.9765. Found 395.9756.

2-(*Tert*-butyl-diphenylsilyloxymethyl)anthraquinone, 66.[141]

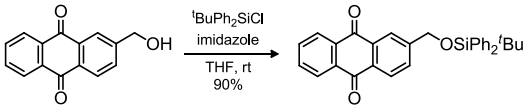

65 **66**

To a solution of 2-hydroxymethyl-9,10-antraquinone **65** (1.00 g, 4.20 mmol) in dry THF (50 mL) at rt, *tert*-butyl(chloro)diphenylsilane (1.32 g, 1.25 mL, 5.03 mmol), and imidazol (1.43 g, 21.00 mmol), were added. The mixture was stirred for 16 h at rt. H_2O (75 mL) was added and the residue extracted with AcOEt. The combined extracts were dried ($MgSO_4$), filtered out, and the solvent was removed under reduced pressure. Purification of the product was achieved by FC (SiO_2, hexane/DCM, 3:1) and washing with MeOH. Compound **66** (1.74 g, 90%) was obtained as a yellow solid.

[141] S. González, N. Martín and D. M. Guldi, *J. Org. Chem.* **2002**, *68*, 779.

^{1}H NMR (300 MHz, $CDCl_3$) δ: 8.33-8.25 (m, 4H), 7.83-7.79 (m, 3H), 7.73-7.70 (m, 4H), 7.47-7.38 (m, 6H), 4.92 (s, 2H), 1.16 (s, 9H).

2-(*Tert*-butyl-diphenylsilyloxymethyl)-exTTF, 67.[141]

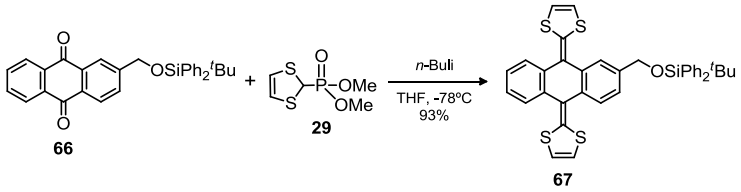

66 29 67

To a solution of phosphonate ester **29** (212 mg, 1.00 mmol) in dry THF (20 mL) at -78ºC, *n*-BuLi (1.6 M in hexanes) (0.70 mL, 1.12 mmol) was added dropwise with a syringe. After 30 min at -78ºC, a solution of **66** in dry THF (119 mg, 0.25 mmol) was added with a syringe into the solution of the phosphonate carbanion. The mixture was stirred for 1 h at -78ºC and then allowed to warm to rt, and let to stand overnight. The THF was evaporated under reduced pressure, H_2O (75 mL) added and the residue extracted with DCM. The combined extracts were dried ($MgSO_4$), filtered out, and the solvent was removed under reduced pressure. Purification of the product was achieved by FC (SiO_2, hexane/DCM, 3:1). Compound **67** was obtained as a yellow solid (603 mg, 93%).

^{1}H NMR (200 MHz, $CDCl_3$) δ: 7.72-7.64 (m, 7H), 7.44-7.22 (m, 10H), 6.30-6.27 (m, 4H), 4.84 (d, *J* = 13.3 Hz, 1H), 4.81 (d, *J* = 13.3 Hz, 1H), 1.12 (s, 9H).

2-Hydroxymethyl-exTTF, 68.[141]

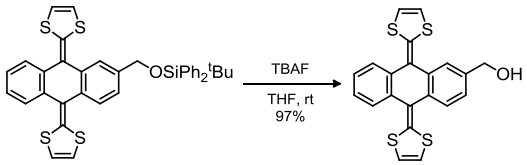

67 68

To a solution of **67** (325mg, 0.50 mmol) in dry DMF (50 mL) at rt, *n*-Bu_4NF (1M in THF) (0.75 mL, 0.75 mmol) was added. The mixture was stirred at rt for 16 h. H_2O (75 mL) was added and the residue extracted with DCM. The combined extracts were dried ($MgSO_4$), filtered out, and the solvent was removed under reduced pressure.

Purification of the product was achieved by FC (SiO_2, hexane/DCM, 3:1). Compound **68** was obtained as a yellow solid (199 mg, 97%).

^{1}H NMR (200 MHz, DMSO) δ: 7.66-7.57 (m, 4H), 7.36-7.23 (m, 3H), 6.74-6.73 (m, 4H), 5.29 (t, *J* = 5.6 Hz, 1H), 4.54 (d, *J* = 5.6 Hz, 2H).

Methyl 3,5-*Bis*(5-chloro-3-oxapentyloxy)benzoate, 71.[142]

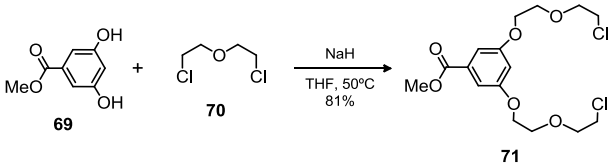

NaH (2.92 g, 73.00 mmol, 60% in mineral oil) was added to a solution of methyl 3,5-dihydroxybenzoate **69** (6.06 g, 36.04 mmol) in DMF (30 mL). The mixture was stirred 2 h at 110ºC and cooled to rt; the resulting suspension of dianion was added to a solution of 2-chloroethyl ether **70** (51.81 g, 362.28 mmol, 10 equiv.) in DMF (30 mL) over 6 h and then the mixture was stirred for five days at 50ºC and filtered (Celite) to remove NaCl. DMF and excess dichloride were removed *in vacuo*. Purification of the residue by FC (SiO_2, DCM/EtOAc, 20: 1) gave **71** (11.1 g, 81%) as an oil.

^{1}H NMR (300 MHz, $CDCl_3$) δ: 7.21 (d, *J* = 2.2 Hz, 2H), 6.53 (t, *J* = 2.2 Hz, 1H), 4.16 (t, *J* = 4.6 Hz, 4H), 3.88 (m, 7H), 3.83 (t, *J* = 5.8 Hz, 4H), 3.66 (t, *J* = 5.8 Hz, 4H).

***Bis*(5-methoxycarbonyl-1,3-phenylene)[20]crown, 72.**[142]

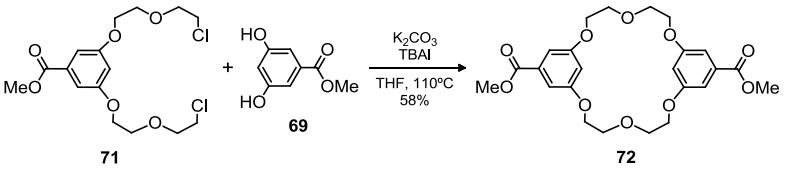

A solution of methyl 3,5-*bis*(5-chloro-3-oxapentyloxy)benzoate **71** (6.04 g, 15.84 mmol) and methyl 3,5-dihydroxybenzoate **69** (2.66 g, 15.84 mmol) in DMF (22 mL) was added *via* a syringe pump at 0.75 mL/h to a suspension containing K_2CO_3 (22.04 g, 159.47 mmol) and *n*-Bu_4NI (20 mg) in DMF (750 mL) at 110ºC. After complete

[142] D. S. Nagvekar and H. W. Gibson, *Org. Prep. Proced. Int.* **1997**, *29*, 237.

addition, the mixture was stirred vigorously at 110°C for five days, cooled and evaporated. The residue was taken in DCM and filtered (Celite) to remove salts and subjected to FC (SiO_2, Et_2O) to give pure **72** (4.36 g, 58%).

mp: 186-188°C.

^{1}H NMR (300 MHz, $CDCl_3$) δ: 7.09 (d, *J* = 2.4 Hz, 4H), 6.67 (br s, 2H), 4.12 (br s, 8H), 3.83 (br s, 14H).

***Bis*(5-methoxycarbonyl-1,3-phenylene)[20]crown-6, 73.**[143]

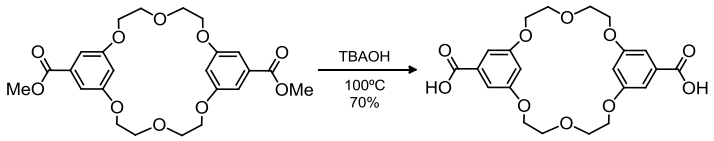

72 **73**

A solution of 1.25 g (2.62 mmol) of bis(5-carbomethoxy-m-phenylene)[20]crown-6 **72** in 50 mL of 40% aq *n*-Bu_4NOH was refluxed for 24 h, cooled, acidified with 4M HCl (50 mL), cooled to 0-5°C and filtered (Celite). The solid was washed with H_2O, dried and recrystallized from py to afford compound **73** (822 mg, 70%) as a colorless solid.

^{1}H NMR (DMSO) δ: 13.5-12.4 (br s), 7.03 (d, *J* = 1.0 Hz, 4H), 6.67 (m, 2H), 4.13 (t, *J* = 2.0 Hz, 8H), 3.79 (t, *J* = 2.0 Hz, 8H).

^{13}C NMR (75 MHz, $CDCl_3$) δ: 166.8, 159.5, 132.6, 107.6, 107.3, 68.9, 67.7.

[143] H. W. Gibson, D. S. Nagvekar, J. Powell, C. Gong and W. S. Bryant, *Tetrahedron* **1997**, *53*, 15197.

***Bis*[5-(2-exTTF-oxycarbonyl)-1,3-phenylene][20]crown-6, 74.**

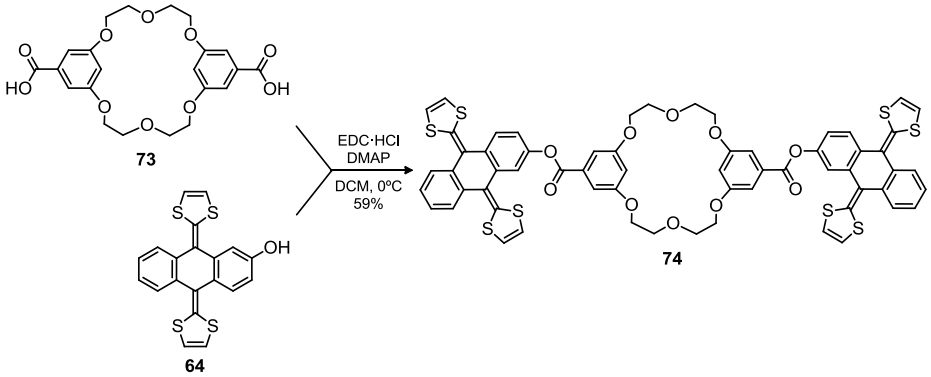

73 **64** **74**

To a stirring solution of 2-hydroxy-exTTF **64** (110 mg, 0.23 mmol) and dicarboxylic acid **73** (50 mg, 0.11 mmol) in dry DCM (20 mL) at 0°C, EDC hydrochloride (54 mg, 0.28 mmol) and DMAP (34 mg, 0.28 mmol) were added portionwise. The resulting solution was allowed to slowly warm up to rt and then stirred overnight. The reaction mixture was diluted with 20 mL of DCM and sequentially washed with $NaHCO_3$ sat. aq solution, HCl 1 M, and H_2O, dried over Na_2SO_4, filtered and evaporated under reduced pressure. The resulting residue was purified by FC (SiO_2, DCM, then DCM/AcOEt 95:5). Receptor **74** was obtained as a yellow solid (79 mg, 59 %).

^{1}H NMR (700 MHz, DMSO) δ 7.70 – 7.61 (m, 5H), 7.55 (d, *J* = 8.4 Hz, 1H), 7.51 (d, *J* = 2.4 Hz, 1H), 7.48 (d, *J* = 2.4 Hz, 1H), 7.39 – 7.31 (m, 4H), 7.25 (m, 1H), 7.22 – 7.16 (m, 5H), 6.79 – 6.68 (m, 8H), 6.65 (d, *J* = 6.6 Hz, 2H), 4.27 – 4.15 (m, 8H), 3.84-3.82 (m, 8H).

^{13}C NMR (176 MHz, DMSO) δ 164.6, 164.6, 160.2, 148.7, 148.7, 138.4, 138.2, 137.2, 136.5, 136.4, 135.1, 135.0, 134.9, 133.0, 132.9, 130.9, 128.7, 126.8, 126.2, 126.1, 125.8, 125.2, 125.1, 120.5, 120.3, 120.1, 119.8, 119.7, 118.7, 118.7, 118.6, 118.5, 108.9, 108.6, 69.5, 69.5, 68.5.

FTIR (DCM) ν: 3068, 2925, 1732, 1596, 1546, 1513, 1453, 1420, 1370, 1322, 1300, 1264, 1204, 1173, 1109, 1088, 1064, 1006, 953, 865, 800, 755, 735, 702, 675, 650, 633 cm^{-1}.

MS (MALDI) *m/z*: 1204.1 $[M]^+$, 1227.0 $[M + Na]^+$.

HRMS (MALDI) *m/z* calcd for $C_{62}H_{44}O_{10}S_8$ 1204.0695 found 1204.0654

***Bis*[5-(2-exTTF-methyloxycarbonyl)-1,3-phenylene][20]crown-6, 75.**

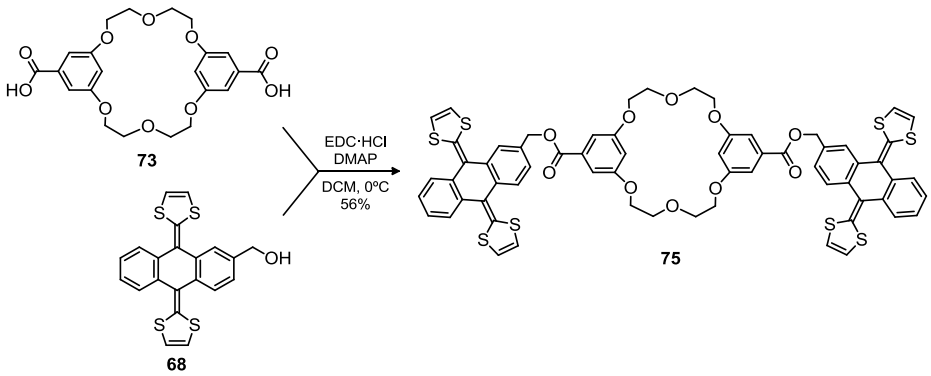

73 68 75

To a stirring solution of 2-hydroxymethyl-exTTF **68** (96 mg, 0.23 mmol) and dicarboxylic acid **73** (50 mg, 0.1 mmol) in dry DCM (20 mL) at 0ºC, EDC·HCl (54 mg, 0.28 mmol) and DMAP (34 mg, 0.28 mmol) were added portionwise. The resulting solution was allowed to slowly warm up to rt and then stirred overnight. The reaction mixture was diluted with 20 mL of DCM and sequentially washed with $NaHCO_3$ sat. aq solution, HCl 1 M, and H_2O, dried over Na_2SO_4, filtered and evaporated under reduced pressure. The resulting residue was purified by FC (SiO_2, DCM, then DCM/AcOEt 1:1). Receptor **75** was obtained as a yellow solid (77 mg, 56 %).

^{1}H NMR (700 MHz, DMSO) δ: 7.71 (m, 2H), 7.66 – 7.59 (m, 6H), 7.35 (d, *J* = 8.0 Hz, 2H), 7.34 – 7.27 (m, 4H), 7.08 (s, 4H), 6.76 – 6.69 (m, 6H), 6.68 – 6.63 (m, 4H), 5.33 (s, 4H), 4.17 – 4.08 (m, 8H), 3.82 – 3.72 (m, 8H).

^{13}C NMR (175 MHz, DMSO) δ: 165.2, 159.7, 136.9, 134.9, 134.7, 134.6, 134.4, 134.0, 131.2, 126.3, 125.5, 124.8, 124.7, 123.7, 120.5, 120.4, 118.3, 118.2, 118.1, 117.8, 107.7, 69.1, 68.0, 65.9.

FTIR (DCM) v: 3062, 2925, 2864, 1717, 1596, 1546, 1512, 1449, 1298, 1264, 1224, 1171, 1068, 733, 702, 649 cm^{-1}.

MS (MALDI) *m/z*: 1232.1 $M]^+$, 1255.1 $[M + Na]^+$.

HRMS (MALDI) *m/z* calcd for $C_{64}H_{48}O_{10}S_8$ 1232.1008. Found 1232.0990.

Annexes

ANNEX I. A SHORT MANUAL ON TITRATION EXPERIMENTS

I.1. INTRODUCTION

As we have seen along this manuscript, one of the most important data about a supramolecular system is the stability of the complex formed, i.e. the free energy (ΔG) associated to the system.

The easiest way of obtaining this information is through the equilibrium constant of the system (K_a), which measures the binding affinity of the molecular building blocks and which is directly related to ΔG through the equation (**6**).

$$\Delta G = -RT\ln K_a \qquad \textbf{(6)}$$

Many authors have written excellent book chapters and articles about how to obtain the binding constant from titration experiments[115],[144] and, therefore, in this annex we will only mention those aspects more relevant to this study.

Through this manuscript the following nomenclature has been systematically used:

- *Host* (H), is the building block whose physical or chemical properties are experimentally observed. Usually its concentration is maintained constant.
- *Guest* (G), is the building block whose concentration is the independent variable (the titrating agent).

In principle, the assignment of which molecule is the host and which the guest is arbitrary. In practice, it depends on the properties that are going to be observed and the solubilities of the building blocks. For practical reasons, the larger, more expensive or more synthetic demanding component is usually the host.[144c]

[144] a) H. Tsukube, H. Furuta, A. Odani, Y. Takeda, Y. Kudo, Y. Inoue, Y. Liu, H. Sakamoto and K. Kimura, in *Comprehensive Supramolecular Chemistry, Vol. 8* (Eds.: J.-M. Lehn, J. L. Atwood, J. E. D. Davies, D. D. Macnicol and F. Vögtle), Pergamon/Elsevier, Oxford, **1996**; b) C. S. Wilcox, in *Frontiers in supramolecular organic chemistry and photochemistry* (Eds.: H. J. Schneider and H. Dürr), VCH, **1991**; c) P. Thordarson, *Chem. Soc. Rev.* **2011**, *40*, 1305; d) P. Thordarson, in *Supramol. Chem.* (Eds.: J. W. Steed and P. A. Gale), John Wiley & Sons, Ltd, **2012**; e) E. M. Pérez and N. Martín, in *Supramolecular Chemistry of Fullerenes and Carbon Nanotubes* (Eds.: N. Martín and J.-F. Nierengarten), Wiley-VCH, Weinheim, **2012**; f) K. Hirose, in *Analytical Methods in Supramolecular Chemistry* (Ed.: C. Schalley), Wiley-VCH Verlag GmbH & Co. KGaA, **2007**, p. 17.

I.2. A NOTE ON THE USE OF SALTS IN NON-AQUEOUS SOLVENTS

If we consider a supramolecular complex formed by a host and a guest molecule in a 1:1 stoichiometry, its equilibrium will be given by (**7**) and its association constant K_a will thus be **(8)**, where 'a_X' are the activity coefficients of the different species present.

$$H + G \rightleftharpoons HG \qquad \textbf{(7)}$$

$$K_a = \frac{a_{HG}}{a_H \, a_G} \qquad \textbf{(8)}$$

For the sake of simplicity, it is a very common practice to replace the activity coefficients by the concentration of the species. While this assumption is correct in the case of neutral molecules or salts in aqueous media, it is important to recall that salts tend to ion pair in low dielectric constant organic solvents (ε < 30) as those typically used in supramolecular chemistry.[145] For example, at an ionic strength of 0.01 M, the activity coefficient of a monovalent ion in water (ε = 80.2) is 0.99 whereas in chloroform (ε = 4.8) is 0.46.

As a result, in order to account for ionic strength effects, we need to consider that both the ion pair and the free form of a building block may intervene in the formation of the supramolecular complex (Scheme I.1) and assume that the electrolyte exists in solution as a monomer and there are no other species present.[146]

$G^+X^- \rightleftharpoons G^+ + X^-$	Ion pair dissociation.
$G^+ + H \rightleftharpoons HG^+$	Complexation of the free guest.
$G^+X^- + H \rightleftharpoons HG^+X^-$	Complexation of the ion pair.

Scheme I.1. Possible equilibria for a salt acting as guest in non-aqueous media.

Thus, unless operating in very diluted conditions ([salt] < 10^{-4} M) in which the salt is nearly completely ionized one may not assume that concentration approximates activity for charged species in non-aqueous media. Luckily this was the case for the supramolecular systems developed in this study, simplifying the calculations.

[145] N. Isaacs, *Physical Organic Chemistry*, 2nd ed., Longmans England, **1995**.
[146] J. W. Jones, Thesis, Virginia Polytechnic Institute and State University (Blacksburg), **2004**.

I.3. DETERMINATION OF THE CONCENTRATION RANGE

Determining the right concentration range of both the host and the guest molecules is one of the key steps in a titration experiment. It is easy to understand why if we consider the problem from a qualitative point of view.

On the one hand, if the concentration of the system is too low, the host molecule will not "find" the guest molecule among the "sea" of solvent molecules and the complex will not be effectively formed.

On the other, if the concentration of the system is too high, the equilibria will be completely shifted towards the complex and problems such as solubility limitations, non-ideal binding behavior and other experimental difficulties may arise.

Several authors have also dealt with this problem from a quantitative point of view, proving that, in a titration experiment, measurements below 20% and above 80% complexation yield uncertain values (Figure I.1).[115]

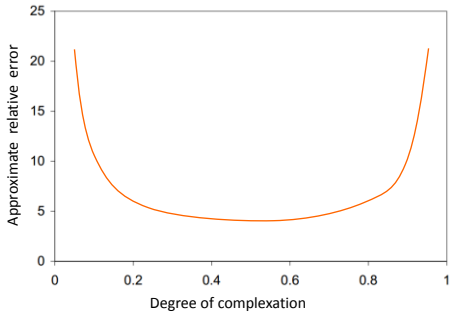

Figure I.1. Measures out of the 20%-80% complexation range yield very uncertain values.

While the initial concentration of host $[H]^o$ can be limited either by the technique employed (e.g. NMR requires concentrations in the range of 0.01 M) or the intrinsic properties of the system (e.g. the molar absorptivity is too low for UV-vis measurements), the starting concentration of the guest $[G]^o$ can be set up in a wider range. It is important though, to ensure that enough equivalents of guest are added to avoid an unending experiment.

A practical manner to know how concentrated should the host be and how many equivalents of guest are necessary in a titration experiment is offered by the p-value developed by Weber, which informs on the "probability of binding" of the system. It is defined as the concentration of the complex divided by the initial concentration of the minor component (the limiting reagent) and thus, in order to avoid very uncertain values, this p-value should be between 0.2 and 0.8.[147]

If we consider a system with a 1:1 stoichiometry and defined by (**7**), its p-values will be then obtained by (**9**) or (**10**), where $[H]^o$ and $[G]^o$ are quantities established by us.

$$p = \frac{[HG]}{[H]^o}; \text{ when } [H]^o \leq [G]^o \quad \textbf{(9)}$$

$$p = \frac{[HG]}{[G]^o}; \text{ when } [H]^o > [G]^o \quad \textbf{(10)}$$

p	p-value. Probability of binding of the system.
[H]	Equilibrium concentrations of the free host.
$[H]^o$	Starting concentration of the free host.
[G]	Equilibrium concentrations of the free guest.
$[G]^o$	Starting concentration of the free guest.
[HG]	Equilibrium concentrations of the complex.

The value of [HG], however, is a little bit more complex to obtain. It can be obtained theoretically if we consider the definition of the binding constant K_a (**8**) (substituting the activity coefficient of the species by its concentrations) and take into account the mass balance of both host (**11**) and guest (**12**).

$$[H] = [H]^o - [HG] \quad \textbf{(11)}$$

$$[G] = [G]^o - [HG] \quad \textbf{(12)}$$

Mixing all these equations together afford equation (**13**), which can be then transformed into (**14**) after expansion and into (**15**) after rearrangement. Solving the real root of this latter equation affords (**16**).

[147] G. Weber, in *Molecular biophysics* (Eds.: B. Pullman and M. Weissbluth), Academic Press, New York, **1965**.

$$K_a = \frac{[HG]}{([H]^o - [HG])([G]^o - [HG])} \quad \textbf{(13)}$$

$$K_a = \frac{[HG]}{[H]^o[G]^o - [HG]([H]^o + [G]^o) + [HG]^2} \quad \textbf{(14)}$$

$$[HG]^2 - \left([H]^o + [G]^o + \frac{1}{K_a}\right)[HG] + [H]^o[G]^o = 0 \quad \textbf{(15)}$$

$$[HG] = \frac{[H]^o + [G]^o + \frac{1}{K_a} - \sqrt{\left([H]^o + [G]^o + \frac{1}{K_a}\right)^2 - 4[H]^o[G]^o}}{2} \quad \textbf{(16)}$$

Equation (**16**) is a powerful one as it involves the three key elements in a titration experiment: the initial concentrations of host $[H]^o$ and guest $[G]^o$ molecules and the association constant K_a, this being the only unknown variable.

This equation also defines a surface that can be perpendicularly cut with an intersecting perpendicular plane to produce a curve relating [HG] with $[G]^o$ (or $[H]^o$). This curve is what we call a binding isotherm. As seen in Figure I.2, when the concentration of guest is high in comparison to K_a, the saturation is quickly reached and the binding isotherms have substantial linear portions (c). However, when the concentrations are lowered, more gently curved isotherms are obtained (a) and (b).[144b]

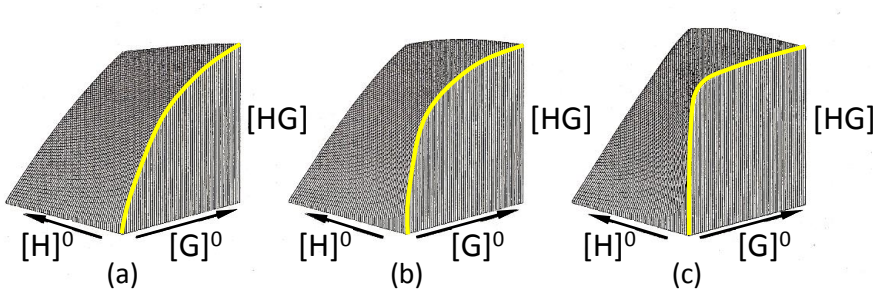

Figure I.2. Three surfaces as defined by (**16**) and their corresponding binding isotherm (in yellow). The three examples differ in the magnitude of K_a being (a) the weakest and (c) the strongest. Vertical axes are not scaled equally.

In order to obtain some numerical values, we need to make some preliminary estimation on the binding constant, the unknown variable in equation (**16**). If possible, a good idea for doing this is to consider analogous systems found in literature. As an arbitrary example, Table I.1 sums up the different p-values (p) and the number of guest molecules equivalents (n) associated for a system where the dissociation constant (K_d = 1/K_a) is 10^{-6} M^{-1}. A close analysis of these values, with the support of their graphical representation (Figure I.3), provides valuable information on the best experimental conditions in a titration experiment.

Table I.1. Dependence of the p-value (p) and the number of guest equivalents (n) added upon different combinations of $[H]^o$ and $[G]^o$.[a]

	$[H]^o/K_d$		$[G]^o/K_d$										
			0.2	0.4	0.6	0.8	1.0	2.0	4.0	6.0	8.0	10	20
A	0.1	p	0.16	**0.27**	**0.36**	**0.43**	**0.49**	**0.66**	**0.80**	0.86	0.89	0.91	0.95
		n	2.00	**4.00**	**6.00**	**8.00**	**10.0**	**20.0**	**40.0**	60.0	80.0	100	200
B	1.0	p	**0.48**	**0.45**	**0.43**	**0.40**	**0.38**	**0.59**	**0.76**	0.81	0.84	0.90	0.95
		n	**0.20**	**0.40**	**0.60**	**0.80**	**1.00**	**2.00**	**4.00**	0.60	0.80	10	20
C	10	p	0.91	0.91	0.90	0.90	0.90	0.89	0.87	0.83	**0.79**	**0.73**	0.92
		n	0.02	0.04	0.06	0.08	0.10	0.20	0.40	0.60	**0.80**	**1.00**	2.00
D	$[G]/K_d$	p	0.15	**0.23**	**0.30**	**0.34**	**0.38**	**0.50**	**0.61**	**0.67**	**0.70**	**0.73**	**0.80**
		n	1.00	**1.00**	**1.00**	**1.00**	**1.00**	**1.00**	**1.00**	**1.00**	**1.00**	**1.00**	**1.00**

[a] As obtained from equations (**9**), (**10**) and (**16**), p-values in the 0.2 - 0.8 range are in bold.

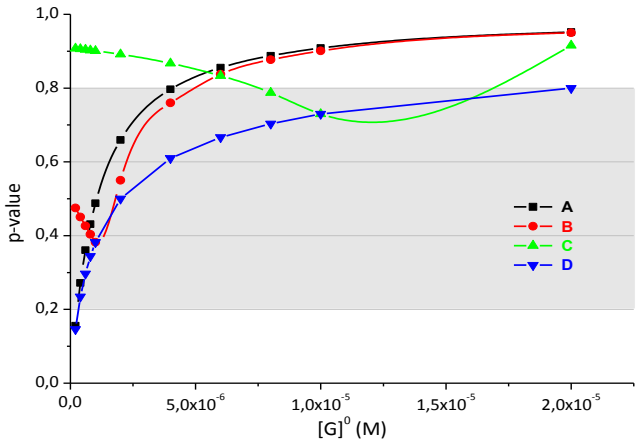

Figure I.3. Graphical representation of values obtained in Table I.1 when $K_a = 10^6$.

A Host concentration $[H]^o$ is approximately one-tenth of the dissociation constant (K_d). These conditions provide the widest range of p-values and thus are considered to be the best. However, they demand a large excess of guest molecule (1-50 equivalents).

B Host concentration $[H]^o$ is fixed at a concentration equal to K_d. Whereas these conditions do not allow to obtain p-values < 0.3 they are still useful if more diluted conditions are difficult to obtain (e.g. NMR). As an advantage, they require a smaller excess of guest molecule (1-5 equivalents).

C Host concentration $[H]^o$ is much larger than the binding constant. In this case appropriate p-values are never attained as the equilibria is directly shifted towards the formation of the complex.

D Host concentration $[H]^o$ is equal to guest concentration $[G]^o$. This is an alternative way for a titration based in a dilution protocol. It can be practical when binding is very strong as it affords the lowest possible p-values for any given analyte concentration.

As a result, the following methodology has been employed in this study:

1. An estimation of the K_a value [the only unknown variable in (**16**)] has been made on the base of previous results in literature of analogous systems.
2. The necessary $[H]^o$ and $[G]^o$ for such a system has been calculated so the p-values remain in the 0.2 - 0.8 range.
3. A titration experiment has been made and an experimental K_a found.
4. The p-values for this system have been recalculated with the experimental K_a value obtained. At this stage two possible situations are possible:
    a. Most of p-values are in the 0.2-0.8 range → Titration experiment is repeated up to 3 times to estimate the errors.
    b. Most of p-values are NOT in the 0.2-0.8 range → Step 2, 3 and 4 are repeated with the experimental K_a previously found.

An example of the Excel tables used in this thesis for setting up the experimental conditions of a titration experiment for host **66** is depicted in Table I.2.

Table I.2. Example of an Excel table used for setting up the experimental conditions in a typical titration experiment.

	[TTF] (M)	3,22E-04	1 mg TTF / 5 mL ClPh	MW 620,78	Kd ?	5,01E-04		Path	1 mm		Host **66**	
	[C60] (M)	8,33E-03	12 mg C60 / 2 mL ClPh	MW 720,64				V tot (mL)	0,60			
	SOLUTION TTF			**SOLUTION C60**				**ClPh**		**FORESEEN VALUES**		
	Vol (mL)	*mol (TTF)*	*[TTF] in the cell*	*Vol (mL)*	*mol (C60)*	*[C60] in the cell*	*[C60]/Kd*	*Vol (mL)*	*Eq C60*	*[TTF::C60]*	*p*	
1	0,2	6,44E-08	1,07E-04	0,000	0,00E+00	0,00E+00	0,0	0,400	0,00	0,00E+00	0,00	
2	0,2	6,44E-08	1,07E-04	0,010	8,33E-08	1,39E-04	0,3	0,390	1,29	2,05E-05	0,19	
3	0,2	6,44E-08	1,07E-04	0,020	1,67E-07	2,78E-04	0,6	0,380	2,58	3,50E-05	0,33	
4	0,2	6,44E-08	1,07E-04	0,030	2,50E-07	4,16E-04	0,8	0,370	3,88	4,57E-05	0,43	
5	0,2	6,44E-08	1,07E-04	0,040	3,33E-07	5,55E-04	1,1	0,360	5,17	5,37E-05	0,50	
6	0,2	6,44E-08	1,07E-04	0,050	4,16E-07	6,94E-04	1,4	0,350	6,46	6,00E-05	0,56	
7	0,2	6,44E-08	1,07E-04	0,060	5,00E-07	8,33E-04	1,7	0,340	7,75	6,50E-05	0,60	
8	0,2	6,44E-08	1,07E-04	0,070	5,83E-07	9,71E-04	1,9	0,330	9,05	6,90E-05	0,64	
9	0,2	6,44E-08	1,07E-04	0,080	6,66E-07	1,11E-03	2,2	0,320	10,34	7,24E-05	0,67	
10	0,2	6,44E-08	1,07E-04	0,090	7,49E-07	1,25E-03	2,5	0,310	11,63	7,53E-05	0,70	
11	0,2	6,44E-08	1,07E-04	0,100	8,33E-07	1,39E-03	2,8	0,300	12,92	7,77E-05	0,72	
12	0,2	6,44E-08	1,07E-04	0,110	9,16E-07	1,53E-03	3,0	0,290	14,21	7,98E-05	0,74	
13	0,2	6,44E-08	1,07E-04	0,120	9,99E-07	1,67E-03	3,3	0,280	15,51	8,16E-05	0,76	
14	0,2	6,44E-08	1,07E-04	0,130	1,08E-06	1,80E-03	3,6	0,270	16,80	8,32E-05	0,77	
15	0,2	6,44E-08	1,07E-04	0,140	1,17E-06	1,94E-03	3,9	0,260	18,09	8,46E-05	0,79	
	3			1,050				4,950				

The volume and number of aliquots of the guest solution added depend both on the expected dissociation constant and on the number of data points we wish to obtain. As a general rule it is wise to maintain the concentration of the guest solution more concentrated than the solution of the host (e.g. $[G]^o = 100[H]^o$) to cover a large range of complexation within a reasonable volume. It is also important to note that both $[H]^o$ and $[G]^o$ can be changed in any manner during the titration experiment as far as the p-values remain in the appropriate range.

In order to avoid dilution factors, it is a common practice to use the solution of host as solvent in the solution of guest rather than use pure solvent.

An alternative procedure consists in preparing a fresh solution for each titration point. This was the approach employed with the exTTF derivatives, given the photosensitizer role that fullerenes have in these systems.

I.4. CHOOSING THE SPECTROSCOPIC METHOD

Now that we have seen how to calculate [HG] theoretically and the importance of the p-values, an important question remains open: how to measure [HG] experimentally. The answer to this question is intimately linked with the chosen spectroscopic method as most of the time we are not observing the complex concentration itself but a physical change proportional to it. Even though there is a myriad of techniques available for a supramolecular titration,[115] in this annex we will only mention the techniques employed in this study.

I.4.1. NMR spectroscopy

It is based in studying the complexation-induced shift of the NMR signals of the host. It is one of the most commonly used techniques due to the high structural information provided, its tolerance towards minor impurities and wide availability. However, its limited sensitivity demands the use of moderate concentration ($[H]^o \approx 10^{-4}$ M) and thus, appropriate p-values can only be obtained for weak association constants ($\leq 10^4$ M) as seen before. Two different scenarios can be found:

a) Case 1: Slow exchange rate (in the NMR time scale)

In this regime two chemically different environments exist at a single moment and, thus, both the signals of the building blocks and the signal of the complex are seen (Figure I.4). As a result of the evolution of the complexation, during the titration experiment, the signal of the host will decrease and the one of the complex increase.

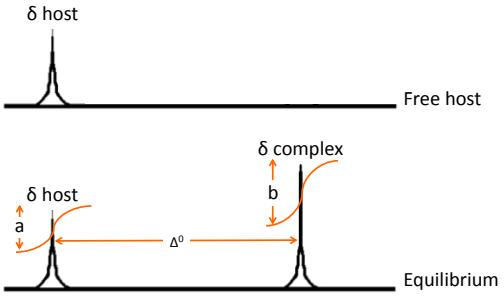

Figure I.4. Representative NMR spectra for a slow exchange of the complexation equilibrium.

In this case, [HG] can be measured directly by considering the integration of the host peak in the complex over the total integration of the host parts as expressed by **(17)** which can be then rewritten into equation **(18)** to provide the sought [HG]. Replacing this value into equation (**13**) affords the value of the binding constant.

$$\frac{[HG]}{[H]^o} = \frac{b}{a+b} \quad \textbf{(17)}$$

$$[HG] = \frac{b}{a+b}[H]^o \quad \textbf{(18)}$$

b) Case 1: Fast exchange rate (in the NMR time scale)

This is by far, the most common situation found in supramolecular systems. In this case a single time-averaged signal is observed (Figure I.5).

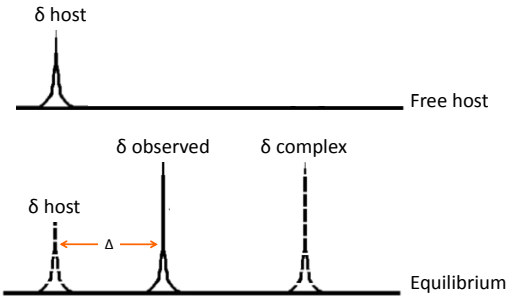

Figure I.5. Representative NMR spectra for a fast exchange of the complexation equilibrium.

In this case the observed chemical shift (δ_{obs}) is the weighted average of the free host and the bound host in the complex as seen in equation **(19)** where χ is the mole fraction as defined by **(20)**, **(21)** and **(22)**.

$$\delta_{obs} = \chi_H\delta_H + \chi_{HG}\delta_{HG} \quad \textbf{(19)}$$

$$\chi_{HG} + \chi_H = 1 \quad \textbf{(20)}$$

$$\chi_{HG} = \frac{[HG]}{[H]+[HG]} \quad \textbf{(21)}$$

$$\chi_H = \frac{[H]}{[H]+[HG]} = 1 - \frac{[HG]}{[H]+[HG]} \quad \textbf{(22)}$$

Then, δ_{obs} (**19**) can be rewritten with the help of $[H]^o$ definition (**11**) into (**23**), which in turn can then be reorganized into (**24**).

$$\delta_{obs} = \delta_H + \frac{[HG]}{[H]+[HG]}(\delta_{HG}-\delta_H) = \delta_H + \frac{[HG]}{[H]^0}(\delta_{HG}-\delta_H) \quad \textbf{(23)}$$

$$[HG] = \frac{[H]^o(\delta_{obs}-\delta_H)}{(\delta_{HG}-\delta_H)} = [H]^o\left(\frac{\Delta}{\Delta^o}\right) \quad \textbf{(24)}$$

Where $\Delta = \delta_{obs} - \delta_H$ and $\Delta^o = \delta_{HG} - \delta_H$. The Δ/Δ^o ratio is called the saturation fraction, and is equal to χ_{HG}. As Δ^o remains an unknown variable, it is not possible to obtain the value of the binding constant by direct substituting in equation (**13**). However, there are several approximations to overcome this limitations (Rose-Drago, Benesi-Hildebrand, Scott-Scatchard…) which are based in simplifications of the system.[144a]

An alternative equation is obtained by combining together equations (**16**) and (**23**) to afford the exact expression for the complexation-induced shift of an NMR signal as a function of $[H]^o$, $[G]^o$, K_a, Δ^o and δ_H (**25**) where K_a and Δ^o remain unknown parameters.

$$\delta_{obs} = \delta_H + \frac{\Delta^o}{2[H]^o}\left\{[H]^o + [G]^o + \frac{1}{K_a} - \sqrt{\left([H]^o + [G]^o + \frac{1}{K_a}\right)^2 - 4[H]^o[G]^o}\right\} \quad \textbf{(25)}$$

This equation can be solved with the help of computational methods and non-linear curve fitting methods. In a nutshell, these methods start from an estimated value of K_a (proposed by the user) and then take the data points corresponding to the largest $[G]^o$ (when the equilibrium should be fully displaced towards the formation of the complex) to estimate the value of Δ^o. With these values of K_a and Δ^o, a calculated chemical shift δ_{calc} is obtained for each experimental value of $[G]^o$ and $[H]^o$ and the difference between δ_{obs} and δ_{calc} ($\delta_{obs} - \delta_{calc}$) calculated. If the sum of these differences is positive (or negative), the proposed K_a is modified by increasing (or decreasing) its value. Then the entire process is repeated until convergence.[148]

[148] R. S. Macomber, *J. Chem. Educ.* **1992**, *69*, 375.

I.4.2. UV-visible spectroscopy

Is based in studying the complexation-induced absorption changes of the host moiety. It has been the most important technique in this thesis and globally it is probably the second most important method for determining binding constants as it is cheap, simple and insensitive to non-absorbing impurities.

Its main limitation arises from the fact that UV-vis titration needs to be carried out within a concentration range where an ideal behavior is followed (A < 1). In spite of this, the range of K_a available to obtain with this technique is rather large ($10^3 \leq K_a \leq 10^7$ M^{-1}). In addition, as indicated by the Beert-Lambert law ($A = l \cdot [H] \cdot \varepsilon_H$) the absorption of the host molecule (A) depends on its concentration [H] governed by the binding constant, its relative molar absorptivity (ε_H) fixed by its chemical nature, and the pathlength of the cell (l) which can be set freely by us. Therefore, a practical solution to widen the concentration range available to use consists in employing cells with different pathlengths, from 0.1 to 1 cm.

In contrast to NMR spectroscopy, the timescale for UV-vis transitions (< 10^{-12} s) is much smaller than the lifetime of any supramolecular complex and, thus, the exchange rate will always be in the slow regime.

Therefore, at a given wavelength (λ_{obs}) the observed absorbance (A_{obs}) will be the sum of the absorbance of the host (A_H), the guest (A_G) and the complex (A_{HG}) as seen in equations (**27**)-(**29**) where the length of the cell has been fixed to 1 cm as a premise for ease of the calculations and as depicted in Figure I.6.

$$A_{obs} = A_H + A_G + A_{HG} \quad \textbf{(26)}$$

$$A_H = \varepsilon_H [H] = \varepsilon_H ([H]^o - [HG]) \quad \textbf{(27)}$$

$$A_G = \varepsilon_G [G] = \varepsilon_G ([G]^o - [HG]) \quad \textbf{(28)}$$

$$A_{HG} = \varepsilon_{HG} [HG] \quad \textbf{(29)}$$

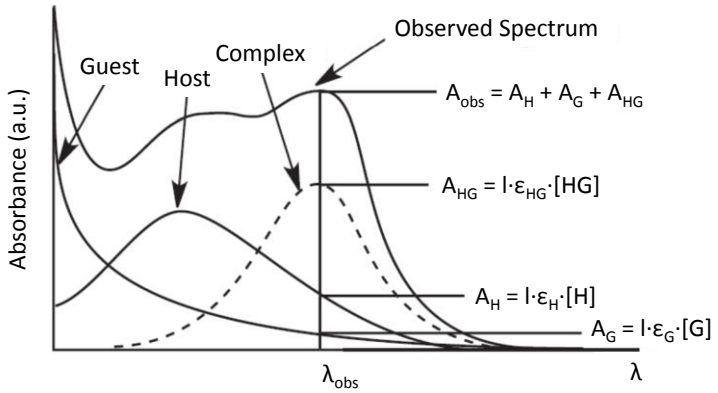

Figure I.6. Representative UV-vis spectra of a supramolecular titration.

Combining together equations (**27**)-(**29**) we can obtain equation (**30**), which in turn can be rewritten as (**31**) where $\varepsilon_{\Delta HG} = \varepsilon_{HG} - \varepsilon_H - \varepsilon_G$.

$$A_{obs} = \varepsilon_H ([H]^o - [HG]) + \varepsilon_G ([G]^o - [HG]) + \varepsilon_{HG} [HG] \quad \textbf{(30)}$$

$$A_{obs} = A_{H^o} + A_{G^o} + \varepsilon_{\Delta HG}[HG] \quad \textbf{(31)}$$

Also, by combining (**31**) with equation (**16**) we obtain expression **(32)**, which defines the complexation-induced change in the absorption.

$$A_{obs} = A_{H^o} + A_{G^o} + \frac{\varepsilon_{\Delta HG}}{2} \left\{ [H]^o + [G]^o + \frac{1}{K_a} - \sqrt{\left([H]^o + [G]^o + \frac{1}{K_a}\right)^2 - 4[H]^o[G]^o} \right\} \quad \textbf{(32)}$$

As in the case of NMR titrations, this is a single equation with 2 unknown variables (K_a and $\varepsilon_{\Delta HG}$) and, therefore, it will be resolved by non-linear curve fitting methods (with the SPECFIT/32™ software in our case) rather than making bold assumptions in the search of shortcuts.

It is important to note that the molar absorptivity of the guest molecule (ε_G) can be either determined independently in a separate set of measures or added to the list of unknown parameters that will be obtained from the fitting program.

a) The 1 : 2 equilibria

In this study we have also used UV-vis spectroscopy to study 1 : 2 equilibria (Chapter 3.2. and 3.3.) which is another common situation in supramolecular chemistry. This equilibria can be considered both as a stepwise process of two guest molecules binding to one host (**33**) and (**34**) or as an overall equilibrium between the two guest molecules and a host (**35**). Even though in some cases it may be easier to consider the overall equilibrium, it is important to consider that it is extremely unlikely that a supramolecular complex HG_2 can be formed by simultaneous collision of one host and two guest molecules.

$$H + G \rightleftharpoons HG \; ; K_1 \qquad \textbf{(33)}$$

$$HG + G \rightleftharpoons HG_2 \; ; K_2 \qquad \textbf{(34)}$$

$$H + 2G \rightleftharpoons HG_2 \; ; \beta_{12} \qquad \textbf{(35)}$$

The corresponding binding constants for each of this equilibria will respectively be:

$$K_1 = \frac{[HG]}{[H][G]} \qquad \textbf{(36)}$$

$$K_2 = \frac{[HG_2]}{[HG][G]} = \frac{[HG_2]}{K_1[H][G]^2} \qquad \textbf{(37)}$$

$$\beta_{12} = \frac{[HG_2]}{[H][G]^2} = K_1 K_2 \qquad \textbf{(38)}$$

The rationale to obtain the equations defining the complexation induced spectroscopic changes in the host molecule can be obtained with an analogous treatment as seen before. However, for the sake of shortness it will not be developed here as an excellent step-by-step explanation can be found elsewhere.[144d]

$$A_{obs} = A\frac{\varepsilon_{\Delta HG} K_1 [H]^o [G] (1 + 2 K_2 [G])}{1 + K_1 [G] + K_1 K_2 [G]^2} \qquad \textbf{(39)}$$

b) About Specfit software

SPECFIT/32™ has been the software used in this study for analyzing the experimental titration data. It is a multivariate data analysis program for modeling and fitting equilibrium titration data by adjusting the stability constants and the corresponding molar absorptivity over a selected range of wavelengths.

The spectral information is introduced as three dimensional data from multi-wavelength spectrophotometric measurements. Typically, these 3D data sets consist of simultaneous measurements of Absorbance *vs.* Wavelength as a function of $[G]^o$ as the independent variable. A complete exposition of the mathematical principles used and descriptive details of the original version is available in the bibliography.[149] Unfortunately for new users, this program is no longer supported or sold.

I.4.3. Fluorescence spectroscopy

Is based in studying the complexation-induced quenching (or enhancement) of the host's fluorescence. It is perhaps the most sensitive of all the methods used in determining binding constants, allowing to measure binding constants >> 10^6 M^{-1}. It is important, however, to work with diluted conditions (absorption of the species at the wavelength used for excitation < 0.05) so the fluorescence follows a Beert-Lambert-type relationship. With this technique it is also necessary to consider whether the fluorescence is quenched through static (relevant to host-guest association) or dynamic (collisional) mechanism as they will respond to different equations. This problem do not arise if what we are looking at is quenching enhancement.

Fluorescence experiments are being carried out in collaboration with Prof. Dirk M. Guldi in Erlangen and full explanation on the different equations can be found in the literature.[144d] Details will not be discussed here for the sake of shortness. The underlying principles though remain analogue to those seen before.

[149] H. Gampp, M. Maeder, C. J. Meyer and A. D. Zuberbühler, *Talanta* **1985**, *32*, 257.

ANNEX II. COOPERATIVITY

Cooperativity is a phenomenon arising when two molecules bind non-covalently through two or more interactions, so that the system as a whole behaves differently from what would be expected based on the properties of the individual interactions acting in isolation.[150] The synergy of these interactions can lead to an increase of the overall stability of the complex (positive cooperativity), to a weakening of the system (negative cooperativity) or have no significant impact at all (non-cooperativity). Depending on the nature of the interactions present, we can differentiate three types of cooperativity (Figure II.1):

- *Allosteric chelate*: arises from the interplay of two or more intermolecular binding interactions. The archetypal example is the binding of oxygen to hemoglobin, where binding of one molecule increases the affinity of the rest.
- *Chelate cooperativity*: arises from the presence of one or more intramolecular binding interactions. It can be attributed to the fact that intermolecular interactions require an extra loss of translational and rotational entropy when compared with intramolecular interactions.
- *Interannular cooperativity*: arises from the interplay of two or more intramolecular binding interactions, in which the binding of a first guest chelate "freezes" the system facilitating the insertion of a second one. As a result, interannular cooperativity implies the presence of chelate cooperativity, but the opposite is not true.

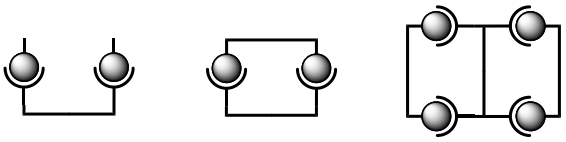

Allosteric cooperativity | Chelate cooperativity | Interannular cooperativity

Figure II.1. Different types of cooperativity.

[150] C. A. Hunter and H. L. Anderson, *Angew. Chem. Int. Ed.* **2009**, *48*, 7488.

A detailed theoretical analysis of these systems is beyond the scope of this annex and can be found in a recent publication by Ercolani and Schiaffino.[151] Thus, we will merely outline here the subject of cooperativity in the more relevant cases for this study, namely allosteric and chelate cooperativity.

II.1. ALLOSTERIC COOPERATIVITY

The first evidence of allosteric cooperativity can be found by looking at the shape of the binding isotherm. As seen before, the standard form of the isotherm of a supramolecular complex is a rectangular hyperbola (Figure I.2). However, in some cases this curve is transformed into a sigmoidal one, reflecting the essence of positive cooperativity, i.e. that the unbound-bound transition occurs with a different gradient, over a smaller range of guest concentration, than in a non-cooperative system.[115]

Figure II.2 represents three possible modifications in the shape of the binding isotherm according to the extent of the cooperative effect: a) represents a manifestation of positive cooperativity where the increase is not so large to alter the shape of the curve, b) represents the expected sigmoidal binding curve for a cooperative system and c) represents a phase transition, which is the ultimate form of cooperative behavior, an all-or-none phenomenon. In the case of negative cooperativity, the result is usually a binding curve that looks like the non-cooperative binding one, but approaches maximal binding more slowly.

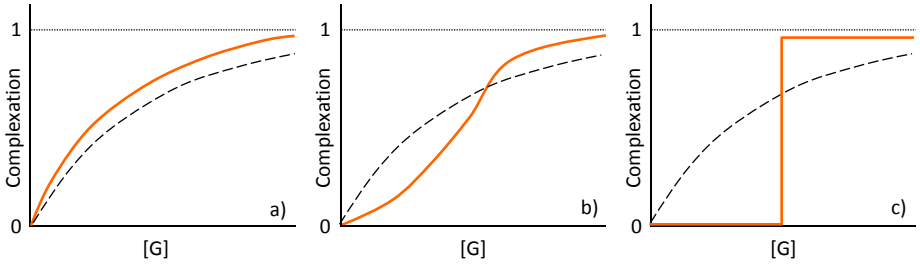

Figure II.2. Forms of binding isotherms derived from cooperative behavior in comparison with the hyperbolic non-cooperative binding curve (dashed). a) Non-sigmoidal, non-hyperbolic. b) Sigmoid binding curve. c) A phase transition.

[151] G. Ercolani and L. Schiaffino, *Angew. Chem. Int. Ed.* **2011**, *50*, 1762.

This graphical approach, however, can lead to confusion. A better alternative arises by considering the constants involved. So, if we consider the simpler case –the binding of a monovalent guest molecule G to a divalent host molecule H to form a 1 : 2 complex– its stability will be characterized by two stepwise binding constants, identical (*K*) in the absence of cooperativity and different (K_1 and K_2) in a cooperative system.[*] Thus, the allosteric cooperativity factor (α) can be viewed as the equilibrium constant for the conversion of the non-cooperative system into the cooperative one (Figure II.3) quantifying the magnitude of the allosteric effect exerted between the two sites.

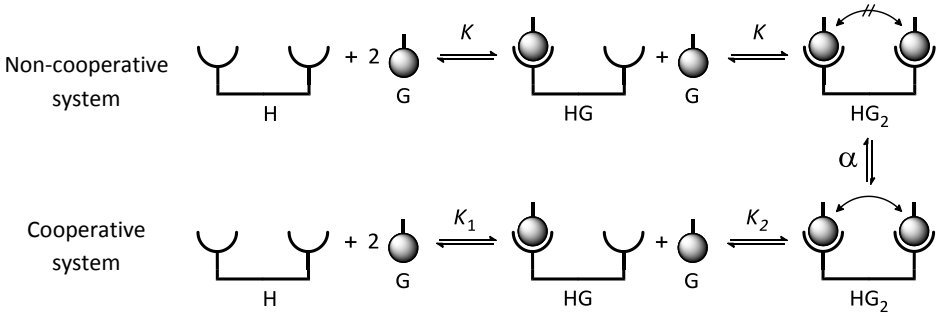

Figure II.3. The allosteric cooperativity factor α has been defined as the equilibrium constant for the conversion of a non-cooperative system into a cooperative one.

As a result, the overall cooperative factor, α, will be defined by (**40**).

$$\alpha = \frac{K_1 K_2}{K^2} \qquad \textbf{(40)}$$

Values > 1 denote positive cooperativity. For example, α = 10 means that the affinity towards the guest is increased by a factor of 10. Values < 1 denotes negative cooperativity. For example α = 0.1 means a 10-fold decrease in the affinity. α = 1 characterizes a non-cooperative system where the affinity remains unaltered.

The value of *K* can be evaluated by studying the binding of the monovalent guest to a monovalent model of the host, or alternatively, by directly taking the value of the constant K_1 as the reference constant.[151]

[*] Some authors prefer to consider the microscopic association constants K_1' and K_2' which take into account the statistical factor reflecting the degeneracy of the partially bound intermediate. In that case $K_1 = 2K_1'$ and $K_2 = \frac{1}{2}K_2'$. In this case a non-cooperative system will be characterized y

II.2. CHELATE COOPERATIVITY

In contrast with the well-established allosteric cooperativity, the assessment of chelate cooperativity remains a controversial issue due to its concentration dependence.[150-151] Therefore, only a simplified description will be given here.

For this, we will introduce a key concept, the effective molarity (EM), which is a physicochemical parameter accounting for the easier formation of an intramolecular reaction over its intermolecular analogous (Scheme II.1).[152]

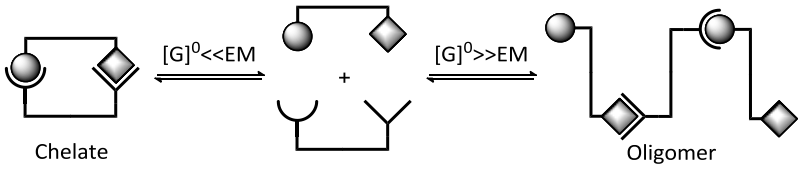

Scheme II.1. EM quantifies the ease of cyclization *vs.* oligomerization.

Thus, it can be defined as the equilibrium constant between the intramolecular and the intermolecular reaction as illustrated by Scheme II.2 and equation (**41**).[124] Even though it has been argued that EM cannot be taken as the chelate cooperativity factor due to dimension inconsistence,[151] it will be used in this study as a rough estimation on the influence of chelate cooperativity in our system.

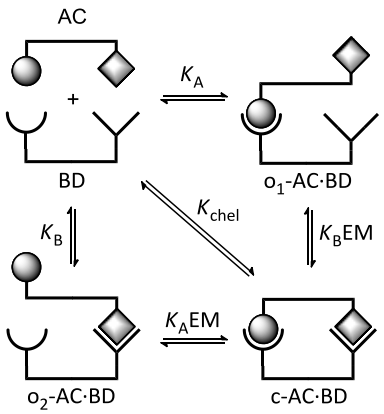

Scheme II.2. Formation of a heterotopic chelate complex.

$$EM = \frac{K_{intra}}{K_{inter}} = \frac{K_{chel}}{K_A K_B} \text{ (mol L}^{-1}\text{)} \qquad \textbf{(41)}$$

[152] G. Ercolani and L. Schiaffino, in *Bioinspiration and Biomimicry in Chemistry*, John Wiley & Sons, Inc., **2012**, p. 47.

ANNEX III. SUPPORTING FIGURES

III.1. CHAPTER 4.1.

III.1.1. UV-VIS TITRATIONS

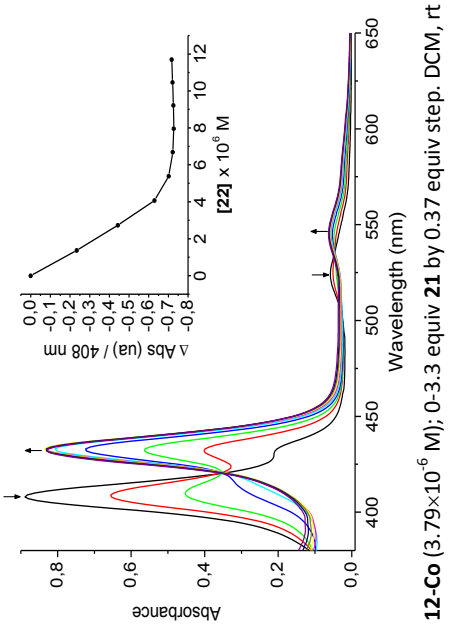

12-Co (3.79×10^{-6} M); 0-3.3 equiv **21** by 0.37 equiv step. DCM, rt

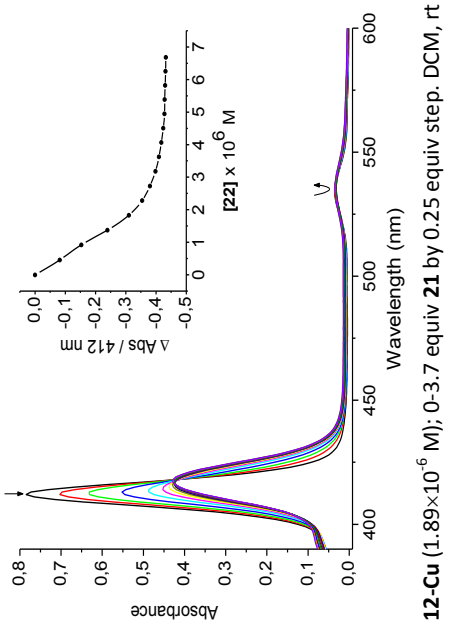

12-Cu (1.89×10^{-6} M); 0-3.7 equiv **21** by 0.25 equiv step. DCM, rt

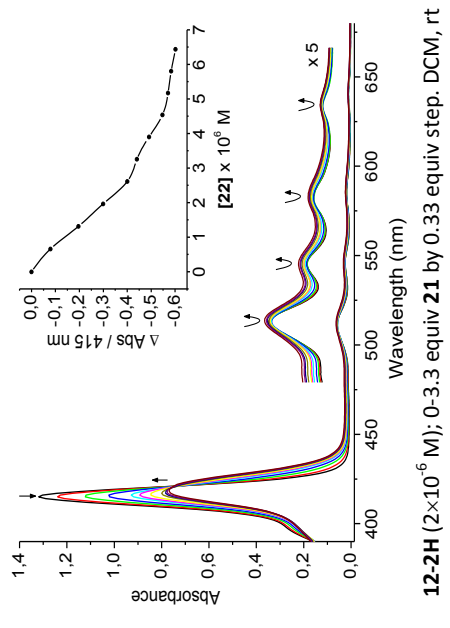

12-2H (2×10^{-6} M); 0-3.3 equiv **21** by 0.33 equiv step. DCM, rt

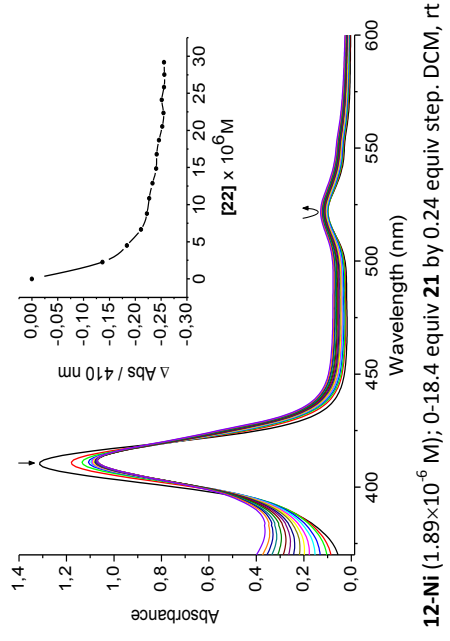

12-Ni (1.89×10^{-6} M); 0-18.4 equiv **21** by 0.24 equiv step. DCM, rt

III.1.2. ESI-MS STUDIES

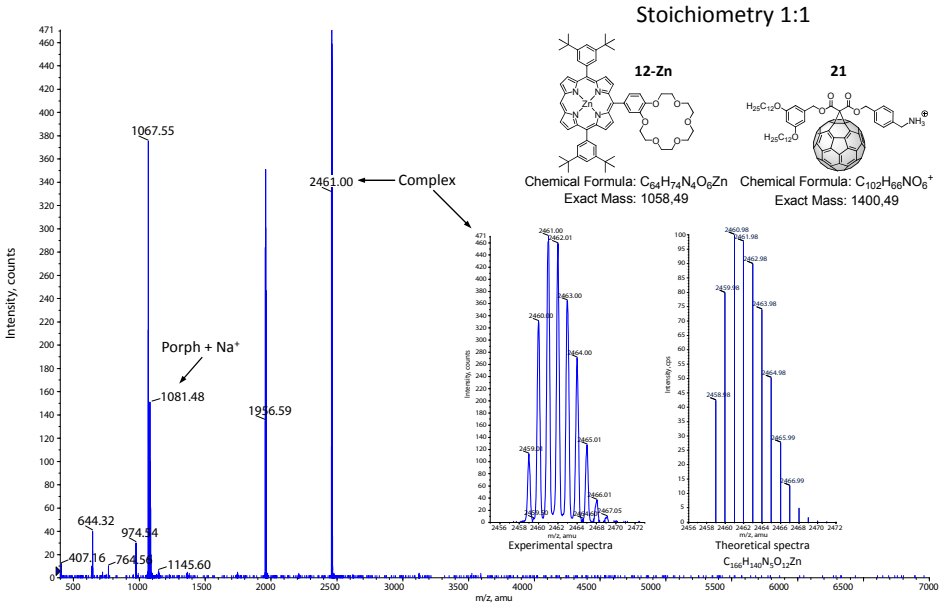

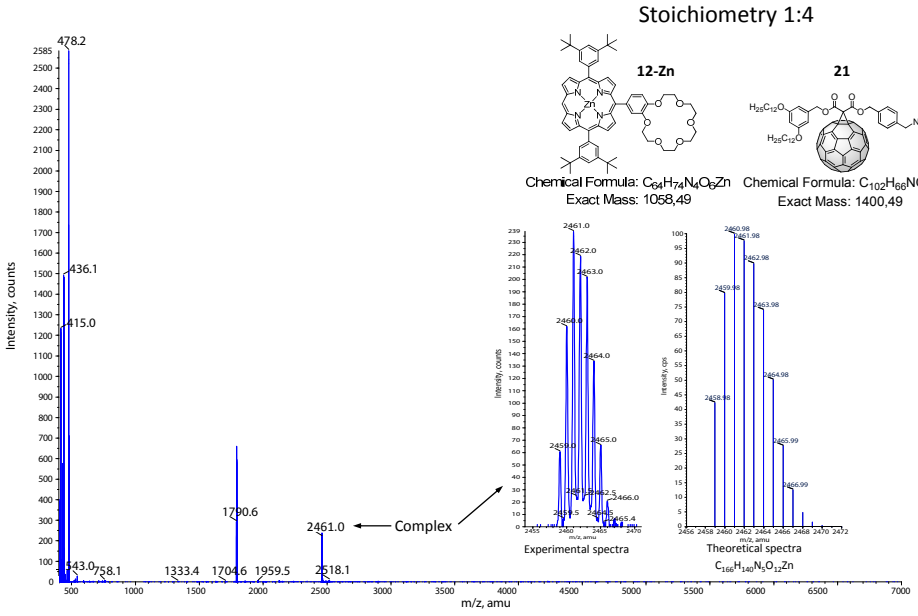

III.1.3. ASSESMENT OF THE CHELATE COOPERATIVITY

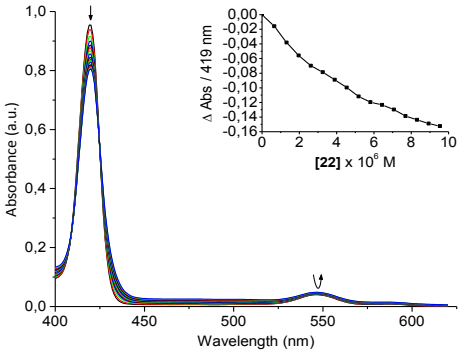

12-Zn (1.89×10^{-6} M); 0-5.2 equiv **21** by 0.55 equiv step. $CHCl_3$, rt.

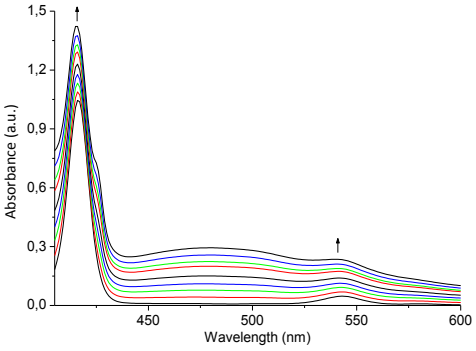

12-Zn (1.89×10^{-6} M); 0-84 equiv **20** by 10.5 equiv step. $CHCl_3$, rt.

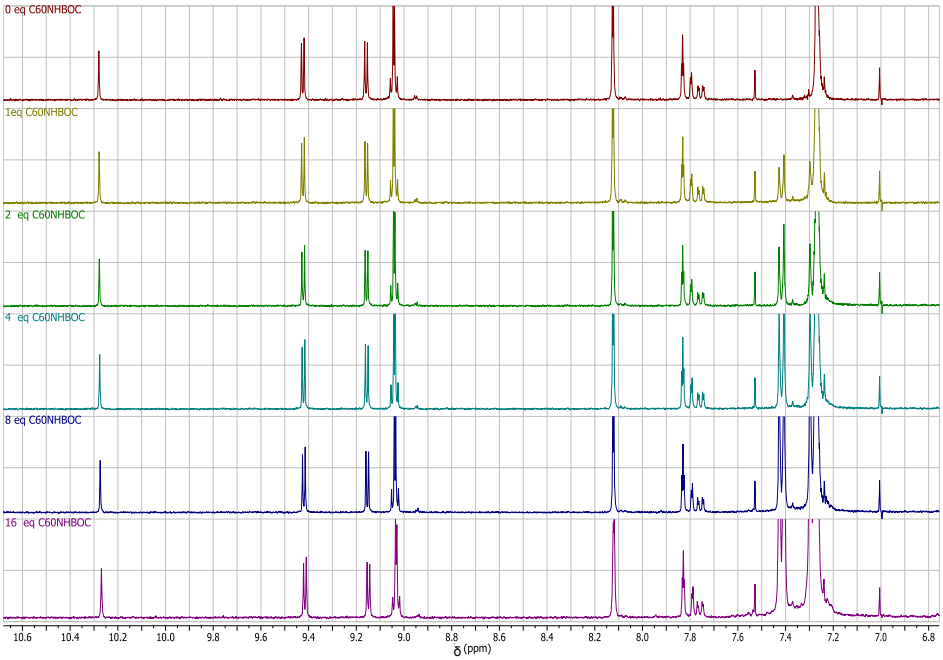

12-Zn (1.51×10^{-3} M); 0-16 equiv **20** $CDCl_3$, rt.

III.1.4. ^{1}H-NMR STUDIES

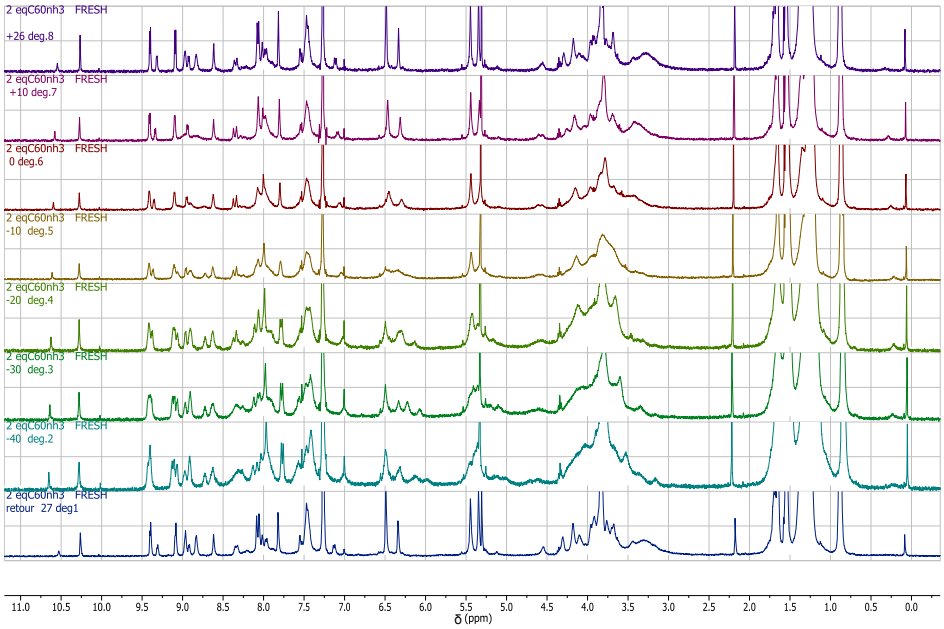

^{1}H-NMR VT experiments over a 1:2 mixture of **12-Zn** (1.51×10^{-3} M) and **21**. $CDCl_3$, rt.

III.2. CHAPTER 4.2.

III.2.1. VARIABLE TEMPERATURE STUDIES

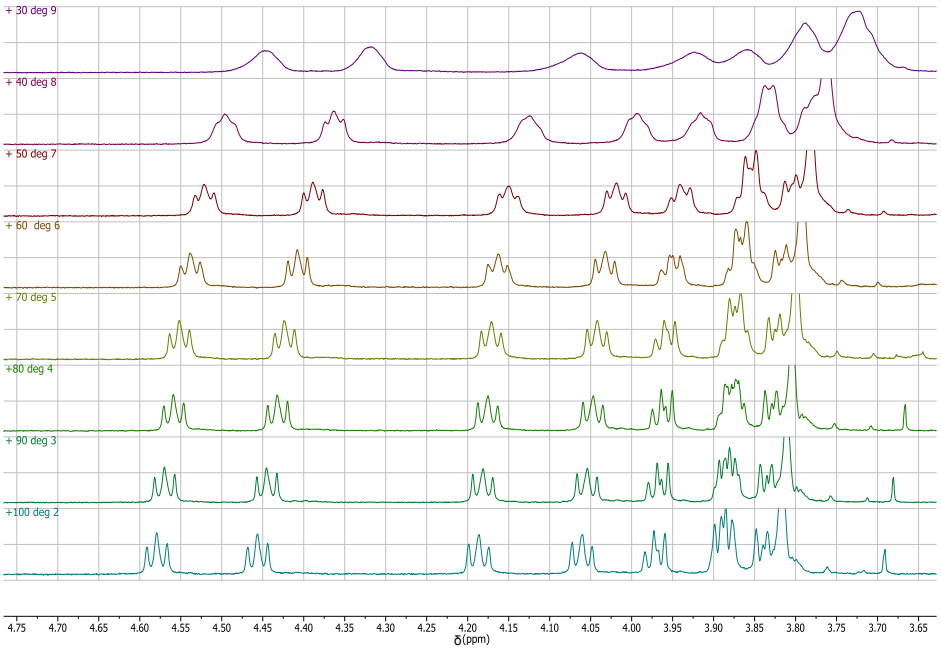

^{1}H-NMR VT experiments of **23** in $ClCD_2CD_2Cl$.

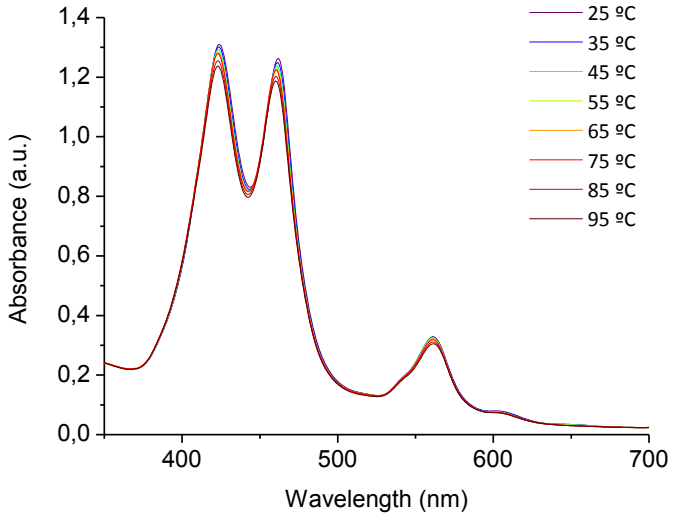

UV-vis VT experiments of **23** in ClPh.

III.2.2. ESI-MS STUDIES

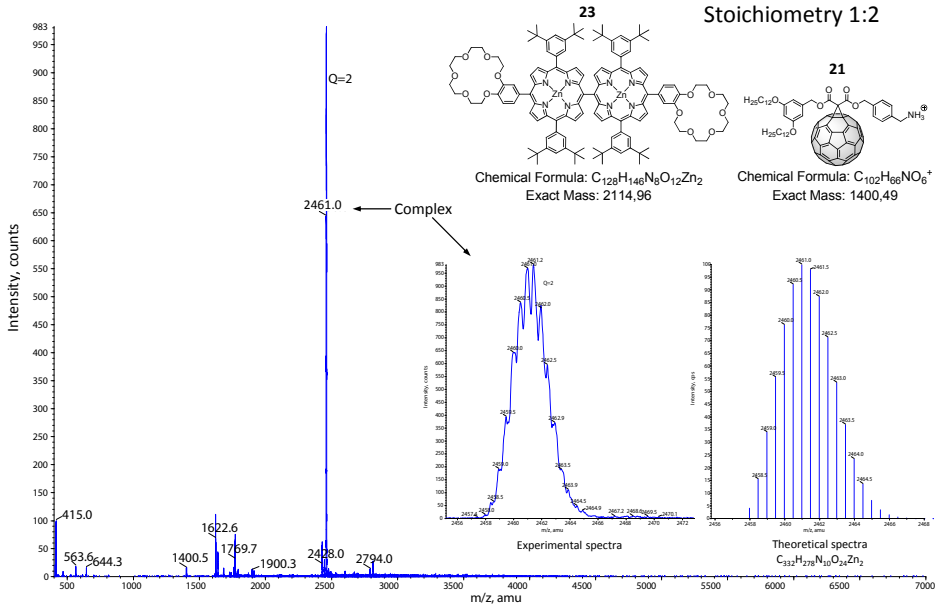

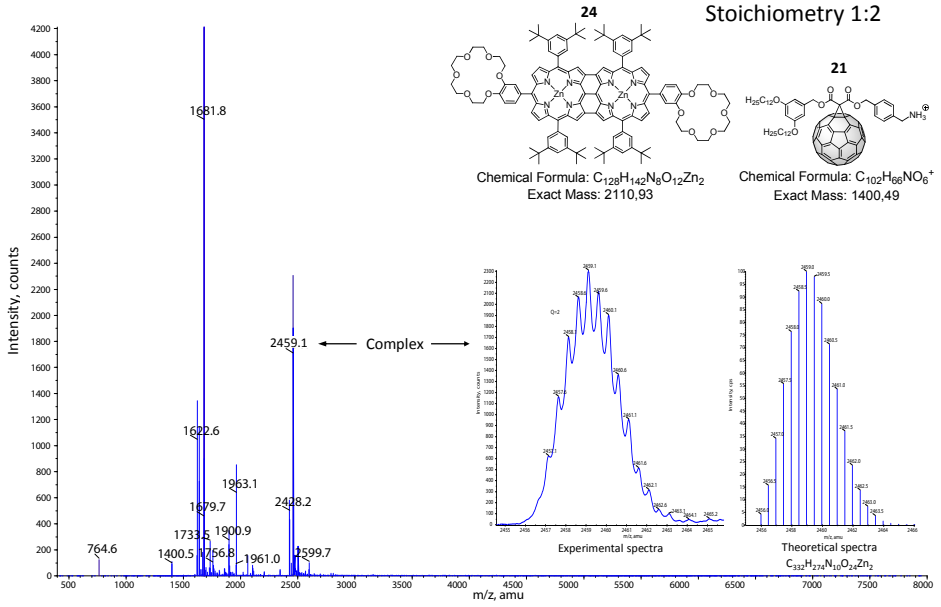

III.3. CHAPTER 4.3.

III.3.1. ESI-MS STUDIES

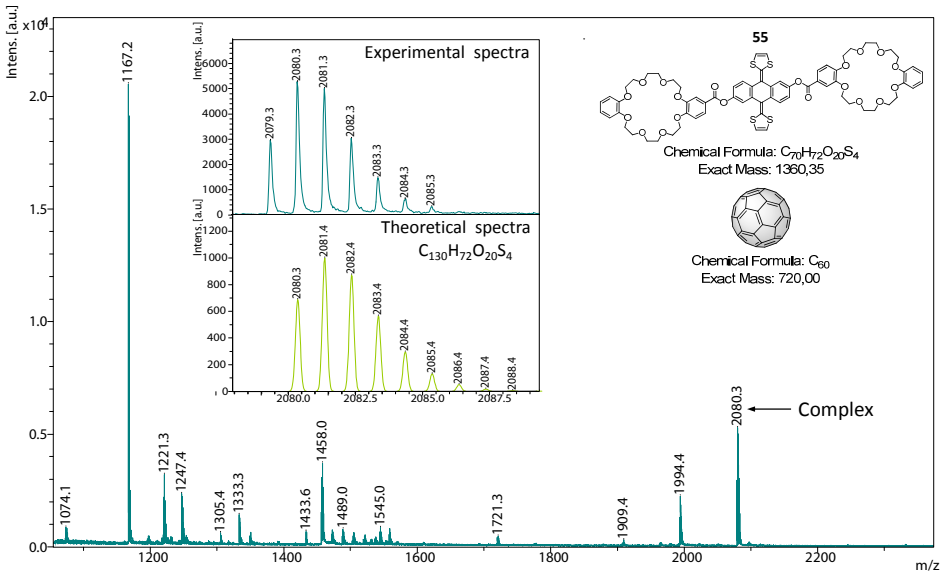

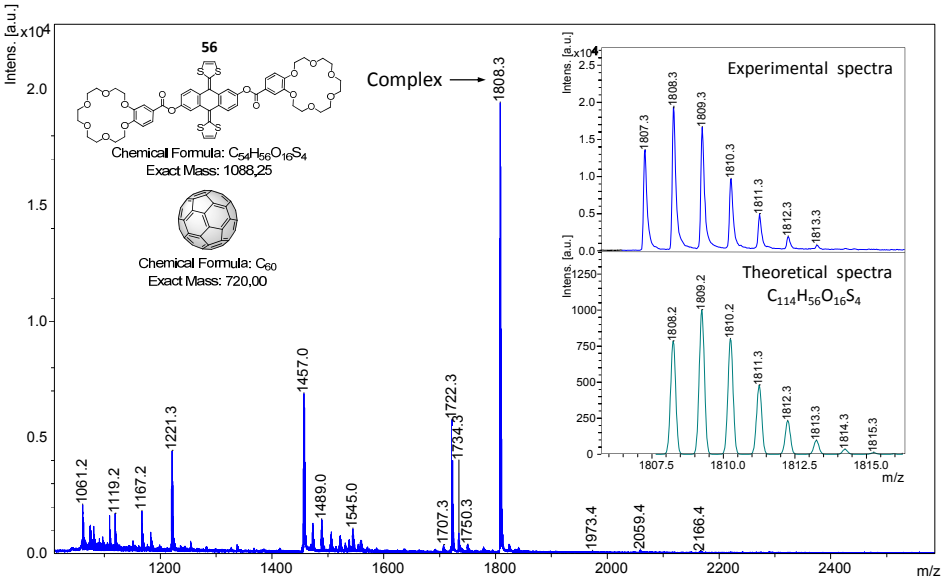

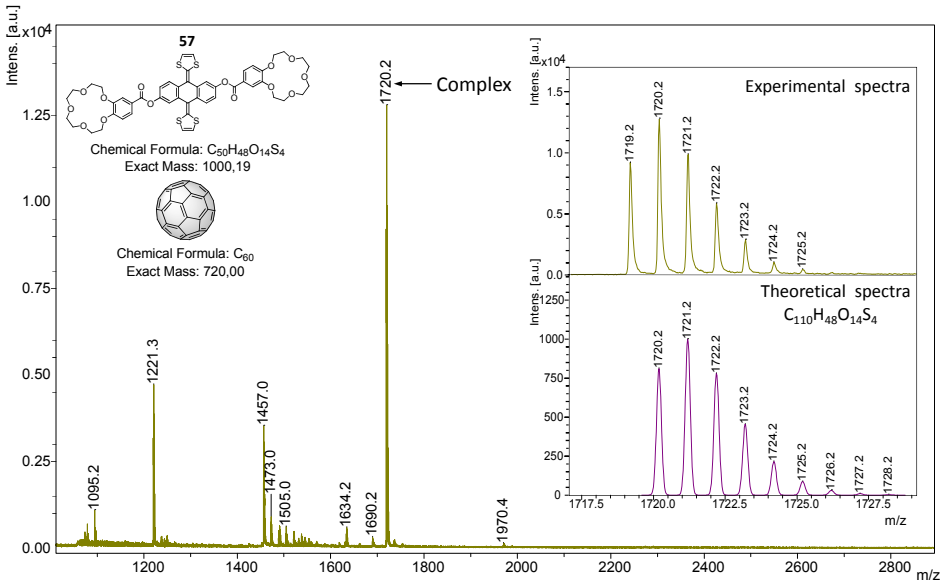
57
Chemical Formula: C50H48O14S4
Exact Mass: 1000,19
Chemical Formula: C60
Exact Mass: 720,00
Complex
Experimental spectra
Theoretical spectra
C110H48O14S4
Intens. [a.u.]
m/z

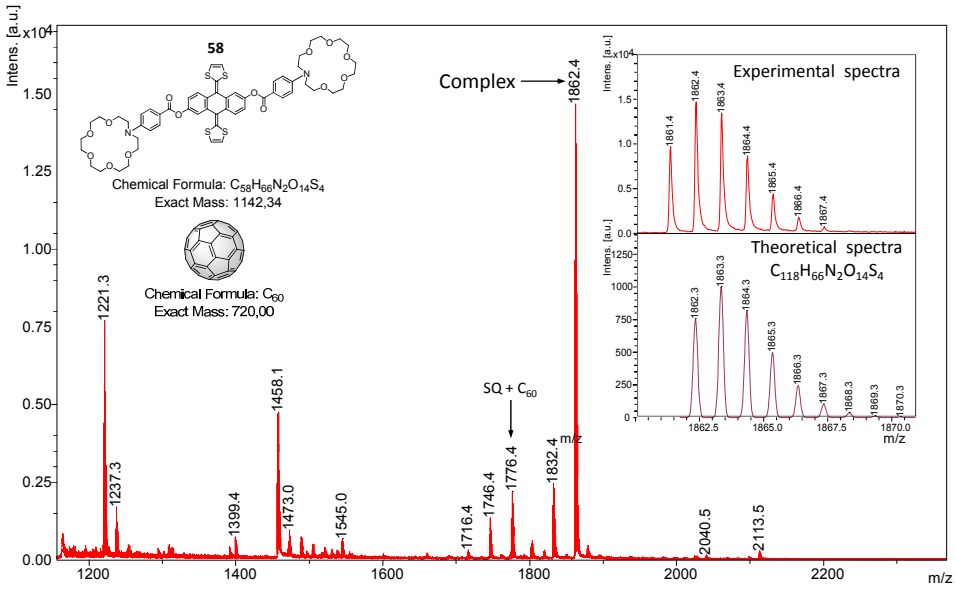
58
Chemical Formula: C58H66N2O14S4
Exact Mass: 1142,34
Chemical Formula: C60
Exact Mass: 720,00
Complex
SQ + C60
Experimental spectra
Theoretical spectra
C118H66N2O14S4
Intens. [a.u.]
m/z

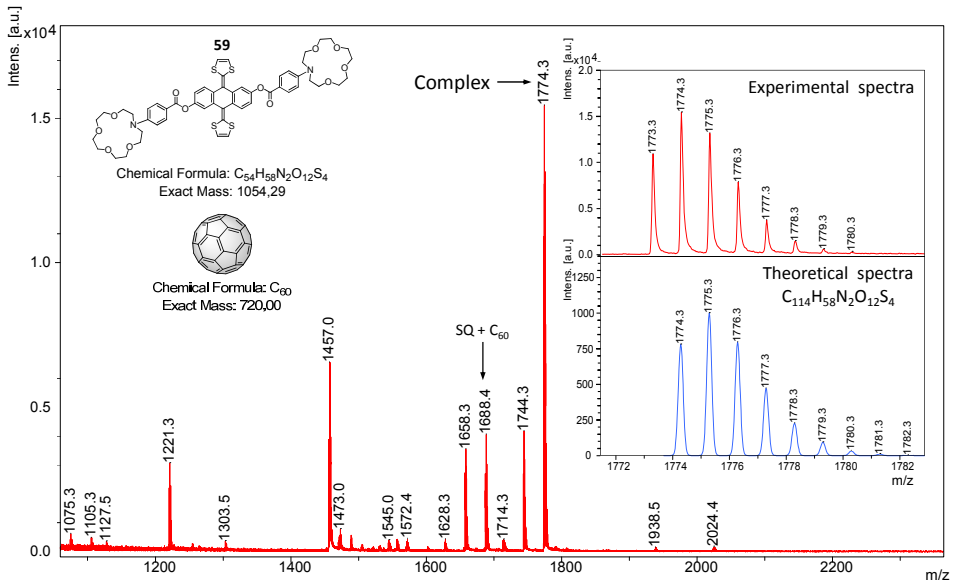
59
Chemical Formula: C54H58N2O12S4
Exact Mass: 1054,29
Chemical Formula: C60
Exact Mass: 720,00
Complex
SQ + C60
Experimental spectra
Theoretical spectra
C114H58N2O12S4
Intens. [a.u.]
m/z

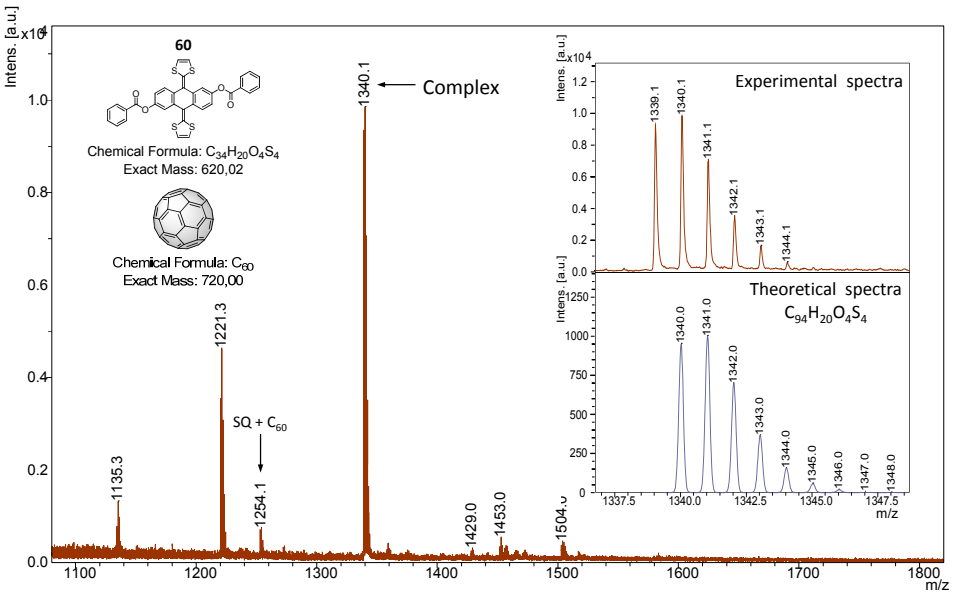
60
Chemical Formula: C34H20O4S4
Exact Mass: 620,02
Chemical Formula: C60
Exact Mass: 720,00
Complex
SQ + C60
Experimental spectra
Theoretical spectra
C94H20O4S4
Intens. [a.u.]
m/z

III.3.2. ELECTROCHEMICAL STUDIES

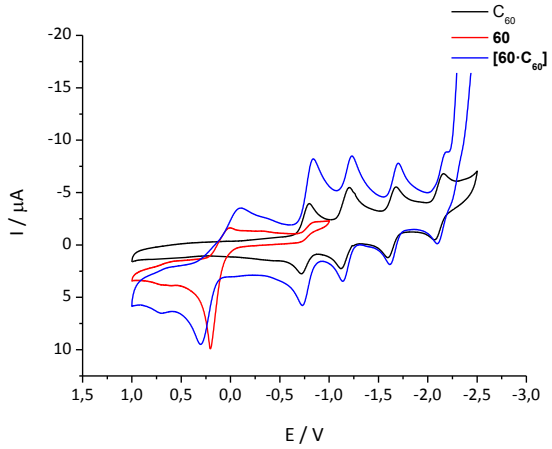

60

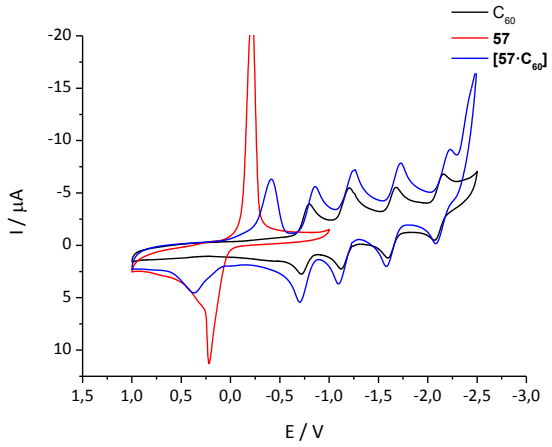

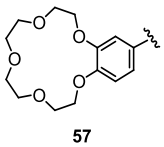

57

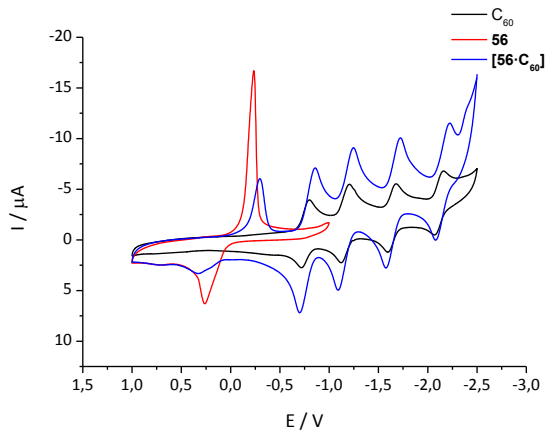

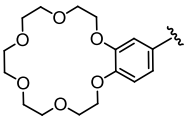

56

III.3.3. COMPUTATIONAL STUDIES

Conformational analysis of the host system (Relative energies)

Conformer	PM7 (kcal/mol)	Conformer	PM7 (kcal/mol)
c1 uu	0.00	c2 uu	0.60
c1 dd	0.35	c2 dd	0.60
c1 ud	0.08	c2 ud	0.55

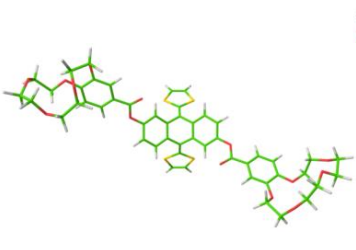

c1 uu

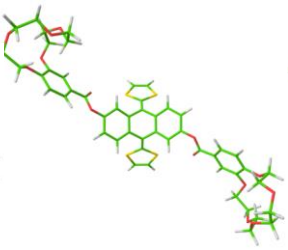

c1 dd

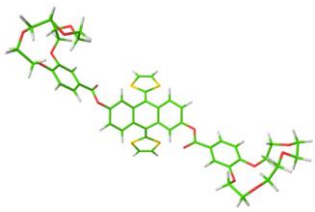

c1 ud

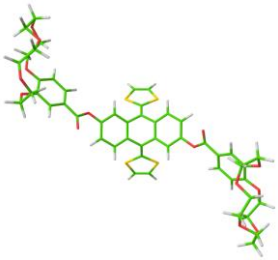

c2 uu

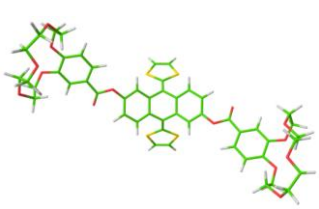

c2 dd

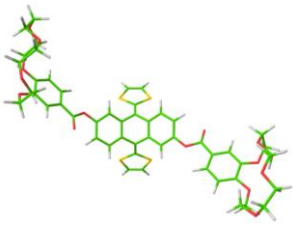

c2 ud

Optimized Geometries (DFT level)

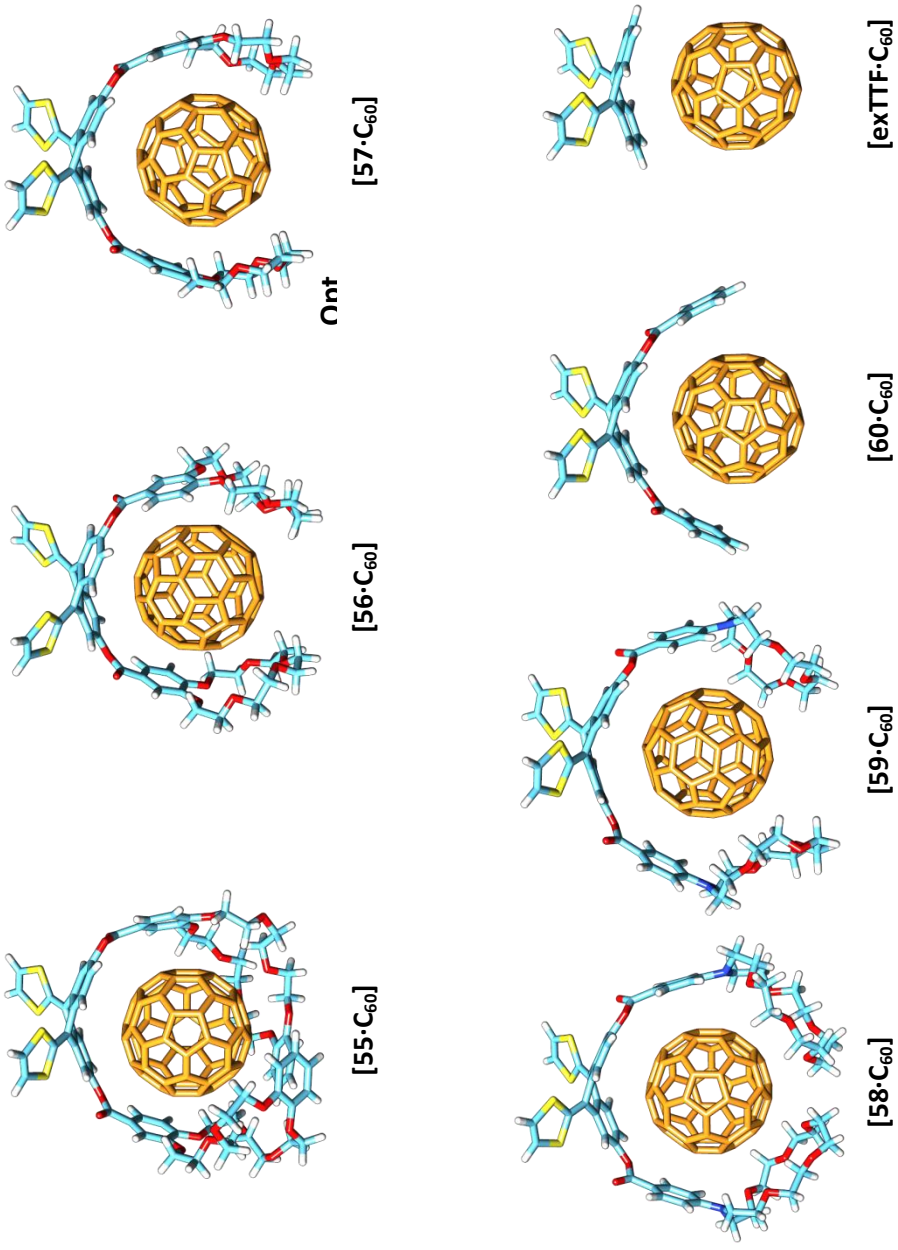

III.4. CHAPTER 4.4.

III.4.1. ESI-MS STUDIES

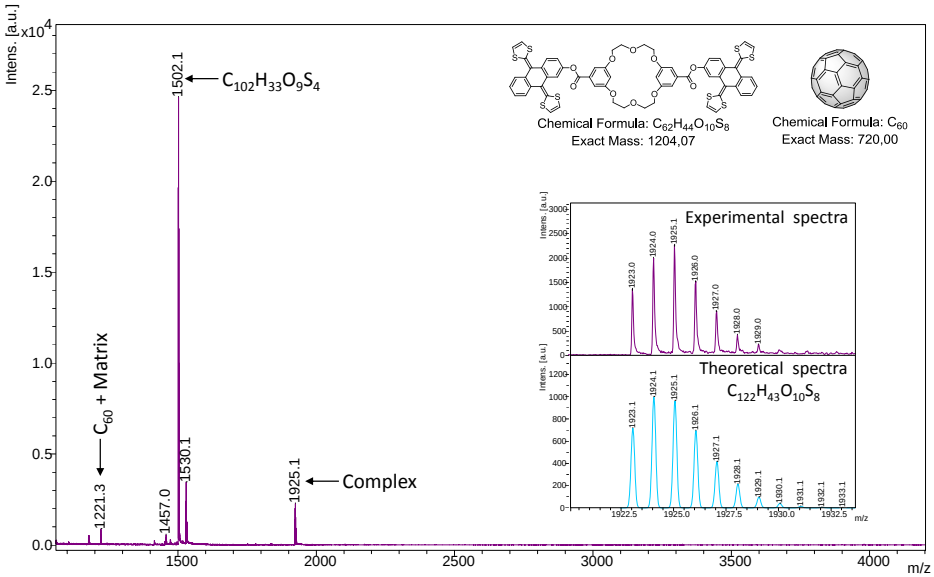

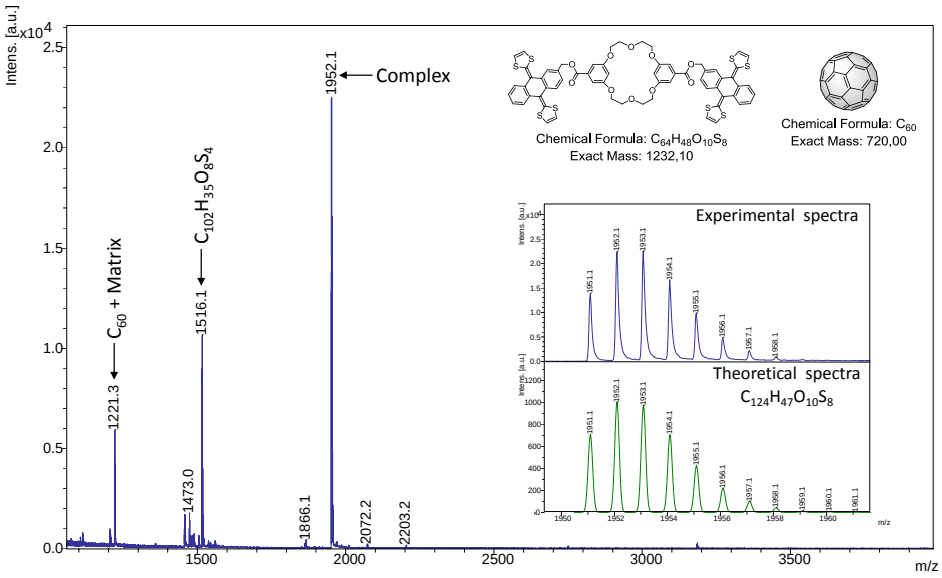

III.4.2. ELECTROCHEMICAL STUDIES

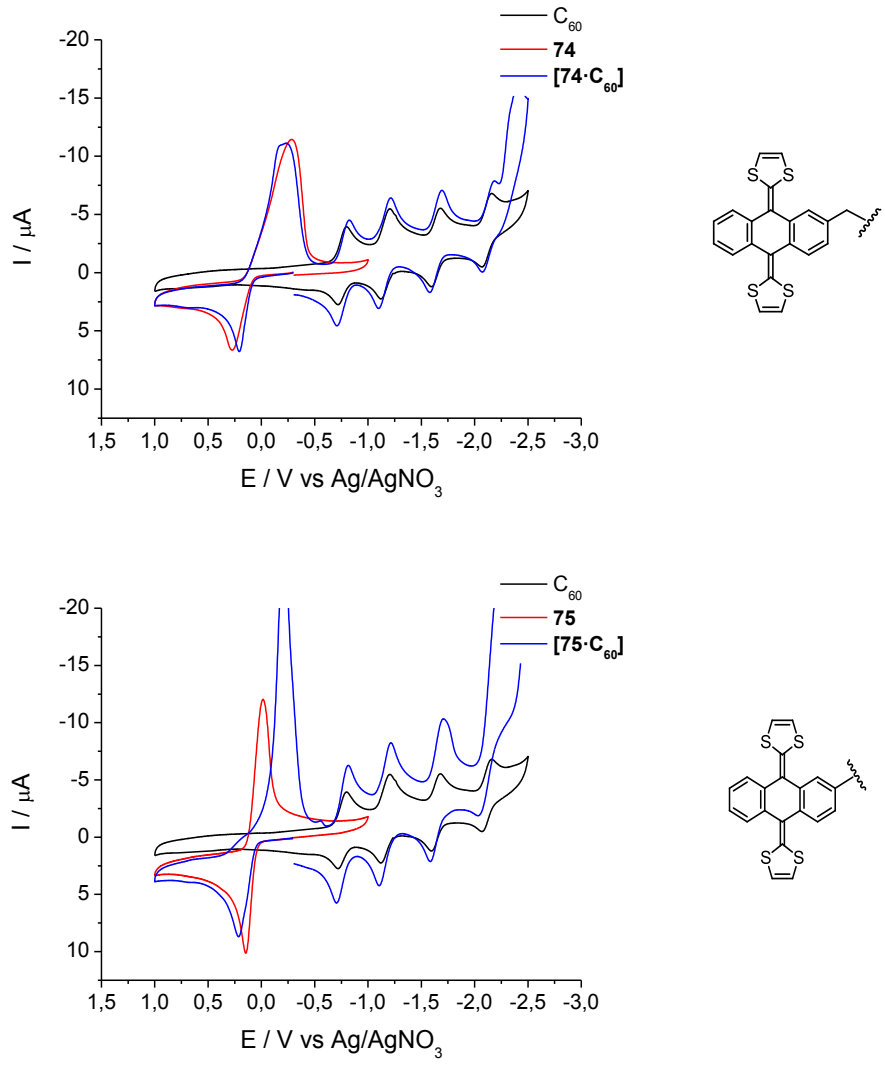

CV of C_{60}, host exTTF and a 1:1 exTTF/C_{60} mixture. Top: **74**, Bottom: **75**.
(SR: 100 mV/s. ClPh/MeCN 4:1. SE: *n*-Bu_4NPF_6 (0.1 M). WE: GCE. CE: Pt wire. 298 K).

The irregular shape of the exTTF waves can be explained on the basis of adsorption over the working electrode surface.

Summary

Introduction

One of the major issues humanity faces nowadays is the increasing dependency to non-renewable fossil fuels in order to get electricity, without which our society would move back into the 1800s. As a result, tremendous efforts have been made to find new and better sources of energy. Within them, solar light is one of the most promising given the outstanding potential of sun, which sheds over the Earth more energy in one year than the one that will ever be obtained from all the non-renewable sources available in the planet together.[1]

From all the technologies available to transform light energy into electricity, solar cells are the most common devices. Among them, organic cells have emerged as cheap and flexible alternatives which unfortunately do not posses high efficiencies yet. However, it should be possible to obtain much better efficiencies from them, as organic devices able to harvest light and convert it into electrochemical potential energy with near quantum efficiency do already exist on Earth. They are the photosynthetic apparatuses and are the base of life in the planet.

So, if we consider that both solar cells and the photosynthetic apparatus share a basic functioning (absorption of light to produce a separation of charges which then recombine) why no human-made device has come even close to the efficiency of nature? The answer is not yet clear, but a clue seems to be in the size of the photosynthetic apparatus, lying in the nano-scale, (Figure 1) where properties of matter no longer respond to standard physics but to quantum mechanics.

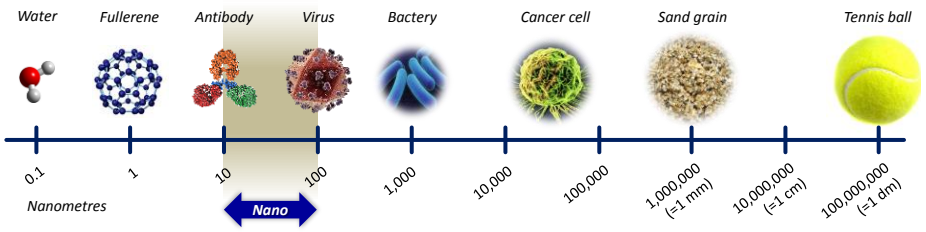

Figure 1. How small is "nano"?.

In order to reach that scale chemists have often resorted to the bottom-up approach, consisting in arranging smaller components (i.e. molecules) into more complex ensembles.

One of the main tools for obtaining an ordered assembly and not a random combination of the building blocks is supramolecular chemistry, which is interested in the self-assembly of the building blocks by using weak intermolecular forces[2] and is the main focus of the present study.

In this context, we have dealt with the formation of supramolecular donor-acceptor ensembles which are able to reproduce the key step of the photosynthetic process, i.e. the formation of a charge separated state. The interest will be focused in understanding how electron donor and acceptor molecules can form stable ensembles in a controlled manner.

For this, two different molecules have been used in the donor moiety: porphyrins and extended TTF (exTTF), whereas fullerene C_{60} has been used in the receptor moiety.

Porphyrins are 18 π-electron aromatic macrocycles composed of a tetra pyrrolic core with three different positions for functionalization. Two of them on the periphery, the *meso* and *β*-pyrrolic positions, and a third in the inner NH positions, where it is possible to coordinate a metal cation (Figure 2).[39]

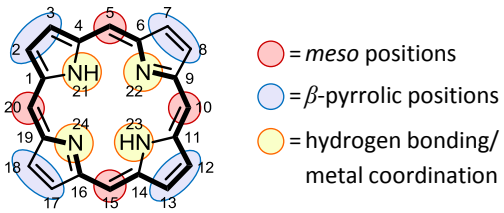

Figure 2. Porphyrin structure with its aromatic ring (bold) and numbering.

They are excellent donor molecules due to their strong UV-vis absorption bands, tunable oxidation potential and long lived singlet excited state.

It is also noteworthy the use of both *meso-meso* singly linked and *meso-meso*, *β-β*, *β-β* triply linked porphyrin arrays, obtained by oxidative coupling of a free *meso* position metalloporphyrin (Scheme 1).

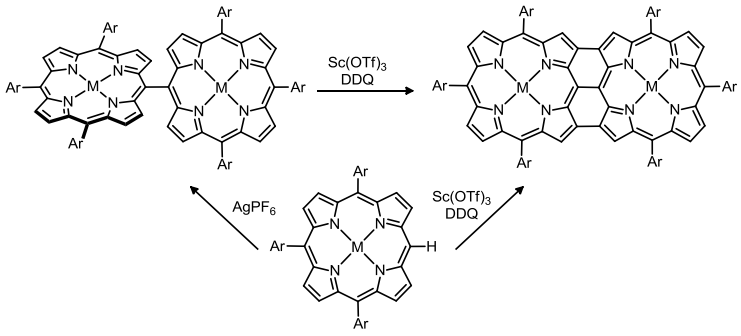

Scheme 1. Formation of porphyrin arrays.

9,10-di(1,3-dithiol-2-ylidene)-9,10-dihydroanthracene (exTTF) is a conjugated tetrathiafulvalene (TTF) analogue incorporating two 1,3-dithiole rings connected through a *p*-quinoid spacer (Figure 3).[90]

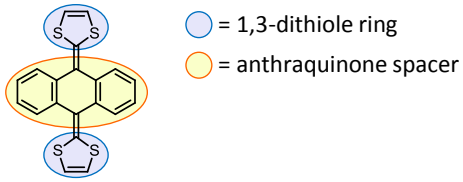

Figure 3. exTTF structure.

This pro-aromatic molecule has been widely used in the donor moiety due to its low oxidation potential and non-planar geometry. Remarkably, when oxidized the geometry of the molecule dramatically changes from a horse saddle structure, where both the electron donor and the aromatic face are clearly differentiated, into a planar D_{2h}, where the aromaticity is extended through the whole molecule and the 1,3-dithiolium aromatic rings are orthogonal to the anthracene unit (Figure 4).[92]

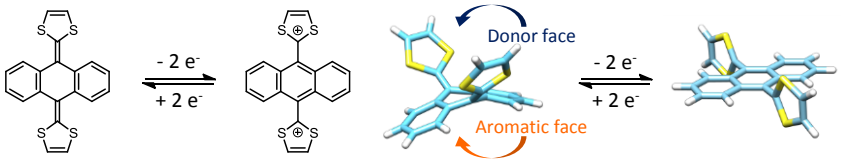

Figure 4. The oxidation of exTTF derives leads to a dramatic change of the geometry.

[60]fullerene, a closed carbon cage molecule (Figure 5), has been systematically used as the acceptor moiety due to its tridimensional structure, low reduction potential, UV-vis absorption at a large range and low reorganization energies in electron transfer reactions.

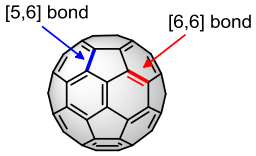

Figure 5. C_{60}.

Whereas [60]fullerene, porphyrins and exTTFs have been extensively combined by covalent methods, little research has been done in supramolecular ensembles due to the difficulties in obtaining stable complexes in solution in a controlled manner. The typical toolbox used for non-covalent assemblies involves π–π stacking, ionic interactions, Lewis base – acid reactions, ammonium – crown ether complementarity and mechanical bond. When used alone, these interactions lead to rather weak complexes, however, a wise combination of them can lead to very stable ensembles.

In our study we have used the aforementioned toolbox in combination with different crown ethers, producing a series of stable crown ether containing donor-acceptor ensembles.

Objectives and results

Effect of the metal atom on the binding constant between metalated porphyrins and C_{60}

First, we were interested in gaining a deeper understanding in the nature of π-π interactions between porphyrins and fullerenes, which remains controversial as it is believed to arise from an electronic donation from the fullerene to the porphyrin. This counter-instinctive conclusion may be rationalized if we consider the fullerene at the specific level of the double bond rather than at the global one.[59]

Therefore, a new series of stable supramolecular metalloporphyrin·C_{60} dyads were obtained by combining π-π stacking and ammonium-crown ether interactions (Figure 6). The optimal complementarity of these interactions had previously been evidenced in our laboratory in Strasbourg, where their combination led to a two orders of magnitude increase of the binding constant.[86]

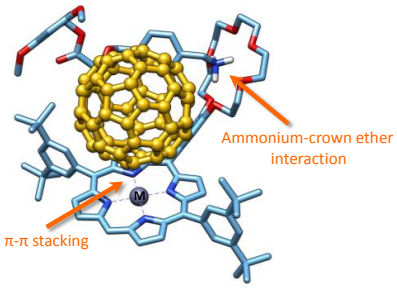

Figure 6. Supramolecular complexes obtained from the new metalloporphyrin·crown ether conjugates. M = 2H, Co, Ni, Cu, Zn.

Given the supposed electrostatic nature of π-π interactions, the central metal atom in the porphyrin moiety was systematically changed in order to evaluate its impact in the binding constants and electrochemical behavior of the formed complexes.

Targeted host porphyrins **12-M** (M = 2H, Co, Ni, Cu, Zn) were obtained by a Suzuki-Miyaura cross-coupling reaction over derivative **9**, which was in turn obtained by a regioselective iodination of substrate **8**, resulting from the mixed condensation of dipyrromethane **3** and aldehyde **6** (Scheme 2).

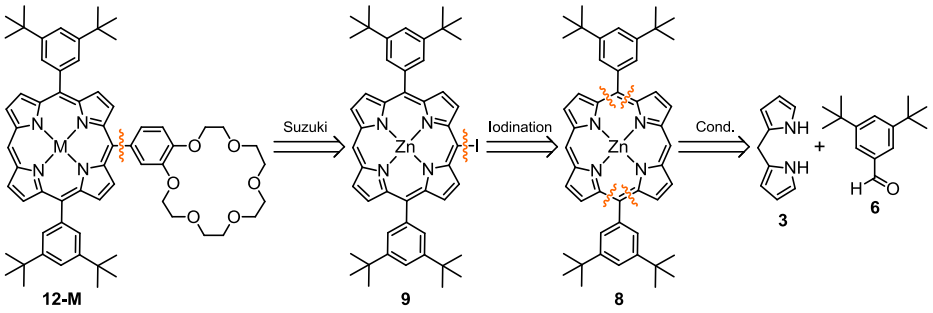

Scheme 2. Retrosynthetic analysis of host porphyrins **12-M**.

Guest molecule **22**, was obtained via a Bingel cycloaddition over C_{60} from derivative **20**. This asymmetric malonate was in turn obtained by esterification reaction of molecule **19**, derived from alcohol **17** (Scheme 3).

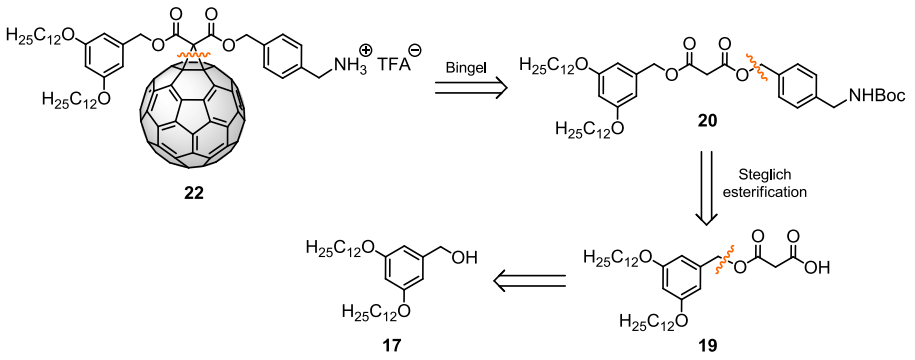

Scheme 3. Retrosynthetic analysis of guest methanofullerene **22**.

Complexation studies of supramolecular ensembles **[12-M·21]** were realized by monitoring the changes in the absorption spectra of the porphyrin moiety **12-M** after addition of increasing quantities of fullerene derivative **21** at rt (Scheme 4).

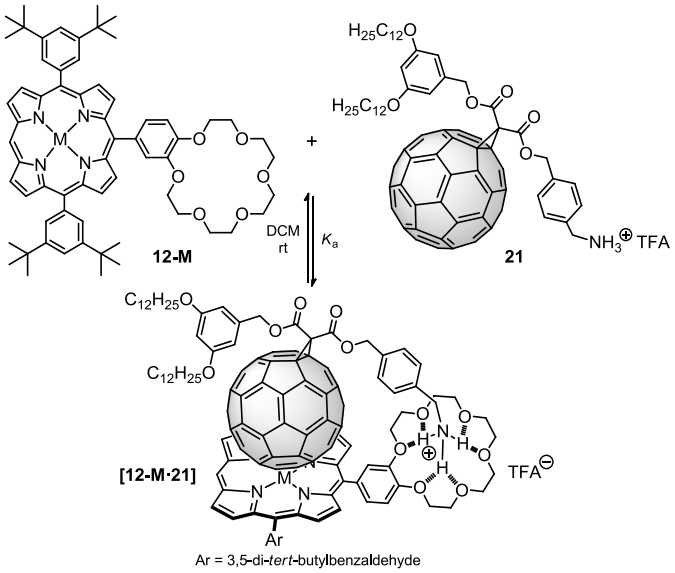

Scheme 4. Formation of the supramolecular complexes **[12-M·21]** from their building blocks.

Non-linear curve fitting of the titration data by Specfit analysis software estimated the different K_a values for the formation of **[12-M·21]** as reported in Table 1.

Table 1. Binding constants of systems **[12-M·21]**.

Complex	log K_a ± 3σ
[12-2H·21]	5.5 ± 0.2
[12-Co·21]	6.3 ± 0.2
[12-Ni·21]	5.9 ± 0.1
[12-Cu·21]	6.3 ± 0.3
[12-Zn·21]	6.9 ± 0.2

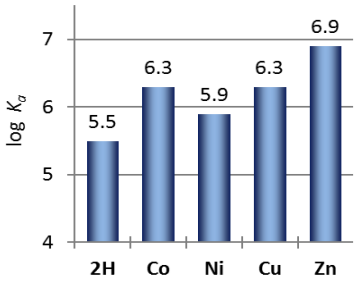

The binding constants obtained were very high, nicely evidencing the complementarity of ammonium-crown ether and π stacking in the system and the influence of the chelate cooperativity.

Interestingly, the K_a values obtained for **[12-Zn·21]** and **[12-2H·21]** were very different to those previously reported in the literature where host systems based in free base porphyrins systematically bound pristine fullerene with a similar strength than their analogous with Zn(II).[61a],[62],[63b]

The values obtained in our series correlate with the ones expected for a porphyrin·C_{60} system governed by van der Waals forces, where K_a becomes larger when the number of electrons in the porphyrin increase. The exception to this "rule of thumb" would be the great stability of **[12-Co·21]**, which can be explained on the base of the strong interactions between fullerenes and group 9 metals (Co, Rh, Ir).[63b]

It is also important to note that previous examples in the literature complexed pristine C_{60}, whose low solubility limited the crucial choice of solvents for the titration experiment. Indeed, it has been suggested that desolvation of C_{60} is a major contributor to the energetics of its binding in solution.[62] The use of methanofullerene **21** has elegantly circumvented this limitation while basically retaining the original properties of the fullerene moiety.

Supramolecular properties of porphyrin arrays

Inspired by the results of the previous systems, we decided to further functionalize the porphyrin moiety to obtain both a *meso-meso* appended porphyrin dimer and a triply linked *meso-meso*, *β-β*, *β'-β'*, porphyrin tape. The supramolecular properties of these arrays -largely unexplored up to date- have been studied by complexing the same guest methanofullerene.

Despite the great molecular complexity of dimers **23** and **24**, their high symmetry allowed to carry out the respective synthesis in a relatively easy divergent experimental procedure from porphyrin **12-Zn**, as depicted in Scheme 5.

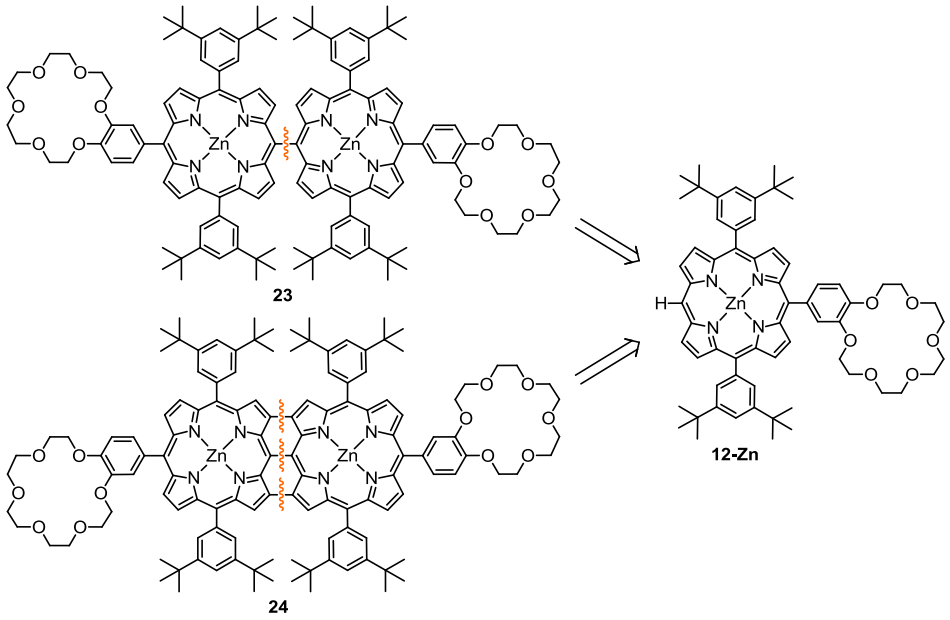

Scheme 5. Retrosynthetic analysis of porphyrin arrays **23** and **24**.

Complexation studies of **[23·21]** and **[23·21$_2$]** were performed by monitoring the changes in the absorption spectra of the porphyrin dimer **23** in DCM after addition of increasing quantities of fullerene derivative **21** at rt (Scheme 6).

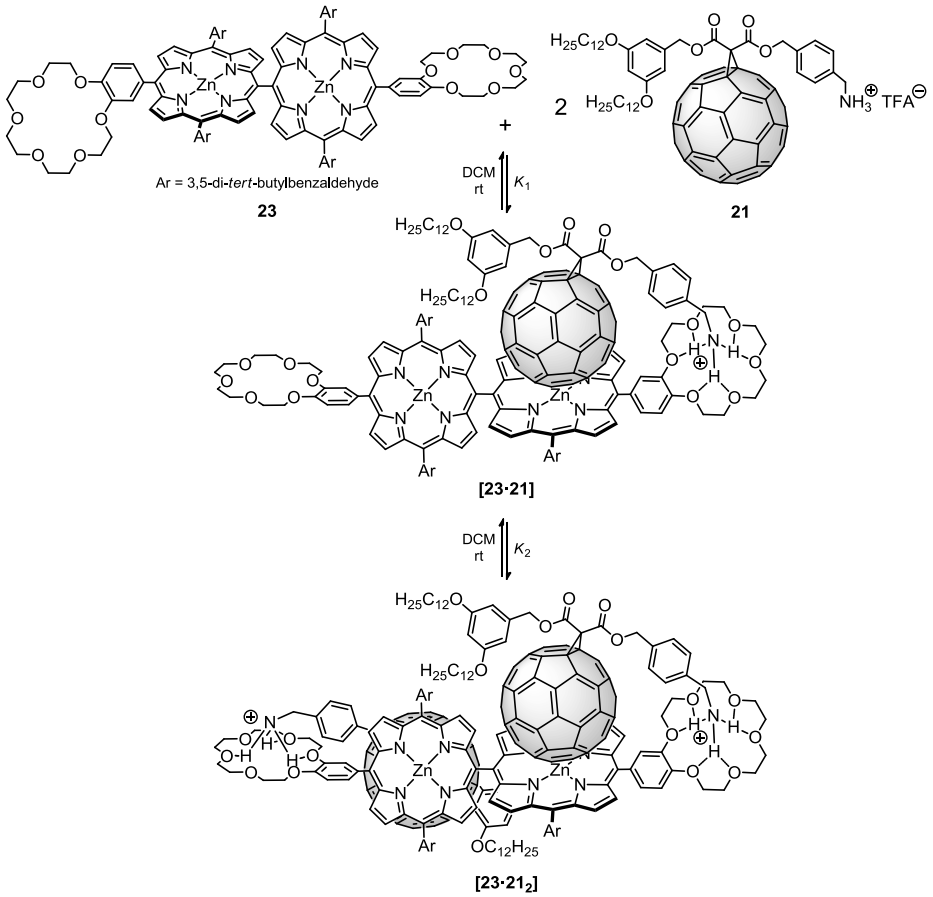

Scheme 6. Supramolecular complexes obtained from building blocks **23** and **21**.

Non-linear curve fitting to a 1:2 model yielded the binding constants of this system as reported by Table 2.

Table 2. Stepwise binding constants obtained for **[23·21$_2$]**.

log K_a ± 3σ	
log K_1	8.7 ± 1.4
log K_2	5.4 ± 0.9

Surprisingly, the binding constant obtained for K_1 is much larger than that obtained in the case of the monoporphyrin (log K_1=8.7 *vs.* log K_a=6.9 respectively). Modelization of the system evidenced a close distance between the fullerene moiety and both porphyrin subunits (Figure 7), suggesting the existence of an additional interaction with the neighbor porphyrin moiety. This complementary recognition motif can be thus a plausible explanation for the experimental findings.

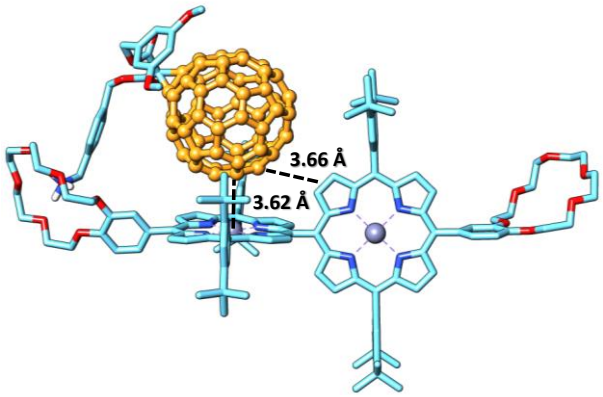

Figure 7. Spartan Modelization of **[23·21]** (semi-empirical PM3 method, dodecyl chains have been substituted by methyl groups for ease of calculations) suggesting the existence of fullerene-porphyrin interactions with both porphyrin subunits.

A look at the shape of the binding isotherm also evidenced that it was not a standard hyperbola, thus pointing to possible cooperative effects (see Annex II). Even though each of the porphyrin subunits exhibit chelate cooperativity, we could consider the interaction between subunits as allosteric and, therefore, calculate the cooperative factor α as shown in **(I)** where $K \approx K_1$. It clearly shows a negative cooperativity.

$$\alpha = \frac{K_1 K_2}{K^2} = \frac{K_2}{K_1} = \frac{10^{5.4}}{10^{8.7}} = 0.0005 \qquad \textbf{(I)}$$

This result can be explained on the base of the electronic communication between porphyrin moieties as in the porphyrin tape-sandwich developed by Aida.[89] Thus a complexation of a first fullerene molecule by a porphyrin subunit can deplete the electronic density of that porphyrin and its neighbor's, thus decreasing the affinity of the latter towards fullerenes.

Complexation of **24** by **21** at rt was followed by monitoring the changes in the absorption spectra of the porphyrin array **24** (Scheme 7).

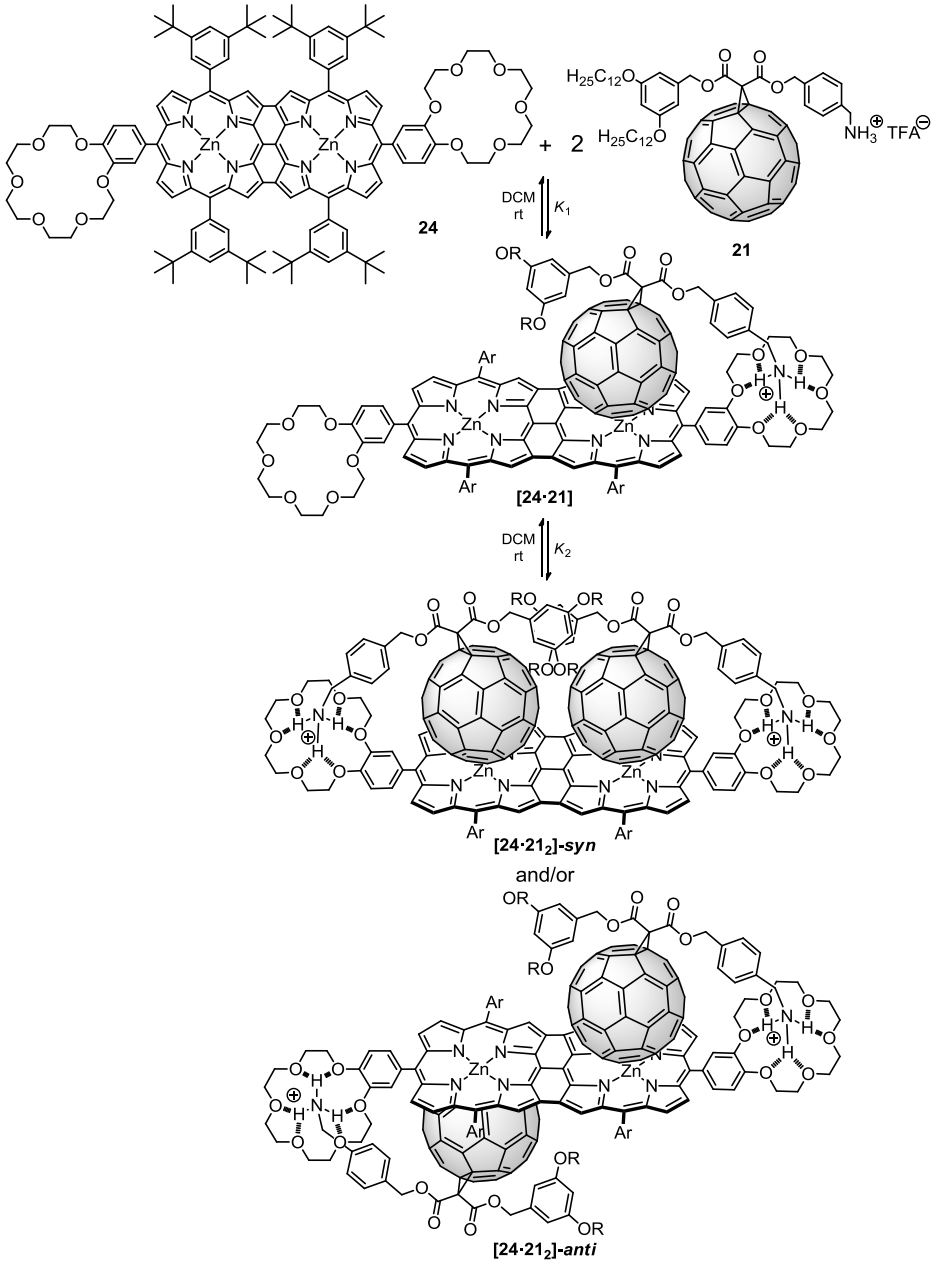

Scheme 7. Supramolecular complex obtained from building blocks **24** and **21**.

Non-linear curve fitting was adjusted for a 1:2 system yielding the binding constants of the process as reported in Table 3.

Table 3. Stepwise binding constants obtained for **[24·21$_2$]**.

log K_a ± 3σ	
log K_1	6.8 ± 0.5
log K_2	5.4 ± 0.3

Calculations of the allosteric cooperativity factor by equation **(II)** evidenced a negative cooperativity in the system which can be explained by a similar rationale than the one used for the *meso-meso* dimer, i.e. complexation of a fullerene moiety lowers the electronic density of the complexing porphyrin and its neighbor's. Interestingly, the cooperativity factor obtained this time is much larger than the one in **[23·21$_2$]**.

$$\alpha = \frac{K_2}{K_1} = \frac{10^{5.4}}{10^{6.8}} = 0.04 \qquad \textbf{(II)}$$

As depicted in Scheme 7, the combination of 1 equivalent of host molecule **24** and two of guest molecule **21** can yield two different regioisomers, **[24·21$_2$]-*syn*** and **[24·21$_2$]-*anti***. Although it is not possible to ascertain which conformer is preferred in solution, modelization of **[24·21$_2$]-*syn*** (Figure 8) evidenced the possibility of having additional π-π interactions between both moieties, which are not possible to obtain in **[24·21$_2$]-*anti***. The presence of this complementary interaction could be an explanation for the larger α value obtained in **[24·21$_2$]**, thus pointing to the *syn* conformer as that preferred in solution.

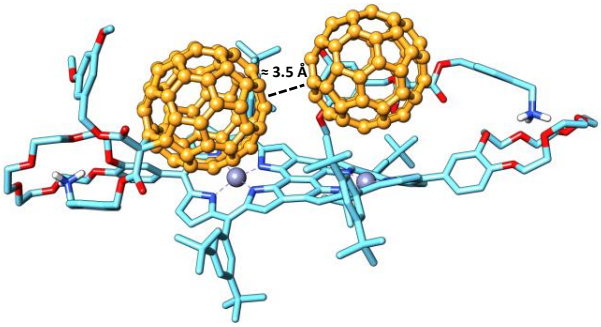

Figure 8. Spartan modelization of **[24·21$_2$]-*syn*** (semi-empirical PM3 method, dodecyl chains have been substituted by methyl groups for ease of calculations).

Unveiling the nature of crown ether-C_{60} interactions

In this chapter we further explored the nature of fullerene-crown ether interactions in exTTF based receptors following the results previously obtained in our lab which led to very strong binding constants for pristine C_{60}.[103]

While supposed to arise from n-π or CH-π interactions, the precise nature of the additional stability conferred by crown ethers remains an open question. As a result we have synthesized a new series of crown ether containing exTTF derivatives with a twofold objective, studying the impact of size modification and the introduction of heteroatoms (i.e. nitrogen) to tune the affinity for [60]fullerene.

The exTTF based receptors were synthesized by a common route consisting in the esterification reaction of a carboxylic acid and 2,6-dihydroxy-exTTF **33**, obtained in turn by a Horner-Wadsworth-Emmons reaction over quinone **30** (Scheme 8).

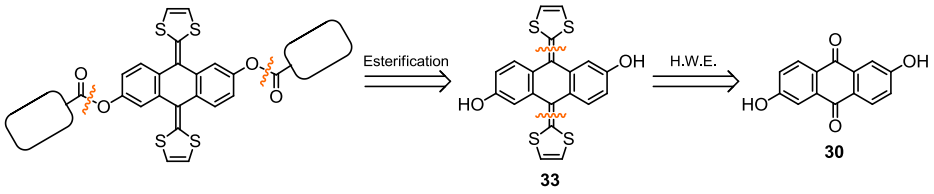

Scheme 8. Retrosynthetic analysis of the exTTF receptors.

While receptors **56**, **57** and **60** were obtained from commercially available carboxylic acids, other crown ether carboxylic acids had to be synthesized. Thus, compound **41** was obtained from catechol **36** by two successive *O*-alkylations and via intermediate **38** (Scheme 9).

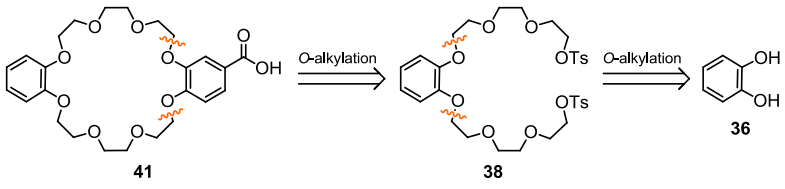

Scheme 9. Retrosynthetic analysis of carboxylic acid **41**.

Azacrown ether **47** synthesis involved a *N*-alkylation over molecule **42** followed by an *O*-alkylation on intermediate **44** (Scheme 10).

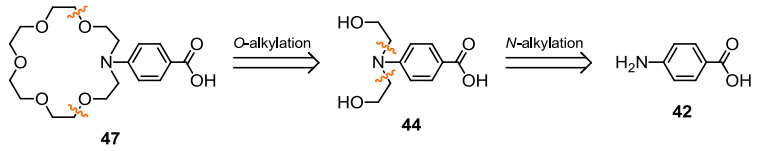

Scheme 10. Retrosynthetic analysis of carboxylic acid **47**.

Finally, azacrown ether **51** was obtained from **49** by a Hartwig-Buchwald cross coupling (Scheme 11).

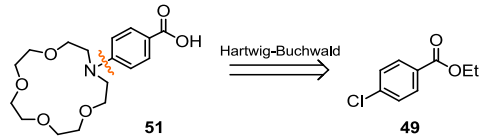

Scheme 11. Retrosynthetic analysis of carboxylic acid **51**.

Complexation studies were realized by monitoring the changes in the exTTF moiety spectra after adding increasing quantities of C_{60} in ClPh at rt (Scheme 12).

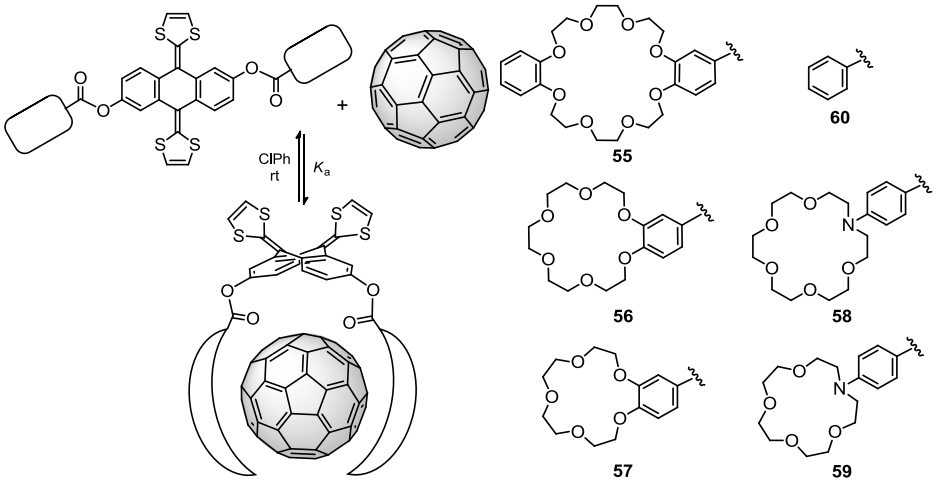

Scheme 12. Complexes obtained from exTTF based tweezers **55**, **56**, **57**, **58**, **59** and **60**.

Non-linear curve fitting of titration data afforded the binding constants for each of the receptors as reported in Table 4.

Table 4. Binding constants of the exTTF based receptors.

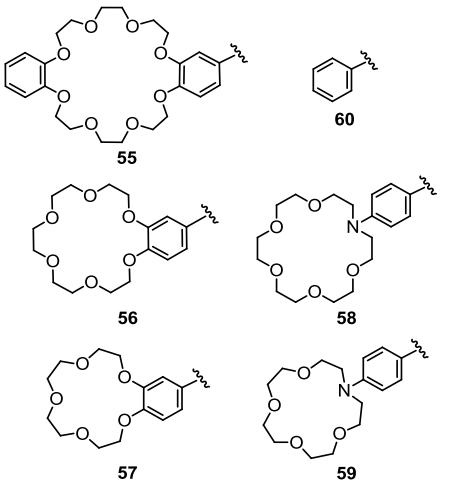

Host	log K_a ± 3σ
55	> 7
56*	6.7 ± 0.2
57	4.1 ± 0.1
60	3.3 ± 0.4
58	5.1 ± 0.3
59	3.4 ± 0.3

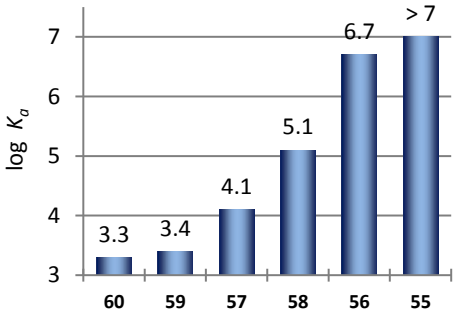

* Results previously published.[103]

As can be seen from the experimental findings, the nature and size of the crown ether has a clear impact on the affinity towards [60]fullerene leading to a range of binding constants oscillating more than three orders of magnitude. Azacrown ethers led to slightly lower binding constants whereas larger crown ether, led to larger K_a.

The donor-acceptor interaction in the ground state between the exTTF and the C_{60} was evidenced by electrochemical studies but there was no direct correlation between the binding constants and the electrochemical properties of the complexes, suggesting the presence of other interactions.

Study of the geometrical parameters of the modeled complexes (DFT level) confirmed that the affinity towards C_{60} arises from an interplay of CH-π, n-π and π-π interactions (Table 5). The key parameters seems to be the CH-π and n-π interactions from the crown ether moiety, as the larger they become, the larger the binding energy is, and as π-π and n-π interactions from the exTTF moiety/peripheral aromatic rings remain in the same range for all complexes. However, the later still play an important role in the binding of C_{60} as evidenced in **[60·C_{60}]**.

Table 5. Geometrical parameters of the complexes obtained from the exTTF based tweezers.

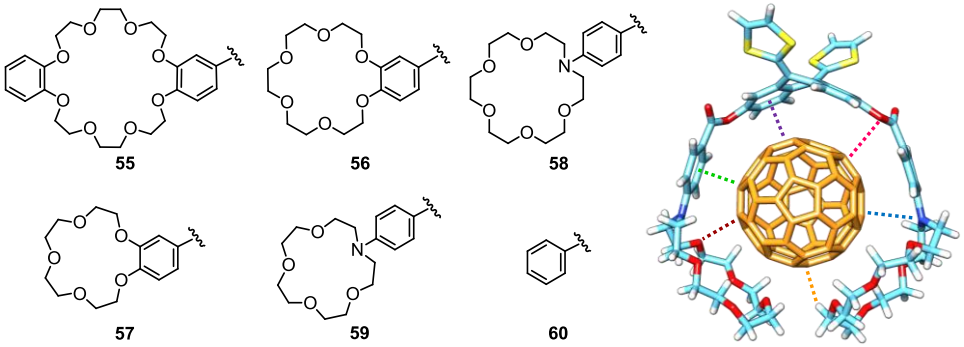

Host	nº H-C (< 3.20 Å)	nº O-C (< 3.80 Å)	bz-C (Å)	bz-bz (Å)	O-C (Å)	N-C (Å)	E_a (kcal/mol)	log K_a ± 3σ (rt, ClPh, UV)
55	12	10	2.96*	3.36*	3.37*	—	-54.36	> 7
56	10	12	2.95	3.45	3.42	—	-44.76	6.7 ± 0.2
58	10	10	3.06	3.37	3.14	3.50	-43.33	5.1 ± 0.3
57	8	8	2.99	3.46	3.30	—	-39.69	4.1 ± 0.1
59	10	4	3.41	3.37	3.25	4.14	-36.77	3.4 ± 0.3
60	—	—	3.25	3.45	3.16	—	-22.85	3.3 ± 0.4
exTTF	—	—	—	3.42	—	—	-10.24	—

* Asymmetric structure. The second bz-C, bz-bz and O-C distances are 2.99, 3.60 and 3.52 Å, respectively.

The influence of embracing the fullerene by the crown ether was also studied, evidencing that this movement provides a stabilization of around 25-30% of the total binding energy.

Design and synthesis of new (exTTF)$_2$-crown ether molecular tweezers

Interested by the influence of crown ethers in the recognition of C_{60} we developed two new receptors with a (exTTF)$_2$-crown ether structure. The synthetic route to receptors **75** and **76** was based on the esterification of the corresponding exTTF derivative over the carboxylic acid **74**, which in turn was obtained from catechol **69** after two *O*-alkylation reactions (Scheme 13).

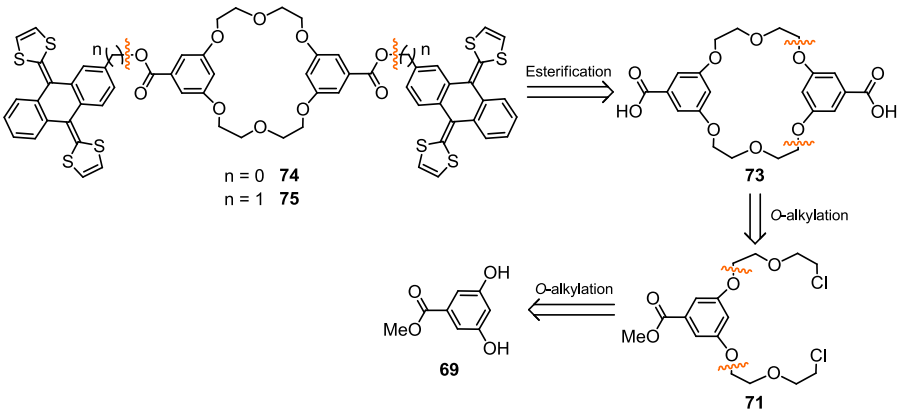

Scheme 13. Retrosynthetic analysis of receptors **74** and **75**.

The key reaction to obtain exTTF derivatives **64** and **68** was a Horner-Wadsworth-Emmons reaction over their corresponding alcohol, **61** and **65** (Scheme 14).

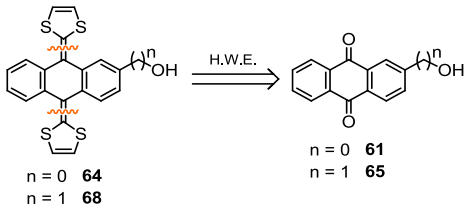

Scheme 14. Retrosynthetic analysis of the exTTF derivative moieties **64** and **68**.

Complexation studies were realized by UV-vis spectroscopy (Scheme 15).

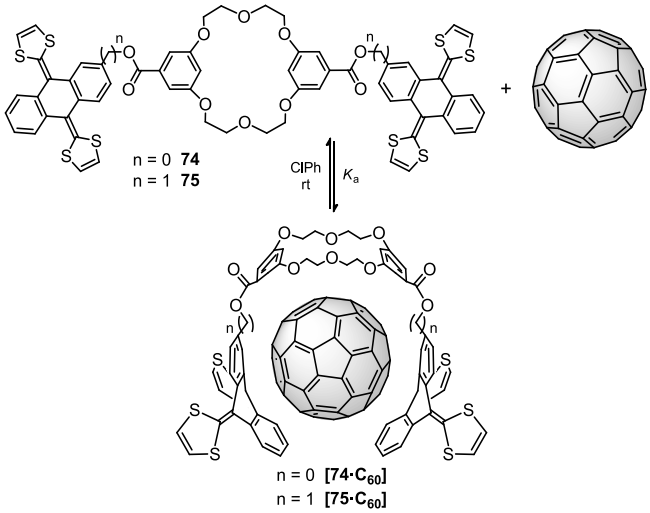

Scheme 15. Supramolecular complex obtained from building blocks **74**, **75** and C_{60}.

Binding constants of the systems were obtained as reported in Table 6.

Table 6. Binding constants of the $(exTTF)_2$-crown ether molecular tweezers.

Complex	log K_a ± 3σ
[74·C_{60}]	5.0 ± 0.4
[75·C_{60}]	6.5 ± 0.6

In spite of the widespread principle of preorganization,[122] the use of rigid host molecule **74** led to a lower binding constant than in more flexible **75**. This proves that an increase in the preorganization of the host molecule does not always lead to higher affinities towards the guest, being also important to search a proper complementarity between host and guest

Noteworthy, the binding constant obtained with **[74·C_{60}]** is lower than its exTTF-$(crown\ ether)_2$ analogue **[56·C_{60}]**. This demonstrates the great potential of crown ethers as recognition motifs for fullerenes, comparable –or even better– than that of the well established complementarity of exTTF.

Conclusions

The work developed in this study has provided valuable information on the key role of crown ethers in the supramolecular chemistry of fullerenes.

Notably, we have gained further knowledge in the nature of two supramolecular interactions which were not very well understood previously: π-π stacking between C_{60} and porphyrins and the affinity of crown ethers towards fullerenes.

We have also further studied the supramolecular properties of porphyrin arrays, largely unexplored up to now.

All these results will lead to the design of new supramolecular receptors towards fullerenes.

Resumen

Introducción

Uno de los mayores retos a los que se enfrenta la humanidad hoy en día es nuestra creciente dependencia a los combustibles fósiles para generar electricidad, sin la cual nuestra sociedad retrocedería hasta comienzos del siglo XIX. Como respuesta a esta situación, se han realizado enormes esfuerzos para encontrar nuevas y mejores fuentes de energía entre las que destaca la luz solar debido a su extraordinario potencial: el sol irradia sobre la tierra más energía en un año de la que jamás se conseguiría juntando todas las fuentes de energía no renovables del planeta.[1]

De todas las tecnologías existentes para transformar la energía solar en electricidad, los paneles fotovoltaicos son, tal vez, los dispositivos más comunes. Entre ellos, las células orgánicas son especialmente prometedoras puesto que, a pesar de no ofrecer eficiencias demasiado altas, son baratas y flexibles. Además, mejorar su rendimiento debe de ser posible ya que en la naturaleza existen actualmente dispositivos orgánicos tales como el aparato fotosintético, capaces de capturar la luz y transformarla en un potencial electroquímico con un rendimiento casi cuantitativo.

Entonces, ¿por qué si tanto las células solares como el aparato fotosintético comparten un mismo esquema de funcionamiento (absorción de la luz para producir un estado de separación de cargas que posteriormente se recombina) ningún dispositivo artificial ha sido capaz de acercarse a la eficiencia de las plantas? La respuesta parece estar relacionada con el tamaño del aparato fotosintético, en la escala nanométrica, (Figura 1) donde es la física cuántica quien gobierna.

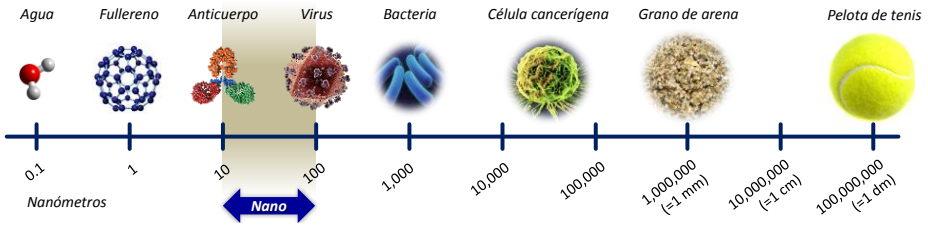

Figura 1. ¿Cómo de pequeñas son las "nano-cosas"?

Con el objetivo de alcanzar esa escala de tamaño los químicos recurren a menudo a una aproximación de tipo ascendente (bottom-up), en la que componentes pequeños (las moléculas) son ordenados para obtener dispositivos más complejos.

Una de las herramientas más utilizadas para conseguir un ensamblaje ordenado en lugar de una mezcla aleatoria de los componentes es la química supramolecular, interesada en su auto-ensamblado a través de fuerzas intermoleculares débiles[2] y que es el objetivo central del presente estudio.

Así, hemos tratado la formación de ensamblajes supramoleculares dador-aceptor capaces de reproducir la etapa clave de la fotosíntesis, esto es, la formación de un estado de separación de cargas estable. Nuestro interés se centrará principalmente en estudiar cómo obtener sistemas estables de forma controlada.

Para ello, se ha trabajado con dos moléculas dadoras diferentes: las porfirinas y los TTF extendidos (exTTF), mientras que el C_{60} se ha usado como molécula aceptora.

Las porfirinas son macrociclos aromáticos con 18 electrones π constituidas por un centro tetrapirrólico y tres posiciones diferentes para la funcionalización, dos de ellas en la periferia, las posiciones *meso* y β-pirrólicas, y una tercera en los grupos NH, donde es posible coordinar un catión metálico (Figura 2).[39]

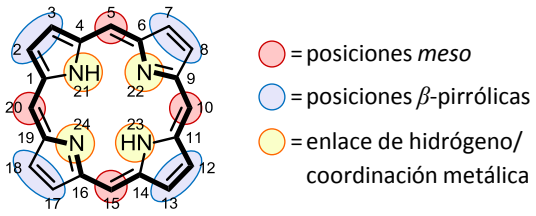

Figura 2. Estructura de las porfirinas con su anillo aromático (en negrita) y numeración.

Son unas excelentes moléculas dadoras debido a sus fuertes bandas de absorción UV-vis, potencial de oxidación modulable y largo tiempo de vida del estado excitado singlete.

Asimismo, hay que destacar también el uso que hemos hecho de dímeros porfirínicos unidos tanto por las posiciones *meso-meso* como por las posiciones *meso-meso*, *β-β* y *β-β*. Estos sistemas fueron obtenidos mediante una reacción de acoplamiento oxidante sobre una porfirina metálica con una posición *meso* libre (Esquema 1).

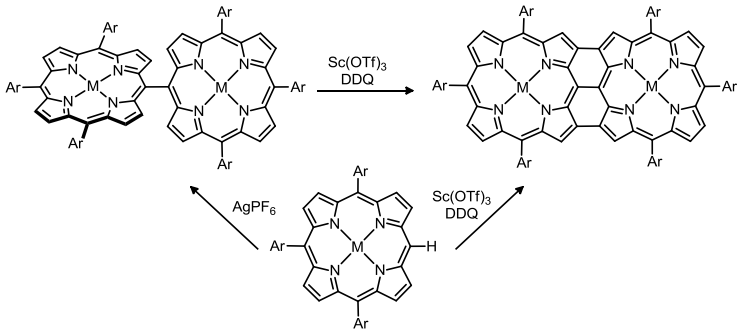

Esquema 1. Formación de los dímeros porfirínicos.

El 9,10-di(1,3-ditiol-2-yliden)-9,10-dihidroantraceno (exTTF) es un análogo conjugado del tetratiafulvaleno (TTF) que incorpora un espaciador *p*-quinoide entre los dos anillos de 1,3-ditiol (Figura 3).[90]

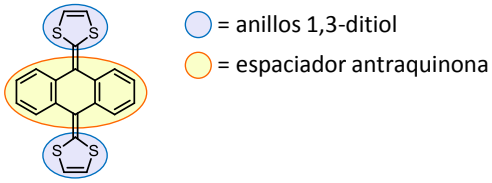

Figura 3. Estructura del exTTF.

Esta molécula pro-aromática ha sido ampliamente usada como dador de electrones debido a su bajo potencial de oxidación y geometría tridimensional. Al oxidarse, su conformación cambia drásticamente desde una forma de silla de caballo, en la que la cara dadora y la aromática se diferencian claramente, a una conformación plana D_{2h} donde la aromaticidad se extiende por toda la molécula y los anillos de 1,3-ditiol se disponen ortogonales al anillo de antraceno central (Figura 4).[92]

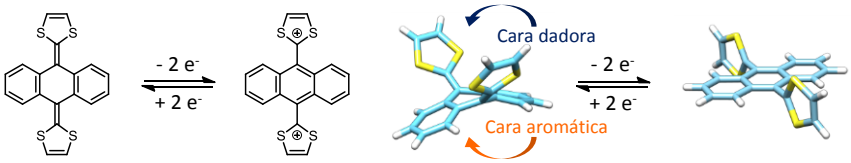

Figura 4. La oxidación del exTTF produce un cambio dramático de la geometría.

El [60]fullereno (Figura 5) se ha usado como aceptor debido a su estructura tridimensional, potencial de reducción, amplio rango de absorción UV-vis y baja energía de reorganización en reacciones de transferencia electrónica.

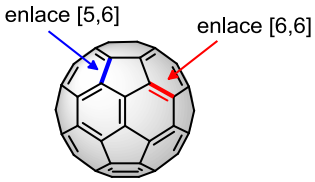

Figura 5. Estructura molecular del C_{60}.

A pesar de la extensa bibliografía existente sobre conjugados covalentes de fullerenos, porfirinas y exTTFs, su combinación supramolecular ha sido mucho menos explorada debido a las dificultades inherentes en la obtención de complejos supramoleculares de composición conocida y controlada. Las interacciones que se usan normalmente para la obtención de estos compuestos son de tipo π–π, iónicas, catión amonio-éter corona, reacciones ácido-base de Lewis o enlaces mecánicos. Usadas individualmente, estas interacciones derivan en complejos de baja estabilidad, sin embargo, su combinación estratégica permite obtener complejos muy estables.

En nuestro estudio se han combinado algunas ellas con diferentes éteres corona para obtener una serie de nuevos complejos supramoleculares dador-aceptor.

Objetivos y resultados

Influencia del metal en la constante de asociación entre distintas porfirinas metaladas y el C_{60}.

En primer lugar nos interesamos en conseguir un mayor conocimiento sobre las interacciones π-π entre porfirinas y fullerenos. La naturaleza de esta atracción es un tema controvertido, ya que parece implicar una transferencia de carga desde el fullereno a la porfirina, hecho que sólo se puede racionalizar considerando el fullereno al nivel local del doble enlace y no en su conjunto.[59]

Así, se construyeron una serie de díadas supramoleculares donde el C_{60} y la porfirina se combinaron a través de interacciones π-π y catión amonio-éter corona (Figura 6) cuya óptima complementariedad se demostró en un trabajo previo de nuestro laboratorio en Estrasburgo, en el que se consiguió aumentar la estabilidad de los complejos en dos órdenes de magnitud.[86]

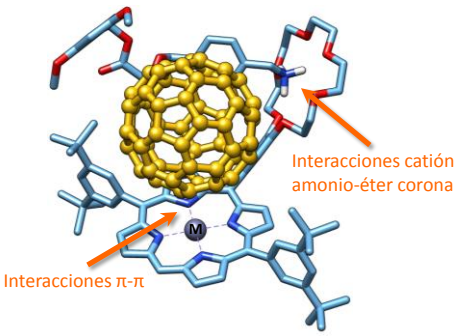

Figura 6. Estructura de los nuevos complejos supramoleculares. M = 2H, Co, Ni, Cu, Zn.

En esta serie, el metal de la porfirina se cambió sistemáticamente con el objetivo de alterar su entorno, ya que dado el origen electrostático de las interacciones π-π esta modificación debería tener un claro impacto en las constante de asociación de los complejos formados.

Las porfirinas **12-M** (M = 2H, Co, Ni, Cu, Zn) se obtuvieron a través de un acoplamiento de Suzuki-Miyaura sobre el derivado **9**, que a su vez se obtuvo de la yodación regioselectiva de la molécula **8**, procedente de la condensación mixta del dipirrometano **3** y el aldehído **6** (Esquema 2).

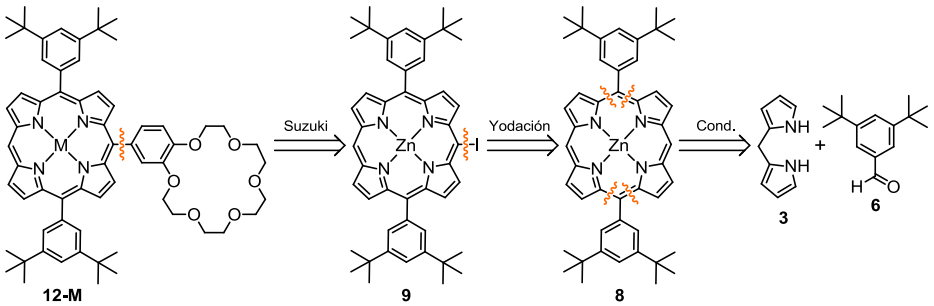

Esquema 2. Análisis retrosintético de las porfirinas **12-M**.

El sustrato **22**, se obtuvo mediante una cicloadición de tipo Bingel de la molécula **20** sobre el C_{60}. El malonato asimétrico usado se obtuvo mediante una reacción de esterificación sobre la molécula **19**, procedente del alcohol **17** (Esquema 3).

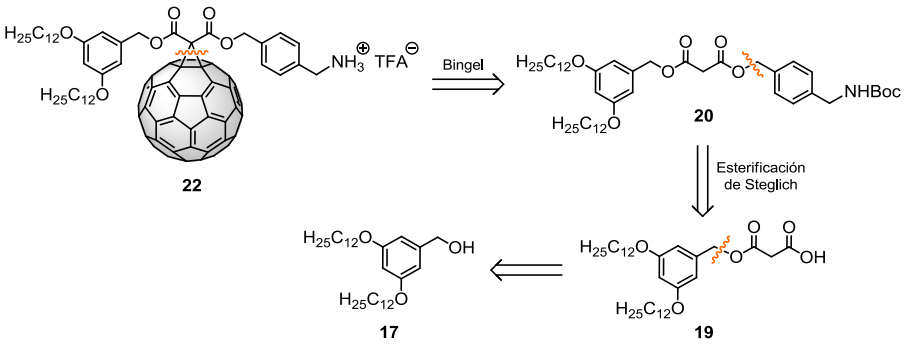

Esquema 3. Análisis retrosintético del metanofullereno **22**.

Los estudios de complejación de los sistemas **[12-M·21]** se realizaron monitorizando los cambios espectroscópicos de la unidad porfirínica **12-M** después de adicionar cantidades crecientes del derivado **21** a temperatura ambiente (Esquema 4).

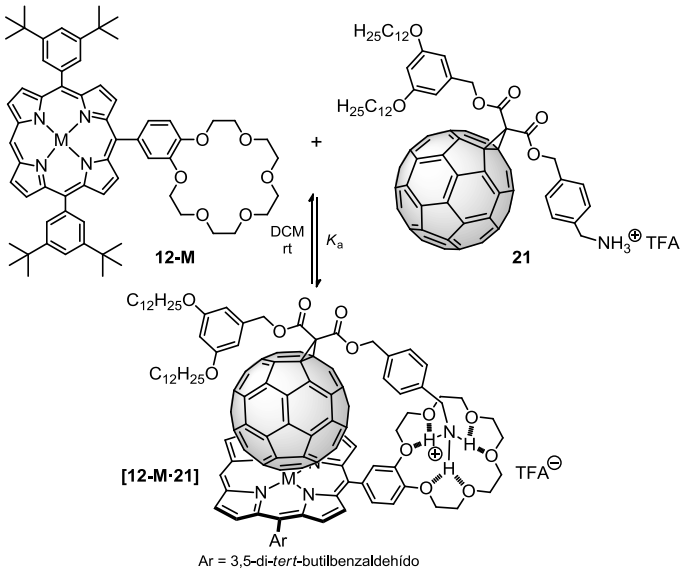

Esquema 4. Formación de los complejos supramoleculares **[12-M·21]** a partir de sus unidades.

El ajuste no lineal de los datos de la valoración mediante el programa de análisis Specfit permitió obtener el valor de las diferentes constantes de formación K_a de los complejos **[12-M·21]** tal y como aparecen en la Tabla 1.

Tabla 5.1. Constantes de asociación de los sistemas **[12-M·21]**.

Complejo	log K_a ± 3σ
[12-2H·21]	5.5 ± 0.2
[12-Co·21]	6.3 ± 0.2
[12-Ni·21]	5.9 ± 0.1
[12-Cu·21]	6.3 ± 0.3
[12-Zn·21]	6.9 ± 0.2

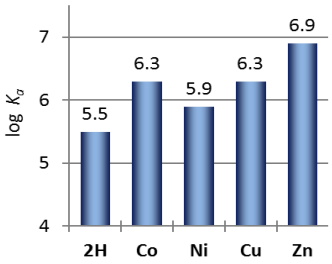

Las constantes de asociación obtenidas fueron muy altas, evidenciando tanto la buena complementariedad de las interacciones catión amonio-éter corona y π-π del sistema, como la influencia de la cooperatividad quelato.

Es de destacar que los valores de K_a obtenidos para **[12-Zn·21]** y **[12-2H·21]** son muy diferentes de los descritos previamente en la bibliografía, donde receptores basados en porfirinas de base libre sistemáticamente se unían al fullereno con una afinidad similar a la de sus análogas de Zn(II).[61a],[62],[63b]

Sin embargo, los valores que hemos obtenido correlacionan con los esperados para una díada porfirina·C_{60} unida mediante fuerzas de van der Waals, en las que K_a aumenta al aumentar el número de electrones en la porfirina. La excepción a esta "regla" sería la gran estabilidad de **[12-Co·21]**, atribuible a las fuertes interacciones existentes entre el fullereno y los metales del grupo 9 (Co, Rh, Ir).[63b]

Asimismo, hay que destacar que los trabajos precedentes complejan C_{60} no funcionalizado, cuya baja solubilidad limita el rango de disolventes que se pueden utilizar. De hecho, se ha sugerido que la desolvatación del C_{60} es uno de los principales contribuyentes en la energía libre de complejación en solución.[62] El uso del metanofullereno **21** ha evitado elegantemente estas limitaciones, manteniendo prácticamente intactas las propiedades originales del fullereno.

Propiedades supramoleculares de las díadas de porfirinas

Inspirados por los resultados del sistema anterior decidimos funcionalizar aún más nuestra porfirina con el objetivo de obtener dímeros porfirínicos de tipo *meso-meso* y *meso-meso*, *β-β*, *β'-β'*. Las propiedades supramoleculares de estas díadas, ampliamente desconocidas, se estudiaron mediante la complejación del mismo metanofullereno, **21**, usado como sustrato anteriormente.

A pesar de la gran complejidad de los dímeros **23** y **24**, su alta simetría nos permitió obtenerlos fácilmente a través de una ruta sintética divergente a partir de la porfirina **12-Zn**, tal y como se observa en el Esquema 5.

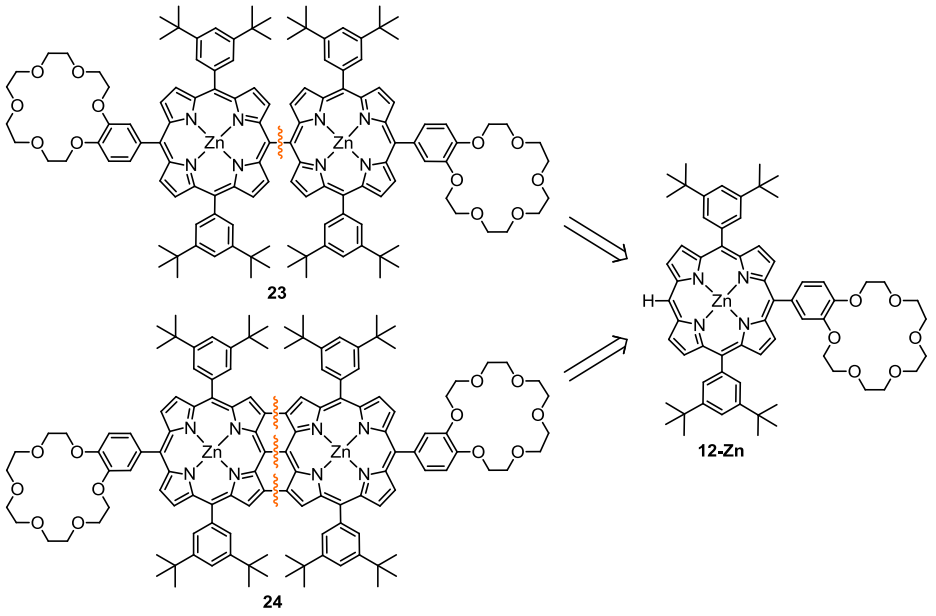

Esquema 5. Análisis retrosintético de los dímeros **23** y **24**.

Los estudios de complejación de **[23·21]** y **[23·21$_2$]** se realizaron monitorizando los cambios espectroscópicos de la porfirina **23** tras adicionar cantidades crecientes del derivado fullerénico **21** a temperatura ambiente en DCM (Esquema 6).

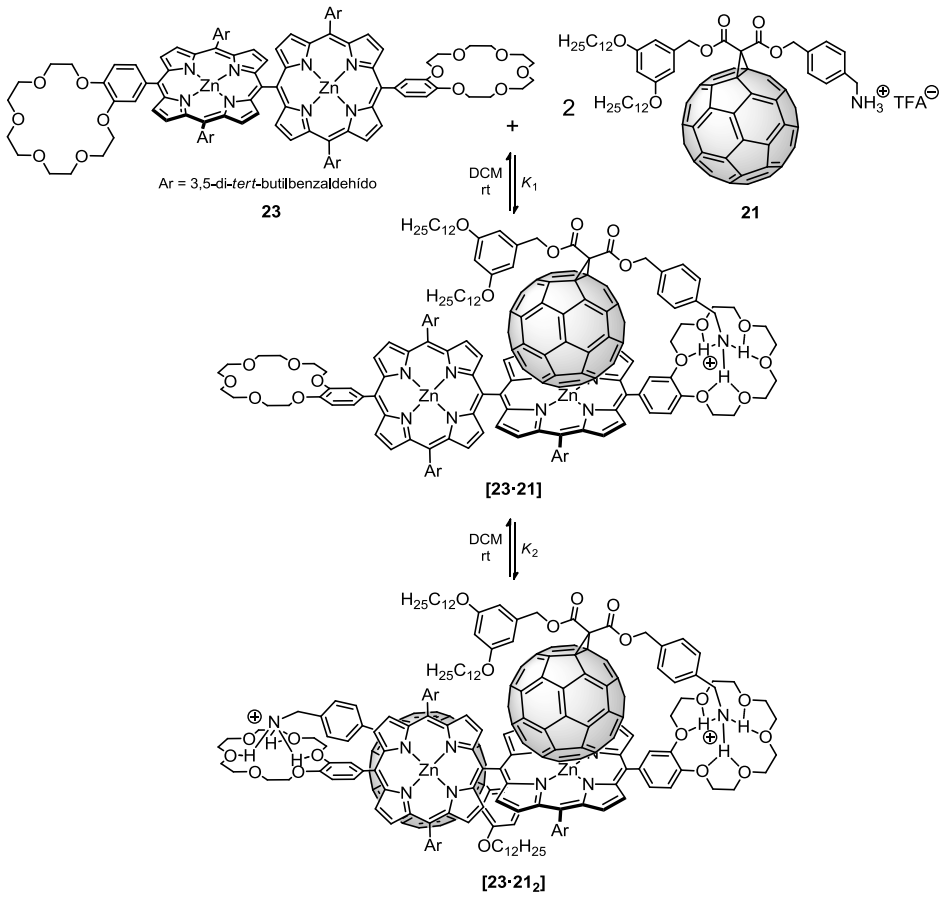

Esquema 6. Complejos supramoleculares obtenidos a partir de **23** y **21**.

El ajuste no lineal de los valores experimentales se realizó para una estequiometría 1:2 obteniéndose los distintos valores de K_a tal y como muestra la Tabla 5.2.

Tabla 5.2. Constantes de asociación obtenidas para **[23·21$_2$]**.

log K_a ± 3σ	
log K_1	8.7 ± 1.4
log K_2	5.4 ± 0.9

Sorprendentemente, la constante de asociación obtenida para K_1 es mucho mayor que la obtenida para la monoporfirina (log K_1=8.7 *vs.* log K_a=6.9 respectivamente). La modelización del sistema puso en relieve la existencia de una distancia corta entre el

fullereno y ambas porfirinas (Figura 7), sugiriendo la existencia de interacciones supramoleculares con ambas unidades. Este punto de reconocimiento adicional podría, por tanto, justificar la mayor estabilidad observada.

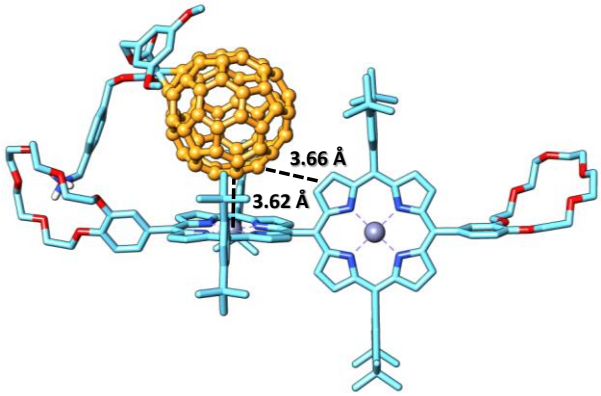

Figura 7. Modelización Spartan de **[23·21]** (método semi-empírico PM3, las cadenas de dodecilo se han sustituido por grupos metilos para facilitar los cálculos) sugiriendo la existencia de interacciones fullereno-porfirina con ambas subunidades porfirínicas.

Por otra parte, el aspecto de la isoterma de enlace de este sistema no se corresponde con una hipérbola estándar, sugiriendo la existencia de posibles efectos cooperativos (ver Anexo II). A pesar de que el tipo de cooperatividad presente en cada subunidad es de tipo quelato, podemos considerar las interacciones entre subunidades de tipo alostérico y, por tanto, calcular el factor de cooperatividad α a través de **(I)** (donde $K \approx K_1$) evidenciándose claramente una cooperatividad negativa.

$$\alpha = \frac{K_1 K_2}{K^2} = \frac{K_2}{K_1} = \frac{10^{5.4}}{10^{8.7}} = 0.0005 \qquad \textbf{(I)}$$

Este resultado se puede explicar atendiendo a la comunicación electrónica entre las dos porfirinas, en línea con los resultados obtenidos en los 'sándwiches' de Aida.[89] Así, la complejación del fullereno con una porfirina resulta en la disminución de la densidad electrónica de esta, así como la de la porfirina vecina, disminuyendo por tanto la afinidad de esta última hacia los fullerenos.

La complejación de **24** por **21** se estudió monitorizando los cambios espectroscópicos en el espectro UV-vis del dímero **24** (Esquema 7).

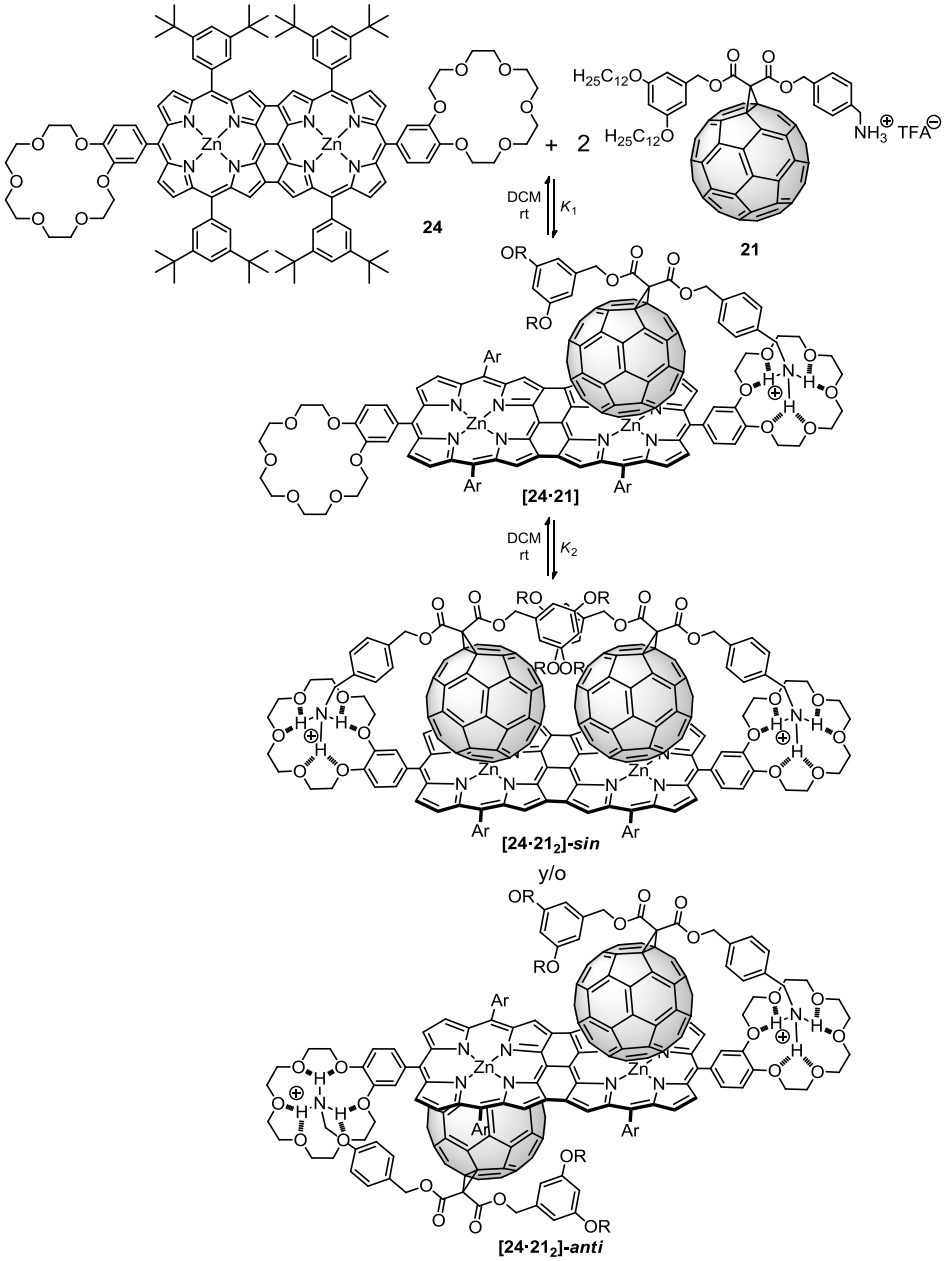

Esquema 7. Complejos supramoleculares obtenidos a partir de **24** y **21**.

El ajuste no lineal de los datos experimentales obtenidos para un sistema 1:2 devolvió las constantes de asociación del proceso tal y como se recogen en la Tabla 5.3.

Tabla 5.3. Constantes de asociación de cada etapa de formación de **[24·21$_2$]**.

log K_a ± 3σ	
log K_1	6.8 ± 0.5
log K_2	5.4 ± 0.3

El cálculo del factor de cooperatividad alostérico mediante **(II)** evidenció la cooperatividad negativa del sistema, motivada probablemente por un proceso análogo al visto anteriormente, en el que la complejación de una unidad de fullereno disminuye la densidad electrónica en todo el dímero. Sorprendentemente, el valor de α obtenido es mucho mayor que el obtenido para **[23·21$_2$]**.

$$\alpha = \frac{K_2}{K_1} = \frac{10^{5.4}}{10^{6.8}} = 0.04 \qquad \textbf{(II)}$$

Tal y como se muestra en el Esquema 7, la combinación de 1 equiv del receptor **24** con 2 equiv de **21** puede derivar en la obtención de dos regiosiómeros diferentes, **[24·21$_2$]-*sin*** y **[24·21$_2$]-*anti***. Aunque en principio no es posible averiguar qué isómero es el mayoritario en disolución, la modelización de **[24·21$_2$]-*sin*** (Figura 8) evidenció la posibilidad de establecer interacciones π-π adicionales entre los dos fullerenos de una forma no posible en **[24·21$_2$]-*anti***. La presencia de esta interacción adicional podría ser, por tanto, una explicación para el mayor valor de α obtenido en **[24·21$_2$]**, apuntando así a que sea el confórmero *sin* el mayoritario en disolución.

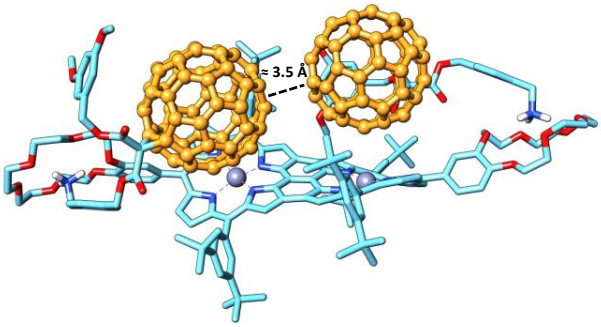

Figura 8. Modelización Spartan de **[24·21$_2$]-*sin*** (método semi-empírico PM3, las cadenas de dodecilo se han sustituido por grupos metilos para facilitar los cálculos).

Descubriendo la naturaleza de las interacciones entre los éteres corona y el C_{60}

En este capítulo exploramos la naturaleza de las interacciones fullereno-éter corona continuando el trabajo realizado previamente en Madrid en el que un conjugado exTTF-éter corona presentó una afinidad muy alta hacia el C_{60}.[103]

A pesar de que esta atracción entre los éteres corona y el C_{60} se supone resultante de interacciones n-π o CH-π, su origen concreto es todavía una pregunta abierta. Para responderla, se sintetizó una serie de nuevos conjugados de exTTF-éter corona con un doble objetivo: estudiar el impacto de la modificación del tamaño y la introducción de heteroátomos (i.e. nitrógeno) para modular la afinidad hacia el [60]fullereno.

Los receptores se sintetizaron siguiendo una ruta sintética común consistente en la esterificación de un ácido carboxílico derivado del éter corona correspondiente y el 2,6-dihidroxy-exTTF **33**, obtenido a través de una reacción de Horner-Wadsworth-Emmons sobre la quinona **30** (Esquema 8).

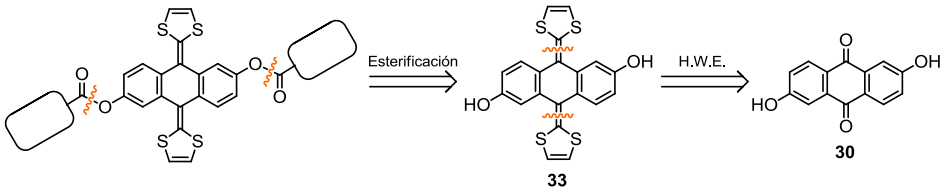

Esquema 8. Análisis retrosintético de los receptores de exTTF.

Mientras que los receptores **56**, **57** y **60** se obtuvieron a partir de ácidos comerciales, otros tuvieron que ser sintetizados. Así, el compuesto **41** se obtuvo a partir del catecol **36** mediante dos *O*-alquilaciones sucesivas y el intermedio **38** (Esquema 9).

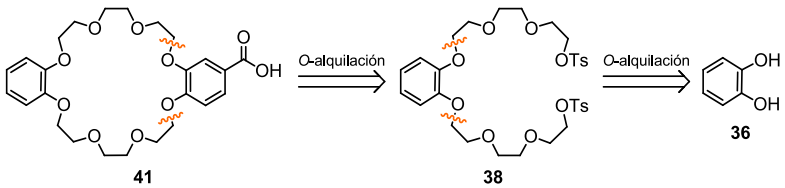

Esquema 9. Análisis retrosintético del ácido carboxílico **41**.

La síntesis del azaéter corona **47** se realizó a través de una *N*-alquilación sobre la molécula **42** seguida de una *O*-alquilación en el intermedio **44** (Esquema 10).

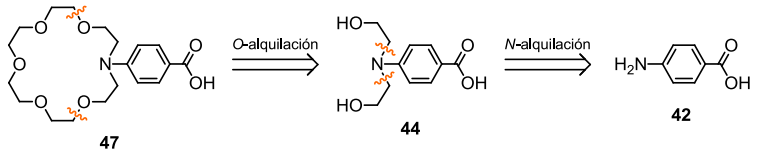

Esquema 10. Análisis retrosintético del ácido carboxílico **47**.

Por último, el azaéter corona **51** se obtuvo a partir de la molécula **49** y un acoplamiento cruzado de Hartwig-Buchwald (Esquema 11).

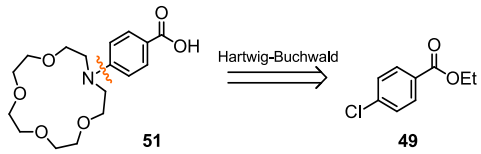

Esquema 11. Análisis retrosintético del ácido carboxílico **51**.

Los estudios de complejación se realizaron siguiendo los cambios espectroscópicos del exTTF tras adicionar cantidades crecientes de C_{60} en ClPh (Esquema 12).

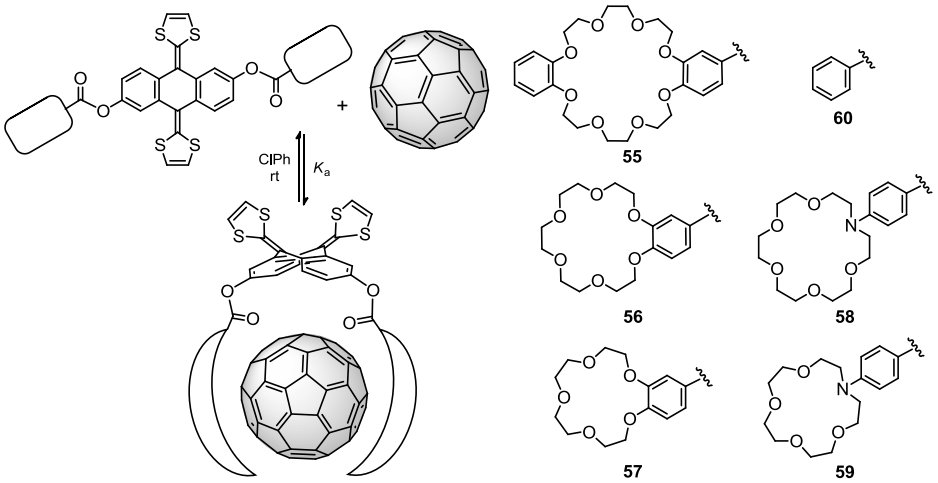

Esquema 12. Complejos derivados de las pinzas de exTTF **55**, **56**, **57**, **58**, **59** y **60**.

El ajuste no lineal de los datos experimentales permitió obtener el valor de las constantes de asociación tal y como se recogen en la Tabla 5.4.

Tabla 5.4. Constantes de asociación de las pinzas de exTTF.

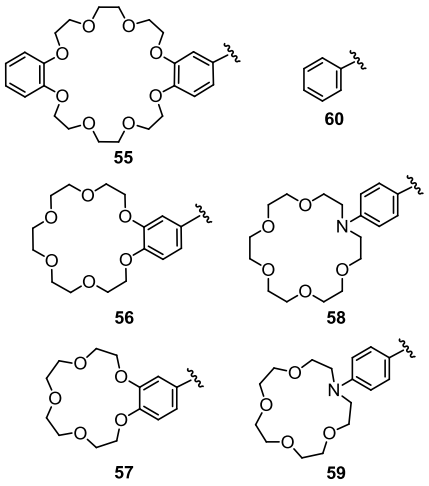

* Resultados publicados previamente.[103]

Receptor	log K_a ± 3σ
55	> 7
56*	6.7 ± 0.2
57	4.1 ± 0.1
60	3.3 ± 0.4
58	5.1 ± 0.3
59	3.4 ± 0.3

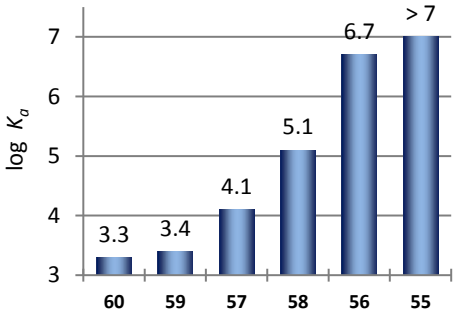

La naturaleza y el tamaño del éter corona tienen un claro impacto en la afinidad hacia el [60]fullereno, traduciéndose en cambios en las constantes de asociación de más de 3 órdenes de magnitud. Los azaéteres corona presentaron una afinidad ligeramente menor, mientras que éteres mayores incrementaron los valores de K_a.

La interacción dador-aceptor en el estado fundamental entre el exTTF y el C_{60} se evidenció mediante estudios electroquímicos, pero no se obtuvo ninguna correlación directa entre las constantes de asociación y las variaciones de los potenciales redox observados para los complejos, sugiriendo así la participación de otras interacciones.

El estudio de los parámetros geométricos de los modelos computacionales de los complejos (nivel DFT) confirmó que la afinidad hacia el C_{60} surge de una combinación de interacciones CH-π, n-π y π-π (Tabla 5.5). Los parámetros clave parecen ser las interacciones CH-π y n-π de los éteres corona, ya que cuanto más numerosas son, mayor es la energía de enlace y puesto que las interacciones π-π y n-π del exTTF/anillos aromáticos permanecen en el mismo rango en todos los casos. Estas últimas, sin embargo, tienen un papel importante, evidenciado en **[60·C_{60}]**.

Tabla 5.5. Parámetros geométricos de los complejos obtenidos con las pinzas de exTTF.

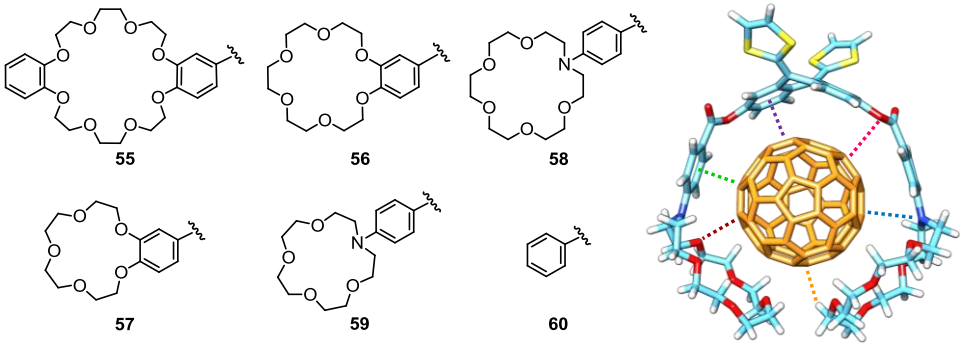

Host	nº H-C (< 3.20 Å)	nº O-C (< 3.80 Å)	bz-C (Å)	bz-bz (Å)	O-C (Å)	N-C (Å)	E_a (kcal/mol)	log K_a ± 3σ (rt, ClPh, UV)
55	12	10	2.96*	3.36*	3.37*	—	-54.36	> 7
56	10	12	2.95	3.45	3.42	—	-44.76	6.7 ± 0.2
58	10	10	3.06	3.37	3.14	3.50	-43.33	5.1 ± 0.3
57	8	8	2.99	3.46	3.30	—	-39.69	4.1 ± 0.1
59	10	4	3.41	3.37	3.25	4.14	-36.77	3.4 ± 0.3
60	—	—	3.25	3.45	3.16	—	-22.85	3.3 ± 0.4
exTTF	—	—	—	3.42	—	—	-10.24	—

* Estructura asimétrica. Las 2^{as} distancias bz-C, bz-bz y O-C miden 2.99, 3.60 y 3.52 Å respectivamente.

La influencia del "abrazo" del fullereno por el éter corona también fue estudiado, evidenciándose que este movimiento produce una estabilización de aproximadamente el 25-30% de la energía total de enlace.

Diseño y síntesis de nuevas pinzas moleculares de tipo (exTTF)$_2$-éter corona

Interesados por la influencia de los éteres corona en el reconocimiento del C_{60}, desarrollamos dos nuevos receptores de estructura (exTTF)$_2$-éter corona. La ruta sintética seguida para los receptores **75** y **76** se basó en la esterificación de los correspondientes derivados de exTTF sobre el ácido carboxílico **74**, que a su vez se obtuvo del derivado de catecol **69** tras dos *O*-alquilaciones sucesivas (Esquema 13).

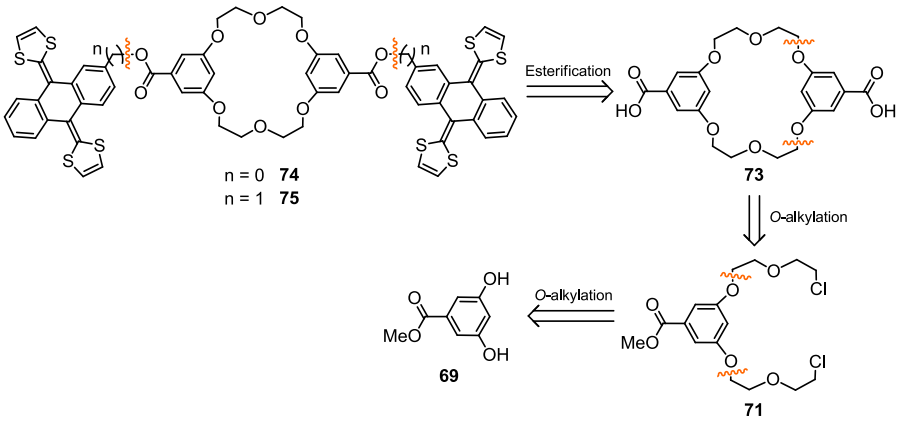

Esquema 13. Análisis retrosintético de los receptores **74** y **75**.

La etapa clave en la síntesis de los exTTF **64** y **68** es una reacción de Horner-Wadsworth-Emmons sobre los correspondientes alcoholes **61** y **65** (Esquema 14).

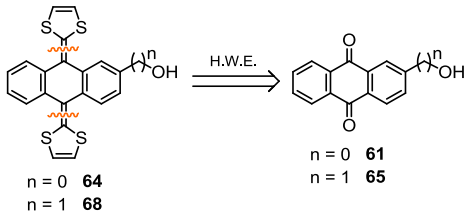

Esquema 14. Análisis retrosintético de los derivados de exTTF **64** y **68**.

Los estudios de complejación se realizaron por espectroscopía UV-vis (Esquema 15).

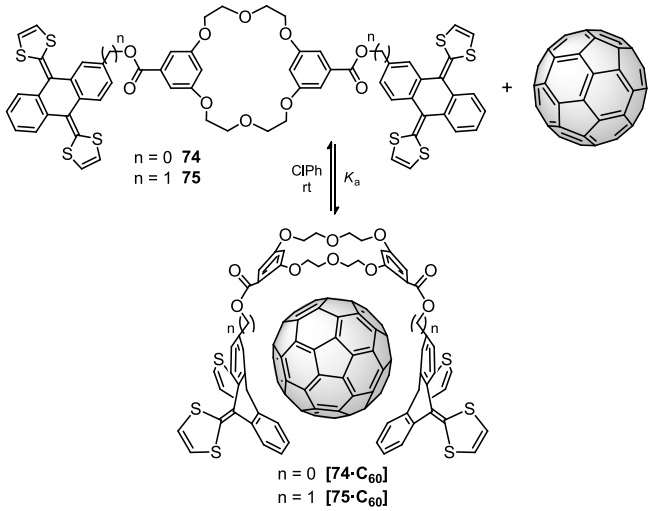

Esquema 15. Complejos supramoleculares obtenidos a partir de **74**, **75** y C_{60}.

Las constantes de asociación obtenidas para estos sistemas se recogen en la Tabla 5.6.

Tabla 5.6. Constantes de asociación de los complejos de tipo $(exTTF)_2$-eter corona.

Complex	log K_a ± 3σ
[74·C_{60}]	5.0 ± 0.4
[75·C_{60}]	6.5 ± 0.6

A pesar de lo generalizado del "principio de preorganización",[122] el uso del receptor **74**, más rígido que **75**, produjo complejos con constantes de formación más bajas, probando así que un incremento en la preorganización del sistema no siempre produce mayores afinidades, y siendo también importante buscar una buena complementariedad entre receptor y sustrato.

Hay que destacar también que la constante de formación de **[75·C_{60}]** está en el mismo rango que la obtenida en su complejo exTTF-$(éter\ corona)_2$ análogo, **[56·C_{60}]**. Esto demuestra el gran potencial de los éteres corona como elementos de reconocimiento para los fullerenos, comparable al de los exTTF.

Conclusiones

El trabajo desarrollado en este estudio ha proporcionado información valiosa sobre el papel clave de los éteres corona en la química supramolecular de los fullerenos.

En concreto, hemos obtenido un mayor conocimiento sobre el origen de dos interacciones supramoleculares poco conocidas anteriormente: las interacciones π-π entre el C_{60} y las porfirinas y la afinidad de éteres corona hacia los fullerenos.

Asimismo, hemos estudiado las propiedades supramoleculares de las díadas porfirínicas, ampliamente desconocidas hasta ahora.

Todos estos resultados conducirán a la obtención de nuevos receptores supramoleculares para los fullerenos.

Résumé

Présentation

L'un des plus grands défis auxquels fait face l'humanité aujourd'hui, est la dépendance croissante des combustibles fossiles non renouvelables afin d'obtenir de l'électricité, sans laquelle notre société serait renvoyée au début du XIXe. En conséquence, des efforts considérables ont été déployés pour trouver de nouvelles sources d'énergie, parmi lesquelles l'énergie solaire est l'une des plus prometteuses : le soleil envoie sur la terre plus d'énergie en une année que celle qui ne sera jamais obtenue à partir de toutes les sources d'énergie non renouvelables combinées.[1]

De toutes les technologies disponibles pour transformer l'énergie solaire en électricité, les cellules photovoltaïques sont les dispositifs les plus courants. Parmi celles-ci, les cellules photovoltaïques organiques sont particulièrement prometteuses, car en dépit de ne pas offrir de très bonnes performances, elles ne sont pas onéreuses et sont flexibles. Cependant, il doit être possible d'améliorer leurs performances, car ils existent déjà des dispositifs organiques, tel que le système photosynthétique naturel, capable de collecter la lumière pour la transformer en un potentiel électrochimique avec un rendement presque quantitatif.

Si les cellules solaires et l'appareil photosynthétique ont un mode de fonctionnement analogue (absorption de la lumière pour produire une séparation de charges qui ensuite se recombinent), pourquoi aucun dispositif artificiel n'a pu à ce jour égaler l'efficacité de la nature ? La réponse n'est pas encore claire, mais semble être liée à la taille de l'appareil photosynthétique, qui est à l'échelle nanométrique (Figure 1) où les propriétés de la matière répondent à la physique quantique.

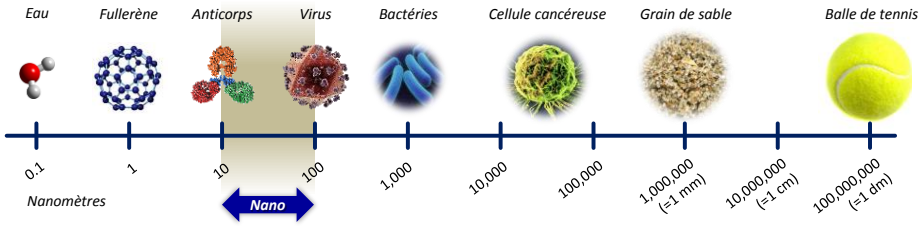

Figure 1. Quelle est la taille des "nano-objets"?

Afin d'atteindre cette échelle les chimistes ont souvent utilisé une approche ascendante (bottom-up) dans laquelle des petits composants (des molécules) sont organisés pour donner des dispositifs plus complexes.

Un des outils les plus courants pour obtenir l'assemblage désiré plutôt qu'un mélange aléatoire est la chimie supramoléculaire. Celle-ci s'intéresse à l'auto-assemblage ordonné des blocs de construction par des forces intermoléculaires faibles,[2] c'est aussi le thème central de la présente étude.

Dans ce contexte, ce travail porte sur la formation d'ensembles supramoléculaires donneur-accepteur capables de reproduire l'étape clé de la photosynthèse, à savoir la formation d'un état à charges séparées. L'intérêt sera particulièrement porté sur la manière dont les molécules donneuses d'électrons et les molécules acceptrices peuvent former des ensembles discrets stables d'une manière contrôlée.

Pour cela, nous avons utilisé des porphyrines et des TTF étendues comme molécules donneuses, tandis que le C_{60} a été choisi pour la construction de la partie acceptrice.

Les porphyrines sont des macrocycles aromatiques à 18 électrons π constitués d'un noyau tétrapyrrolique avec trois positions susceptibles d'être fonctionnalisées, deux dans la périphérie, les positions *méso* et les β-pyrroliques et une troisième au niveau des groupements NH, où il est aussi possible de complexer des cations métalliques (Figure 2).[39]

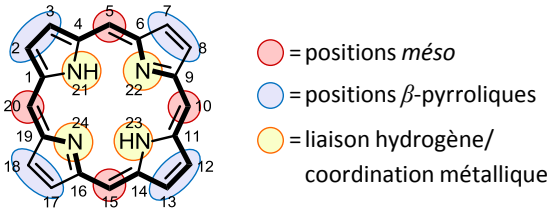

Figure 2. Structure des porphyrines avec leur anneau aromatique (en gras).

Elles sont intéressantes en raison de leur forte absorption, de leur potentiel d'oxydation modulable et du temps de vie relativement long de leur état excité singulet.

Il faut mentionner aussi, l'utilisation des dimères porphyriniques liés soit en positions *méso-méso*, soit en position *méso-méso*, *β-β* et *β'-β'*. Ces systèmes ont été obtenus par une réaction de couplage oxydant de métalloporphyrines ayant une position *méso* libre (Schéma 1).

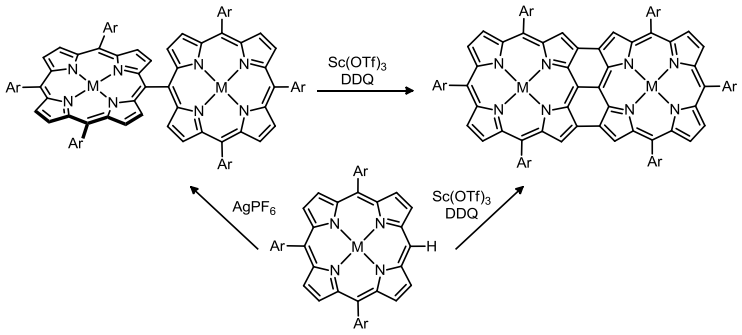

Schéma 16. Formation de dimères de porphyrines.

Le 9,10-di(1,3-dithiol-2-ylidène)-9,10-dihydroantracène (exTTF) est un analogue conjugué du tétrathiafulvalène avec un motif centrale *p*-quinonique (Figure 3).[90]

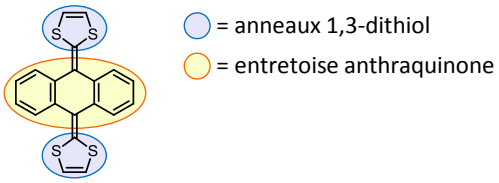

Figure 3. Structure du exTTF.

Cette molécule pro-aromatique a été largement utilisée comme système donneur en raison de son faible potentiel d'oxydation et sa géométrie à trois dimensions. Son oxydation produit un changement de conformation en passant d'une structure en 'selle de cheval' où le coté donneur et le coté aromatique sont clairement différents, à une conformation plane de symétrie D_{2h}, où l'aromaticité s'étend tout au long de la molécule et les anneaux 1,3-dithiol sont orthogonaux à l'entretoise (Figure 4).[92]

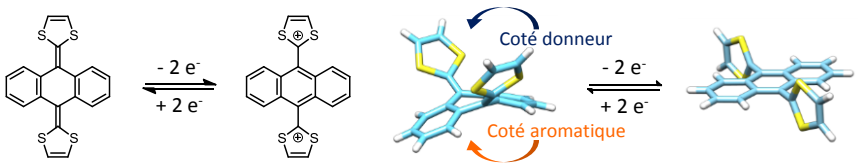

Figure 4. L'oxydation de exTTF produit un changement important de sa conformation.

Le C_{60} (Figure 5) a été utilisé en raison de sa structure tridimensionnelle, son faible potentiel de réduction, son absorption UV-vis dans une large gamme et sa faible énergie de réorganisation dans les réactions de transfert d'électrons.

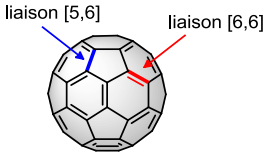

Figure 5. Structure moléculaire du C_{60}.

Malgré une vaste littérature disponible sur les conjugués covalents associant fullerènes et porphyrines ou exTTFs, la préparation d'analogues supramoléculaires a été beaucoup moins explorée en raison des difficultés à obtenir des complexes stables en solution. Les interactions généralement utilisées pour leur assemblage non-covalent sont le π-π stacking, la complémentarité cation ammonium-éther couronne, les interactions acide-base de Lewis, et finalement les liaisons mécaniques. Utilisées individuellement, ces interactions conduisent généralement à des complexes de faibles stabilités. Cependant, la combinaison de plusieurs d'entre elles peut permettre d'obtenir des complexes très stables.

Lors de cette étude, nous avons combiné différentes interactions pour obtenir une nouvelle série des complexes supramoléculaires donneur-accepteur. Dans tous les cas, nos systèmes utilisent un éther-couronne.

Objectifs et résultats

Effet des métaux sur la constante d'association entre porphyrines métalliques et le C_{60}

Tout d'abord, nous nous sommes intéressés à mieux comprendre les interactions π-π entre les porphyrines et les fullerènes. La nature de cette attraction reste controversée, car elle semble provenir d'un transfert électronique du fullerène à la porphyrine. Cette conclusion contre-intuitive peut être rationalisée si l'on considère le fullerène au niveau de sa double liaison plutôt que dans sa globalité.[59]

Ainsi, nous avons construit une nouvelle série de dyades supramoléculaires où le C_{60} et les porphyrines ont été assemblés grâce à des interactions π-π et cation ammonium-éther couronne (Figure 6). La complémentarité optimale de ces interactions à été démontrée dans une étude précédente dans notre laboratoire à Strasbourg où elles ont augmenté la stabilité du complexe de 2 ordres de grandeur.[86]

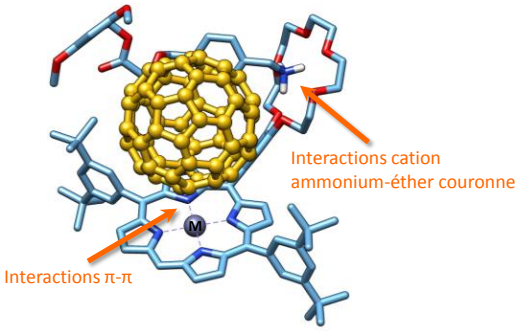

Figure 6. Structure des nouveaux complexes supramoléculaires. M = 2H, Co, Ni, Cu, Zn.

Dans cette série, le métal de la porphyrine a été systématiquement changé afin de modifier leur environnement. En raison de l'origine électrostatique des interactions π-π cette modification devrait avoir un clair impact sur la stabilité des complexes.

Les porphyrines **12-M** (M = 2H, Co, Ni, Cu, Zn) ont été obtenues par un couplage de Suzuki-Miyaura avec le dérivé **9**, qui à son tour a été obtenu par iodation régiosélective de la molécule **8**, résultant elle-même de la condensation entre le dipyrrométhane **3** et l'aldéhyde **6** (Schéma 2).

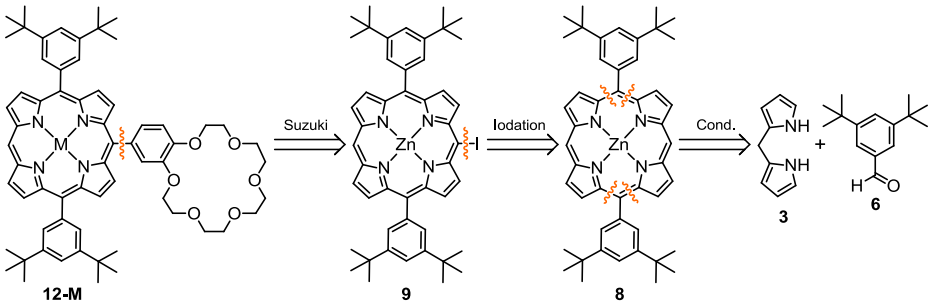

Schéma 2. Analyse rétrosynthétique des porphyrines **12-M**.

La molécule **22** a été obtenue par une cycloaddition de Bingel de **20** sur le C_{60}. Ce malonate asymétrique a été obtenu par une réaction d'estérification entre la molécule **19** et dérivé de l'alcool **17** (Schéma 3).

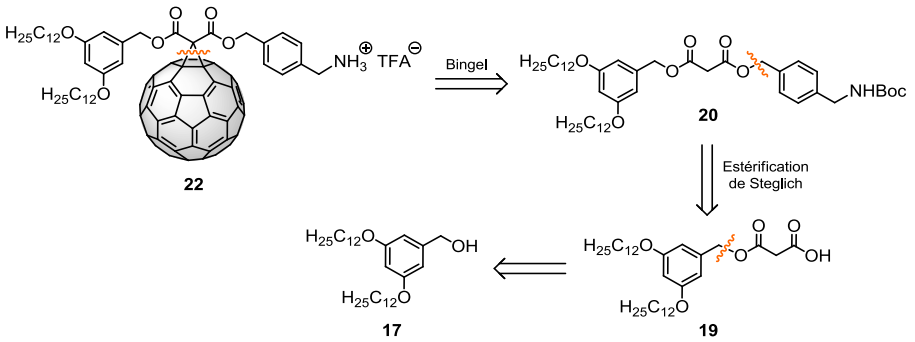

Schéma 3. Analyse rétrosynthétique du methanofullerène **22**.

Les études de complexation conduisant aux ensembles supramoléculaires **[12-M·21]** ont été réalisées par spectrophotométrie en réalisant un ajout dosé de **21** à une solution des porphyrines **12-M** (Schéma 4).

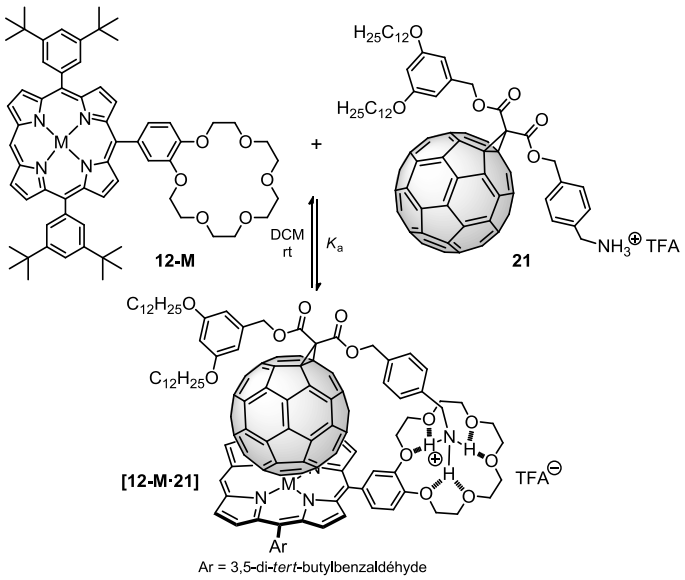

Schéma 4. Formation des complexes supramoléculaires **[12-M·21]** à partir de leurs unités.

Le traitement des données des différentes titrations par le logiciel d'analyse Specfit a permis d'obtenir les différentes valeurs de K_a pour la formation de **[12-M·21]**, les valeurs sont résumées dans le Tableau 1.

Tableau 1. Constantes d'association des systèmes **[12-M·21]**.

Complex	log K_a ± 3σ
[12-2H·21]	5.5 ± 0.2
[12-Co·21]	6.3 ± 0.2
[12-Ni·21]	5.9 ± 0.1
[12-Cu·21]	6.3 ± 0.3
[12-Zn·21]	6.9 ± 0.2

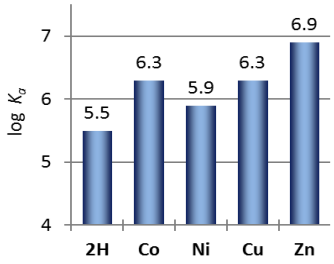

Les constantes d'association obtenues sont très élevées, montrant la bonne complémentarité entre les interactions π-π et cation ammonium-éther couronne ainsi que l'influence de la coopérativité chélate.

Notamment, les valeurs de K_a obtenues pour **[12-Zn·21]** et **[12-2H·21]** sont très différentes de celles précédemment décrites dans la littérature, où les récepteurs à base de porphyrines bases libres ont systématiquement une affinité pour le C_{60} similaire à leurs homologues de Zn(II).[61a],[62],[63b]

Cependant, les valeurs obtenues dans notre série sont en corrélation avec celles attendues pour une dyade porphyrine·C_{60} interagissant par des forces de van der Waals, où K_a augmente lorsque la densité électronique de la porphyrine augmente. L'exception à cette «règle» est la grande stabilité de **[12-Co·21]**, attribuable aux fortes interactions entre les fullerènes et les métaux du groupe 9 (Co, Rh, Ir).[63b]

Il est également important de noter que les travaux précédents utilisaient du C_{60} non fonctionnalisé, dont la faible solubilité limite le choix des solvants utilisables. En fait, il a été suggéré que la désolvatation du C_{60} représente la contribution majeure à l'énergie libre de complexation en solution.[62] L'utilisation du methanofullerène **21** a élégamment évité ces limitations, tout en conservant presque intactes les propriétés originelles du fullerène.

Propriétés supramoléculaires des dimères de porphyrine

Inspirés par les résultats des systèmes précédents, nous avons décidé d'augmenter la complexité du système afin d'obtenir des dimères *méso-méso* et *méso-méso*, *β-β*, *β'-β'*. Les propriétés supramoléculaires de ces dimères, largement inexplorés, ont été étudiées en utilisant le méthanofullerène **21**.

Malgré la grande complexité des dimères **23** et **24**, leur grande symétrie nous a permis de les obtenir aisément par une voie de synthèse divergente en partant de la porphyrine **Zn-12** comme présenté dans le Schéma 5.

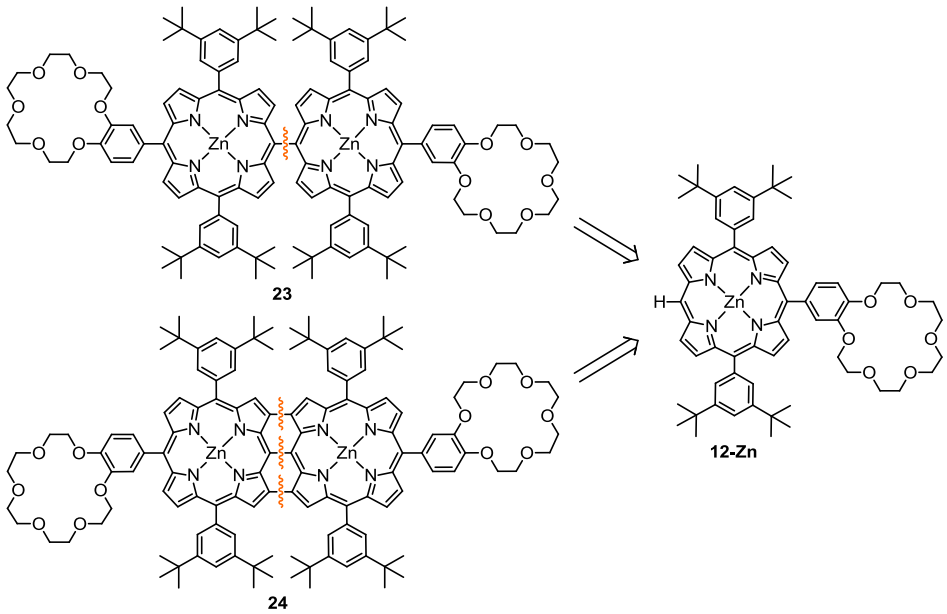

Schéma 5. Analyse rétrosynthétique des dimères **23** et **24**.

Les études de complexation de **[23·21]** et de **[23·21$_2$]** ont été réalisées par spectrophotométrie en effectuant un ajout dosé de **21** à une solution de porphyrine **23** à température ambiante dans du DCM (Schéma 6).

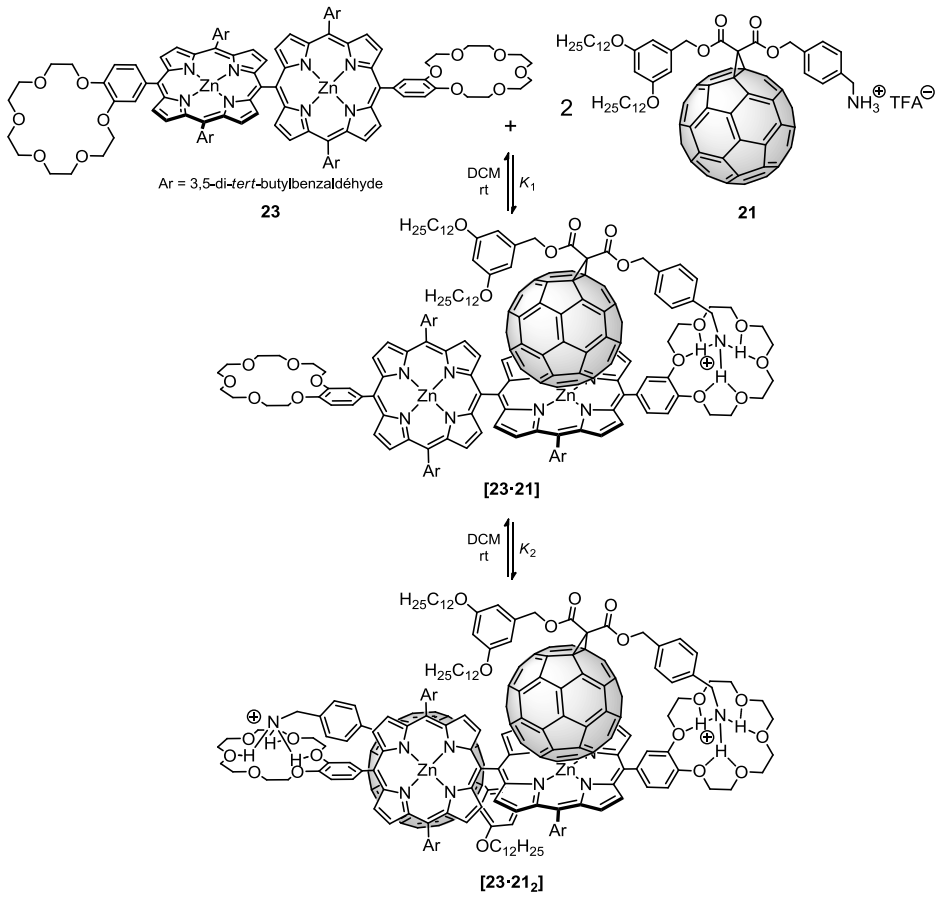

Schéma 6. Complexes supramoléculaires obtenus à partir de **23** et **21**.

Le traitement des données expérimentales a été fait pour un système 1:2, permettant ainsi d'obtenir les valeurs de K_a résumées dans le Tableau 2.

Tableau 2. Constantes d'association obtenues pour **[23·21$_2$]**.

log K_a ± 3σ	
log K_1	8.7 ± 1.4
log K_2	5.4 ± 0.9

Contrairement aux attentes, la constante d'association obtenue pour K_1 est beaucoup plus grande que celle obtenue dans le cas de la monoporphyrine (log K_1=8.7 *vs.* logK_a=6.9). La modélisation du système a mis en évidence l'existence d'une faible

distance entre le fullerène et les deux sous-unités porphyriniques (Figure 7), ce qui suggère l'existence d'une interaction supplémentaire avec la porphyrine voisine. Ce motif de reconnaissance supplémentaire peut donc être une explication plausible des résultats expérimentaux.

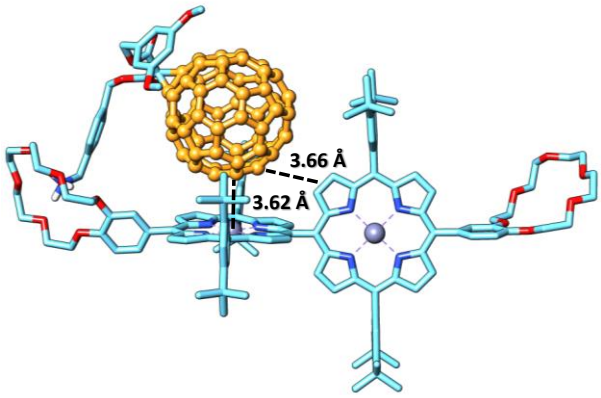

Figure 7. Modélisation Spartan de **[23·21]** (méthode semi-empirique PM3, les chaînes dodécyle ont été remplacées par des groupes méthyle pour faciliter les calculs) suggérant l'existence d'interactions porphyrine-fullerène avec les deux sous-unités porphyriniques.

En outre, la forme de l'isotherme de liaison de ce système ne correspond pas à celle d'une hyperbole, suggérant également l'existence d'effets coopératifs (voir Annexe II).

Le coefficient de coopérativité α démontre clairement l'existence d'une coopérativité négative.

$$\alpha = \frac{K_1 K_2}{K^2} = \frac{K_2}{K_1} = \frac{10^{5.4}}{10^{8.7}} = 0.0005 \qquad \textbf{(I)}$$

Ce résultat peut être expliqué en considérant la communication électronique entre les deux porphyrines, en accord avec les résultats du système décrit par Aida.[89] Ainsi, la complexation de **21** par la porphyrine produit une diminution de la densité électronique sur l'ensemble du dimère, diminuant ainsi l'affinité pour l'association du second fullerène.

La complexation de **24** par **21** a également été étudiée par titrages photométriques (Schéma 7).

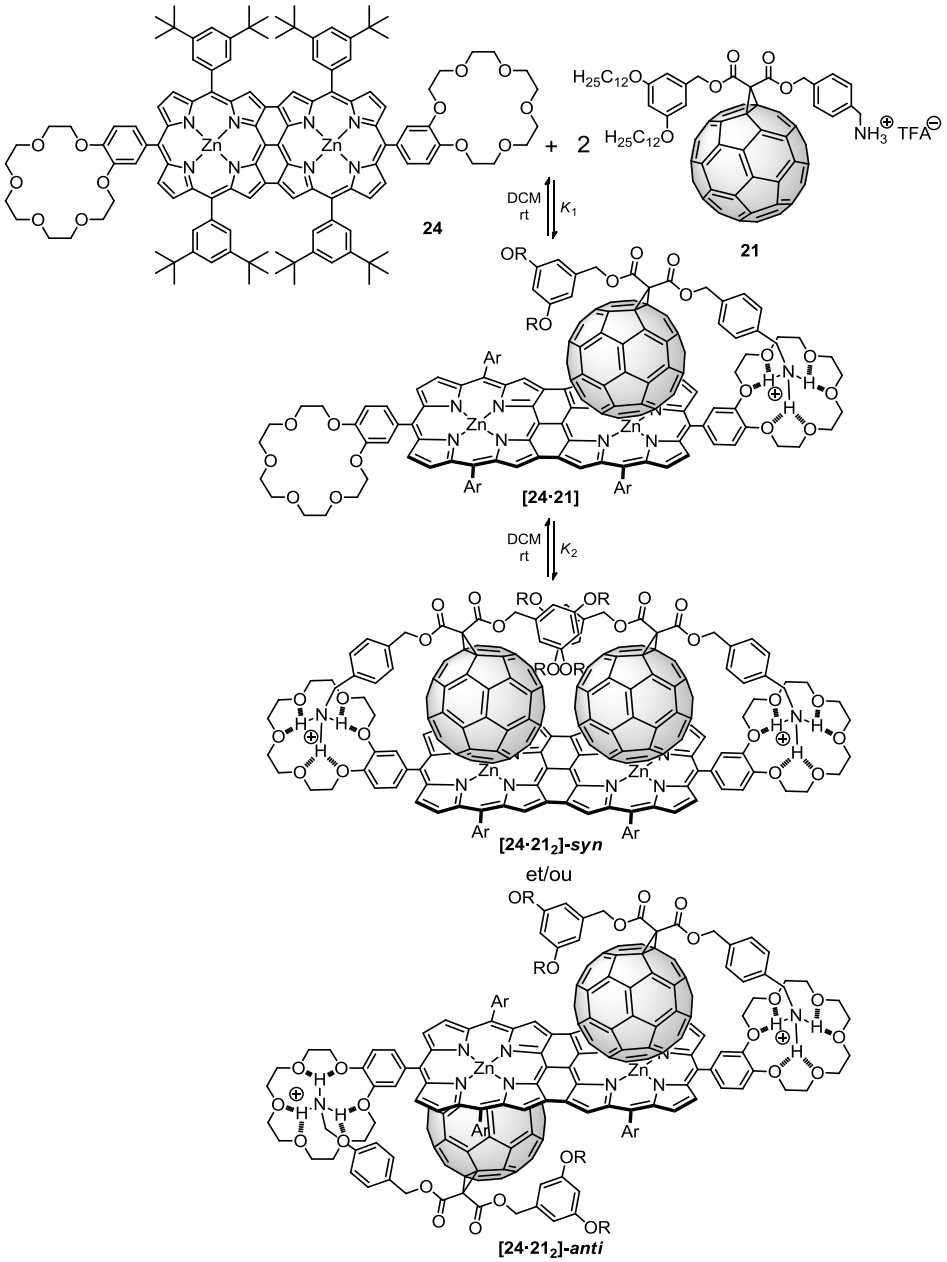

Schéma 7. Complexes supramoléculaires obtenus à partir de **24** et **21**.

Le traitement des données expérimentales pour un système 1:2 a permis d'obtenir les valeurs de constantes d'associations montrées dans le Tableau 3.

Tableau 3. Constantes d'association pour la formation de **[24·21$_2$]**.

log K_a ± 3σ	
log K_1	6.8 ± 0.5
log K_2	5.4 ± 0.3

Le calcul du facteur de coopérativité allostérique, α, par **(II)** montre une coopérativité négative du système, probablement causée par un mécanisme analogue à celui vu précédemment, dans lequel la complexation d'une unité fullerène abaisse la densité électronique du dimère entier. De manière inattendue, la valeur de α obtenue est beaucoup plus élevée que celle de **[23.21$_2$]**.

$$\alpha = \frac{K_2}{K_1} = \frac{10^{5.4}}{10^{6.8}} = 0.04 \qquad \textbf{(II)}$$

Comme illustré dans le Schéma 7, la combinaison d'un équivalent de **24** et de deux équivalents de **21** conduit à deux diastéréoisomères différents, **[24·21$_2$]-*syn*** et **[24·21$_2$]-*anti***. Bien qu'en principe il n'est pas possible de déterminer lequel est favorisé en solution, la modélisation de **[24·21$_2$]-*syn*** (Figure 8) montre la possibilité d'avoir des interactions π-π supplémentaires entre les deux fullerènes alors que cela est impossible pour **[24·21$_2$]-*anti.*** La présence de cette interaction supplémentaire peut donc expliquer la valeur plus grande de α dans **[24·21$_2$]**, suggérant ainsi que la conformation *syn* est celle préférée en solution.

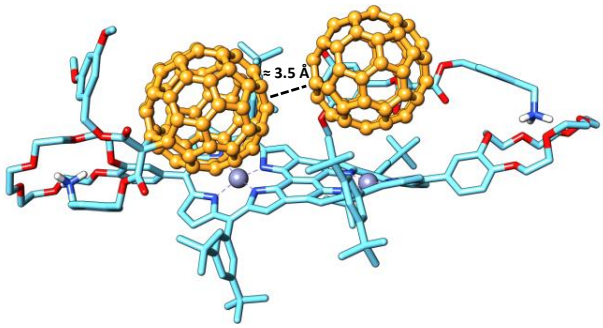

Figure 8. Modélisation Spartan de **[24·21$_2$]-syn** (méthode semi-empirique PM3, les chaînes dodécyle ont été remplacées par des groupes méthyle pour faciliter les calculs).

Nature des interactions entre les éthers couronne et le C_{60}

Dans ce chapitre, nous avons étudié la nature des interactions fullerène-éther couronne en poursuivant des travaux initiés à Madrid dans lesquels un conjugué exTTF-éther couronne présentait une très forte affinité pour le C_{60}.[103]

Bien que provenant en principe des interactions n-π ou CH-π, la nature précise de la stabilité supplémentaire conférée par les éthers couronnes reste une question ouverte. En conséquence, nous avons synthétisé une nouvelle série de dérivés d'exTTF contenant des éther couronnes avec deux objectifs : étudier l'effet de la modification de la taille du macrocycle et/ou de l'introduction d'un atome d'azote dans le cycle sur l'affinité pour le C_{60}.

Les récepteurs ont été obtenus par une voie de synthèse impliquant l'estérification d'un acide carboxylique et le 2,6-dihydroxy-exTTF **33,** lui-même obtenu par une réaction de Horner-Wadsworth-Emmons sur la quinone **30** (Schéma 8).

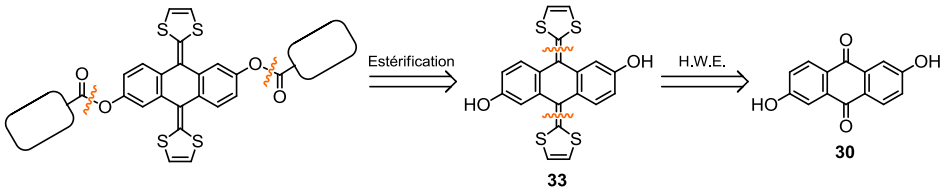

Schéma 8. Analyse rétrosynthétique des récepteurs de exTTF.

Alors que les récepteurs **56**, **57** et **60** ont été préparés à partir d'acides carboxyliques commerciaux, des autres dérivés ont dû être synthétisées.

Ainsi, le composé **41** a été obtenu à partir du catéchol **36** par deux *O*-alkylations successives *via* l'intermédiaire **38** (Schéma 9).

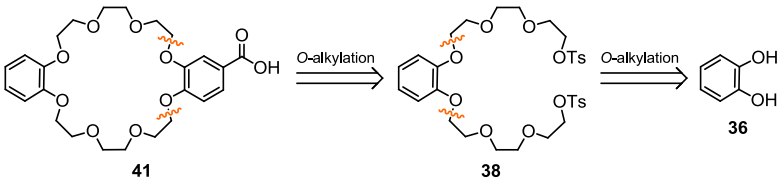

Schéma 9. Analyse rétrosynthétique de l'acide carboxylique **41**.

La synthèse du aza-éther couronne **47** a été réalisée à l'aide d'une *N*-alkylation du composé **42** suivie d'une *O*-alkylation de l'intermédiaire **44** (Schéma 10).

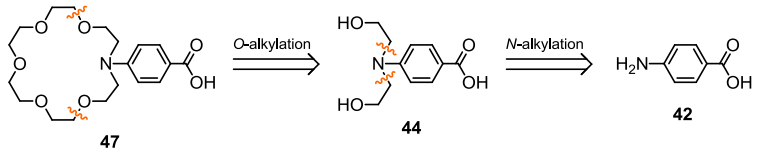

Schéma 10. Analyse rétrosynthétique de l'acide carboxylique **47**.

Enfin, l'aza-éther couronne **51** a été obtenue à partir de la molécule **49** par un couplage de Hartwig-Buchwald (Schéma 11).

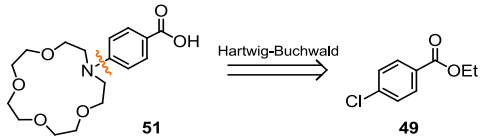

Schéma 11. Analyse rétrosynthétique de l'acide carboxylique **51**.

Les études de complexation ont été réalisées par spectrophotométrie en effectuant des ajouts dosés de C_{60} à des solutions des dérivés exTTF (Schéma 12).

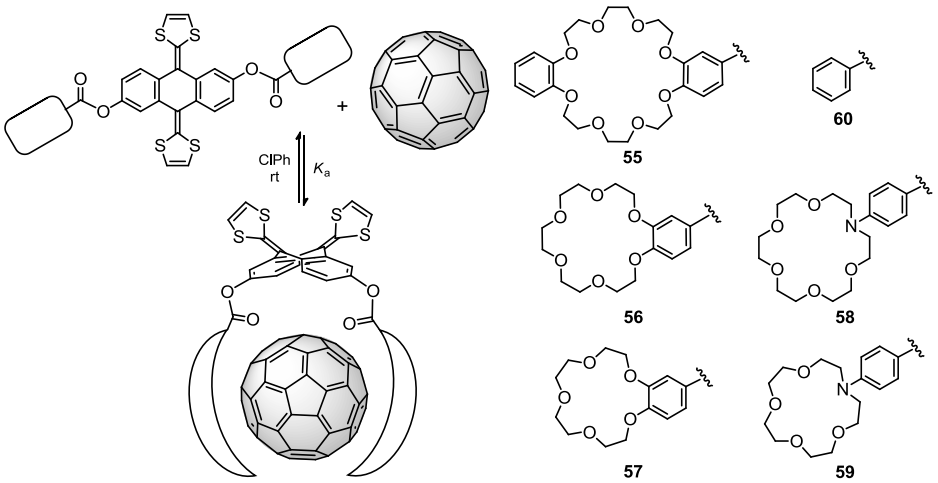

Schéma 12. Complexes dérivés des pinces d'exTTF **55**, **56**, **57**, **58**, **59** et **60**.

Le traitement des données expérimentales a permis d'obtenir les valeurs des constantes d'associations résumées dans le Tableau 4.

Tableau 4. Constantes d'association des pinces exTTF.

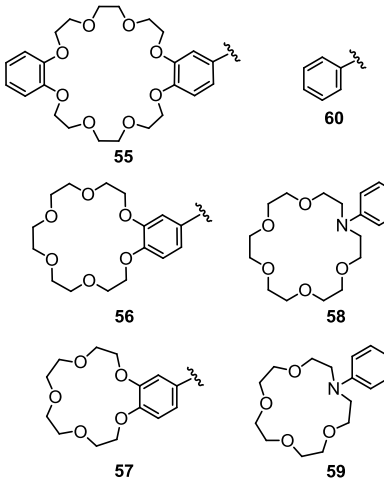

Récepteur	log K_a ± 3σ
55	> 7
56*	6.7 ± 0.2
57	4.1 ± 0.1
60	3.3 ± 0.4
58	5.1 ± 0.3
59	3.4 ± 0.3

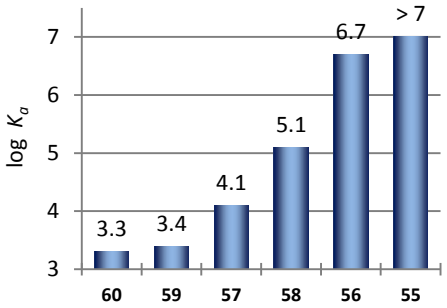

* Résultats publiés précédemment.[103]

La nature et la taille de l'éther couronne ont un effet évident sur l'affinité pour le [60]fullerène, entraînant des changements dans les constantes d'association de plus de 3 ordres de grandeur. Les aza-éther couronnes ont montré une affinité légèrement inférieure alors que les valeurs de K_a augmentent avec l'augmentation de la taille des macrocycles.

L'interaction donneur-accepteur dans l'état fondamental entre la partie exTTF et le C_{60} a été démontrée par des études électrochimiques. Néanmoins une corrélation directe entre les constantes d'association et les propriétés électrochimiques des complexes n'a pu être obtenue, suggérant de fait l'existence d'autres interactions.

L'étude des paramètres géométriques des complexes modélisés (niveau DFT) a confirmé que l'affinité envers le C_{60} résulte d'une combinaison d'interactions CH-π, n-π et π-π (Tableau 5). Les principaux paramètres semblent être les interactions CH-π et n-π des éthers couronnes, car plus elles sont nombreuses et plus l'énergie de liaison augmente. Dans le même temps, l'énergie de liaison des interactions π-π et n-π du TTF ou des cycles aromatiques périphériques restent dans la même gamme dans tous les cas. Cependant, ces dernières jouent aussi un rôle important comme en témoigne le système **[60·C_{60}]**.

Tableau 5. Paramètres géométriques des complexes obtenus à partir des pinces d'exTTF.

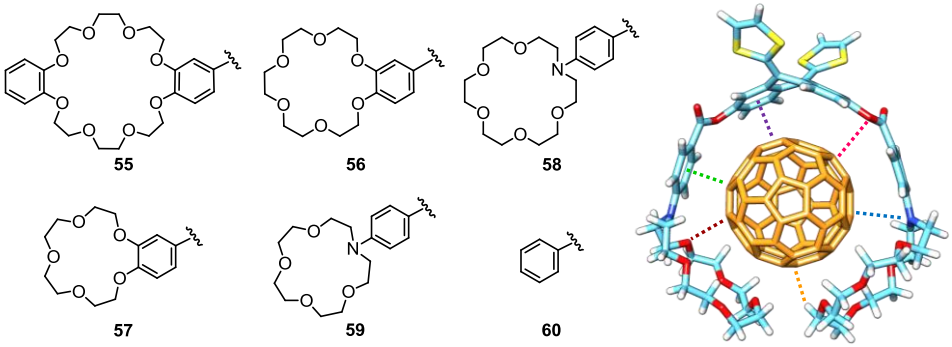

Host	nº H-C (< 3.20 Å)	nº O-C (< 3.80 Å)	bz-C (Å)	bz-bz (Å)	O-C (Å)	N-C (Å)	E_a (kcal/mol)	log K_a ± 3σ (rt, ClPh, UV)
55	12	10	2.96*	3.36*	3.37*	—	-54.36	> 7
56	10	12	2.95	3.45	3.42	—	-44.76	6.7 ± 0.2
58	10	10	3.06	3.37	3.14	3.50	-43.33	5.1 ± 0.3
57	8	8	2.99	3.46	3.30	—	-39.69	4.1 ± 0.1
59	10	4	3.41	3.37	3.25	4.14	-36.77	3.4 ± 0.3
60	—	—	3.25	3.45	3.16	—	-22.85	3.3 ± 0.4
exTTF	—	—	—	3.42	—	—	-10.24	—

* Structure asymétrique. Les 2èmes distances bz-C, bz-bz et O-C sont 2.99, 3.60 et 3.52 Å, respectivement.

Conception et synthèse de nouveaux clips moléculaires (exTTF)$_2$-éther couronne.

Toujours intéressés par l'influence des éthers couronnes sur la reconnaissance du C_{60}, nous avons développé deux nouveaux récepteurs de type (exTTF)$_2$-éther couronne. La voie de synthèse suivie pour les récepteurs **75** et **76** est fondée sur l'estérification du dérivé d'exTTF correspondant avec l'acide carboxylique **74**, lui même obtenu à partir du catéchol **69** par deux réactions d'*O*-alkylation successives (Schéma 13).

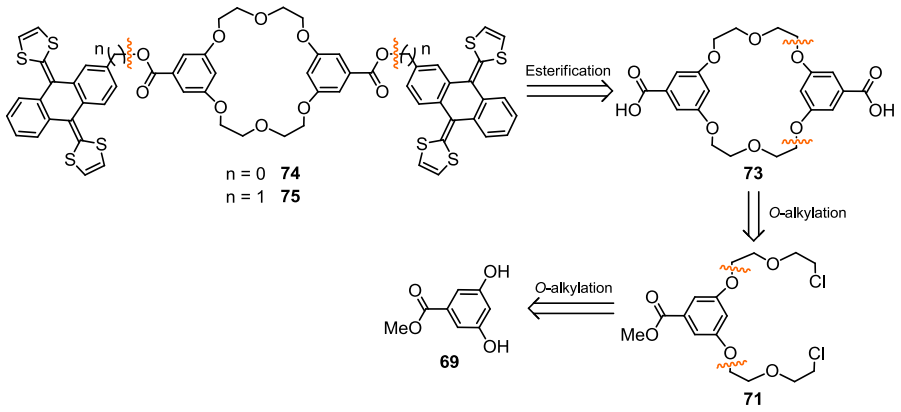

Schéma 13. Analyse rétrosynthétique des récepteurs **74** et **75**.

L'étape clé pour la synthèse des exTTF **64** et **68** est une réaction de Horner-Wadsworth-Emmons sur les alcools **61** et **65** (Schéma 14).

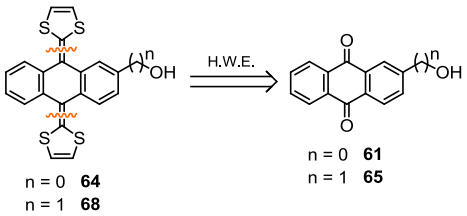

Schéma 14. Analyse rétrosynthétique des composés exTTF **64** et **68**.

Les études de complexation ont été faites par spectroscopie UV-vis (Schéma 15).

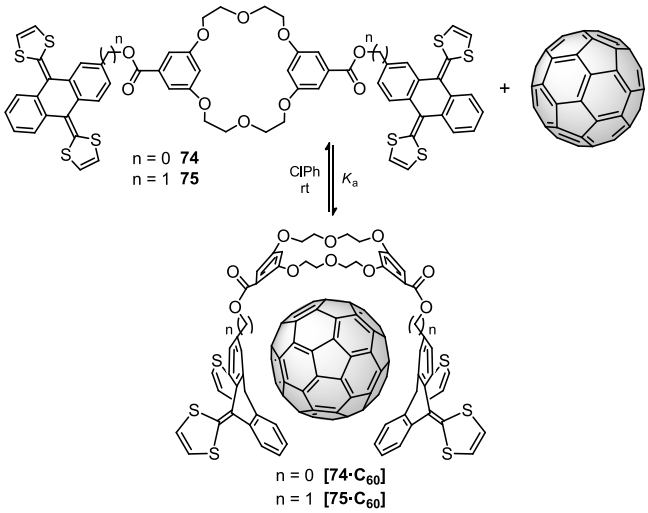

Schéma 15. Complexes supramoléculaires obtenus à partir de **74**, **75** et C_{60}.

Les résultats des études de complexation ont sont résumés dans le Tableau 6.

Tableau 6. Constantes d'association des pinces $(exTTF)_2$-éther couronne.

Complexe	log K_a ± 3σ
[74·C_{60}]	5.0 ± 0.4
[75·C_{60}]	6.5 ± 0.6

Malgré l'omniprésence du «principe de préorganisation»,[122] l'utilisation du récepteur **74**, plus rigide que **75** a conduit a l'obtention d'un complexe avec une constante de stabilité plus faible, prouvant ainsi qu'une augmentation de la préorganisation du système ne conduit pas forcément à des affinités plus élevées, car celle-ci n'amène pas forcément une bonne complémentarité entre le récepteur et le substrat

Il faut également noter que la constante de formation **[75·C_{60}]** est du même ordre de grandeur que celle obtenue pour son complexe exTTF-(éther couronne)$_2$ analogue **[56·C_{60}]**. Cela démontre l'énorme potentiel des éthers couronnes comme éléments de reconnaissance pour les fullerènes.

Conclusions

Les travaux développés dans cette étude ont fourni des informations précieuses sur le rôle clé des éthers couronnes en chimie supramoléculaire des fullerènes.

Notamment, nous avons obtenu une meilleure compréhension de la nature de deux interactions supramoléculaires peu connus jusque-là: les interactions π-π entre C_{60} et porphyrines et l'affinité des éthers couronnes vis-à-vis des fullerenes.

Nous avons également étudié les propriétés supramoléculaires de dyades porphyriniques en grande partie inconnus jusqu'à présent.

Tous ces résultats apportent une base importante pour l'ingénierie moléculaire de nouveaux récepteurs supramoléculaires des fullerènes.

Bibliography

[1] Greenpeace, EPIA, "Solar Generation. The global solar photovoltaic outlook.", **2010**.

[2] a) J.-M. Lehn, *Supramolecular Chemistry. Concepts and Perspectives*, Wiley-VCH, Weinheim, **1995**; b) P. D. Beer, P. A. Gale, D. K. Smith, *Supramolecular Chemistry*, Oxford University Press, Oxford, **1999**; c) J. W. Steed, J. L. Atwood, *Supramolecular Chemistry*, 2nd ed., John Wiley & Sons, Wiltshire, **2009**; d) *Comprehensive Supramolecular Chemistry, Vol. 1-11*, (Ed. J.-M. Lehn, J. L. Atwood, J. E. D. Davies, D. D. Macnicol, F. Vögtle), Pergamon/Elsevier, Oxford, **1996**; e) *Supramolecular Chemistry of Fullerenes and Carbon Nanotubes*, (Ed. N. Martín, J.-F. Nierengarten), Wiley-VCH, Weinheim, **2012**; f) *Supramolecular Chemistry: From Molecules to Nanomaterials*, (Ed. J. W. Steed, P. A. Gale), John Wiley & Sons, **2012**; g) *Analytical Methods in Supramolecular Chemistry*, 2nd ed., (Ed. C. A. Schalley), Wiley-VCH, Weinheim, **2012**.

[3] J.-M. Lehn, "Supramolecular Chemistry—Scope and Perspectives Molecules, Supermolecules, and Molecular Devices (Nobel Lecture)", *Angew. Chem. Int. Ed.*, **1988**, *27*, 89.

[4] A. Werner, "Beitrag zur Konstitution anorganischer Verbindungen", *Z. anorg. Chem.*, **1893**, *3*, 267.

[5] E. Fischer, "Einfluss der Configuration auf die Wirkung der Enzyme", *Ber. Deutsch. Chem. Ges.*, **1894**, *27*, 2985.

[6] P. Ehrlich, C. B. Bolduan, *Collected Studies on Immunity*, Wiley, **1906**.

[7] C. J. Pedersen, "Cyclic polyethers and their complexes with metal salts", *J. Am. Chem. Soc.*, **1967**, *89*, 7017.

[8] B. Dietrich, J. M. Lehn, J. P. Sauvage, "Diaza-polyoxa-macrocycles et macrobicycles", *Tetrahedron Lett.*, **1969**, *10*, 2885.

[9] D. J. Cram, T. Kaneda, R. C. Helgeson, G. M. Lein, "Spherands - ligands whose binding of cations relieves enforced electron-electron repulsions", *J. Am. Chem. Soc.*, **1979**, *101*, 6752.

[10] C. O. Dietrich-Buchecker, J.-P. Sauvage, "A Synthetic Molecular Trefoil Knot", *Angew. Chem. Int. Ed.*, **1989**, *28*, 189.

[11] K. S. Chichak, S. J. Cantrill, A. R. Pease, S.-H. Chiu, G. W. V. Cave, J. L. Atwood, J. F. Stoddart, "Molecular Borromean Rings", *Science*, **2004**, *304*, 1308.

[12] M. Fujita, D. Oguro, M. Miyazawa, H. Oka, K. Yamaguchi, K. Ogura, "Self-assembly of ten molecules into nanometre-sized organic host frameworks", *Nature*, **1995**, *378*, 469.

[13] B. Olenyuk, J. A. Whiteford, A. Fechtenkotter, P. J. Stang, "Self-assembly of nanoscale cuboctahedra by coordination chemistry", *Nature*, **1999**, *398*, 796.

[14] E. V. Anslyn, D. A. Dougherty, *Modern Physical Organic Chemistry*, Univ. Science Books, **2006**.

[15] a) P. Metrangolo, H. Neukirch, T. Pilati, G. Resnati, "Halogen Bonding Based Recognition Processes: A World Parallel to Hydrogen Bonding", *Acc. Chem. Res.*, **2005**, *38*, 386; b) P. Metrangolo, F. Meyer, T. Pilati, G. Resnati, G. Terraneo, "Halogen Bonding in Supramolecular Chemistry", *Angew. Chem. Int. Ed.*, **2008**, *47*, 6114.

[16] R. G. Pearson, "Hard and Soft Acids and Bases", *J. Am. Chem. Soc.*, **1963**, *85*, 3533.
[17] a) O. Takahashi, Y. Kohno, M. Nishio, "Relevance of Weak Hydrogen Bonds in the Conformation of Organic Compounds and Bioconjugates: Evidence from Recent Experimental Data and High-Level ab Initio MO Calculations", *Chem. Rev.*, **2010**, *110*, 6049; b) T. Steiner, "The Hydrogen Bond in the Solid State", *Angew. Chem. Int. Ed.*, **2002**, *41*, 48.
[18] L. M. Salonen, M. Ellermann, F. Diederich, "Aromatic Rings in Chemical and Biological Recognition: Energetics and Structures", *Angew. Chem. Int. Ed.*, **2011**, *50*, 4808.
[19] A. S. Mahadevi, G. N. Sastry, "Cation−π Interaction: Its Role and Relevance in Chemistry, Biology, and Material Science", *Chem. Rev.*, **2012**, *113*, 2100.
[20] D.-X. Wang, M.-X. Wang, "Anion−π Interactions: Generality, Binding Strength, and Structure", *J. Am. Chem. Soc.*, **2012**, *135*, 892.
[21] C. A. Hunter, K. R. Lawson, J. Perkins, C. J. Urch, "Aromatic interactions", *J. Chem. Soc., Perkin Trans. 2*, **2001**, 651.
[22] G. J. Bartlett, A. Choudhary, R. T. Raines, D. N. Woolfson, "n→π* interactions in proteins", *Nat. Chem. Biol.*, **2010**, *6*, 615.
[23] I. Dance, "What is supramolecular?", *New J. Chem.*, **2003**, *27*, 1.
[24] a) J. F. Stoddart, "The chemistry of the mechanical bond", *Chem. Soc. Rev.*, **2009**, *38*, 1802; b) C. Bruns, J. F. Stoddart, "The Mechanical Bond: A Work of Art" in *Beauty in Chemistry*, *Vol. 323* (Ed.: L. Fabbrizzi), Springer Berlin Heidelberg, **2012**, pp. 19.
[25] a) K. A. Jolliffe, S. J. Langford, M. G. Ranasinghe, M. J. Shephard, M. N. Paddon-Row, "Design and Synthesis of Two (Pseudo)symmetric Giant Trichromophoric Systems Containing the C_{60} Chromophore", *J. Org. Chem.*, **1999**, *64*, 1238; b) J.-P. Sauvage, http://www-chimie.u-strasbg.fr/~lcom/Recherche/transfert1.html
[26] H. W. Kroto, J. R. Heath, S. C. O'Brien, R. F. Curl, R. E. Smalley, "C_{60}: Buckminsterfullerene", *Nature*, **1985**, *318*, 162.
[27] a) *Fullerenes. Chemistry and reactions.*, (Ed. A. Hirsch, M. Brettreich), Wiley-VCH, **2005**; b) D. M. Guldi, N. Martin, *Fullerenes: From Synthesis to Optoelectronic Properties*, Springer, **2002**.
[28] a) Q. Xie, E. Pérez-Cordero, L. Echegoyen, "Electrochemical detection of C_{60}^{6-} and C_{70}^{6-}: Enhanced stability of fullerides in solution", *J. Am. Chem. Soc.*, **1992**, *114*, 3978; b) N. Martín, L. Sánchez, B. Illescas, I. Pérez, "C60-Based Electroactive Organofullerenes", *Chem. Rev.*, **1998**, *98*, 2527.
[29] H. Ajie, M. M. Alvarez, S. J. Anz, R. D. Beck, F. Diederich, K. Fostiropoulos, D. R. Huffman, W. Kraetschmer, Y. Rubin, K. E. Schriver, D. Sensharma, R. L. Whetten, "Characterization of the soluble all-carbon molecules C_{60} and C_{70}", *J. Phys. Chem.*, **1990**, *94*, 8630.
[30] I. Hiroshi, H. Kiyoshi, A. Tsuyoshi, A. Masanori, T. Seiji, O. Tadashi, S. Masahiro, S. Yoshiteru, "The small reorganization energy of C_{60} in electron transfer", *Chem. Phys. Lett.*, **1996**, *263*, 545.
[31] C. Pedersen, "The discovery of crown ethers", *J. Inclusion Phenom.*, **1988**, *6*, 337.

[32] a) E. Weber, F. Vögtle, "Classification and nomenclature of coronands, cryptands, podands, and of their complexes", *Inorg. Chim. Acta*, **1980**, *45*, L65; b) D. J. Cram, "Preorganization—From Solvents to Spherands", *Angew. Chem. Int. Ed.*, **1986**, *25*, 1039.

[33] E. Weber, F. Vögtle, "Crown-type compounds — An introductory overview" in *Host Guest Complex Chemistry I*, *Vol. 98*, Springer, **1981**, pp. 1.

[34] J. Effing, U. Jonas, L. Jullien, T. Plesnivy, H. Ringsdorf, F. Diederich, C. Thilgen, D. Weinstein, "C_{60} and C_{70} in a Basket? – Investigations of Mono- and Multilayers from Azacrown Compounds and Fullerenes", *Angew. Chem. Int. Ed.*, **1992**, *31*, 1599.

[35] F. Lara, R. Cruz, M. Martínez, R. Martíneza, B. Villaneda, A. Ramírez, E. Moreno, I. Martínez, E. Angeles, "A Novel Crown Ether. $2C_{60}$ Complex", *Supramol. Chem.*, **1999**, *10*, 185.

[36] a) S. Bhattacharya, A. Sharma, S. K. Nayak, S. Chattopadhyay, A. K. Mukherjee, "NMR Study of Complexation of Crown Ethers with [60]- and [70]Fullerenes", *J. Phys. Chem. B*, **2003**, *107*, 4213; b) A. Saha, S. K. Nayak, S. Chottopadhyay, A. K. Mukherjee, "Spectrophotometric Study of Complexation of Dicyclohexano-24-crown-8 with [60]- and [70]Fullerenes and Other Acceptors", *J. Phys. Chem. B*, **2003**, *107*, 11889.

[37] Y. Yamaguchi, Z.-I. Yoshida, "Shape-persistency and Molecular Function in Heteromacrocycles: Creation of Heteroarenecyclynes and Arene–Azaarenecyclynes", *Chem. Eur. J.*, **2003**, *9*, 5430.

[38] Y. Liu, J.-R. Han, Y.-L. Zhao, H.-Y. Zhang, Z.-Y. Duan, "Synthesis of Some Selenacrown Ethers and the Thermodynamic Origin of Their Complexation with C_{60}", *J. Inclusion Phenom. Macrocyclic Chem.*, **2005**, *51*, 191.

[39] J. L. Sessler, E. Karnas, E. Sedenberg, "Porphyrins and Expanded Porphyrins as Receptors" in *Supramol. Chem.* (Eds.: J. W. Steed, P. A. Gale), John Wiley & Sons, Ltd, **2012**.

[40] a) S. I. Yang, J. Seth, J.-P. Strachan, S. Gentemann, D. Kim, D. Holten, J. S. Lindsey, D. F. Bocian, "Ground and excited state electronic properties of halogenated tetraarylporphyrins. Tuning the building blocks for porphyrin-based photonic devices", *J. Porphyrins Phthalocyanines*, **1999**, *3*, 117; b) J. H. Fuhrhop, D. Mauzerall, "One-electron oxidation of metalloporphyrins", *J. Am. Chem. Soc.*, **1969**, *91*, 4174.

[41] a) S. Tobita, Y. Kaizu, H. Kobayashi, I. Tanaka, "Study of higher excited singlet states of zinc(II)-tetraphenylporphin", *J. Chem. Phys.*, **1984**, *81*, 2962; b) R. A. Reed, R. Purrello, K. Prendergast, T. G. Spiro, "Resonance Raman characterization of the radical anion and triplet states of zinc tetraphenylporphine", *J. Phys. Chem.*, **1991**, *95*, 9720; c) A. Harriman, G. Porter, N. Searle, "Reversible photo-oxidation of zinc tetraphenylporphine by benzo-1,4-quinone", *J. Chem. Soc., Faraday Trans. 2*, **1979**, *75*, 1515.

[42] A. D. Adler, F. R. Longo, J. D. Finarelli, J. Goldmacher, J. Assour, L. Korsakoff, "A simplified synthesis for meso-tetraphenylporphine", *J. Org. Chem.*, **1967**, *32*, 476.

[43] a) J. S. Lindsey, H. C. Hsu, I. C. Schreiman, "Synthesis of tetraphenylporphyrins under very mild conditions", *Tetrahedron Lett.*, **1986**, *27*, 4969; b) J. S. Lindsey, I. C. Schreiman, H. C. Hsu, P. C. Kearney, A. M. Marguerettaz, "Rothemund and Adler-Longo reactions revisited: synthesis of tetraphenylporphyrins under equilibrium conditions", *J. Org. Chem.*, **1987**, *52*, 827.

[44] P. D. Rao, S. Dhanalekshmi, B. J. Littler, J. S. Lindsey, "Rational Syntheses of Porphyrins Bearing up to Four Different Meso Substituents", *J. Org. Chem.*, **2000**, *65*, 7323.

[45] J. S. Lindsey, "Synthetic Routes to meso-Patterned Porphyrins", *Acc. Chem. Res.*, **2009**, *43*, 300.

[46] a) M. O. Senge, "Stirring the porphyrin alphabet soup-functionalization reactions for porphyrins", *Chem. Commun.*, **2011**, *47*, 1943; b) B. M. J. M. Suijkerbuijk, R. J. M. Klein Gebbink, "Merging Porphyrins with Organometallics: Synthesis and Applications", *Angew. Chem. Int. Ed.*, **2008**, *47*, 7396.

[47] a) A. Tsuda, A. Osuka, "Discrete conjugated porphyrin tapes with an exceptionally small bandgap", *Adv. Mater.*, **2002**, *14*, 75; b) A. Naoki, O. Atsuhiro, "Directly linked porphyrin arrays", *Chem. Rec.*, **2003**, *3*, 225.

[48] A. Osuka, H. Shimidzu, "*meso*, *meso*-Linked Porphyrin Arrays", *Angew. Chem. Int. Ed.*, **1997**, *36*, 135.

[49] T. Ogawa, Y. Nishimoto, N. Ono, N. Yoshida, A. Osuka, "One-pot electrochemical formation of *meso*,*meso*-linked porphyrin arrays", *Chem. Commun.*, **1998**, 337.

[50] a) X. Shi, L. S. Liebeskind, "3-Cyclobutenyl-1,2-dione-substituted Porphyrins. 2. A Simple and General Entry to Quinone−Porphyrin−Porphyrin−Quinone Tetrads and Related Molecules", *J. Org. Chem.*, **2000**, *65*, 1665; b) J. Wojaczyński, L. Latos-Grażyński, P. J. Chmielewski, P. Van Calcar, A. L. Balch, "^{1}H NMR Investigations of Triphenylporphyrin Metal Complexes and Electronic Interactions in Iron(III) Complexes of meso−meso-Linked 5,5'-Bis(10,15,20-triphenylporphyrin)", *Inorg. Chem.*, **1999**, *38*, 3040; c) L.-M. Jin, L. Chen, J.-J. Yin, C.-C. Guo, Q.-Y. Chen, "A Facile and Potent Synthesis of meso,meso-Linked Porphyrin Arrays Using Iodine(III) Reagents", *Eur. J. Org. Chem.*, **2005**, *2005*, 3994.

[51] T. Ogawa, Y. Nishimoto, N. Yoshida, N. Ono, A. Osuka, "Completely Regioselective Synthesis of Directly Linked *meso*,*meso* and *meso*,β Porphyrin Dimers by One-Pot Electrochemical Oxidation of Metalloporphyrins", *Angew. Chem. Int. Ed.*, **1999**, *38*, 176.

[52] Y. H. Kim, D. H. Jeong, D. Kim, S. C. Jeoung, H. S. Cho, S. K. Kim, N. Aratani, A. Osuka, "Photophysical Properties of Long Rodlike *Meso*−*Meso*-Linked Zinc(II) Porphyrins Investigated by Time-Resolved Laser Spectroscopic Methods", *J. Am. Chem. Soc.*, **2001**, *123*, 76.

[53] a) A. Tsuda, A. Osuka, "Fully Conjugated Porphyrin Tapes with Electronic Absorption Bands That Reach into Infrared", *Science*, **2001**, *293*, 79; b) S. Hiroto, A. Osuka, "*meso*-Alkyl-Substituted *meso*-*meso* Linked Diporphyrins and meso-Alkyl-Substituted *meso*-*meso*, β-β, β-β Triply Linked Diporphyrins", *J. Org. Chem.*, **2005**, *70*, 4054.

[54] Y. Sun, T. Drovetskaya, R. D. Bolskar, R. Bau, P. D. W. Boyd, C. A. Reed, "Fullerides of Pyrrolidine-Functionalized C_{60}", *J. Org. Chem.*, **1997**, *62*, 3642.

[55] D. R. Evans, N. L. P. Fackler, Z. Xie, C. E. F. Rickard, P. D. W. Boyd, C. A. Reed, "π-Arene/Cation Structure and Bonding. Solvation versus Ligand Binding in Iron(III) Tetraphenylporphyrin Complexes of Benzene, Toluene, p-Xylene, and [60]Fullerene", *J. Am. Chem. Soc.*, **1999**, *121*, 8466.

[56] M. M. Olmstead, D. A. Costa, K. Maitra, B. C. Noll, S. L. Phillips, P. M. Van Calcar, A. L. Balch, "Interaction of Curved and Flat Molecular Surfaces. The Structures of Crystalline Compounds Composed of Fullerene (C_{60}, $C_{60}O$, C_{70}, and $C_{120}O$) and Metal Octaethylporphyrin Units", *J. Am. Chem. Soc.*, **1999**, *121*, 7090.

[57] P. D. W. Boyd, M. C. Hodgson, C. E. F. Rickard, A. G. Oliver, L. Chaker, P. J. Brothers, R. D. Bolskar, F. S. Tham, C. A. Reed, "Selective Supramolecular Porphyrin/Fullerene Interactions", *J. Am. Chem. Soc.*, **1999**, *121*, 10487.

[58] E. M. Pérez, N. Martín, "Curves ahead: molecular receptors for fullerenes based on concave-convex complementarity", *Chem. Soc. Rev.*, **2008**, *37*, 1512.

[59] P. D. W. Boyd, C. A. Reed, "Fullerene−Porphyrin Constructs", *Acc. Chem. Res.*, **2004**, *38*, 235.

[60] M. Kimura, Y. Saito, K. Ohta, K. Hanabusa, H. Shirai, N. Kobayashi, "Self-Organization of Supramolecular Complex Composed of Rigid Dendritic Porphyrin and Fullerene", *J. Am. Chem. Soc.*, **2002**, *124*, 5274.

[61] a) D. Sun, F. S. Tham, C. A. Reed, L. Chaker, M. Burgess, P. D. W. Boyd, "Porphyrin−Fullerene Host−Guest Chemistry", *J. Am. Chem. Soc.*, **2000**, *122*, 10704; b) D. Sun, F. S. Tham, C. A. Reed, L. Chaker, P. D. W. Boyd, "Supramolecular Fullerene-Porphyrin Chemistry. Fullerene Complexation by Metalated "Jaws Porphyrin" Hosts", *J. Am. Chem. Soc.*, **2002**, *124*, 6604.

[62] A. Hosseini, S. Taylor, G. Accorsi, N. Armaroli, C. A. Reed, P. D. W. Boyd, "Calix[4]arene-Linked Bisporphyrin Hosts for Fullerenes: Binding Strength, Solvation Effects, and Porphyrin−Fullerene Charge Transfer Bands", *J. Am. Chem. Soc.*, **2006**, *128*, 15903.

[63] a) K. Tashiro, T. Aida, J.-Y. Zheng, K. Kinbara, K. Saigo, S. Sakamoto, K. Yamaguchi, "A Cyclic Dimer of Metalloporphyrin Forms a Highly Stable Inclusion Complex with C_{60}", *J. Am. Chem. Soc.*, **1999**, *121*, 9477; b) J.-Y. Zheng, K. Tashiro, Y. Hirabayashi, K. Kinbara, K. Saigo, T. Aida, S. Sakamoto, K. Yamaguchi, "Cyclic Dimers of Metalloporphyrins as Tunable Hosts for Fullerenes: A Remarkable Effect of Rhodium(III)", *Angew. Chem. Int. Ed.*, **2001**, *40*, 1857.

[64] G. Gil-Ramírez, S. D. Karlen, A. Shundo, K. Porfyrakis, Y. Ito, G. A. D. Briggs, J. J. L. Morton, H. L. Anderson, "A Cyclic Porphyrin Trimer as a Receptor for Fullerenes", *Org. Lett.*, **2010**, *12*, 3544.

[65] J. Song, N. Aratani, H. Shinokubo, A. Osuka, "A Porphyrin Nanobarrel That Encapsulates C_{60}", *J. Am. Chem. Soc.*, **2010**, *132*, 16356.

[66] W. Meng, B. Breiner, K. Rissanen, J. D. Thoburn, J. K. Clegg, J. R. Nitschke, "A Self-Assembled M_8L_6 Cubic Cage that Selectively Encapsulates Large Aromatic Guests", *Angew. Chem. Int. Ed.*, **2011**, *50*, 3479.

[67] M. Yanagisawa, K. Tashiro, M. Yamasaki, T. Aida, "Hosting Fullerenes by Dynamic Bond Formation with an Iridium Porphyrin Cyclic Dimer: A “Chemical Friction” for Rotary Guest Motions", *J. Am. Chem. Soc.*, **2007**, *129*, 11912.

[68] A. Satake, Y. Kobuke, "Dynamic supramolecular porphyrin systems", *Tetrahedron*, **2005**, *61*, 13.

[69] a) N. Armaroli, F. Diederich, L. Echegoyen, T. Habicher, L. Flamigni, G. Marconi, J.-F. Nierengarten, "A new pyridyl-substituted methanofullerene derivative. Photophysics, electrochemistry and self-assembly with zinc(II) *meso*-tetraphenylporphyrin (ZnTPP)", *New J. Chem.*, **1999**, *23*, 77; b) F. D'Souza, G. R. Deviprasad, M. S. Rahman, J.-P. Choi, "Self-Assembled Porphyrin–C_{60} and Porphycene–C_{60} Complexes via Metal Axial Coordination", *Inorg. Chem.*, **1999**, *38*, 2157.

[70] F. D'Souza, P. M. Smith, M. E. Zandler, A. L. McCarty, M. Itou, Y. Araki, O. Ito, "Energy Transfer Followed by Electron Transfer in a Supramolecular Triad Composed of Boron Dipyrrin, Zinc Porphyrin, and Fullerene: A Model for the Photosynthetic Antenna-Reaction Center Complex", *J. Am. Chem. Soc.*, **2004**, *126*, 7898.

[71] A. Trabolsi, M. Elhabiri, M. Urbani, J. L. Delgado, F. Ajamaa, N. Solladié, A.-M. Albrecht-Gary, J.-F. Nierengarten, "Supramolecular click chemistry for the self-assembly of a stable Zn(II)-porphyrin-C_{60} conjugate", *Chem. Commun.*, **2005**, 5736.

[72] a) J. L. Sessler, B. Wang, A. Harriman, "Long-range photoinduced electron transfer in an associated but non-covalently linked photosynthetic model system", *J. Am. Chem. Soc.*, **1993**, *115*, 10418; b) P. de Rege, S. Williams, M. Therien, "Direct evaluation of electronic coupling mediated by hydrogen bonds: implications for biological electron transfer", *Science*, **1995**, *269*, 1409.

[73] L. Sánchez, M. Sierra, N. Martín, A. J. Myles, T. J. Dale, J. Rebek, W. Seitz, D. M. Guldi, "Exceptionally Strong Electronic Communication through Hydrogen Bonds in Porphyrin–C_{60} Pairs", *Angew. Chem. Int. Ed.*, **2006**, *45*, 4637.

[74] S. K. Chang, A. D. Hamilton, "Molecular recognition of biologically interesting substrates: synthesis of an artificial receptor for barbiturates employing six hydrogen bonds", *J. Am. Chem. Soc.*, **1988**, *110*, 1318.

[75] F. Wessendorf, B. Grimm, D. M. Guldi, A. Hirsch, "Pairing Fullerenes and Porphyrins: Supramolecular Wires That Exhibit Charge Transfer Activity", *J. Am. Chem. Soc.*, **2010**, *132*, 10786.

[76] V. Rüdiger, H.-J. Schneider, V. P. Solov'ev, V. P. Kazachenko, O. A. Raevsky, "Crown Ether–Ammonium Complexes: Binding Mechanisms and Solvent Effects", *Eur. J. Org. Chem.*, **1999**, *1999*, 1847.

[77] C. J. Pedersen, H. K. Frensdorff, "Macrocyclic Polyethers and Their Complexes", *Angew. Chem. Int. Ed.*, **1972**, *11*, 16.

[78] A. Späth, B. König, "Molecular recognition of organic ammonium ions in solution using synthetic receptors", *Beilstein J. Org. Chem.*, **2010**, *6*, 32.

[79] F. D'Souza, C. A. Wijesinghe, M. E. El-Khouly, J. Hudson, M. Niemi, H. Lemmetyinen, N. V. Tkachenko, M. E. Zandler, S. Fukuzumi, "Ultrafast excitation

transfer and charge stabilization in a newly assembled photosynthetic antenna-reaction center mimic composed of boron dipyrrin, zinc porphyrin and fullerene", *Phys. Chem. Chem. Phys.*, **2011**, *13*, 18168.

[80] D. Balbinot, S. Atalick, D. M. Guldi, M. Hatzimarinaki, A. Hirsch, N. Jux, "Electrostatic Assemblies of Fullerene−Porphyrin Hybrids: Toward Long-Lived Charge Separation", *J. Phys. Chem. B*, **2003**, *107*, 13273.

[81] N. Watanabe, N. Kihara, Y. Furusho, T. Takata, Y. Araki, O. Ito, "Photoinduced Intrarotaxane Electron Transfer between Zinc Porphyrin and [60]Fullerene in Benzonitrile", *Angew. Chem. Int. Ed.*, **2003**, *42*, 681.

[82] K. Li, D. I. Schuster, D. M. Guldi, M. Á. Herranz, L. Echegoyen, "Convergent Synthesis and Photophysics of [60]Fullerene/Porphyrin-Based Rotaxanes", *J. Am. Chem. Soc.*, **2004**, *126*, 3388.

[83] Z.-Q. Wu, X.-B. Shao, C. Li, J.-L. Hou, K. Wang, X.-K. Jiang, Z.-T. Li, "Hydrogen-Bonding-Driven Preorganized Zinc Porphyrin Receptors for Efficient Complexation of C_{60}, C_{70}, and C_{60} Derivatives", *J. Am. Chem. Soc.*, **2005**, *127*, 17460.

[84] F. D'Souza, P. M. Smith, S. Gadde, A. L. McCarty, M. J. Kullman, M. E. Zandler, M. Itou, Y. Araki, O. Ito, "Supramolecular Triads Formed by Axial Coordination of Fullerene to Covalently Linked Zinc Porphyrin−Ferrocene(s): Design, Syntheses, Electrochemistry, and Photochemistry", *J. Phys. Chem. B*, **2004**, *108*, 11333.

[85] A. Trabolsi, M. Urbani, J. L. Delgado, F. Ajamaa, M. Elhabiri, N. Solladié, J.-F. Nierengarten, A.-M. Albrecht-Gary, "Large photoactive supramolecular ensembles prepared from C_{60}-pyridine substrates and multi-Zn(II)-porphyrin receptors", *New J. Chem.*, **2008**, *32*, 159.

[86] N. Solladié, M. E. Walther, M. Gross, T. M. F. Duarte, C. Bourgogne, J.-F. Nierengarten, "A supramolecular cup-and-ball C_{60}-porphyrin conjugate system", *Chem. Commun.*, **2003**, 2412.

[87] N. Solladié, M. E. Walther, H. Herschbach, E. Leize, A. V. Dorsselaer, T. M. F. Duarte, J.-F. Nierengarten, "Supramolecular complexes obtained from porphyrin–crown ether conjugates and a fullerene derivative bearing an ammonium unit", *Tetrahedron*, **2006**, *62*, 1979.

[88] F. D'Souza, R. Chitta, S. Gadde, M. E. Zandler, A. L. McCarty, A. S. D. Sandanayaka, Y. Araki, O. Ito, "Potassium Ion Controlled Switching of Intra- to Intermolecular Electron Transfer in Crown Ether Appended Free-Base Porphyrin−Fullerene Donor−Acceptor Systems", *J. Phys. Chem. A*, **2006**, *110*, 4338.

[89] H. Sato, K. Tashiro, H. Shinmori, A. Osuka, Y. Murata, K. Komatsu, T. Aida, "Positive Heterotropic Cooperativity for Selective Guest Binding via Electronic Communications through a Fused Zinc Porphyrin Array", *J. Am. Chem. Soc.*, **2005**, *127*, 13086.

[90] a) F. G. Brunetti, J. L. López, C. Atienza, N. Martín, "π-Extended TTF: a versatile molecule for organic electronics", *J. Mater. Chem.*, **2012**, *22*, 4188; b) Y. Yamashita, Y. Kobayashi, T. Miyashi, "p-Quinodimethane Analogues of Tetrathiafulvalene", *Angew. Chem. Int. Ed.*, **1989**, *28*, 1052.

[91] N. Martín, L. Sánchez, C. Seoane, E. Ortí, P. M. Viruela, R. Viruela, "Synthesis, Properties, and Theoretical Characterization of Largely π-Extended Tetrathiafulvalene Derivatives with Quinonoid Structures", *J. Org. Chem.*, **1998**, *63*, 1268.

[92] N. Martín, E. Ortí, "Chapter 6 - Quinonoid π-extended tetrathiafulvalenes (TTFs)" in *Handbook of Advanced Electronic and Photonic Materials and Devices* (Ed.: N. Hari Singh), Academic Press, Burlington, **2001**, pp. 245.

[93] E. Ortí, *Personal communication*.

[94] E. M. Pérez, M. Sierra, L. Sánchez, M. R. Torres, R. Viruela, P. M. Viruela, E. Ortí, N. Martín, "Concave Tetrathiafulvalene-Type Donors as Supramolecular Partners for Fullerenes", *Angew. Chem. Int. Ed.*, **2007**, *46*, 1847.

[95] E. M. Pérez, L. Sánchez, G. Fernández, N. Martín, "exTTF as a Building Block for Fullerene Receptors. Unexpected Solvent-Dependent Positive Homotropic Cooperativity", *J. Am. Chem. Soc.*, **2006**, *128*, 7172.

[96] S. S. Gayathri, M. Wielopolski, E. M. Pérez, G. Fernández, L. Sánchez, R. Viruela, E. Ortí, D. M. Guldi, N. Martín, "Discrete Supramolecular Donor–Acceptor Complexes", *Angew. Chem. Int. Ed.*, **2009**, *48*, 815.

[97] E. M. Pérez, A. L. Capodilupo, G. Fernández, L. Sánchez, P. M. Viruela, R. Viruela, E. Ortí, M. Bietti, N. Martín, "Weighting non-covalent forces in the molecular recognition of C_{60}. Relevance of concave-convex complementarity", *Chem. Commun.*, **2008**, 4567.

[98] D. Canevet, M. Gallego, H. Isla, A. de Juan, E. M. Pérez, N. Martín, "Macrocyclic Hosts for Fullerenes: Extreme Changes in Binding Abilities with Small Structural Variations", *J. Am. Chem. Soc.*, **2011**, *133*, 3184.

[99] G. Fernández, E. M. Pérez, L. Sánchez, N. Martín, "Self-Organization of Electroactive Materials: A Head-to-Tail Donor–Acceptor Supramolecular Polymer", *Angew. Chem. Int. Ed.*, **2008**, *47*, 1094.

[100] G. Fernández, E. M. Pérez, L. Sánchez, N. Martín, "An Electroactive Dynamically Polydisperse Supramolecular Dendrimer", *J. Am. Chem. Soc.*, **2008**, *130*, 2410.

[101] E. Huerta, H. Isla, E. M. Pérez, C. Bo, N. Martín, J. de Mendoza, "Tripodal exTTF-CTV Hosts for Fullerenes", *J. Am. Chem. Soc.*, **2010**, *132*, 5351.

[102] J. Santos, B. Grimm, B. M. Illescas, D. M. Guldi, N. Martín, "Cooperativity between π-π and H-bonding interactions-a supramolecular complex formed by C_{60} and exTTF", *Chem. Commun.*, **2008**, 5993.

[103] B. Grimm, J. Santos, B. M. Illescas, A. Muñoz, D. M. Guldi, N. Martín, "A New exTTF-Crown Ether Platform To Associate Fullerenes: Cooperative n−π and π−π Effects", *J. Am. Chem. Soc.*, **2010**, *132*, 17387.

[104] J.-B. Giguere, J.-F. Morin, "New strapped porphyrins as hosts for fullerenes: synthesis and complexation study", *Org. Biomol. Chem.*, **2012**, *10*, 1047.

[105] M. C. Díaz, B. M. Illescas, N. Martín, J. F. Stoddart, M. A. Canales, J. Jiménez-Barbero, G. Sarova, D. M. Guldi, "Supramolecular pseudo-rotaxane type complexes from π-extended TTF dimer crown ether and C_{60}", *Tetrahedron*, **2006**, *62*, 1998.

[106] B. M. Illescas, J. Santos, M. C. Díaz, N. Martín, C. M. Atienza, D. M. Guldi, "Supramolecular Threaded Complexes from Fullerene–Crown Ether and π-Extended TTF Derivatives", *Eur. J. Org. Chem.*, **2007**, *2007*, 5027.

[107] a) M. Sommelet, "Sur un mode de décomposition des halogénoalcoylates d'hexaméthylène - tétramine", *C. R. Chim.*, **1913**, *157*, 852; b) Z. Wang, "Sommelet Reaction" in *Comprehensive Organic Name Reactions and Reagents*, John Wiley & Sons, Inc., **2010**.

[108] A. Nakano, H. Shimidzu, A. Osuka, "Facile regioselective *meso*-iodination of porphyrins", *Tetrahedron Lett.*, **1998**, *39*, 9489.

[109] P. Even, B. Boitrel, "Crown porphyrins", *Coord. Chem. Rev.*, **2006**, *250*, 519.

[110] B. Neises, W. Steglich, "Simple Method for the Esterification of Carboxylic Acids", *Angew. Chem. Int. Ed.*, **1978**, *17*, 522.

[111] C. Bingel, "Cyclopropanierung von Fullerenen", *Chem. Ber.*, **1993**, *126*, 1957.

[112] C. A. Hunter, "Quantifying Intermolecular Interactions: Guidelines for the Molecular Recognition Toolbox", *Angew. Chem. Int. Ed.*, **2004**, *43*, 5310.

[113] M. Nappa, J. S. Valentine, "The influence of axial ligands on metalloporphyrin visible absorption spectra. Complexes of tetraphenylporphinatozinc", *J. Am. Chem. Soc.*, **1978**, *100*, 5075.

[114] F. D'Souza, O. Ito, "Supramolecular donor-acceptor hybrids of porphyrins/phthalocyanines with fullerenes/carbon nanotubes: electron transfer, sensing, switching, and catalytic applications", *Chem. Commun.*, **2009**, 4913.

[115] K. A. Connors, *Binding Constants: The Measurement of Molecular Complex Stability*, Wiley, **1987**.

[116] J. Fenn, M. Mann, C. Meng, S. Wong, C. Whitehouse, "Electrospray ionization for mass spectrometry of large biomolecules", *Science*, **1989**, *246*, 64.

[117] P. G. Young, K. A. Jolliffe, "Selective recognition of sulfate ions by tripodal cyclic peptides functionalised with (thio)urea binding sites", *Org. Biomol. Chem.*, **2012**, *10*, 2664.

[118] D. Kim, A. Osuka, "Photophysical Properties of Directly Linked Linear Porphyrin Arrays", *J. Phys. Chem. A*, **2003**, *107*, 8791.

[119] H. Günther, *NMR spectroscopy: basic principles, concepts, and applications in chemistry*, Wiley, **1995**.

[120] J. F. Hartwig, "Transition Metal Catalyzed Synthesis of Arylamines and Aryl Ethers from Aryl Halides and Triflates: Scope and Mechanism", *Angew. Chem. Int. Ed.*, **1998**, *37*, 2046.

[121] A. E. Jones, C. A. Christensen, D. F. Perepichka, A. S. Batsanov, A. Beeby, P. J. Low, M. R. Bryce, A. W. Parker, "Photochemistry of the π-Extended 9,10-Bis(1,3-dithiol-2-ylidene)- 9,10-dihydroanthracene System: Generation and Characterisation of the Radical Cation, Dication, and Derived Products", *Chem. Eur. J.*, **2001**, *7*, 973.

[122] J. B. Wittenberg, L. Isaacs, "Complementarity and Preorganization" in *Supramol. Chem.*, John Wiley & Sons, Ltd, **2012**.

[123] a) M. C. Misuraca, T. Grecu, Z. Freixa, V. Garavini, C. A. Hunter, P. W. N. M. van Leeuwen, M. D. Segarra-Maset, S. M. Turega, "Relationship Between Conformational Flexibility and Chelate Cooperativity", *J. Org. Chem.*, **2011**, *76*, 2723; b) Z. Zhong, X. Li, Y. Zhao, "Enhancing Binding Affinity by the Cooperativity between Host Conformation and Host–Guest Interactions", *J. Am. Chem. Soc.*, **2011**, *133*, 8862.

[124] H. J. Hogben, J. K. Sprafke, M. Hoffmann, M. Pawlicki, H. L. Anderson, "Stepwise Effective Molarities in Porphyrin Oligomer Complexes: Preorganization Results in Exceptionally Strong Chelate Cooperativity", *J. Am. Chem. Soc.*, **2011**, *133*, 20962.

[125] W. L. F. Armarego, C. L. L. Chai, *Purification of Laboratory Chemicals*, Elsevier, **2003**.

[126] T. E. Nielsen, S. L. Quement, M. Juhl, D. Tanner, "Cu-mediated Stille reactions of sterically congested fragments: towards the total synthesis of zoanthamine", *Tetrahedron*, **2005**, *61*, 8013.

[127] a) J. K. Laha, S. Dhanalekshmi, M. Taniguchi, A. Ambroise, J. S. Lindsey, "A Scalable Synthesis of Meso-Substituted Dipyrromethanes", *Org. Process Res. Dev.*, **2003**, *7*, 799; b) M. J. Plater, S. Aiken, G. Bourhill, "A new synthetic route to donor–acceptor porphyrins", *Tetrahedron*, **2002**, *58*, 2405.

[128] D. Bonifazi, G. Accorsi, N. Armaroli, F. Song, A. Palkar, L. Echegoyen, M. Scholl, P. Seiler, B. Jaun, F. Diederich, "Oligoporphyrin Arrays Conjugated to [60]Fullerene: Preparation, NMR Analysis, and Photophysical and Electrochemical Properties", *Helv. Chim. Acta*, **2005**, *88*, 1839.

[129] C.-L. Chuang, O. dos Santos, X. Xu, J. W. Canary, "Synthesis and Cyclic Voltammetry Studies of Copper Complexes of Bromo- and Alkoxyphenyl-Substituted Derivatives of Tris(2-pyridylmethyl)amine: Influence of Cation−Alkoxy Interactions on Copper Redox Potentials", *Inorg. Chem.*, **1997**, *36*, 1967.

[130] A. Zistler, S. Koch, A. Dieter Schluter, "Dendronized polyacrylates with glucose units in the periphery", *J. Chem. Soc., Perkin Trans. 1*, **1999**, 501.

[131] J.-F. Eckert, J.-F. Nicoud, J.-F. Nierengarten, S.-G. Liu, L. Echegoyen, F. Barigelletti, N. Armaroli, L. Ouali, V. Krasnikov, G. Hadziioannou, "Fullerene−Oligophenylenevinylene Hybrids: Synthesis, Electronic Properties, and Incorporation in Photovoltaic Devices", *J. Am. Chem. Soc.*, **2000**, *122*, 7467.

[132] D. Felder, M. Gutiérrez Nava, M. P. Carreón, J.-F. Eckert, M. Luccisano, C. Schall, P. Masson, J.-L. Gallani, B. Heinrich, D. Guillon, J.-F. Nierengarten, "Synthesis of Amphiphilic Fullerene Derivatives and Their Incorporation in Langmuir and Langmuir-Blodgett Films", *Helv. Chim. Acta*, **2002**, *85*, 288.

[133] a) A. J. Moore, M. R. Bryce, "Generation and Trapping of Phosphorus Stabilized 4,5-Ethylenedithio-1,3-dithiol-2-ide Carbanions: Synthesis of Ethylenedithio-1,3-dithiafulvalenes", *Synthesis*, **1991**, *1991*, 26; b) L. Sánchez, Thesis *Síntesis y propiedades de compuestos dadores derivados de TTF y de sistemas dador-aceptor de electrones*, Universidad Complutense de Madrid, **1997**.

[134] A. J. Moore, M. R. Bryce, "Highly conjugated π-electron donors for organic metals: synthesis and redox chemistry of new 1,3-dithiole and 1,3-selenathiole derivatives", *J. Chem. Soc., Perkin Trans. 1*, **1991**, 157.

[135] G. J. Marshallsay, M. R. Bryce, "Synthesis and Multistage Redox Properties of 9,10-Bis(1,3-dithiol-2-ylidene)-9,10-dihydroanthracene Derivatives Functionalized with Ferrocenyl and Tetrathiafulvalenyl Units", *J. Org. Chem.*, **1994**, *59*, 6847.

[136] J. Santos, Thesis *Síntesis y propiedades de sistemas electroactivos derivados de C_{60}*, Universidad Complutense de Madrid, **2010**.

[137] X.-Z. Zhu, C.-F. Chen, "A Highly Efficient Approach to [4]Pseudocatenanes by Threefold Metathesis Reactions of a Triptycene-Based Tris[2]pseudorotaxane", *J. Am. Chem. Soc.*, **2005**, *127*, 13158.

[138] F. Diederich, L. Echegoyen, M. Gómez-López, R. Kessinger, J. Fraser Stoddart, "The self-assembly of fullerene-containing [2]pseudorotaxanes: formation of a supramolecular C_{60} dimer", *J. Chem. Soc., Perkin Trans. 2*, **1999**, 1577.

[139] N. Yamaguchi, L. M. Hamilton, H. W. Gibson, "Dendritic Pseudorotaxanes", *Angew. Chem. Int. Ed.*, **1998**, *37*, 3275.

[140] W. C. J. Ross, "43. Aryl-2-halogenoalkylamines. Part I", *J. Chem. Soc.*, **1949**, 183.

[141] S. González, N. Martín, D. M. Guldi, "Synthesis and Properties of Bingel-type Methanofullerene–π-Extended-TTF Diads and Triads", *J. Org. Chem.*, **2002**, *68*, 779.

[142] D. S. Nagvekar, H. W. Gibson, "Improved syntheses of 20- and 26-membered bis(5-carbomethoxy-1,3-phenylene) crown ethers", *Org. Prep. Proced. Int.*, **1997**, *29*, 237.

[143] H. W. Gibson, D. S. Nagvekar, J. Powell, C. Gong, W. S. Bryant, "Polyrotaxanes by in situ self threading during polymerization of functional macrocycles. Part 2: Poly(ester crown ether)s", *Tetrahedron*, **1997**, *53*, 15197.

[144] a) H. Tsukube, H. Furuta, A. Odani, Y. Takeda, Y. Kudo, Y. Inoue, Y. Liu, H. Sakamoto, K. Kimura, "Determination of Stability Constants" in *Comprehensive Supramolecular Chemistry*, *Vol. 8* (Eds.: J.-M. Lehn, J. L. Atwood, J. E. D. Davies, D. D. Macnicol, F. Vögtle), Pergamon/Elsevier, Oxford, **1996**; b) C. S. Wilcox, "Design, Synthesis, and Evaluation of an Efficacious Functional Group Dyad. Methods and Limitations in the Use of NMR for Measuring Host-Guest Interactions" in *Frontiers in supramolecular organic chemistry and photochemistry* (Eds.: H. J. Schneider, H. Dürr), VCH, **1991**; c) P. Thordarson, "Determining association constants from titration experiments in supramolecular chemistry", *Chem. Soc. Rev.*, **2011**, *40*, 1305; d) P. Thordarson, "Binding Constants and Their Measurement" in *Supramol. Chem.* (Eds.: J. W. Steed, P. A. Gale), John Wiley & Sons, Ltd, **2012**; e) E. M. Pérez, N. Martín, "Experimental determination of association constants involving fullerenes" in *Supramolecular Chemistry of Fullerenes and Carbon Nanotubes* (Eds.: N. Martín, J.-F. Nierengarten), Wiley-VCH, Weinheim, **2012**; f) K. Hirose, "Determination of Binding Constants" in *Analytical Methods in Supramolecular Chemistry* (Ed.: C. Schalley), Wiley-VCH Verlag GmbH & Co. KGaA, **2007**, pp. 17.

[145] N. Isaacs, *Physical Organic Chemistry*, 2nd ed., Longmans England, **1995**.
[146] J. W. Jones, Thesis *Quantification of Supramolecular Complexes Involving Charged Species in Non-Aqueous Solvents: Theory and Application*, Virginia Polytechnic Institute and State University (Blacksburg), **2004**.
[147] G. Weber, in *Molecular biophysics* (Eds.: B. Pullman, M. Weissbluth), Academic Press, New York, **1965**.
[148] R. S. Macomber, "An introduction to NMR titration for studying rapid reversible complexation", *J. Chem. Educ.*, **1992**, *69*, 375.
[149] H. Gampp, M. Maeder, C. J. Meyer, A. D. Zuberbühler, "Calculation of equilibrium constants from multiwavelength spectroscopic data—II32, 95.: Specfit: two user-friendly programs in basic and standard fortran 77", *Talanta*, **1985**, *32*, 257.
[150] C. A. Hunter, H. L. Anderson, "What is Cooperativity?", *Angew. Chem. Int. Ed.*, **2009**, *48*, 7488.
[151] G. Ercolani, L. Schiaffino, "Allosteric, Chelate, and Interannular Cooperativity: A Mise au Point", *Angew. Chem. Int. Ed.*, **2011**, *50*, 1762.
[152] G. Ercolani, L. Schiaffino, "Bioinspired Self-Assembly II: Principles of Cooperativity in Bioinspired Self-Assembling Systems" in *Bioinspiration and Biomimicry in Chemistry*, John Wiley & Sons, Inc., **2012**, pp. 47.